ABSTRACT

BOOKMAN, LAKE DAWSON. Approximate Solitons of the Landau-Lifshitz Equation . (Under the direction of Dr. Mark Hoefer.)

Under highly idealized assumptions the model for a thin ferromagnetic film supports a family of large amplitude, localized waves in the magnetization, termed droplet solitons [Kos90; HS12]. In physical systems, these highly idealized assumptions cannot be met, yet there have been recent observations of structures similar to droplet solitons in experiments where both damping and spin-transfer torque effectively cancel each other out [Moh13; Mac14]. Typically, damping and forcing are small and may be viewed as a perturbation of the classical model. This thesis derives a general framework for investigating such perturbations, as well as many others, using the techniques of soliton perturbation theory. The method utilized here is generalized to a broad class of Hamiltonian systems which includes the model of magnetic systems studied here. Also derived is an approximate, analytical representation of the droplet soliton, which is valid for low frequencies and low velocities. Leveraging the approximate droplet, many analytical results can be obtained for quite complex systems. A wide range of physically relevant effects are explored determining the particle-like dynamics of the droplet. The most important of these applications is the nanocontact spin torque oscillator which corresponds to the experimental conditions where the droplet has been observed. The framework here is used to probe the existence and stability of the droplet in certain parameter regimes utilizing classical tools from dynamical systems theory. The validity of the approximate theory is tested by comparison with careful numerical experiments.

Approximate Solitons of the Landau-Lifshitz Equation

by
Lake Dawson Bookman

A dissertation submitted to the Graduate Faculty of
North Carolina State University
in partial fulfillment of the
requirements for the Degree of
Doctor of Philosophy

Applied Mathematics

Raleigh, North Carolina

2015

APPROVED BY:

Mansoor Haider	Kazufumi Ito
Dan Stancil	Mark Hoefer Chair of Advisory Committee

DEDICATION

ἠντεβόλεσα τὸν ὁδίτην ἐκ τοῖ δήμου παλαιοῦ ὅς ἔφη: “δύο σκέλοι τοῦ λίθου
σπίδεις καὶ ἄνευ κόρμων ἐν τῇ ἐρημίας κείμονται
περὶ τόυτους ἐν τῇ ἀμμῷ ἡμιβύθιον τὸ προσκλαλμένον
πρόσωπον κείται, ὁῦ ἡ κατανομαξία μέλαινα,
καὶ τὸν φαρκιδώδες μύλλον καὶ ἡ ἐμψύρου ἀναξίου
μνκτερίσμα λέγει ὅτι ὁ τόυτου ἀγαλματογλύφος
ἐῦ ἔγνω ἤδειλτὰς μαργότας ἐκείνας ἃι ἔτι ἐπιζώσι χαράκται
ἐπὶ ταῦτα τὰ ἄψυχα ἥ χεὶρ ἥ κερτήσε ταῦτα
καὶ ἥ καρδία ἥ ἔθρεψε καὶ ἐπι τοῦ ὑποβάθρου
ὁι ᾽ουτοε λόγοι φαίνονται: ‘τὸ ὄνομα ἐμοῦ ἔστιν Οζιμάνδιας
ὁ βασιλεὺς τῶν βασιλέων σκοπεῖτε τὰ ἔργα ἐμοῦ ὑμεῖς
δυνατοὶ καὶ ἄλγεῖτε’ οὐδέν ἄλλο μένει
περὶ τὴν τοῦ ἐρείπιου ἓκείνου πελώρου φθορὰν
ἀπείρον καὶ ἀκρόψιλον τόν ἐρῆμον καὶ ἁρπεδὲς
ἁλίπεδον πόρρω ἐπέκτεινει."

- Πέρσι βιχ Ξέλλι

(Thanks, Mom)

BIOGRAPHY

The author was born an undisclosed number of years ago in North Carolina, spending his entire childhood at the same home in Chapel Hill, NC. In 2003, Lake achieved the rank of Eagle Scout in the Boy Scouts. To date, he regards this as his proudest accomplishment since it reflects not only upon achievement, but also on civic engagement and personal integrity. In 2008, he graduated from Swarthmore College double majoring in Mathematics and Physics. During his final two years at Swarthmore, Lake had the opportunity to work on the Swarthmore Spheromak Experiment, a project focusing on the magnetic confinement of plasmas with the long term goal of contributing to viable controlled fusion. Immediately following his time at Swarthmore, Lake went to work for the now dissolved “Institute for Earth Science and Engineering" at the University of Auckland in New Zealand . While there, Lake conducted research in aid of geothermal exploration. Having left New Zealand for N.C. Sate, Lake has never forgotten his passionate conviction that scientific research should serve the pressing needs of the world and in his opinion, the need for clean renewable energies sources remain such an area of important exploration.

ACKNOWLEDGEMENTS

I would like to thank my advisor for his help and guidance. Graduate school can be a trying time for many students and it is only through Mark's assistance that I have made it through to completion.

I would also like to acknowledge the tireless support of my wife. Her support helped carry me through. I would also to thank my parents and brothers all of whom have been steadfast in their encouragement of me throughout graduate school.

Additionally, I would like to thank all the educators who contributed to my development. While I cannot begin to list them all, several names stand out. Laurie Alexander without whom I may never have learned to read. Peter Reichert and Bob Robinson for challenging me at a young age and recognizing my aptitude for mathematical thinking long before I had recognized it myself. Dr. Brad Miller for making my introduction to Physics a challenge and a joy. Mimi Cross for her patience and reminding me that education and civic engagement go hand in hand. Drs. Thomas Hunter, Janet Talvacchia and Cheryl Grood who each helped in their own way to help me understand what abstract math was and to come to love it. Dr. Michael Brown for his tireless commitment to my success in Physics and Dr. Carl Grossman for reminding me that it is possible to be human and study science. Eylon Shalev and Peter Malin for mentoring beyond geophysics with advice that has served me in all corners of my life. I would like to acknowledge my parents again, who taught me not only as all parents teach their children, but also as teachers themselves. In both capacities, as parent and instructor, both contributed to my diverse interests, my passion for learning and the values that guide me.

Finally, I would like to acknowledge my friends at N.C. State from whom I learned a great deal. Chief among peers, I would like to thank Will Cousins, for the many hours he spent learning new material with me, counseling me and most importantly for his suggestion that I work with Mark. I would also like to acknowledge the free support and frequent discussions with Nick Lowman, Jeffery Willert and Lucus Van Blaircum, all of whom contributed in their own way to the academic work in this thesis.

TABLE OF CONTENTS

LIST OF TABLES

LIST OF FIGURES

CHAPTER

1

INTRODUCTION

Even the most elementary study of magnetic materials reveals the importance of coherent structures. The tendency of ferromagnetic materials to form domains of aligned magnetization was well known in quite early models and experiments [CG11]. When using a continuous model for the magnetization, solitons or domain walls, as localized solutions, offer a mathematical explanation for the rapid transition which occurs between magnetic domains. Accordingly, solitons are a rich area of research in ferromagnetic materials where a wide array of such structures can be observed[Kos90]. In this context, solitons correspond to regions of a magnetic material where the direction of the magnetization vector, $\mathbf{M} = [M_x, M_y, M_z]$, exhibits a significant deviation from a uniform background. Solitons in magnetic media are of particular interest as a mechanism for data storage or information transfer. Since the discovery of the spin torque effect by Slonczewski[Slo96] and Berger[Ber96], magnetic vortices, domain walls and skyrmions have all been created and studied with exactly that application in mind [Cow07; Par08; Fer13]. This thesis focuses primarily on a different localized structure, the magnetic droplet soliton (or droplet from here on), illustrated in Fig. 1.1. There is a current need

for more theory relating to the droplet because of its recent observation in experiment [Moh13; Mac14]. Broadly speaking, solitons are special solutions of nonlinear partial differential equations that receive significant attention because of their nontrivial dynamics and often appear in the long time behavior of solutions.

In a more precise sense, solitons are a particular class of analytical solution to integrable partial differential equations. The model for a one-dimensional ferromagnet is integrable, but the focus of this thesis is for a ferromagnetic film where the model is non-integrable. The droplet here is a two-dimensional analogue of the exact solution to the one-dimensional model, but no analytical solution is known to exist. The droplet can be computed numerically and its stability numerically verified [HS12]. It is also possible to approximate the droplet in certain parameter regimes, as will be done later in this chapter. The mathematical term soliton is often reserved for integrable systems, and the droplet is more properly dubbed a solitary wave. However, this mathematical distinction is often ignored in physical systems and the terms soliton and solitary wave will be used interchangeably throughout this thesis.

Figure 1.1(a) shows a plot of an approximate solution for the droplet (an explicit formula will be given later in this chapter). An assumption on the model here is that the ferromagnetic layer is saturated so that the magnetization vector is of uniform length (M_s) throughout the medium. It is therefore convenient to work with a nondimensionalized magnetization, $\mathbf{m} = \mathbf{M}/M_s = (m_x, m_y, m_z)$. The arrows represent the in-plane component of the magnetization vector, (m_x, m_y), and the color corresponds to the out of plane component of the magnetization, m_z. Far from the origin, the magnetization is pointing nearly straight up: the arrows in plane are small and all the magnitude is concentrated in m_z. Near the origin, the magnetization is nearly, but not quite, pointing straight down and in between there is a rapid transition region where $m_z \approx 0$ (the white band). Figure 1.1(b) plots the m_z profile along the line $y = 0$. Superimposed on this profile is the vector (m_x, m_z). Moving from left to right, the vector can clearly be observed to point (at least slightly) to the left. If instead the vector transitioned from pointing left to pointing right, a nonzero winding number

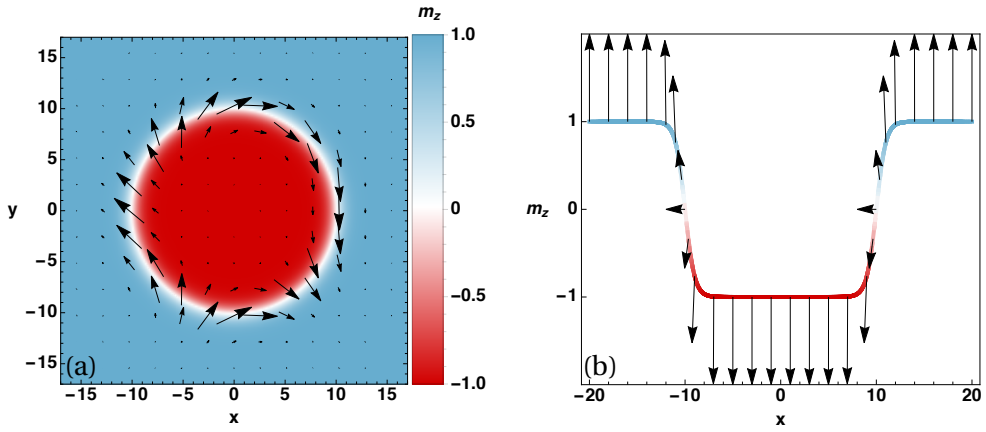

Figure 1.1 (a) A representation of the approximate droplet with precessional frequency, ω, of 0.1 and propagation velocity, $\mathbf{V}$, of $[.02, 0]$. In this figure, the arrows represent the in-plane component of the magnetization and the color the out of plane component. One key contribution of this thesis is the extension of the approximate droplet to the propagating case. The non-trivial phase contribution can clearly be seen in the variation of the arrows. (b) A slice down the $x-$axis of the plot in (a). The vectors representing (m_x, m_z) are superimposed on the vertical profile of the droplet to illustrate the manner in which the droplet transitions from the far-field to the nearly reversed state and back.

would be necessary to transition between the left and right states, commonly called topological charge [Kos90]. For the droplet, this is prevented by the restriction that the magnetization never fully reverse, since any such transition would require an instant of full reversal. Hence the droplet has no overall topological charge which is one of the most fundamental properties distinguishing it from other magnetic solitons.

One of the key differences between the droplet and other magnetic solitons is that the droplet is fundamentally a dynamic structure. As time advances, the arrows will rotate in plane with a fixed frequency. This contrasts to other magnetic solitons where the magnetization may remain static or is characterized by a switching frequency (e.g. magnetic bubbles) [DL80; Fin13]. As will be clarified later in this chapter, the precession of the droplet plays a vital role in stabilizing the droplet and preventing it from relaxing to the uniform state. Such a mechanism is necessary since the droplet has no topological charge and hence is not stabilized by its topology as happens with other magnetic solitons. Additionally, droplets can propagate through a medium and are not fixed to a particular

point. This propagation is made possible by the fact that the magnetization never fully reverses. A single reversal of the magnetization vector in a homogenous medium leads to pinning (as happens with vortices), by general arguments involving conserved quantities [PT91].

The droplet in Fig. 1.1 is one example from a six-parameter family of solutions to an idealized model. This model, the Landau-Lifshitz equation, is elaborated on in the next section (Section 1.1). The model presented there includes certain physical assumptions: a sufficiently thin ferromagnetic layer, strong perpendicular anisotropy (preferred direction of the magnetization due to its crystal structure) and perpendicular applied field. These assumptions introduce certain symmetries in the mathematical model, which in turn generate free parameters in the general solution. As will be further clarified later, the typical parameterization involves the rest precession frequency, ω, and a propagation velocity, $\mathbf{V}$, as well as parameters corresponding to the initial state for these angular and linear velocities.

The main goal of this thesis is to characterize the influence of additional physical effects (e.g. damping and forcing) on these solitons. The strategy employed involves a combination of numerical investigation and careful asymptotic analysis to elucidate the underlying physics. To accomplish this analysis, these previously neglected physical effects must be added back into the underlying model. However, many of these effects are small and it is natural to consider the adiabatic evolution of the solitons along the soliton manifold. This strategy has been broadly employed in the field of nonlinear waves (see [KM89] for an exhaustive review). Additionally, the Landau-Lifshitz equation is a Hamiltonian system and this structure can be utilized to simplify the asymptotic calculation involved.

Hamiltonian systems are among the most common models in physics. Examples within the context of nonlinear partial differential equations are the Nonlinear Schrödinger (NLS), Korteweg-de Vries equation (KdV) and the Sine-Gordon equation. Such systems are characterized by a skew-

adjoint operator J and the Hamiltonian, $\mathcal{E}$:

$$\frac{\partial z}{\partial t} = J\nabla\mathcal{E}(z) \tag{1.1}$$

where z is the state variable. $\mathcal{E}$ is typically viewed as the energy of the system, since the structure of Hamiltonian systems guarantees that this quantity remains constant in time. To extend to possibly non-Hamiltonian systems, the model is augmented by adding a small perturbation, P, to the equation. Soliton solutions can often be found in these systems and the general question of soliton stability has been characterized in the celebrated works [Gri87; Gri90]. In what follows, the existence of a stable soliton solution is assumed.

The core principle is that the complicated dynamics of the perturbed system can be projected onto a lower dimensional space, similar to the strategy employed in a truncated Galerkin discretization. Much information can be gleaned form simply projecting onto a family of functions which contains most of the key features of the target solution as has been done recently for modifications of the NLS equation in [CS14]. However, greater physical insight can be gained into perturbed, soliton-supporting equations by projecting onto the soliton solution manifold. The dynamics of the perturbed problem reduce to the dynamics of a few parameters with specific physical meaning. In this way the solitons are thus ascribed particle like qualities, and the reduced-order system can be viewed as analogous to Newton's laws in a field theoretic context.

One standard approach is to consider the conserved quantities of the $P = 0$ model. This idea is immediately sensible since the existence of soliton solutions is intimately connected with the existence of symmetries of an equation (and via Noether's theorem with the existence of conserved quantities). When $P \neq 0$ these quantities will no longer be conserved, but balance laws can be derived relating the change in time of these quantities to the perturbation (See Appendix C for an example). Evaluating along the soliton manifold, the dynamics of these conserved quantities can be mapped to the dynamics of the soliton parameters. Such approaches have been used in

many applications, e.g. for NLS and optics [KS95; Abl09]. The main obstacle here is that often many conserved quantities are unknown and ad hoc approaches of balance laws must be employed to determine equations for all the parameters. Systematic approaches can be taken to determining these conserved quantities, but such strategies require full knowledge of the underlying symmetries of an equation which may be difficult to determine.

In Chapter 2, a singular perturbation theory approach, previously applied to NLS in [Wei85], is generalized to a broad class of Hamiltonian systems. The main advantage of this approach is that no knowledge of the conserved quantities or symmetries of the system are needed, only knowledge of the parameters. This is in contrast to more ad hoc approaches involving conserved quantities [KS95]. The main obstacle is the need to characterize the generalized null space of a linear operator, which in general is a difficult problem. With the addition of a physically motivated assumption, however, enough elements from the generalized null space can be obtained to close the modulation equations even in this very abstract setting. Thus the aim is to recover a practical method to describe perturbed soliton dynamics in general systems, much like the stability criterion of Grillakis, Shatah and Strauss, [Gri87; Gri90]. Note that these equations only govern the leading order dynamics, but do not give the next order correction and neglect coupling to dispersive radiation. In most physical contexts understanding the modification of the soliton is sufficient, but finding these corrections could be done in principle.

Using the general machinery developed for Hamiltonian systems, Chapters 3 and 4 derive and utilize the modulation equations for a range of perturbations of physical interest. These examples include the effect of field gradients, damping and forcing. The combination of these different perturbations are sufficient to make qualitative comparison to the recent experimental work of [Moh13; Mac14] and offer possible insight into the usefulness of droplets in nanoscale magnetic devices. Finally, Chapter 5 discusses numerical approaches to computing solitons for the perturbed models without appealing to asymptotic theory.

1.1 Mathematical Model

1.1.1 Torque Equation

The mathematical model considered here is the following torque equation for the vector field magnetization **M**

$$\begin{aligned} \frac{\partial \mathbf{M}}{\partial t} &= -\left|\gamma\right| \mu_0 \mathbf{M} \times \mathbf{H}_{\text{eff}} + \mathbf{P}, \\ \mathbf{H}_{\text{eff}} &= \frac{2A}{\mu_0 M_{\text{s}}^2} \nabla^2 \mathbf{M} + \left(H_0 + \frac{2K_{\text{u}}}{\mu_0 M_{\text{s}}^2} M_z \right) \mathbf{z} + \mathbf{H}_{\text{m}}. \end{aligned} \tag{1.2}$$

The ferromagnetic material is taken to be of infinite extent in the x-y directions and of finite thickness δ in z. The parameters are the gyromagnetic ratio γ, the permeability of free space μ_0, the exchange stiffness parameter A, the perpendicular magnetic field amplitude H_0, the crystalline anisotropy constant K_{u}, and the saturation magnetization M_{s}. **P** represents any perturbation that maintains the magnetization's total length, i.e. $\mathbf{P} \cdot \mathbf{M} \equiv 0$. The structure of Eq. 1.2 immediately guarantees that $\frac{\partial |\mathbf{M}|}{\partial t} = 0$. The Landau-Lifshitz equation refers specifically to a model which includes a specific form of damping. The torque equation becomes the Landau-Lifshitz equation when $\mathbf{P} = \alpha \mathbf{M} \times (\mathbf{M} \times H_{\text{eff}})$ where α, the damping parameter, is typically small but nonzero. Note that this choice of **P** satisfies the constraint that $\mathbf{P} \cdot \mathbf{M} = 0$.

The boundary conditions are $\lim_{x^2+y^2 \to \infty} \mathbf{M} = M_{\text{s}} \mathbf{z}$ and $\partial \mathbf{M} / \partial z = 0$ when $z = \pm \delta / 2$. $\mathbf{H}_{\text{m}}$ is the magnetostatic field resulting from Maxwell's equations. That is, $\mathbf{H}_{\text{m}}$ satisfies $\nabla \times \mathbf{H}_{\text{m}}$ and can be written in terms of a potential $\mathbf{H}_{\text{m}} = -\nabla U$. Additionally in the ferromagnetic layer, $\nabla \cdot \mathbf{H}_{\text{m}} = -\nabla \cdot \mathbf{M}$.

In terms of the potential U this requirement becomes

$$\nabla^2 U = \begin{cases} \nabla \cdot \mathbf{M} & |z| < \frac{\delta}{2} \\ 0 & |z| > \frac{\delta}{2} \end{cases} \tag{1.3}$$

$$\left.\frac{\partial U}{\partial z}\right|_{z=\pm\frac{\delta}{2}} = \mp m_z(x, y, \pm\frac{\delta}{2}) \tag{1.4}$$

Altogether, H_{eff} represents a net effective magnetic field, due to the combined effects of magnetic exchange, applied field, anisotropy and the long range effects of the magnetostatic field. By assuming a uniform in z magnetization distribution, the two-dimensional (2D), film thickness averaged magnetostatic field can be greatly simplified. As derived in [GC04a], the magnetostatic energy for a z independent magnetization can be given in Fourier space as

$$\begin{aligned} \mathcal{E}_{\text{m}} = \frac{\delta}{2} \int_{\mathbb{R}^2} \Bigg\{ & \frac{|\mathbf{k} \cdot \widehat{\mathbf{M}}_\perp|^2}{k^2} [1 - \widehat{\Gamma}(k\delta)] \\ & + |\widehat{M_z - M_{\text{s}}}|^2 \widehat{\Gamma}(k\delta) \Bigg\} \, \mathrm{d}\mathbf{k}, \end{aligned} \tag{1.5}$$

where

$$\widehat{\Gamma}(\kappa) = \frac{1 - e^{-\kappa}}{\kappa}. \tag{1.6}$$

Computing the negative variational derivative of $\mathcal{E}_{\text{m}}$ with respect to $\mathbf{M}$ and expanding $\widehat{\Gamma}(k\delta)$ for $|k\delta| \ll 1$ gives the result

$$\begin{aligned} \mathbf{H}_{\text{m}} &\sim -M_z \mathbf{z} + \frac{\delta}{2} \mathbf{H}_{\text{nl}}, \\ \mathbf{H}_{\text{nl}} &= \mathbf{z} \sqrt{-\nabla^2} (M_z - M_{\text{s}}) + \frac{1}{\sqrt{-\nabla^2}} \nabla (\nabla \cdot \mathbf{M}_\perp), \end{aligned} \tag{1.7}$$

where $\mathbf{M}_\perp = (M_x, M_y)$, δ is assumed to be small relative to the typical transverse wavelength of excitation, i.e., the exchange length, and the operators are interpreted in Fourier space, e.g., $\widehat{\sqrt{-\nabla^2} f} = |\mathbf{k}| \widehat{f}$ and $\widehat{f}(\mathbf{k})$ is the two-dimensional Fourier transform of f at wavevector $\mathbf{k}$. We will absorb the

nonlocal magnetostatic correction $-\delta\mathbf{M}\times\mathbf{H}_{\rm nl}/2$ into the small perturbation $\mathbf{P}$.

Nonlocal magnetostatic corrections have also been used to study domain patterns and vortices in materials with easy-plane anisotropy [GCE01]. Further simplification can be obtained using the magnetic exchange length $l_{\rm ex}=\sqrt{2A/(\mu M_{\rm s}^2)}$ and the dimensionless quality factor $Q=2K_{\rm u}/(\mu_0 M_{\rm s}^2)$, assumed to be greater than unity to guarantee the existence of droplet solutions in the unperturbed ($\mathbf{P}=0$, $\delta=0$) problem [Kos90]. Nondimensionalizing time by $[\left|\gamma\right|\mu_0 M_{\rm s}(Q-1)]^{-1}$, lengths by $l_{\rm ex}/\sqrt{Q-1}$, fields by $M_{\rm s}(Q-1)$, and setting $\mathbf{m}=\mathbf{M}/M_{\rm s}$, eq. (1.2) becomes the 2D model

$$\begin{aligned}\frac{\partial\mathbf{m}}{\partial t}&=-\mathbf{m}\times\left(\nabla^2\mathbf{m}+(m_z+h_0)\mathbf{z}\right)+\mathbf{p},\\ \mathbf{p}&=\frac{\mathbf{P}}{|\gamma|\mu_0 M_{\rm s}^2(Q-1)}-\frac{\delta}{2}\mathbf{m}\times\mathbf{h}_{\rm nl},\quad (x,y)\in\mathbb{R}^2.\end{aligned}\tag{1.8}$$

While the presentation of the torque equation in vectorial form (Eq. (1.8)) is natural, it is not always the most convenient form to work in. Since $\mathbf{m}(\mathbf{x},t)\in S^2$ for all $\mathbf{x}$, t, one can use different parameterizations of the sphere to give different expressions for the range space of $\mathbf{m}$. In this way the constraint that $|\mathbf{m}|=1$ is encoded in the equations. Two natural choices are used extensively in this work: 1) classical spherical coordinates and 2) stereographic projection of the coordinates.

To make the transformation to spherical variables, set $\mathbf{m}=[\sin(\Theta)\cos(\Phi),\sin(\Theta)\sin(\Phi),\cos(\Theta)]$ (See Figure 1.2). Substituting into Eq. (1.8) and solving for $\frac{\partial\Theta}{\partial t}$ and $\frac{\partial\Phi}{\partial t}$, yields

$$\frac{\partial\Theta}{\partial t}=F[\Theta,\Phi]+P_\Theta\tag{1.9}$$

$$\sin(\Theta)\frac{\partial\Phi}{\partial t}=G[\Theta,\Phi]-h_0\sin(\Theta)+P_\Phi\tag{1.10}$$

where

$$F[\Theta,\Phi] = \frac{\nabla\cdot\left(\sin^2(\Theta)\nabla\Phi\right)}{\sin(\Theta)} \tag{1.11}$$

$$G[\Theta,\Phi] = \frac{1}{2}\sin(2\Theta)\left(|\nabla\Phi|^2+1\right) - \nabla^2\Theta \tag{1.12}$$

and $P_\Theta = \mathbf{p}\cdot\mathbf{e}_\Theta$, $P_\Phi = \mathbf{p}\cdot\mathbf{e}_\Phi$ where $\mathbf{e}_\Theta, \mathbf{e}_\Phi$ are the canonical polar and azimuthal basis vectors. The primary advantage of this coordinate system stems from its relationship to the Hamiltonian variables for the torque equation: $\cos(\Theta), \Phi$ [HS12]. As a result, many analytical computations are greatly simplified by working in these variables.

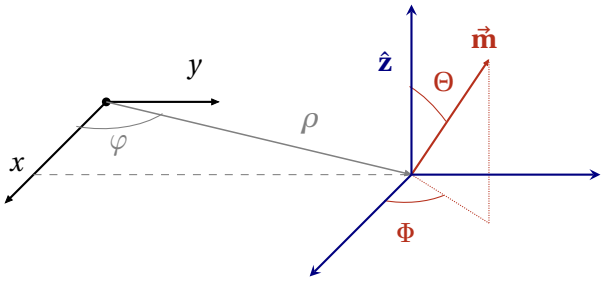

Figure 1.2 A representation of the relationship between the polar variables (Θ,Φ) parameterizing the magnetization (range-space), which differs from a polar representation of the plane (ρ,φ) for the domain.

The stereographic projection motivates the change of variables $w = \frac{m_x+im_y}{1+m_z}$ (See Figure 1.3). There is a singularity of this transformation as $m_z \to -1$, but this transformation remains useful for the droplet as this case corresponds to full reversal of the magnetization which is excluded from consideration. Differentiating this expression for w with respect to t, substituting into Eq. (1.8) and simplifying yields the equation

$$i\frac{\partial w}{\partial t} = \nabla^2 w - \frac{2w^*\nabla w\cdot\nabla w + w(1-w^*w)}{1+w^*w} - h_0 w + P_w \tag{1.13}$$

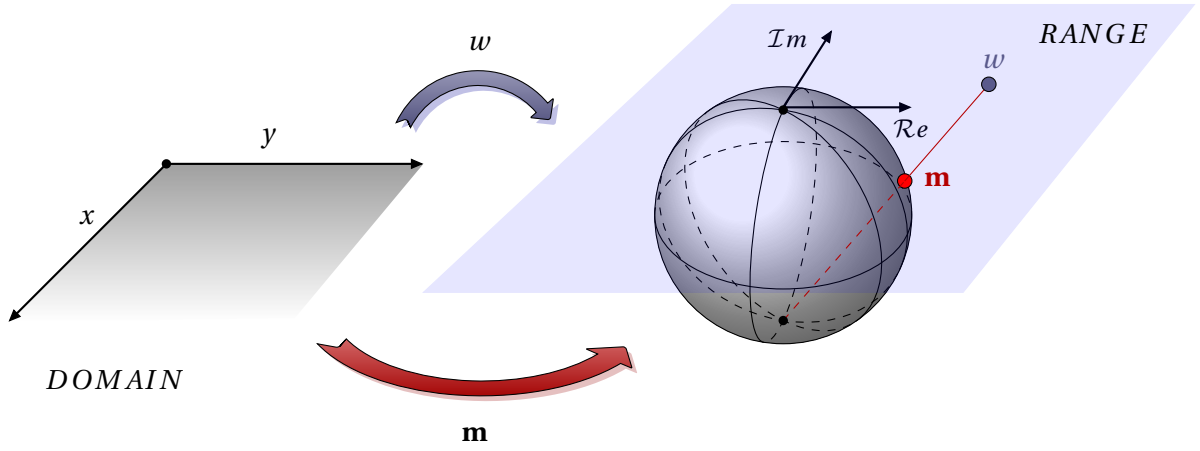

Figure 1.3 An illustration of the relationship between w and $\mathbf{m}$ via the stereographic projection. While both sets have the same domain $\mathbb{R}^2$, w takes on a value in the complex plane such that $\mathbf{m} \in S^2$, w and the south pole are collinear. This introduces a singularity as $\mathbf{m}$ approaches pointing straight down. This projection is reverse of the more common stereographic projection from the northern pole, but is convenient here as the droplet never fully reverses.

where z^* denotes the complex conjugate of z and

$$P_w = \frac{1}{2}\left[i p_x \left(1+|w|^2\right) - p_y \left(1-|w|^2\right) - i p_z w \left(1+|w|^2\right)\right] \tag{1.14}$$

and p_x, p_y, p_z are defined by $\mathbf{p} = [p_x, p_y, p_z]$. Eq. (1.13) is frequently more convenient for numerical calculations since it reformulates the torque system as a single equation for a complex-valued function. Furthermore, in the weakling nonlinear regime Eq. (1.13) reduces to the Nonlinear Schrödinger equation. However, the nonlinear gradient terms offer significant complexity to the equation. The similarity to NLS makes the droplet analogous to the Townes mode, with the important distinction that the droplet is a stable structure. Throughout this thesis, all three presentations of the Landau-Lifshitz equation will be extensively used.

In the case that $\mathbf{p} = 0$, the torque equation admits several conserved quantities which will be used throughout this work. The total energy (also the Hamiltonian for this system) is given by

$$\mathcal{E}[\mathbf{m}] = \frac{1}{2}\int_{\mathbb{R}^2} \left(\|D\mathbf{m}\|_F^2 + (1-m_z^2) + h_0(1-m_z) \right) d\mathbf{x} \tag{1.15}$$

where $D\mathbf{m}$ denotes the usual matrix derivative of $\mathbf{m}$ and $\|\cdot\|_F$ denotes the Frobenius norm of a matrix. Equivalently, in spherical variables the energy is given by

$$\mathcal{E}[\Theta,\Phi] = \frac{1}{2}\int_{\mathbb{R}^2} \left[|\nabla\Theta|^2 + \sin^2(\Theta)\left(1+|\nabla\Phi|^2\right) + h_0(1-\cos(\Theta)\right] d\mathbf{x} \tag{1.16}$$

or

$$\mathcal{E}[w] = 2\int_{\mathbb{R}^2} \frac{\nabla w^* \cdot \nabla w + w^* w}{(1+w^* w)^2} + \frac{h_0 w^* w}{1+w^* w} d\mathbf{x} \tag{1.17}$$

in stereographic variables. The total spin, given by

$$\mathcal{N}[\mathbf{m}] = \int_{\mathbb{R}^2} (1-m_z) d\mathbf{x}, \tag{1.18}$$

$$\mathcal{N}[\Theta,\Phi] = \int_{\mathbb{R}^2} (1-\cos(\Theta)) d\mathbf{x}, \tag{1.19}$$

or

$$\mathcal{N}[w] = 2\int_{\mathbb{R}^2} \frac{w^* w}{1+w^* w} d\mathbf{x}, \tag{1.20}$$

is also conserved. The total momentum,

$$\mathcal{P}[m] = \int_{\mathbb{R}^2} \left(\frac{m_y \nabla m_x - m_x \nabla m_y}{1+m_z} \right) d\mathbf{x}, \tag{1.21}$$

$$\mathcal{P}[\Theta,\Phi] = -\int_{\mathbb{R}^2} (1-\cos(\Theta)) \nabla\Phi d\mathbf{x}, \tag{1.22}$$

or

$$\mathcal{P}[w] = -2\int_{\mathbb{R}^2} \left(\frac{\mathcal{I}m(w^* \nabla w)}{1+w^* w} \right) d\mathbf{x}, \tag{1.23}$$

is the final conserved quantity that this thesis uses extensively. Via Noether's theorem, each of these

conserved quantities corresponds to a symmetry of the equation. For instance, the momentum is generated by translation invariance of the torque equation. There are additional conserved quantities corresponding to other symmetries of the equation (e.g. rotational invariance of the domain or range leading to angular momentum)[PT91]. Solitons are often formulated as energy minimizing solutions subject to specific constraints (see [RW88; Siv08] for examples of this procedure applied to NLS). Similarly, the droplet can be viewed as energy minimizing solution subject to the constraints that the momentum and total spin are fixed values. This formulation relates the three conserved quantities with soliton parameters (ω and $\mathbf{V}$) arising as Lagrange multipliers in the optimization problem. This relationship means that these three quantities are not independent for the droplet, which has implications for deriving the modulation equations using the perturbed conservation law approach.

1.1.2 Droplet Solitons

In order to study the droplet, some approximate representation of this soliton, particularly capturing its dependence on the soliton parameters is required. This could be performed numerically with a "database" of droplet solutions as in [HS12]. This section derives an approximate solution to eq. (1.8) when $\mathbf{p} = 0$, a restriction maintained for the remainder of this section. The solution describes a slowly moving droplet with frequency just above the Zeeman frequency. A droplet soliton can be characterized by six parameters: its precession frequency ω above the Zeeman frequency h_0 in these non-dimensional units, propagation velocity $\mathbf{V} = [V_x, V_y]$, initial phase Φ_0, and the coordinates of the droplet center $\boldsymbol{\xi} = [\xi_x, \xi_y] = \mathbf{V}t + \mathbf{x}_0$ (see Fig. 1.4).

Previously, approximate droplet solutions have been found in two regimes: (i) frequencies, velocities near the linear (spin-wave) band edge corresponding to propagating, weakly nonlinear droplets approximated by the NLS Townes soliton $0 < 1 - w - \frac{V^2}{4} \ll 1$ [Iva01] (ii) $0 < \omega \ll 1$ with zero velocity corresponding to stationary, strongly nonlinear droplets approximated by a circular domain wall [Kos86; IS89]. The focus here is on large amplitude propagating solitons where the

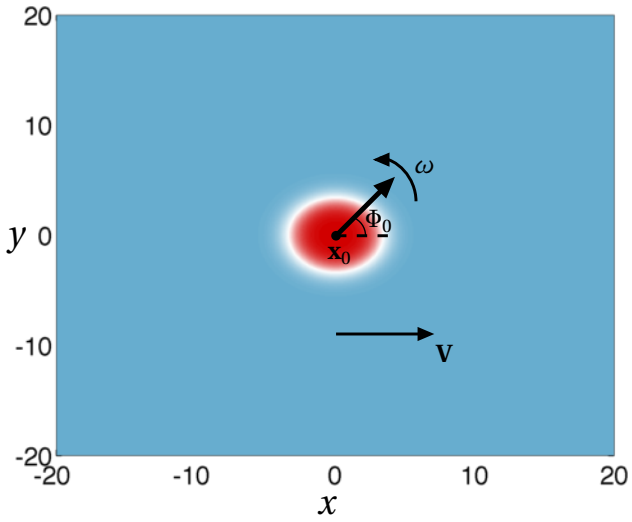

Figure 1.4 Illustration of the droplet parameters. The vector in the middle represents the in-plane component of the magnetization at the center of the droplet.

magnetization is nearly reversed because experiments operate in this regime. Note, however, that the weakly nonlinear regime could also be studied. The defining equation for the droplet can be formulated as a boundary value problem by expressing the magnetization in spherical variables in the frame moving and precessing with the soliton $\Theta \to \Theta(\mathbf{x}-\xi)$, $\Phi \to \Phi_0 + (h_0+\omega)t + \Phi(\mathbf{x}-\xi)$:

$$\begin{cases} -\sin(\Theta)\mathbf{V}\cdot\nabla\Theta = \nabla\cdot\left(\sin^2\Theta\nabla\Phi\right) & (1.24) \\ \sin(\Theta)(\omega-\mathbf{V}\cdot\nabla\Phi) = -\nabla^2\Theta + \dfrac{1}{2}\sin(2\Theta)(1+|\nabla\Phi|^2) & (1.25) \\ \lim\limits_{|\mathbf{x}|\to\infty}\nabla\Phi = -\dfrac{\mathbf{V}}{2}, \quad \lim\limits_{|\mathbf{x}|\to\infty}\Theta = 0. & (1.26) \end{cases}$$

This problem can be further simplified by exploiting the invariance of Eq. (1.8) under rotation of the domain to align the x-axis with the propagation direction. In this coordinate system, $\mathbf{V} = V\mathbf{x}$. Adding the assumptions of small frequency and propagation speed, a simple correction to the known, approximate stationary droplet can be found.

1.1.3 Approximate Stationary Droplet

For the sake of completeness, what follows is a detailed derivation of the small ω approximation for the stationary droplet. First, take as an ansatz

$$\Theta = \Theta_0(\rho) + \omega\Theta_1(\rho,\varphi) + \dots \quad \text{and} \quad \Phi = \text{ a constant }. \tag{1.27}$$

Above, (ρ,φ) are polar variables for the plane, whose origin is centered on the droplet. That is $\rho = \sqrt{(x-\xi_x)^2+(y-\xi_y)^2}$ and $\varphi = \arctan\left(\frac{y-\xi_y}{x-\xi_x}\right)$ (see Fig. 1.2) .

The ansatz in Eq. (1.27) trivially satisfies Eq. (1.24) when $\mathbf{V}=0$. Substituting into Eq. (1.25) yields

$$\begin{cases} -\left(\dfrac{d^2}{d\rho^2}+\dfrac{1}{\rho}\dfrac{d}{d\rho}\right)\Theta_0 + \sin\Theta_0\cos\Theta_0 - \omega\sin\Theta_0 = 0 \\ \dfrac{d\Theta_0}{d\rho}(0;\omega) = 0, \qquad\qquad \lim\limits_{\rho\to\infty}\Theta_0(\rho;\omega) = 0. \end{cases} \tag{1.28}$$

The goal is a uniformly valid approximate solution to this problem in the limit that $0 < \omega \ll 1$. Motivated by the 1D domain wall solution [LL35], begin by introducing a shifted coordinate system $\rho = R + \frac{A}{\omega}$, where A is some constant which will be determined by solvability conditions. In this coordinate, (1.28) becomes

$$-\left(\frac{d^2}{dR^2}+\frac{1}{\left(R+\frac{A}{\omega}\right)}\frac{d}{dR}\right)\Theta_0 + \sin\Theta_0\cos\Theta_0 - \omega\sin\Theta_0 = 0 \tag{1.29}$$

Expanding (1.29) and keeping terms only to first order in ω,

$$-\frac{d^2\Theta_0}{dR^2} + \sin\Theta_0\cos\Theta_0 + \omega\left(-\frac{1}{A}\frac{d\Theta_0}{dR} - \sin\Theta_0\right) = \mathcal{O}\left(\omega^2\right). \tag{1.30}$$

Inserting the asymptotic expansion $\Theta_0 = \Theta_{0,0} + \omega\Theta_{0,1} + \mathcal{O}\left(\omega^2\right)$ into (1.30) and matching terms at

leading order

$$\mathcal{O}(1): \qquad -\frac{d^2\Theta_{0,0}}{dR^2} + \sin\Theta_{0,0}\cos\Theta_{0,0} = 0 \tag{1.31}$$

$$\mathcal{O}(\omega): \qquad -\frac{d^2\Theta_{0,1}}{dR^2} + \cos(2\Theta_{0,0})\Theta_{0,1} = \frac{1}{A}\frac{d\Theta_{0,0}}{dR} + \sin\Theta_{0,0} \tag{1.32}$$

It is readily verified that the solution to (1.31) is $\Theta_{0,0} = \cos^{-1}(\tanh(R+R_0))$ where R_0 is some arbitrary constant. This is the Landau-Lifshitz domain wall solution [LL35]. For simplicity, choose $R_0 = 0$ since it is not restricted unless seeking a higher order solution. Taking $L = -\partial_{RR} + \cos(2\Theta_{0,0})$, equation (1.32) is of the form $L\psi = f$. In this case, L is a Schrödinger operator and hence self-adjoint with kernel spanned by $\operatorname{sech}(R)$. Solvability then requires that

$$\frac{1}{A}\frac{d\Theta_{0,0}}{dR} + \sin\Theta_{0,0} = \left(1 - \frac{1}{A}\right)\operatorname{sech}(R)$$

is orthogonal to the kernel of $L = L^\dagger$. Thus $\left(1-\frac{1}{A}\right)\operatorname{sech}(R)$ will be a nontrivial element of the kernel of L unless $A \equiv 1$. Further, this choice of A means the equation at $\mathcal{O}(\omega)$ is trivially satisfied. Substituting back to the ρ coordinate system, the leading order solution

$$\Theta_0 = \cos^{-1}\left(\tanh\left(\rho - \frac{1}{\omega}\right)\right) + \mathcal{O}\left(\omega^2\right). \tag{1.33}$$

is obtained, which agrees with previous derivations [Kos90; BH13].

This solution is expected to be valid in the regime that R is $\mathcal{O}(1)$, that is ρ is on the same order as $\frac{1}{\omega}$. By examining the residual of eq. (1.29) with the approximate solution (1.33), this solution can be seen to be valid for all ρ. Substituting this approximate solution into (1.28), the residual is $(1-\rho\omega)\operatorname{sech}(\rho - \frac{1}{\omega})/\rho$. For all ρ, as $\omega \to 0$, the residual is no larger than $\mathcal{O}\left(\omega^2\right)$ and the solution is uniformly valid.

Matching the approximate solution (1.33) for $\rho \ll 1$ using regular perturbation theory demonstrates that $\Theta_0(0) = \pi$ *to all orders* in ω. Therefore, the approximate droplet is exponentially close to

being fully reversed at its core.

1.1.4 Approximate Propagating Droplet

The derivation of the approximate *moving* droplet is significantly simplified by exploiting the invariance of Eqs. (1.24)-(1.25) under rotation of the domain and working in the frame where $V_y = 0$ and $|\mathbf{V}| = |V_x| = V$. The derivation proceeds as before by substituting the ansatz

$$\Theta = \Theta_0(\rho) + V\Theta_1(\rho,\varphi) + \mathcal{O}\left(V^2\right) \text{ and } \Phi = \Phi_0 + V\Phi_1(\rho,\varphi) + \mathcal{O}\left(V^2\right) \tag{1.34}$$

into Eqs. (1.24)-(1.25). At order $\mathcal{O}(1)$, this yields one nontrivial equation: precisely Eq (1.28). From here on out, it is further assumed that $0 < \omega \ll 1$. While it is assumed that V is small, the relative ordering of ω and V will be determined during the derivation to guarantee validity of the approximation. At order $\mathcal{O}(V)$,

$$\sin(\Theta_0)\Delta\Phi_1 + \left(\cos(\varphi) + 2\cos(\Theta_0)\frac{\partial\Phi_1}{\partial\rho}\right)\frac{d\Theta_0}{d\rho} = 0, \tag{1.35}$$

$$\Delta\Theta_1 + (\omega\cos(\Theta_0) - \cos(2\Theta_0))\Theta_1 = 0. \tag{1.36}$$

Equation (1.36) is solved by $\Theta_1 = 0$. Substituting the approximate solution for Θ_0 into Eq. (1.35)

$$\left(\Delta\Phi_1 - \cos(\varphi) - 2\tanh\left(\rho - \frac{1}{\omega}\right)\frac{\partial\Phi_1}{\partial\rho}\right)\operatorname{sech}\left(\rho - \frac{1}{\omega}\right) = 0 \tag{1.37}$$

The residual in Eq. (1.37) is determined by two considerations. If $1 \ll \left|\rho \sim \frac{1}{\omega}\right|$, $\operatorname{sech}\left(\rho - \frac{1}{\omega}\right)$ dominates and the residual is exponentially small. In the other case, i.e. $\rho \sim \frac{1}{\omega}$, the residual will only be small if $\Delta\Phi_1 - \cos(\varphi) - 2\tanh\left(\rho - \frac{1}{\omega}\right)\frac{\partial\Phi_1}{\partial\rho}$ is small since $\operatorname{sech}\left(\rho - \frac{1}{\omega}\right)$ is $\mathcal{O}(1)$. This suggests that the boundary condition, $\lim_{\rho\to\infty}\nabla\Phi_1 = -\frac{1}{2}\hat{x}$, may be neglected. It is possible to treat the boundary condition at infinity; however, this requires multiple boundary layers and complicated matched asymptotics. These calculations significantly complicate the form of the final solution and only contribute to

second-order corrections. While these calculations could improve the overall error bounds, for the purposes of this thesis, it is sufficient to capture only the leading order behavior. Assuming Φ_1 is separable of the form $\Phi_1(\rho,\varphi) = f(\rho)\cos(\varphi)$, Eq. (1.37) simplifies to the ordinary differential equation

$$\frac{d^2 f}{d\rho^2} + \left(\frac{1}{\rho} - 2\tanh\left(\rho - \frac{1}{\omega}\right)\right)\frac{df}{d\rho} - \frac{1}{\rho^2} f = 1. \tag{1.38}$$

Numerical solutions of Eq. (1.38) demonstrate that f becomes quite large, approximately $\mathcal{O}\left(\frac{1}{\omega^2}\right)$ near $\rho = \frac{1}{\omega}$. Factoring this into the analysis, changing to the coordinate system $R = \rho - \frac{1}{\omega}$ and expanding f in the series

$$f(\rho) = \frac{f_0(\rho)}{\omega^2} + \frac{f_1(\rho)}{\omega} + f_2(\rho) + \cdots. \tag{1.39}$$

We define the linear operator $L = \frac{d^2}{dR^2} - 2\tanh(R)\frac{d}{dR}$. Substituting the ansatz in Eq. (1.39) into Eq. (1.38) yields,

$$\mathcal{O}\left(\frac{1}{\omega^2}\right): \qquad Lf_0 = 0 \tag{1.40}$$

$$\mathcal{O}\left(\frac{1}{\omega}\right): \qquad Lf_1 = -\frac{df_0}{dR} \tag{1.41}$$

$$\mathcal{O}(1): \qquad Lf_2 = -\frac{df_1}{dR} + 1 + f_0 + R\frac{df_0}{dR} \tag{1.42}$$

Eq. (1.40) admits any constant solution. Take $f_0 = A$. Substituting this expression for f_0 into Eq. (1.41), yields $Lf_1 = 0$. Thus, any constant solution is admissible for f_1 as well. Take $f_1 = B$. Substituting these expressions for f_0 and f_1 into Eq. (1.42), yields $Lf_2 = 1 + A$. $L^\dagger = \frac{d^2}{dR^2} + 2\tanh(R)\frac{d}{dR} + \operatorname{sech}(R)$. $L^\dagger g = 0$ is solved by $g = \operatorname{sech}(R)$. Hence solvability of $Lf_2 = 1 + A$ requires that $\int_{-\infty}^{\infty} \operatorname{sech}(R)(1 + A)dR = 0$ which implies that $A = -1$. Similarly, solvability at $\mathcal{O}(\omega)$ requires $B = 0$. This process can be continued indefinitely, but further higher order corrections will not improve global accuracy unless the boundary condition at infinity is included requiring more complex matched asymptotic methods. Hence, it is sufficient to take $f(\rho) = -\frac{1}{\omega^2} + \mathcal{O}\left(\frac{1}{\omega}\right), \omega \to 0$, which gives rise to the form of

the approximate droplet

$$\Theta = \cos^{-1}\left(\tanh\left(\rho - \frac{1}{\omega}\right)\right) + \mathcal{O}\left(\omega^2, V^2\right) \tag{1.43}$$

$$\Phi = \Phi_0 + (h_0 + \omega)t - \frac{V}{\omega^2}\cos(\varphi) + \mathcal{O}\left(\frac{V}{\omega}\right). \tag{1.44}$$

The error estimates provided here are supported by numerical investigations solving Eqs. (1.28) and (1.38) for Θ_0 and f respectively (see Fig: 1.5)

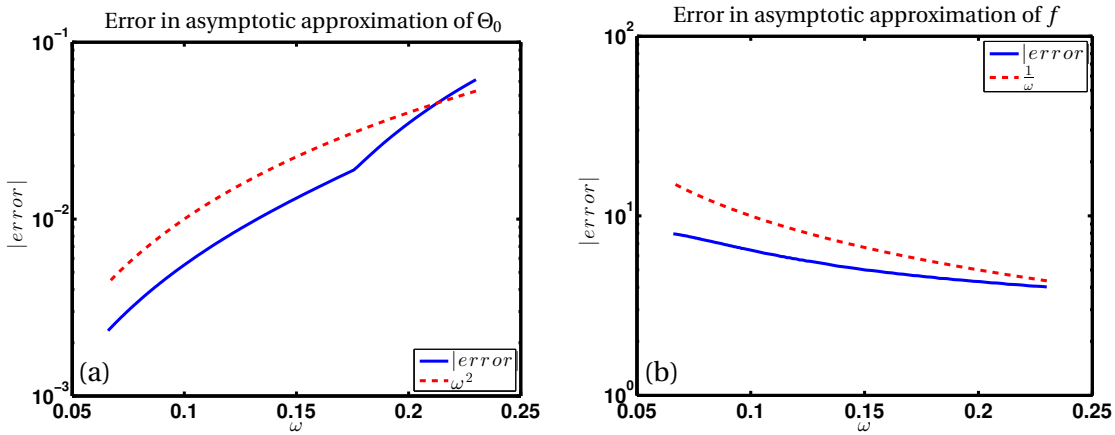

Figure 1.5 (a) Comparison between the numerical solution to Eq. (1.28). The dashed line shows good agreement between the computed error and the theoretical error bound $\mathcal{O}\left(\omega^2\right)$. (b) Comparison between the numerical solution to Eq. (1.38) for f. The dashed line shows good agreement between the computed error and the theoretical error bound $\mathcal{O}\left(\frac{1}{\omega}\right)$, owing to the neglected boundary conditions.

This approximation is valid so long as

$$0 \leq |V| \ll \omega, \quad 0 < \omega \ll 1. \tag{1.45}$$

As for the stationary case, the propagating droplet can be viewed as a precessing, circular domain wall with a radius that is the inverse of the frequency. The new term $-V\cos(\varphi)/\omega^2$ reveals the deviation of the propagating droplet's phase from spatial uniformity. While the relations in (1.45)

may, at first, seem overly restrictive, as demonstrated in Chapter 3 and Chapter 4, important and practical information about propagating droplets can be obtained in this regime. This approximate solution offers both an error estimate and is amenable to further analysis in the context of the perturbed Landau-Lifshitz equation (1.8). Furthermore, it provides a significant improvement over the approximate droplets used in past numerical experiments [PZ98], when the asymptotic relations (1.45) hold.

1.1.5 Approximate Droplet as a Particle-like Dipole

Utilizing the approximate form (1.43), (1.44) for the droplet, a map can be constructed between its parameters and the conserved quantities. Evaluating the integrals in Eqs. (1.15) - (1.23) at the approximate droplet,

$$\mathcal{N} = \frac{2\pi}{\omega^2}, \tag{1.46}$$

$$\mathcal{P} = \frac{2\pi}{\omega^3}\mathbf{V} \tag{1.47}$$

$$\mathcal{E} = \frac{\pi}{\omega^3}\left(|\mathbf{V}|^2 + 4\omega^2 + h_0\omega\right). \tag{1.48}$$

where higher order terms in ω and $|\mathbf{V}|$ have been neglected. These formulae extend the predictions for stationary droplets, see, e.g., [Kos90], and offer an analogy to classical particle dynamics. Rewriting $\mathcal{E}$ in terms of the other conserved quantities,

$$\mathcal{E} = \sqrt{2\pi}\left(\frac{1}{2}\frac{|\mathcal{P}|^2}{\mathcal{N}^{\frac{3}{2}}} + \mathcal{N}^{\frac{1}{2}}\right) + \frac{1}{2}h_0\mathcal{N}. \tag{1.49}$$

By analogy to classical systems, $\sqrt{2\pi}|\mathcal{P}|^2/2\mathcal{N}^{\frac{3}{2}}$ can interpreted as the kinetic energy of the droplet, $\sqrt{2\pi}\mathcal{N}^{\frac{1}{2}}$ as the droplet's potential energy due to precession, and $h_0\mathcal{N}/2$ as the Zeeman energy of the droplet with the net dipole moment $\mathcal{N}$. Inspection of the kinetic energy term shows

that

$$m_{\text{eff}} = \frac{\mathcal{N}^{3/2}}{\sqrt{2\pi}} = \frac{2\pi}{\omega^3} \tag{1.50}$$

serves as the effective mass for the droplet. Therefore, the $0 < \omega \ll 1$ regime corresponds to droplets with large mass. This is a natural interpretation since it is the precession of the droplet which determines its size and prevents the structure from collapsing in on itself. On the other hand, eq. (1.47) implies that the slowly propagating $|\mathbf{V}| \ll \omega$ regime supports droplets with up to $|\mathcal{P}| = \mathcal{O}\left(\frac{1}{\omega}\right)$ momenta. This observation of an effective mass for the droplet will be revisited in Chapter 3,where dynamical equations induced by spatial inhomogeneity in the external magnetic field are derived.

One description of the magnetic droplet is as a bound state of magnons [Kos90]. It is then natural to interpret the potential energy $\sqrt{2\pi}\mathcal{N}^{\frac{1}{2}}$ as the energy released by decay into these constituent "subatomic particles". The expressions (1.46) and (1.47) can also be utilized to verify the Vakhitov-Kolokolov stability criteria [VK73; Gri90] for a propagating droplet (see [HS12]), namely that $\mathcal{N}_\omega < 0$ and $\mathcal{N}_\omega \nabla_V \cdot \mathcal{P} - \nabla_V \mathcal{N} \cdot \mathcal{P}_\omega < 0$.

For the remainder of this work, the approximate droplet in eqs. (1.43), (1.44) will be used whenever an analytical solution is appropriate.

CHAPTER

2

MODULATION THEORY FOR HAMILTONIAN SYSTEMS

This chapter develops an algorithmic approach to soliton perturbation theory for Hamiltonian systems. The technique of soliton perturbation theory has been extensively used in the nonlinear waves community to investigate the behavior of solitary waves in nearly-integrable systems [KM89]. The approach developed in this chapter does not appeal to the underlying integrability of the system, but instead allows for numerical or asymptotic approximations to be used in lieu of an exact solution. While integrability is not required, an assumption is placed on the soliton parameters relating these parameters in a particular way. This statement will be made more precise later in this chapter. The main result of this analysis is Eq. 2.4, which determines the slow time dynamics of the parameters of the soliton. The equations determining the time-evolution of parameters will be referred to as modulation equations. Of course, while this procedure greatly simplifies the derivation of modulation equations, certain knowledge of the base system (e.g. the parameters being allowed to vary) is still required. In practice, however, knowledge of the parameters of the soliton is often easier

to obtain, than knowledge of the conserved quantities [KS95]. Eq. 2.4 reduces to the result of Keener and McLaughlin [KM77b] for perturbations of multi-soliton solutions in (1+1)D, but this derivation makes no assumption on the dimension of the system and provides an alternative approach to their derivation.

In terms of the primary application of this thesis, this analysis is valuable because the Landau-Lifshitz equation is a Hamiltonian system, with canonically conjugate variables $\cos(\Theta)$, Φ. That is, the Landau-Lifshitz system may be written as $\frac{\partial \cos\Theta}{\partial t} = \frac{\delta \mathcal{E}}{\delta \Phi}$ and $\frac{\partial \Phi}{\partial t} = -\frac{\delta \mathcal{E}}{\delta \cos\Theta}$, where the right hand sides are expressed in terms of variational derivatives of the energy $\mathcal{E}$, defined in eq. (1.16). Section 2.4 applies this procedure step by step to derive the modulation equations pertinent for the droplet. For a comparison of the advantages of this approach, a direct approach of calculating the modulation equations for the Landau-Lifshitz equation, without overtly appealing to the Hamiltonian structure is provided in Appendix B.2. The calculation in Appendix B.2 is quite long and involved, but implicitly relies on the Hamiltonian structure. Many of the steps taken in Appendix B.2 are simply long form execution of the ideas of this section. The key advantage to observe between the direct approach and the approach presented here is that a great deal of tedious algebra can be avoided. To demonstrate both the restrictions and generality of the assumptions imposed by this approach, other Hamiltonian systems are discussed in Section 2.2

2.1 General Setup for Hamiltonian Systems

The basic procedure is to allow the parameters to vary on a time scale proportional to the strength of of the perturbation, ϵ. By allowing the parameters to vary in this way, additional degrees of freedom are introduced which can be used to resolve the difficulties arising from singular perturbations. Expanding about the soliton solution in an asymptotic series, one obtains a linear problem at order ϵ. In general, this linear equation will not admit solutions bounded in time. However, as utilized by Weinstein [Wei85], by enforcing orthogonality to the generalized kernel of a linear operator, bounded solutions are assured, guaranteeing that the linear problem at order ϵ does not break the asymptotic

ordering. Imposing these conditions leads to the modulation equations. This procedure is equivalent to projecting the solution of the perturbed model onto the family of solitons, neglecting coupling to small-amplitude dispersive waves. While one might wish to then solve the linear equation at order ϵ to obtain a further correction, this will not be done in this work. As will be demonstrated by the examples in later chapters, quite satisfactory predictions can be made by considering only the leading order dynamics.

A Hamiltonian system requires a real inner product space, X; a functional, $H : X \to \mathbb{R}$; and a skew adjoint operator $J : X \to X$. The notation $\langle \cdot, \cdot \rangle$ denotes the inner product on X. The standard form for a Hamiltonian system is

$$\frac{\partial z}{\partial t} = J\nabla H(z) \tag{2.1}$$

where $z \in X$ is referred to as the state variable. H represents the Hamiltonian, which is often assigned the physical meaning of energy since it is automatically a conserved quantity of such a system. In this context, ∇H means the first variation of this nonlinear function and ΔH refers to the second variation (both taken with respect to the state variable, z). Hamiltonians considered here may depend explicitly upon additional parameters, $\mathbf{q} \in \mathbb{R}^m$ (m is the number of such parameters). Such parameters may arise due to underlying symmetries and a change of coordinates, such as to a comoving reference frame. For the examples which arise in this work, the parameters $\mathbf{q}$ arise from just such a transformation, so this thesis will typically refer to these parameters as “frequencies".

In order to perform perturbation theory, there must exist a base state to perturb around. Therefore it is necessary to assume that Eq. (2.1) admits a solitary wave solution, u.

$$0 = J\nabla H(u, \mathbf{q}). \tag{2.2}$$

If H depends on $\mathbf{q}$, naturally u will depend on $\mathbf{q}$ as well. Typically, the parameters $\mathbf{q}$ do not provide a full parameterization of the solitary wave manifold due to underlying symmetries in the equation such as translation invariance. Accordingly, u may depend on a separate set of parameters $\mathbf{r} \in \mathbb{R}^s$

(s is the number of such parameters). For reasons that will become clear in later examples we refer to these parameters as "phases". Owing to the relationship between frequencies and phases, typically $s = m$; however, the analysis which follows is possible provided $s \geq m$. To express this dependence on these two classes of parameters, the solitary wave will be written $u = u(\mathbf{x}; \mathbf{q}, \mathbf{r})$. There is a formal way to recognize a relationship between q_i and r_i due to the existence of symmetries [CS07]. Symmetry group methods, for example, applied to rotational invariance imply that if q_i is a frequency, then r_i is a phase and the soliton, u, depends on them according to the independent variable $\eta = q_i t + r_i$. Often times, the Hamiltonian system (2.1) admitting solitary wave solutions (2.2) is idealized, neglecting important physical effects. While some such effects may give rise to a different Hamiltonian system, in general such effects do not preserve the Hamiltonian structure. This analysis treats both cases the same by introducing a small perturbation into the equation itself.

The perturbed model is

$$\frac{\partial z}{\partial t} = J\nabla H(z, \mathbf{q}) + \epsilon P \tag{2.3}$$

where $0 < \epsilon \ll 1$ and P is a perturbation. The parameters $\mathbf{q}, \mathbf{r}$ are allowed to vary on a slow time scale, $T = \epsilon t$. In order to apply the solvability condition presented in Section 2.1.1, perturbations will be restricted to depend explicitly on time only through this slow time variable, T. In this case, ordinary differential equations governing the evolution of these parameters can be determined according to the following theorem.

Theorem 2.1.1. *Given the perturbed Hamiltonian system* (2.3). *If*

1. *The solitary wave solution, u, exists for the unperturbed system* (2.3), $\epsilon = 0$, *and is independent of t.*
2. *J has a bounded inverse.*
3. $\Delta H\Big|_{z=u}$ *is self-adjoint for all admissible* $\mathbf{q}$.
4. $\forall\, 1 \leq k \leq m, \exists\, 1 \leq j \leq s$ *such that* $\frac{\partial}{\partial q_k}\nabla H(z, \mathbf{q})\Big|_{z=u} \in \operatorname{span}\left\{J^{-1}\frac{\partial u}{\partial r_j}\right\}$

then letting $\mathbf{v} = [\mathbf{r}, \mathbf{q}]^T \in \mathbb{R}^{s+m}$, *the modulation equations are*

$$\left(\sum_{i=1}^{s+m} \left\langle J^{-1} \frac{\partial u}{\partial v_i}, \frac{\partial u}{\partial v_j} \right\rangle \frac{dv_i}{dT} \right) = \left\langle J^{-1} P, \frac{\partial u}{\partial v_j} \right\rangle \tag{2.4}$$

Equation 2.4 is consistent with previous general results when applied to Hamiltonian systems [KM77b]. The assumptions of Theorem 2.1.1 may seem restrictive at first, but these conditions are frequently met in physical systems of interest. In all systems under consideration here there does exist a solitary wave solution. These solutions generically depend on time, but for the case of a single solitary wave solution, transforming to the reference frame moving, rotating, and/or precessing with the solitary wave can eliminate this explicit dependence on time. Such a transformation will introduce parameters in $\mathbf{q}$ and alter the Hamiltonian but leaves the Hamiltonian structure intact.

The second does offer a restriction. For instance, in the Korteweg-de-Vries equation, J does not admit a bounded inverse and correspondingly the modulation equations require additional considerations [AS81]. Nevertheless, formal calculations are possible and J is frequently invertible for Hamiltonian systems (as it is, e.g., for NLS and the Landau-Lifshitz equation).

With appropriate restrictions on the Hamiltonian, the third assumption always holds. The self-adjoint property of the second variation essentially follows from the same calculation which proves the equality of mixed partial derivatives in finite-dimensional calculus. More care needs to be taken in the corresponding calculation on function spaces, but the Hamiltonians derived in physically relevant systems typically are well enough behaved.

The fourth assumption is restrictive and may seem obscure. However, the parameters of the soliton are often speeds or frequencies. These parameters are typically linked to initial positions or initial phase values so that $\mathbf{q}$ and $\mathbf{r}$ have the same length ($s = m$). In such cases, the dependence of the soliton on the parameters in the laboratory frame will be in the form $\mathbf{r} + t\,\mathbf{q}$. From this temporal dependence, the relations in Assumption (iv) follow directly. As noted earlier, this parametric dependence, $\mathbf{r} + t\,\mathbf{q}$, can follow from symmetry considerations [CS07].

2.1.1 Solvability Condition

Theorem 2.1.1 relies on the lemma proved in Section 2.1.1, which provides a suitable solvability condition.

Lemma 2.1.2. *Let X be a Hilbert space. Let A be a bounded linear operator mapping X to itself. Let $f \in X$. Let $A^\dagger$ be the adjoint of A, i.e. the unique linear operator satisfying $\langle A^\dagger x, y\rangle = \langle x, Ay\rangle$ for all $x, y \in X$. Define $\Upsilon : [0,\infty) \to X$ as the solution of the initial value problem*

$$\begin{cases} \frac{\partial \Upsilon}{\partial t} = A\Upsilon + f \\ \Upsilon(0) = \Upsilon_0 \in X. \end{cases} \tag{2.5}$$

Let $\mu_{-1} = 0$ and $A^\dagger \mu_i = \mu_{i-1}$ for $0 \le i \le N$, where N denotes the highest integer such that $(A^\dagger)^N$ has nontrivial kernel. Then $\Upsilon(t)$ will not be bounded in time unless $\langle \mu_{i-1}, \Upsilon_0\rangle + \langle \mu_i, f\rangle = 0$ for $0 \le i \le N$.

This lemma is a minor generalization of the solvability condition proven in [Wei85].

Proof. Consider the change of variables given by $\psi = \Upsilon - \Upsilon_0$. Equation (2.5) becomes

$$\begin{cases} \frac{\partial \psi}{\partial t} = A\psi + A\Upsilon_0 + f \\ \psi(0) = 0 \end{cases} \tag{2.6}$$

Note, since A is time-independent its (generalized) null vectors, μ_i will be time-independent as well. Consider $i = 1$. By definition $A^\dagger \mu_0 = \mu_{-1} = 0$, hence $\mu_0 \in \ker\left(A^\dagger\right)$. Projecting (2.6) onto μ_0

$$\begin{aligned} \left\langle \mu_0, \frac{\partial \psi}{\partial t} \right\rangle &= \langle \mu_0, A\psi + A\Upsilon_0 + f\rangle \\ &= \langle A^\dagger \mu_0, \psi\rangle + \langle A^\dagger \mu_0, \Upsilon_0\rangle + \langle \mu_0, f\rangle \\ \frac{\partial}{\partial t}\langle \mu_0, \psi\rangle &= \langle \mu_0, f\rangle \end{aligned}$$

Solving this ordinary differential equation yields $\langle \mu_0, \psi \rangle = \langle \mu_0, f \rangle t + \langle \mu_0, \psi(0) \rangle$. Since $\psi(0) = 0$, $\langle \mu_0, \psi(0) \rangle = 0$ as well. It follows that either the mode $\langle \mu_0, \psi \rangle$ grows linearly in time or is 0 for all time. Since $\mu_{-1} = 0$, imposing the condition that $\langle \mu_{-1}, \Upsilon_0 \rangle + \langle \mu_0, f \rangle = 0$ is equivalent to the condition that $\langle \mu_0, f \rangle = 0$.

Next assume that for some value i, $\langle \mu_i, \psi \rangle = 0$ for all time. Projecting (2.6) onto μ_{i+1}

$$\begin{aligned}
\left\langle \mu_{i+1}, \frac{\partial \psi}{\partial t} \right\rangle &= \langle \mu_{i+1}, A\psi + A\Upsilon_0 + f \rangle \\
&= \langle A^\dagger \mu_{i+1}, \psi \rangle + \langle A^\dagger \mu_{i+1}, \Upsilon_0 \rangle + \langle \mu_{i+1}, f \rangle \\
\frac{\partial}{\partial t} \langle \mu_{i+1}, \psi \rangle &= \langle \mu_i, \psi \rangle + \langle \mu_i, \Upsilon_0 \rangle + \langle \mu_{i+1}, f \rangle \\
\frac{\partial}{\partial t} \langle \mu_{i+1}, \psi \rangle &= \langle \mu_i, \Upsilon_0 \rangle + \langle \mu_{i+1}, f \rangle
\end{aligned}$$

As for $i = 0$, the solution the mode $\langle \mu_{i+1}, \psi \rangle$ will grow linearly in time if $\langle \mu_i, \Upsilon_0 \rangle + \langle \mu_{i+1}, f \rangle \neq 0$ or be 0 for all time. Inductively, the lemma follows. □

There are a few key limitations which may not be clear upon first reading the statement of the lemma itself. First, A and f are assumed to be independent of time. Second, all assumptions of smoothness of the function space are bound up in the choice of X which is problem specific. In the context of Hamiltonian systems, X is given and the required smoothness of f is clear. In our intended application, Eq. (2.5) arises from a linearization of a nonlinear problem about a given state. Here, A is an unbounded operator. The rigorous generalization of this lemma to an unbounded operator could be done in principle [Wei85]. In this case, A and f are given, but not X. In order that Lemma 2.1.2 apply, there must exist an X which makes A and f compatible, and it will be in that sense which $\Upsilon(t)$ remains bounded in time. If a given linearization gives rise to $A\psi = \frac{\partial^2 \psi}{\partial x^2}$, then Lemma 2.1.2 would require f be at least twice differentiable in order for there to be a natural choice of the underlying Hilbert space. From here on out, sufficient smoothness in the perturbation that such a Hilbert space is naturally chosen will be assumed. For the perturbations investigated in

Chapter 3 and Chapter 4 this is the case.

2.1.2 Derivation of Equation (2.4)

The proof of Theorem 2.1.1 proceeds by substituting the ansatz

$$z = u(\mathbf{x};\mathbf{r}(T),\mathbf{q}(T)) + \epsilon\, u_1(\mathbf{x},t,T) + \mathcal{O}\left(\epsilon^2\right) \tag{2.7}$$

into (2.3). Expanding in powers of ϵ, the first order equation becomes

$$\mathcal{O}(\epsilon): \qquad \frac{\partial u_1}{\partial t} = J\Delta H(u,\mathbf{q})u_1 - \frac{\partial u}{\partial \mathbf{r}}\frac{d\mathbf{r}}{dT} - \frac{\partial u}{\partial \mathbf{q}}\frac{d\mathbf{q}}{dT} + P \tag{2.8}$$

Note that Eq. (2.8) is of the form in Lemma 2.1.2, allowing for unbounded operators ($A = J\Delta H(u,\mathbf{q})$, $f = P - \frac{\partial u}{\partial \mathbf{r}}\frac{d\mathbf{r}}{dT} - \frac{\partial u}{\partial \mathbf{q}}\frac{d\mathbf{q}}{dT}$). In order that the expansion in (2.7) remain asymptotically ordered, it is necessary that $u_1(x,t,T)$ remain $\mathcal{O}(1)$ for sufficiently long times. Lemma 2.1.2 thus gives a condition that must be satisfied. It remains to characterize the generalized nullspace of $(J\Delta H(u,\mathbf{q}))^\dagger$. Note that since $\Delta H(u,\mathbf{q})$ is self-adjoint, $(J\Delta H(u,\mathbf{q}))^\dagger = -\Delta H(u,\mathbf{q})J$.

Differentiating (2.2) with respect to the parameter r_j for $1 \le j \le s$ and applying J^{-1} to the result yields $\Delta H(u,\mathbf{q})\frac{\partial u}{\partial r_j} = 0$. It follows that $J^{-1}\frac{\partial u}{\partial r_j}$ is in the kernel of $(J\Delta H(u,\mathbf{q}))^\dagger$ for all j. Differentiating (2.2) with respect to the parameter q_k for $1 \le k \le m$ yields

$$\Delta H(u,\mathbf{q})\frac{\partial u}{\partial q_k} + \frac{\partial}{\partial q_k}\nabla H(z,\mathbf{q})\Big|_{z=u} = 0. \tag{2.9}$$

Utilizing assumption (iv), $\nabla H(z,\mathbf{q})\Big|_{z=u} = \beta J^{-1}\frac{\partial u}{\partial r_j}$ for some scalar β and some j. Now, the second term in (2.9) may be replaced to obtain

$$\Delta H(u,\mathbf{q})J\left(J^{-1}\frac{\partial u}{\partial q_k}\right) = -\beta J^{-1}\frac{\partial u}{\partial r_j}. \tag{2.10}$$

Hence, $J^{-1}\frac{\partial u}{\partial q_k} \in \ker(\Delta H(u,\mathbf{q})J)^2$ and therefore in the generalized nullspace. These two sets of vectors do not necessarily fully characterize the generalized nullspace; however, these offer a sufficient number of constraints to uniquely determine the modulation system. Requiring that $f = P - \frac{\partial u}{\partial \mathbf{r}}\frac{d\mathbf{r}}{dT} - \frac{\partial u}{\partial \mathbf{q}}\frac{d\mathbf{q}}{dT}$ be orthogonal to $J^{-1}\frac{\partial u}{\partial q_k}$ and $J^{-1}\frac{\partial u}{\partial r_j}$ yields equations (2.4). The modes $J^{-1}\frac{\partial u}{\partial q_k}$ and $J^{-1}\frac{\partial u}{\partial r_j}$ may not give rise to a complete characterization of the nullspace. As a result, Eqs. (2.4) are only a necessary but not sufficient condition to prevent secular growth. This concludes the proof of Theorem 2.1.1.

2.2 Application to NLS

To better explain the results of the preceding section, this section presents how this theory works to obtain the modulation equations for the Nonlinear Schrödinger equation,

$$i\frac{\partial \psi}{\partial t} + \frac{\partial^2 \psi}{\partial x^2} + 2\left|\psi\right|^2\psi = 0 \tag{2.11}$$

To begin, the assumptions of Theorem 2.1.1 must be verified. Since ψ is complex, it may seem a contradiction that a real Hilbert space is assumed. However, the Hilbert space in question is real, since the relevant inner product is $\langle \Upsilon, \Gamma\rangle = \frac{1}{2}\int_{-\infty}^{\infty}(\Upsilon^*\Gamma + \Upsilon\Gamma^*)dx$. This is only an inner product if the field of scalars is take to be real, which can be readily verified by checking the linearity condition for inner products. The first assumption is that there is a solitary wave solution. A standard presentation of a single, bright soliton solution for NLS is given by [Abl09],

$$\psi(x,t) = \eta e^{i\left(t\left(\alpha^2+\eta^2\right)+\alpha(-2\alpha t+x-x_0)+\phi_0\right)}\operatorname{sech}\left(\eta(-2\alpha t + x - x_0)\right) \tag{2.12}$$

In this presentation, the soliton parameters are η, the amplitude; x_0, an initial position; ϕ_0, an initial phase and α, half the soliton speed. However, the soliton is not independent of time in these variables and a change of coordinates is necessary for Theorem 2.1.1 to apply. For notational

simplicity, the parameters $V = 2\alpha$, the soliton velocity and $\omega = \alpha^2 + \eta^2$ a precession frequency will be used. Note that in these variables, the time dependence of the soliton is related to the parameters by the quantities $x_0 + V t$ and $\omega t + \phi_0$. This motivates the change of coordinates $x \to \xi + V t$ and $\psi \to e^{-i\omega t}\chi(\xi, t)$. Under this transformation, Eq. (2.11) becomes

$$i\frac{\partial \chi}{\partial t} + \frac{\partial^2 \chi}{\partial \xi^2} + 2\left|\chi\right|^2 \chi - \omega\chi - iV\frac{\partial \chi}{\partial \xi} = 0 \tag{2.13}$$

and the solution of Eq. (2.11) given in Eq. (2.12) maps to the time independent function

$$\chi_s(\xi) = \frac{1}{2}\sqrt{4\omega - V^2}\, e^{i\left(\frac{1}{2}V(\xi - x_0) + \phi_0\right)} \operatorname{sech}\left(\frac{1}{2}\sqrt{4\omega - V^2}(\xi - x_0)\right) \tag{2.14}$$

Eq. 2.13 is still a Hamiltonian system, with Hamiltonian

$$H(\chi, \omega, V) = \int_{\mathbb{R}} \left(-\left|\frac{d\chi}{d\xi}\right|^2 + \left|\chi\right|^4 - \omega\left|\chi\right|^2 + V\,\mathcal{I}m\left(\chi^*\frac{d\chi}{d\xi}\right)\right) d\xi \tag{2.15}$$

where $\mathcal{I}m(\cdot)$ denotes the imaginary part of the argument. Note that the Hamiltonian explicitly depends on the soliton parameters, ω and V. In the general terminology used in the previous section, $\mathbf{q} = [\omega, V]$. Note that the soliton in Eq. (2.14) additionally depends on the parameters ϕ_0 and x_0 (i.e. $\mathbf{r} = [\phi_0, x_0]$ using the previous notation). Computing the variational derivative of $H(\chi, \omega, V)$ yields

$$\nabla H(\chi, \omega, V) = \frac{\partial^2 \chi}{\partial x^2} - iV\frac{\partial \chi}{\partial x} + (2\left|\chi\right|^2 - \omega)\chi \tag{2.16}$$

and Eq. (2.13) can be rewritten as

$$\frac{\partial \chi}{\partial t} = i\nabla H(\chi, \omega, V) \tag{2.17}$$

By inspection of Eq. (2.17), the skew adjoint linear operator J for this system is multiplication by the imaginary unit i. It remains to verify the assumptions of Theorem 2.1.1. Eq. 2.13 admits a soliton

solution independent of time and it is to this system that Theorem 2.1.1 will be applied. Since multiplication by i is invertible, J^{-1} exists and the second assumption is satisfied. The second variation of H,

$$\nabla^2 H(\chi,\omega,V)[\Upsilon] = \frac{\partial^2\Upsilon}{\partial x^2} - iV\frac{\partial\Upsilon}{\partial x} + (4|\chi|^2 - \omega)\Upsilon + 2\chi^2\Upsilon^* \tag{2.18}$$

is self-adjoint, independent of the choice of ω and V, which can be verified by a straightforward calculation. The final assumption holds by direct computation. For example,

$$\frac{\partial}{\partial V}\nabla H(\chi)\bigg|_{\chi=\chi_s} = -i\frac{\partial\chi_s}{\partial\xi} = i\frac{\partial\chi}{\partial x_0} = -(-i)^{-1}\frac{\partial\chi}{\partial x_0} = -J^{-1}\frac{\partial\chi}{\partial x_0}. \tag{2.19}$$

therefore $\frac{\partial}{\partial V}\nabla H(\chi)\Big|_{\chi=\chi_s} \in \operatorname{span}\left\{J^{-1}\frac{\partial\chi}{\partial x_0}\right\}$. A similar calculation can be done verifying the relationship between $\frac{\partial}{\partial\omega}\nabla H(\chi)$ and $\frac{\partial\chi}{\partial\phi_0}$, and assumption 4 holds. Introducing a perturbation P to equation (2.13) and applying the result of the previous section, the modulation equations are

$$\begin{pmatrix} 0 & 0 & \frac{1}{2\eta} & -\frac{V}{4\eta} \\ 0 & 0 & 0 & -\frac{\eta}{2} \\ -\frac{1}{2\eta} & 0 & 0 & -\frac{x_0}{4\eta} \\ \frac{V}{4\eta} & \frac{\eta}{2} & \frac{x_0}{4\eta} & 0 \end{pmatrix}\begin{pmatrix} \frac{d\phi_0}{dT} \\ \frac{dx_0}{dT} \\ \frac{d\omega}{dT} \\ \frac{dV}{dT} \end{pmatrix} = \begin{pmatrix} \frac{i}{2}\int_{-\infty}^{\infty}\left(P*\frac{d\psi}{d\phi_0} - P\frac{d\psi}{d\phi_0}^*\right)d\xi \\ \frac{i}{2}\int_{-\infty}^{\infty}\left(P^*\frac{d\psi}{dx_0} - P\frac{d\psi}{dx_0}^*+\right)d\xi \\ \frac{i}{2}\int_{-\infty}^{\infty}\left(P^*\frac{d\psi}{d\omega} - P\frac{d\psi}{d\omega}^*\right)d\xi \\ \frac{i}{2}\int_{-\infty}^{\infty}\left(P^*\frac{d\psi}{dV} - P\frac{d\psi}{dV}^*\right)d\xi \end{pmatrix} \tag{2.20}$$

This result is consistent with references [KS95], [Abl09] under the appropriate change of variables.

2.3 Non-Application to KdV

The famous Korteweg-de Vries (KdV) equation is another Hamiltonian system where adiabatic perturbation theory has been extensively applied [KM77a; Cal78; KM89]. However, in the context

of a dissipative perturbation the modulation equations are known to break down as a shelf forms trailing the soliton [KN78]. Essentially, this means that in the presence of a dissipative perturbation, the resulting solution no longer stays close to the soliton manifold. This manifests as a coupling of higher order effects into the modulation equation governing the phase of the soliton [AS81]. The theorem derived in Section 2.1 does not apply to KdV. Nevertheless, it is instructive to consider the ways in which the theorem fails for KdV and what insight can still be obtained.

To begin, KdV must be expressed in Hamiltonian form. This can be accomplished in multiple ways [Olv84], but for the current purposes the simplest form is

$$H(u) = \int_{-\infty}^{\infty} \left[-u(x)^3 + \frac{1}{2}\left(\frac{\partial u}{\partial x}\right)^2 \right] dx \tag{2.21}$$

with the skew symmetric operator $J = \frac{\partial}{\partial x}$. This yields the standard form of KdV $u_t = J[\nabla H(u)] = -6u\frac{\partial u}{\partial x} - \frac{\partial^3 u}{\partial x^3}$. An expression for the 1-soliton solution to KdV is given by

$$u = \frac{1}{2} c \operatorname{sech}^2\left(\frac{\sqrt{c}}{2}(x - c\,t - a)\right) \tag{2.22}$$

where the soliton parameters are the speed, c and the initial position, a. Boosting to the comoving frame the Hamiltonian becomes, $H[u,c] = \int_{-\infty}^{\infty} \left[-u(x)^3 + \frac{1}{2}\left(\frac{\partial u}{\partial x}\right)^2 - \frac{c}{2}u^2 \right] dx$ and assumptions 1,3 and 4 of Theorem 2.1.1 are all readily verified. However, J is does not have a bounded inverse. The derivation of Eq. 2.4 relies extensively on symbolic manipulation of J^{-1} which is no longer well-defined and these calculations may no longer hold. However, for data decaying smoothly to zero as $x \to -\infty$, $J^+[f] = \int_{-\infty}^{x} f(\xi) d\xi$ satisfies many of the properties one might wish for an inverse. Namely $J[J^+[f]] = J^+[J[f]] = f$. However, this does not mean that J^+ is a sufficient surrogate for J^{-1} for the analysis of the proceeding section to go through. It is immediate that $\ker(J) \subseteq \ker(\nabla^2 H J)$. Therefore whenever the kernel of J is nontrivial, there are additional modes which must be accounted for which were not treated in Section 2.1. The most troubling property that J^+ lacks is that there is no guarantee that $J^+ f \in L^2(\mathbb{R})$ if $f \in L^2(\mathbb{R})$. As a result, the inner products in Eq. 2.4 cease to make sense

and this is what ultimately goes wrong attempting to apply Theorem 2.1.1 substituting J^+ for J^{-1}.

While the calculation in Section 2.1, primarily used the properties of inverse that J^+ has, an additional property was invoked in the calculation: if J is skew-adjoint and J^{-1} exists, J^{-1} is skew adjoint[1]. In addition to simplifying calculations in steps, this property has consequences for the modulation system in Eq. 2.4. The modulation system as presented is in the form of a matrix-vector product. That the matrix multiplying the time derivatives of the soliton parameters is anti-symmetric follows directly from the fact that J^{-1} is skew-adjoint. J^+ is not skew-adjoint, and this structure is lost. To see that J^+ is not skew-adjoint, consider $\langle J^+ f, g\rangle = \int_{-\infty}^{\infty}\left[\left(\int_{-\infty}^{\xi} f(\zeta)d\zeta\right)g(\xi)\right]d\xi$. Integrating by parts, $\langle J^+ f, g\rangle = \left(\int_{-\infty}^{\infty} f(\zeta)d\zeta\right)\left(\int_{-\infty}^{\infty} g(\zeta)d\zeta\right) - \langle f, J^+ g\rangle$. Generically for smooth data in $L^2(\mathbb{R})$, these boundary terms will not vanish.

Nevertheless, substituting J^+ for J^{-1} and formally proceeding with analysis for KdV, the following system is obtained

$$\begin{pmatrix} 0 & -\frac{\sqrt{c}}{2} \\ \frac{\sqrt{c}}{2} & \frac{1}{2c} \end{pmatrix}\begin{pmatrix} \frac{da}{dT} \\ \\ \frac{dc}{dT} \end{pmatrix} = \begin{pmatrix} -\frac{1}{2}c\int_{-\infty}^{\infty}\left[P\,\mathrm{sech}^2\left(\frac{1}{2}\sqrt{c}(x-a)\right)\right]dx \\ \\ \int_{-\infty}^{\infty}\left[P\left(\frac{\frac{e^{\sqrt{c}(x-a)}+1}{\sqrt{c}}-a+x}{2\left(\cosh\left(\sqrt{c}(a-x)\right)+1\right)}\right)\right]dx \end{pmatrix} \tag{2.23}$$

where P stands for an arbitrary perturbation to KdV. Evidently, the matrix multiplying the time derivatives of the parameters is not anti-symmetric, a visible consequence of the lack of a bounded inverse. For the dissipative perturbation, $P = -\gamma u$, considered in [AS81], the integral $\int_{-\infty}^{\infty}\left[P\left(\frac{\frac{e^{\sqrt{c}(x-a)}+1}{\sqrt{c}}-a+x}{2\left(\cosh\left(\sqrt{c}(a-x)\right)+1\right)}\right)\right]dx$ does not converge, which is a consequence of the fact that $J^+\left[\frac{\partial u}{\partial c}\right] \notin L^2(\mathbb{R})$. However, the system decouples and $\frac{dc}{dT}$ can be expressed exclusively in terms of the convergent integral. The resulting modulation equation for $\frac{dc}{dt}$ is equivalent to expressions found in [AS81]. That $\frac{da}{dt}$ cannot be resolved utilizing this method is consistent with the drastically different methods that have been utilized to derive the modulation equation for a in other work.

[1] $JJ^{-1} = I, \Rightarrow (JJ^{-1})^\dagger = I, \Rightarrow (J^{-1})^\dagger J^\dagger = I, \Rightarrow -(J^{-1})^\dagger J = I, \Rightarrow (J^{-1})^\dagger = -J^{-1}$

2.4 Application to Landau-Lifshitz

Now that a general framework has been established, the modulation equations for the Landau-Lifshitz equation may be readily derived. As is carefully verified in Appendix B.1, the Hamiltonian variables for the Landau-Lifshitz equation are $(\cos(\Theta), \Phi)$. For notational simplicity, take $u = \cos(\Theta)$ for the remainder of this section. In these variables, the Landau-Lifshitz equation becomes the system

$$\begin{aligned} \frac{\partial u}{\partial t} &= -\nabla \cdot \left((1-u^2) \nabla \Phi \right) \\ \frac{\partial \Phi}{\partial t} &= \frac{\nabla^2 u}{1-u^2} + \frac{u\,|\nabla u|^2}{(1-u^2)^2} + u(1+|\nabla \Phi|^2) \end{aligned} \tag{2.24}$$

The next step in the analysis is to boost to the co-moving reference frame via the transformation $u(\mathbf{x}, t) \to u(\mathbf{x} - \mathbf{V}t, t)$, $\Phi(\mathbf{x}, t) \to \omega t + \Phi(\mathbf{x} - \mathbf{V}t, t)$ and obtain

$$\begin{aligned} \frac{\partial u}{\partial t} &= -\nabla \cdot \left((1-u^2) \nabla \Phi \right) + \mathbf{V} \cdot \nabla u \\ \frac{\partial \Phi}{\partial t} &= \frac{\nabla^2 u}{1-u^2} + \frac{u\,|\nabla u|^2}{(1-u^2)^2} + u(1+|\nabla \Phi|^2) + \mathbf{V} \cdot \nabla \Phi - \omega \end{aligned} \tag{2.25}$$

The Hamiltonian in the comoving variables, is given by

$$H(u, \Phi, \omega, \mathbf{V}) = \frac{1}{2} \int_{\mathbb{R}^2} \left[\frac{|\nabla u|^2}{1-u^2} + (1-u^2)(1+|\nabla \Phi|^2) + \mathbf{V} \cdot (-u \nabla \Phi + \nabla u \Phi) + 2\omega u \right] d\mathbf{x} \tag{2.26}$$

and the corresponding skew-adjoint operator is $J = \begin{pmatrix} 0 & 1 \\ -1 & 0 \end{pmatrix}$.

Now that the Hamiltonian structure is established, it remains to verify the assumptions of Theorem 2.1.1. The condition of soliton existence is assumed. The specific form is provided by the approximate droplet derived in Chapter 1. That J is invertible is an elementary calculation. Verifying that $\nabla^2 H(u, \Phi, \omega, \mathbf{V})$ is self adjoint requires a somewhat involved if straightforward calculation and is done in Appendix B.1. What remains is the fourth condition. Taking the derivative of ∇H with

respect to ω yields

$$\partial_\omega \nabla H(u,\Phi,\omega,\mathbf{V}) = \begin{pmatrix} 0 \\ 1 \end{pmatrix} \tag{2.27}$$

and with respect to the components of $\mathbf{V}$ yields

$$\partial_{V_i} \nabla H(u,\Phi,\omega,\mathbf{V}) = \begin{pmatrix} \frac{\partial u}{\partial x_i} \\ -\frac{\partial \Phi}{\partial x_i} \end{pmatrix} \tag{2.28}$$

To verify the final condition, derivatives of the soliton with respect to its parameters are necessary, but the analytical form for the droplet is unknown. However, it suffices to differentiate the ansatz made to compute the droplet with respect to the parameters (see Section 1.1.2). For clarity, the soliton takes the form

$$u(\mathbf{x}) = u_0(\mathbf{x}-\mathbf{x}_0-\mathbf{V}t) \tag{2.29}$$

$$\Phi(\mathbf{x}) = \Phi_0 + \omega t + \Psi(\mathbf{x}-\mathbf{x}_0-\mathbf{V}t) \tag{2.30}$$

Differentiating Eq. 2.29 with respect to ω, $\frac{\partial u}{\partial \Phi_0} = 0$ and differentiating Eq. 2.29 with respect to ω, $\frac{\partial u}{\partial \Phi_0} = 1$. Hence

$$J^{-1}\frac{\partial}{\partial \Phi_0}\begin{pmatrix} u \\ \Phi \end{pmatrix} = \begin{pmatrix} 0 & -1 \\ 1 & 0 \end{pmatrix}\begin{pmatrix} 0 \\ 1 \end{pmatrix} = \begin{pmatrix} -1 \\ 0 \end{pmatrix} \tag{2.31}$$

and $\partial_\omega \nabla H(u,\Phi,\omega,\mathbf{V}) \in \text{span}\left\{ J^{-1}\frac{\partial}{\partial \Phi_0}\begin{pmatrix} u \\ \Phi \end{pmatrix} \right\}$. Similarly, differentiating Eq. 2.29 with respect to the components of $\mathbf{x}_0$ (i.e $x_{0,i}$), $\frac{\partial u}{\partial x_{0,i}} = -\frac{\partial u}{\partial x_i}$ and differentiating Eq. 2.29 with respect to $x_{0,i}$, $\frac{\partial \Phi}{\partial x_{0,i}} = -\frac{\partial \Phi}{\partial x_i}$. Thus,

$$J^{-1}\frac{\partial}{\partial x_{0,i}}\begin{pmatrix} u \\ \Phi \end{pmatrix} = \begin{pmatrix} 0 & -1 \\ 1 & 0 \end{pmatrix}\begin{pmatrix} -\frac{\partial u}{\partial x_0} \\ -\frac{\partial \Phi}{\partial x_i} \end{pmatrix} = \begin{pmatrix} \frac{\partial \Phi}{\partial x_i} \\ -\frac{\partial u}{\partial x_{0,i}} \end{pmatrix} \tag{2.32}$$

and $\partial_{V_i}\nabla H(u,\Phi,\omega,\mathbf{V}) \in \text{span}\left\{ J^{-1}\frac{\partial}{\partial x_{0,i}}\begin{pmatrix} u \\ \Phi \end{pmatrix}\right\}$.

Now that the assumptions of the Theorem 2.1.1 are verified, the modulation equations may be written down simply by evaluating Eq. (2.4). Formally, this can be expressed as

$$\begin{pmatrix} 0 & 0 & 0 & -\int_{\mathbb{R}^2}\frac{\partial u}{\partial \omega}d\mathbf{x} & -\int_{\mathbb{R}^2}\frac{\partial u}{\partial V_x}d\mathbf{x} & -\int_{\mathbb{R}^2}\frac{\partial u}{\partial V_y}d\mathbf{x} \\ 0 & 0 & 0 & \int_{\mathbb{R}^2}(\frac{\partial \Phi}{\partial x}\frac{\partial u}{\partial \omega}-\frac{\partial \Phi}{\partial \omega}\frac{\partial u}{\partial x})d\mathbf{x} & \int_{\mathbb{R}^2}(\frac{\partial \Phi}{\partial x}\frac{\partial u}{\partial V_x}-\frac{\partial \Phi}{\partial V_x}\frac{\partial u}{\partial x})d\mathbf{x} & \int_{\mathbb{R}^2}(\frac{\partial \Phi}{\partial x}\frac{\partial u}{\partial V_y}-\frac{\partial \Phi}{\partial V_y}\frac{\partial u}{\partial x})d\mathbf{x} \\ 0 & 0 & 0 & \int_{\mathbb{R}^2}(\frac{\partial \Phi}{\partial y}\frac{\partial u}{\partial \omega}-\frac{\partial \Phi}{\partial \omega}\frac{\partial u}{\partial y})d\mathbf{x} & \int_{\mathbb{R}^2}(\frac{\partial \Phi}{\partial y}\frac{\partial u}{\partial V_x}-\frac{\partial \Phi}{\partial V_x}\frac{\partial u}{\partial y})d\mathbf{x} & \int_{\mathbb{R}^2}(\frac{\partial \Phi}{\partial y}\frac{\partial u}{\partial V_y}-\frac{\partial \Phi}{\partial V_y}\frac{\partial u}{\partial y})d\mathbf{x} \\ \int_{\mathbb{R}^2}\frac{\partial u}{\partial \omega}d\mathbf{x} & -\int_{\mathbb{R}^2}(\frac{\partial \Phi}{\partial x}\frac{\partial u}{\partial \omega}-\frac{\partial \Phi}{\partial \omega}\frac{\partial u}{\partial x})d\mathbf{x} & -\int_{\mathbb{R}^2}(\frac{\partial \Phi}{\partial y}\frac{\partial u}{\partial \omega}-\frac{\partial \Phi}{\partial \omega}\frac{\partial u}{\partial y})d\mathbf{x} & 0 & -\int_{\mathbb{R}^2}(\frac{\partial \Phi}{\partial \omega}\frac{\partial u}{\partial V_x}-\frac{\partial u}{\partial \omega}\frac{\partial \Phi}{\partial V_x})d\mathbf{x} & -\int_{\mathbb{R}^2}(\frac{\partial \Phi}{\partial \omega}\frac{\partial u}{\partial V_y}-\frac{\partial u}{\partial \omega}\frac{\partial \Phi}{\partial V_y})d\mathbf{x} \\ \int_{\mathbb{R}^2}\frac{\partial u}{\partial V_x}d\mathbf{x} & -\int_{\mathbb{R}^2}(\frac{\partial \Phi}{\partial x}\frac{\partial u}{\partial V_x}-\frac{\partial \Phi}{\partial V_x}\frac{\partial u}{\partial x})d\mathbf{x} & -\int_{\mathbb{R}^2}(\frac{\partial \Phi}{\partial y}\frac{\partial u}{\partial V_x}-\frac{\partial \Phi}{\partial V_x}\frac{\partial u}{\partial y})d\mathbf{x} & \int_{\mathbb{R}^2}(\frac{\partial \Phi}{\partial \omega}\frac{\partial u}{\partial V_x}-\frac{\partial u}{\partial \omega}\frac{\partial \Phi}{\partial V_x})d\mathbf{x} & 0 & -\int_{\mathbb{R}^2}(\frac{\partial \Phi}{\partial V_x}\frac{\partial u}{\partial V_y}-\frac{\partial u}{\partial V_x}\frac{\partial \Phi}{\partial V_y})d\mathbf{x} \\ \int_{\mathbb{R}^2}\frac{\partial u}{\partial V_y}d\mathbf{x} & -\int_{\mathbb{R}^2}(\frac{\partial \Phi}{\partial x}\frac{\partial u}{\partial V_y}-\frac{\partial \Phi}{\partial V_y}\frac{\partial u}{\partial x})d\mathbf{x} & -\int_{\mathbb{R}^2}(\frac{\partial \Phi}{\partial y}\frac{\partial u}{\partial V_y}-\frac{\partial \Phi}{\partial V_y}\frac{\partial u}{\partial y})d\mathbf{x} & \int_{\mathbb{R}^2}(\frac{\partial \Phi}{\partial \omega}\frac{\partial u}{\partial V_y}-\frac{\partial u}{\partial \omega}\frac{\partial \Phi}{\partial V_y})d\mathbf{x} & \int_{\mathbb{R}^2}(\frac{\partial \Phi}{\partial V_x}\frac{\partial u}{\partial V_y}-\frac{\partial u}{\partial V_x}\frac{\partial \Phi}{\partial V_y})d\mathbf{x} & 0 \end{pmatrix}\begin{pmatrix} \frac{d\Phi_0}{dT} \\ \frac{dx_0}{dT} \\ \frac{dy_0}{dT} \\ \frac{d\omega}{dT} \\ \frac{dV_x}{dT} \\ \frac{dV_y}{dT} \end{pmatrix} = \begin{pmatrix} -\int_{\mathbb{R}^2}P_u d\mathbf{x} \\ \int_{\mathbb{R}^2}(\frac{\partial \Phi}{\partial x}P_u-\frac{\partial u}{\partial x}P_\Phi)d\mathbf{x} \\ \int_{\mathbb{R}^2}(\frac{\partial \Phi}{\partial y}P_u-\frac{\partial u}{\partial y}P_\Phi)d\mathbf{x} \\ -\int_{\mathbb{R}^2}\frac{\partial \Phi}{\partial \omega}P_u-\frac{\partial u}{\partial \omega}P_\Phi d\mathbf{x} \\ -\int_{\mathbb{R}^2}\frac{\partial \Phi}{\partial V_x}P_u-\frac{\partial u}{\partial V_x}P_\Phi d\mathbf{x} \\ -\int_{\mathbb{R}^2}\frac{\partial \Phi}{\partial V_y}P_u-\frac{\partial u}{\partial V_y}P_\Phi d\mathbf{x} \end{pmatrix}. \quad (2.33)$$

above P_u and P_Φ represent perturbations to the Landau-Lifshitz equation in Hamiltonian form.

It is important to note that this representation can be simplified by recasting in block matrix form and recognizing that some of the integrals can be represented in terms of derivatives of the conserved quantities discussed in Section 1.1 (e.g. $\int_{\mathbb{R}^2}\frac{\partial u}{\partial \omega}d\mathbf{x} = -\frac{\partial \mathcal{N}}{\partial \omega}$).

$$\begin{pmatrix} 0 & \mathbf{0} & -\frac{\partial \mathcal{N}}{\partial \omega} & -\left(\frac{\partial \mathcal{N}}{\partial \mathbf{V}}\right)^T \\ \mathbf{0} & \mathbf{0} & \frac{\partial \mathcal{P}}{\partial \omega} & \left(\frac{\partial \mathcal{P}}{\partial \mathbf{V}}\right)^T \\ \frac{\partial \mathcal{N}}{\partial \omega} & -\frac{\partial \mathcal{P}}{\partial \omega} & 0 & -\mathcal{K}^T \\ \frac{\partial \mathcal{N}}{\partial \mathbf{V}} & -\left(\frac{\partial \mathcal{P}}{\partial \mathbf{V}}\right) & \mathcal{K} & \mathcal{W} \end{pmatrix}\begin{pmatrix} \frac{d\Phi_0}{dT} \\ \frac{d\mathbf{x}_0}{dT} \\ \frac{d\omega}{dT} \\ \frac{d\mathbf{V}}{dT} \end{pmatrix} = \begin{pmatrix} -\int_{\mathbb{R}^2}P_u d\mathbf{x} \\ \int_{\mathbb{R}^2}(\frac{\partial \Phi}{\partial \mathbf{x}}P_u-\frac{\partial u}{\partial \mathbf{x}}P_\Phi)d\mathbf{x} \\ -\int_{\mathbb{R}^2}\frac{\partial \Phi}{\partial \omega}P_u-\frac{\partial u}{\partial \omega}P_\Phi d\mathbf{x} \\ -\int_{\mathbb{R}^2}\frac{\partial \Phi}{\partial \mathbf{V}}P_u-\frac{\partial u}{\partial \mathbf{V}}P_\Phi d\mathbf{x} \end{pmatrix} \quad (2.34)$$

with

$$\mathcal{K} = \begin{pmatrix} \int_{\mathbb{R}^2} (\frac{\partial \Phi}{\partial \omega}\frac{\partial u}{\partial V_x} - \frac{\partial \Phi}{\partial V_x}\frac{\partial u}{\partial \omega}) d\mathbf{x} \\ \int_{\mathbb{R}^2} (\frac{\partial \Phi}{\partial \omega}\frac{\partial u}{\partial V_y} - \frac{\partial \Phi}{\partial V_y}\frac{\partial u}{\partial \omega}) d\mathbf{x} \end{pmatrix} \tag{2.35}$$

and

$$\mathcal{W} = \begin{pmatrix} 0 & -\int_{\mathbb{R}^2} (\frac{\partial \Phi}{\partial V_x}\frac{\partial u}{\partial V_y} - \frac{\partial \Phi}{\partial V_y}\frac{\partial u}{\partial V_x}) d\mathbf{x} \\ \int_{\mathbb{R}^2} (\frac{\partial \Phi}{\partial V_x}\frac{\partial u}{\partial V_y} - \frac{\partial \Phi}{\partial V_y}\frac{\partial u}{\partial V_x}) d\mathbf{x} & 0 \end{pmatrix} \tag{2.36}$$

the structure of the matrix in Eq. (2.33) shows how the method of deriving the modulation equations from conserved quantities is approached. In particular, differentiating $\mathcal{N}$ with respect to the parameters of the droplet would yield exactly the first row. So the first of these equations is simply $\frac{d\mathcal{N}}{dt}$ decomposed via the chain rule into the time dependence of the parameters. The procedure employed here did not require knowledge of the time evolution for the conserved quantities, nor even knowledge of the quantities themselves. However, as the approach employed here is equivalent to the perturbed conservation law approach, it is natural that the conserved quantities would arise.

Substituting in the form of the approximate droplet into Eq. (2.34) gives an explicit expression for the modulation equations. While the Hamiltonian variables are convenient for derivation of the modulation equations, they are not the most physically familiar. Recasting into the spherical variables, the modulation equations utilizing the approximate droplet are given by

$$\frac{d\Phi_0}{dT} = \frac{1}{4\pi}\int_{\mathbb{R}^2} (\mathbf{V}\cdot\hat{\boldsymbol{\rho}})\operatorname{sech}\left(\rho - \frac{1}{\omega}\right) P_\Theta d\mathbf{x} + \frac{\omega}{4\pi}\int_{\mathbb{R}^2} \operatorname{sech}\left(\rho - \frac{1}{\omega}\right) P_\Phi d\mathbf{x}, \tag{2.37}$$

$$\frac{d\mathbf{x}_0}{dT} = \frac{\omega}{2\pi}\int_{\mathbb{R}^2} \operatorname{sech}\left(\rho - \frac{1}{\omega}\right)\hat{\boldsymbol{\rho}}\, P_\Theta d\mathbf{x}, \tag{2.38}$$

$$\frac{d\omega}{dT} = -\frac{\omega^3}{4\pi}\int_{\mathbb{R}^2} \operatorname{sech}\left(\rho - \frac{1}{\omega}\right) P_\Theta d\mathbf{x}, \tag{2.39}$$

$$\frac{d\mathbf{V}}{dT} = -\frac{\omega^2}{2\pi}\int_{\mathbb{R}^2} \left(\frac{3}{2}\mathbf{V} - \frac{(\mathbf{V}\cdot\hat{\boldsymbol{\varphi}})}{\rho\omega}\hat{\boldsymbol{\varphi}}\right)\operatorname{sech}\left(\rho - \frac{1}{\omega}\right) P_\Theta d\mathbf{x} - \frac{\omega^3}{2\pi}\int_{\mathbb{R}^2} \operatorname{sech}\left(\rho - \frac{1}{\omega}\right)\hat{\boldsymbol{\rho}}\, P_\Phi d\mathbf{x}, \tag{2.40}$$

where $\hat{\boldsymbol{\rho}} = [\cos(\varphi), \sin(\varphi)]$, $\hat{\boldsymbol{\varphi}} = [-\sin(\varphi), \cos(\varphi)]$ are the canonical polar basis vectors for the plane.

Eqs. (2.37)-(2.40) will be extensively used throughout Chapters 3&4 to investigate perturbations of physical interest. It is through these applications that the importance of the modulation equations will become clear. In practical applications, the initial soliton center is often of less interest than the actual soliton center $\boldsymbol{\xi} = \mathbf{x_0} + \int_0^t \mathbf{V} d\,t'$. By differentiating this relationship, an equation for the soliton center is obtained $\frac{d\boldsymbol{\xi}}{dT} = \frac{d\mathbf{x}_0}{dT} + \frac{\mathbf{V}}{\epsilon}$, where ϵ measures the slow time scale. When appropriate, this relation will be used instead of Eq. 2.38.

Finally, many of the perturbations investigated in later chapters focus exclusively on the stationary droplet. In this case, the modulation equations greatly simplify, but the equation for $\mathbf{V}$ becomes a constraint on the admissible perturbations which preserve stationarity. The reduced equations for the stationary droplet are given by

$$\frac{d\Phi_0}{dT} = \frac{\omega}{4\pi}\int_{\mathbb{R}^2} \operatorname{sech}(\rho - 1/\omega) P_\Phi \, \mathrm{d}\mathbf{x}, \tag{2.41}$$

$$\frac{d\mathbf{x}_0}{dT} = \frac{\omega}{2\pi}\int_{\mathbb{R}^2} \operatorname{sech}(\rho - 1/\omega) P_\Theta \hat{\boldsymbol{\rho}} \, \mathrm{d}\mathbf{x}, \tag{2.42}$$

$$\frac{d\omega}{dT} = -\frac{\omega^3}{4\pi}\int_{\mathbb{R}^2} \operatorname{sech}(\rho - 1/\omega) P_\Theta \, \mathrm{d}\mathbf{x}, \tag{2.43}$$

$$0 = \int_{\mathbb{R}^2} \operatorname{sech}(\rho - 1/\omega) P_\Phi \hat{\boldsymbol{\rho}} \, \mathrm{d}\mathbf{x}, \tag{2.44}$$

When possible, these simplified equations may be referred to in the applications to specific perturbations in Chapters 3 & 4.

CHAPTER

3

APPLICATION OF THE MODULATION EQUATIONS TO THE TORQUE EQUATION

Chapter 2 developed a framework for exploring general perturbations to a soliton bearing Hamiltonian system. The aim of this chapter is to explore specific perturbations to the magnetic torque equation and demonstrate the kind of physical insight that can be gained utilizing this framework. Section 3.1 considers the impact of a nonuniform applied field and Section 3.2 examines the influence of damping. These examples are intended not only to more closely model real experimental conditions, but to offer a relatively straightforward application of modulation theory for the droplet. One of the primary contributions of this work applied to the Landau-Lifshitz equation is the determination of the evolution of the phase parameters, namely Φ_0 and $\mathbf{x}_0$. In the droplet ansatz of Eqs. 1.24-1.25, in full generality it is not possible to distinguish between a time dependent phase and the frequency. Consequently, it may not be intuitively obvious why the dynamics of the phase parameters are important. In this asymptotic framework, the dynamics of Φ_0 and $\mathbf{x}_0$ represent higher order corrections to the dynamics of ω and $\mathbf{V}$. In many applications these dynamics are critical, a

point which this chapter aims to make clear.

Section 3.3 analyzes the impact of relaxing the thin-film assumption used to reduce Eq. (1.2) to Eq. (1.8). When applied to the stationary droplet, the resulting modulation equations only impact the dynamics of Φ_0 providing a relatively simple example where these higher order effects become significant. Finally, the complex situation of two interacting droplets is considered. This is a strongly nonlinear interaction requiring numerical investigation (Section 3.4.1). While the interactions observed are quite complex, Section 3.4.2 analyzes a simple case of two stationary droplets providing analytic insight into the observations of numerical simulations.

3.0.1 Numerical Methods

In order to validate the theoretical predictions, comparison is made to direct numerical simulations of Eq. (1.8). The numerical simulations (micromagnetics) utilized a periodic, Fourier psuedospectral spatial discretization. For exponentially localized data, the assumption of periodicity is good, provided the domain is large relative to the droplet footprint. In the simulations throughout Chapter 3 and Chapter 4, the spatial domain was chosen to be $[-50,50]\times[-50,50]$, sufficiently large so that the perturbed solitary waves were well-localized within it. In each spatial dimension, 2^9 grid points were used. Time-stepping was done using a version of the Runge-Kutta-Fehlberg algorithm, modified so that the magnetization maintained unit length at every grid point and each time step.

To make comparison to modulation theory, it is also necessary to extract the droplet parameters from micromagnetics. The velocity, $\mathbf{V}$, was extracted from numerical data by computing the center of mass, $\xi(t)=\int_{\mathbb{R}^2}\mathbf{x}(1-m_z(\mathbf{x},t))d\mathbf{x}/\mathcal{N}$. $\mathbf{V}=\frac{d\xi}{dt}$ may then be approximated using a forward difference of $\xi(t)$. This method does not work for perturbations which excite higher order changes in $\frac{d\xi}{dt}$ and $\mathbf{V}$ will not be estimated in such cases.

For the precessional frequency ω, the phase of the in-plane magnetization (m_x,m_y) was extracted at a point a fixed distance from the center of mass ξ. Differentiating this phase with respect

to time yields $\Omega(t)$, the total frequency of the droplet in the moving, droplet reference frame

$$\Omega(T) = h_0(\epsilon\xi(T), T) + \omega(T) + \epsilon\frac{d\Phi_0}{dT}. \tag{3.1}$$

The precessional frequency, ω, was obtained by subtracting h_0 and $\frac{d\Phi_0}{dt}$. In the laboratory frame, the frequency exhibits a doppler shift of $\mathcal{O}\left(V^2\right)$, significantly smaller than the asymptotic accuracy of the approximate droplet [HS12].The contribution from $\frac{d\Phi_0}{dt}$ was estimated via the modulation equation (2.37). An alternative method based on computing the conserved quantities in Eqs. (1.15)-(1.21) was used for comparison. The relations for total spin and momentum of the approximate droplet Eqs. (1.46)-(1.47) were inverted to obtain ω and $\mathbf{V}$. While careful analysis on the degree of agreement of these methods was not performed, when time series data for the parameters computed via both methods were plotted on the same axes, the lines were on top of each other with some small noisy discrepancies.

3.1 Slowly Varying Applied Field

In practical applications, the magnetic field will typically have some spatial variation whose scale is much larger than the scale of the droplet, i.e., the exchange length. This is well modeled by assuming that the perpendicular applied field has the form, $h_0 = h_0(\epsilon t, \epsilon\mathbf{x})$, $0 < \epsilon \ll 1$. This inhomogeneity is best treated by introducing an appropriate perturbation $\mathbf{p}$ in eq. (1.8). Expanding h_0 about the soliton center, ξ,

$$h_0(\epsilon t, \epsilon\mathbf{x}) = h_0(\epsilon t, \epsilon\xi) + \epsilon\tilde{\nabla}h_0\big|_{\mathbf{x}=\xi}\cdot(\mathbf{x}-\xi) + \mathcal{O}\left(\epsilon^2\right), \tag{3.2}$$

where $\tilde{\nabla}$ represents the gradient with respect to the slow variable $\boldsymbol{X} = \epsilon\boldsymbol{x}$. Inserting the expansion (3.2) into the cross product $-\mathbf{m}\times(h_0\hat{\mathbf{z}})$ from eq. (1.8) introduces the perturbation

$$p_\Theta = 0 \text{ and } p_\Phi = \left(\tilde{\nabla}h_0\cdot\hat{\boldsymbol{\rho}}\right)\rho. \tag{3.3}$$

Substituting these into eqs. (2.37)-(2.40) leads to Newton's second law for the droplet center

$$\frac{d^2\boldsymbol{\xi}}{dt^2} = \epsilon \frac{d\mathbf{V}}{dT} = -\omega \nabla h_0. \tag{3.4}$$

Note that ∇ here represents the gradient with respect to the fast variable $\mathbf{x}$, distinguishing it from $\tilde{\nabla}$. The phase Φ_0 and frequency ω are unchanged by the field gradient.

A favorable comparison of direct numerical simulations for eq. (1.8) with the solution to (3.4) is shown in Fig. 3.1. The explicit equation (3.4) agrees with the previous result in [Hoe12] obtained

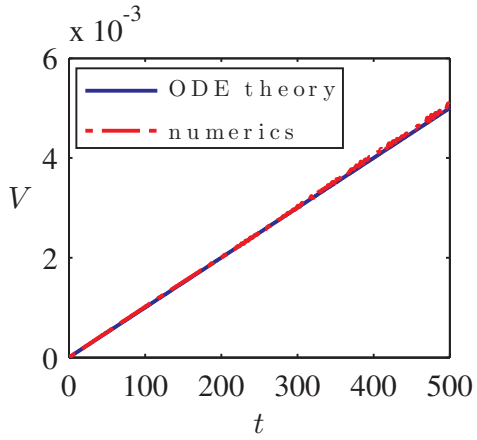

Figure 3.1 Acceleration of the droplet due to the inhomogeneous magnetic field $h_0 = 0.5 - 10^{-4}x$ with $\omega(0) = 0.1$ and $|\mathbf{V}(0)| = 0$. The exact solution to eq. (3.4) (solid) compares favorably to direct numerical simulations of the PDE (dashed).

by perturbing conservation laws and integrating the resulting modulation equations numerically. Previously, the nontrivial dynamical equation was $\frac{d\mathcal{P}}{dt} = -\mathcal{N}\nabla h_0$. To demonstrate the equivalence, transform this equation into eq. (3.4) by using the explicit formulae (1.46), (1.47) for $\mathcal{N}$ and $\mathcal{P}$. Since $\frac{d\omega}{dT} = 0$ and $\mathcal{N}$ depends only on ω, $\frac{d\mathcal{N}}{dT} = 0$. Then

$$\frac{d\boldsymbol{P}}{dT} = \frac{\mathcal{N}^{3/2}}{\sqrt{2\pi}} \frac{d\mathbf{V}}{dT} = \frac{m_{\text{eff}}}{\epsilon} \frac{d^2\boldsymbol{\xi}}{dt^2} = -\frac{\mathcal{N}}{\epsilon} \nabla h_0. \tag{3.5}$$

This is exactly (3.4). The particle-like droplet with mass m_{eff} in eq. (1.50) experiences a conservative force due to the potential $\mathcal{N}h_0$. This interpretation is consistent with the analysis of the effective mass derived from the kinetic energy in Section 1.1.2. Furthermore, it demonstrates that a droplet in a magnetic field gradient behaves effectively like a single magnetic dipole with net dipole moment $\mathcal{N}$.

The effect of an inhomogeneous magnetic field on a massive two-dimensional droplet is markedly different from its effect on a one-dimensional droplet [Kos98] and a vortex [PT91]. A one-dimensional droplet experiences periodic, Bloch-type oscillations for a magnetic field with constant gradient, while a magnetic vortex exhibits motion perpendicular to the field gradient direction.

3.2 Damping

In [Hoe12], it was observed that the droplet accelerates as it decays in the presence of damping alone. Micromagnetic simulations illustrated in Figure 3.2 illustrate this decay of the droplet to the uniform state.

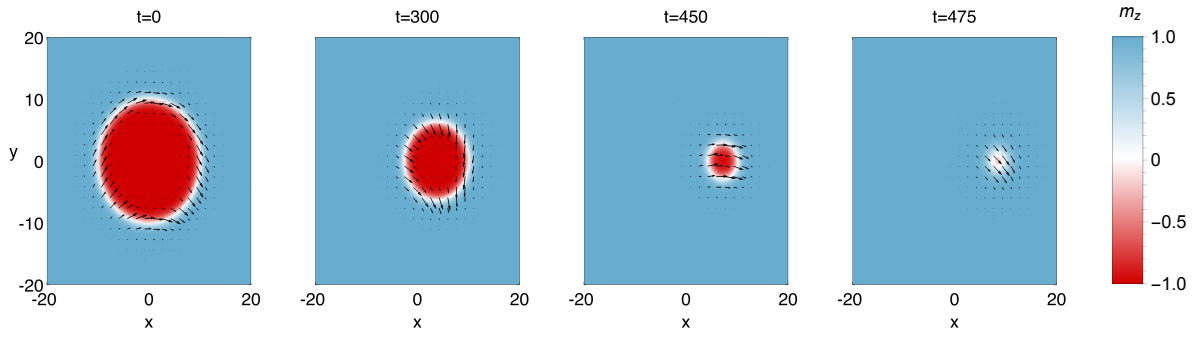

Figure 3.2 Time series plots of an approximate droplet propagating in the presence of damping. The initial droplet parameters for this numerical experiment were $\omega = 0.1$ and $\mathbf{V} = [0.01, 0]^T$ and the nondimensional damping was chosen as $\alpha = 0.1$. As time increases left to right, the droplet radius can clearly be seen to decrease, which corresponds to increasing precessional frequency. The droplet also appears to move farther to the right than a droplet propagating at constant velocity would predict.

The framework presented here offers an analytical tool to understand this slightly counterintuitive result, namely that damping can cause the otherwise steady droplet to speed up. The relevant contributions to eq. 1.8 are

$$p_\Theta = -\alpha(\omega + h_0 - \mathbf{V}\cdot\nabla\Phi)\sin(\Theta) \text{ and } p_\Phi = -\alpha\mathbf{V}\cdot\nabla\Theta \tag{3.6}$$

where the Landau-Lifshitz magnetic damping parameter, usually denoted α, plays the role of the small parameter (ϵ). In many practical situations, the damping parameter is quite small.

Evaluation of equations (2.37)-(2.40) with these perturbations yields two nontrivial equations

$$\frac{d\omega}{dT} = \omega^2(\omega + h_0) \tag{3.7}$$

$$\frac{d\mathbf{V}}{dT} = \omega\mathbf{V}(\omega + 2h_0). \tag{3.8}$$

These equations are again consistent with the perturbed conservation law approach taken in [Hoe12] when evaluated at the approximate solution. When $h_0 = 0$ and $V = 0$, the remaining ODE $\frac{d\omega}{dt} = \alpha\omega^3$ agrees with the result in [Bar86].

Note that the right hand sides of the modulation equations are both positive for $h_0 > -\omega/2$. Hence, the frequency and velocity increase. Equation (3.7) can be interpreted as a dynamical equation for the droplet's mass m_{eff} (eq. (1.50)). The mass is decreasing at a faster rate than the velocity. In light of the interpretation given in Section 3.1, even though the droplet is losing energy consistently, it sheds mass fast enough that its acceleration is not a contradiction. Fig. 3.3 illustrates quite good agreement between the modulation theory and full micromagnetic simulations.

Since Eq. (3.7) decouples in this system, an analytical solution can be found. Elementary application of partial fractions yields an explicit solution in terms of the Lambert W-function; however, the analysis is significantly simplified when $h_0 = 0$. In this case, the analytical solution to Eqs. (3.7)-

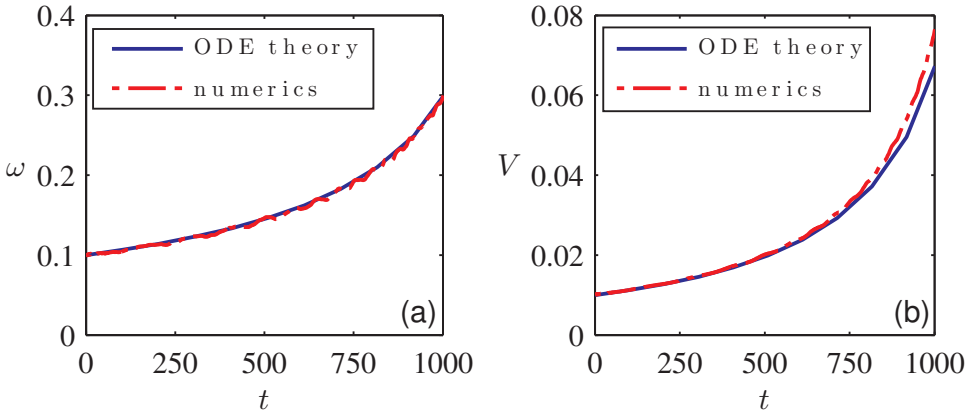

Figure 3.3 The evolution of droplet frequency (a) and velocity (b) due to damping for both numerical solutions of eqs. (3.7), (3.8) (solid) and direct numerical simulations of eq. (1.8) (dashed) when $\epsilon = \alpha = 0.01$, $h_0 = 0.5$, $\omega(0) = 0.1$ and $|\mathbf{V}(0)| = 0.01$.

Eq. (3.8) is

$$\omega(t) = \frac{\omega_0}{\sqrt{1-2\alpha\omega_0^2 t}} \tag{3.9}$$

$$\mathbf{V}(t) = \frac{\mathbf{V}_0}{\sqrt{1-2\alpha\omega_0^2 t}} \tag{3.10}$$

where ω_0 is the initial precession frequency and $\mathbf{V}_0$ the initial velocity. These expressions reveal two facts: a clear time of breakdown for modulation theory and the existence of an adiabatic invariant. Dividing Eq. (3.9) by the components of Eq. (3.10) demonstrates that the quantities ω/V_x and ω/V_y are constant in time.

3.3 Dipolar Field

This section considers the nonlocal impact of the magnetostatic field. As discussed in Section 1.1, this long range coupling of the magnetization through Maxwell's equations can be disregarded for sufficiently thin ferromagnets. Including the first order correction in thickness, δ, gives rise to the

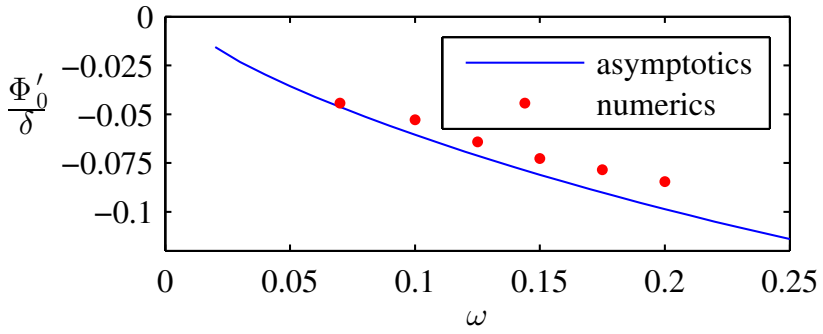

Figure 3.4 Negative frequency shift due to nonlocal, thickness dependent magnetostatic corrections. Equation (3.12) (solid) and micromagnetic simulations with $\delta = 0.1$ (dots).

perturbations (see Appendix B.3 for a derivation)

$$p_\Theta = 0, \quad p_\Phi = -\delta \sin\Theta_0 \sqrt{-\nabla^2}(1-\cos\Theta_0)/2, \tag{3.11}$$

where $\sqrt{-\nabla^2}$ is defined as an operation in Fourier space as discussed in Section 1.1. Consequently, thickness dependent magnetostatic effects only enter in Eqs. (2.44) and (2.41). The constraint equation (2.44) is automatically satisfied because p_Φ depends only on ρ so the φ integrals vanish. What is left is the expression for the slowly varying phase Φ_0. Restricting to the case of the stationary droplet and evaluating (2.41) with (3.11) yields a precessional frequency shift of the droplet

$$\begin{aligned}\frac{d\Phi_0}{dt} = -\frac{\delta\omega}{4}\int_0^\infty &\operatorname{sech}^2(\rho - 1/\omega) \\ &\times \{\sqrt{-\nabla^2}[1-\tanh(\rho-1/\omega)]\}\rho\, d\rho.\end{aligned} \tag{3.12}$$

Recall, the total droplet frequency, Ω, as in Eq (3.1), results from the combined contributions of the applied field, droplet frequency and the higher order phase correction, $\frac{d\Phi_0}{dt}$. Since the integrand is strictly positive for $\rho \in (0,\infty)$, Eq. (3.12) represents a negative frequency shift, which is plotted in Fig. 3.4 as a function of ω. Micromagnetic simulations yield good, asymptotic $\mathcal{O}(\delta\omega)$ agreement as expected.

Further, since $0 < \omega < 1$, stationary droplets in the absence of nonlocal magnetostatics and applied field are always dynamic. The negative frequency shift induced by nonlocal magnetostatics suggests that a droplet in a sufficiently thick film can be static, which would correspond to a magnetic bubble [DL80].

3.4 Interacting Droplets

3.4.1 Summary of Numerical Results

An intriguing, indeed defining aspect of solitary wave dynamics is their interaction behavior. In integrable systems, solitons are known to interact elastically [ZK65] and such interactions are either attractive or repulsive [Gor83]. In more general systems, soliton interactions are more complicated, exhibiting fusion, fission, annihilation or spiraling [SS99; Kra12]. Previous numerical investigations on the interacting droplet revealed that two counter-propagating droplets would merge and then scatter at 90° [PZ98]. In those experiments, the droplets lack sufficient energy to escape the influence of one another. After scattering along the perpendicular, the droplet pair then reverse direction, scattering at 90° again, losing energy after each scattering event. In long time, the interaction settled into a single coherent droplet-like structure. While these experiments suggest droplet interactions can be complex, they do not tell the full story of droplet interaction. As proposed in [Mai14], the study of soliton interaction is of particular interest in magnetic systems as a nonliner method of images offers insight into the interaction of a droplet with either pinned or free boundary conditions common in experiment.

The previous work, [PZ98], did not carefully explore the impact of soliton parameters on the nature of interaction. The relative initial phase, $\Delta\Phi = \Phi_2 - \Phi_1$, of the droplet has a significant impact on determining the resulting interaction. In the experiments presented here, an initial condition was constructed by an appropriate superposition of two droplets (subscripted as 1 and 2 throughout this section). The parameters of the two droplets could be chosen independently, though typically

the velocities and initial positions were chosen to guarantee the two droplets would interact. The precise initial condition chosen for the experiments presented in this chapter was $\mathbf{m} = \tilde{\mathbf{m}}/|\tilde{\mathbf{m}}|$, where $\tilde{m}_x = m_{x,1} + m_{x,2}$, $\tilde{m}_y = m_{y,1} + m_{y,2}$ and $\tilde{m}_z = m_{z,1} + m_{z,2} - 1$. By constructing the initial data in this way, the unit length condition is preserved while also representing a superposition of two droplets. Rather than utilizing the approximate droplet solution, a database of numerically exact solitons computed in [HS12] was utilized. By doing so, the influence of radiation on the interaction is minimized.

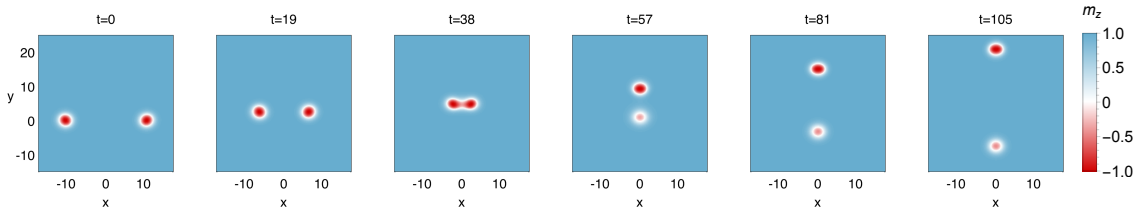

Figure 3.5 Time series of m_z during the attractive interaction of two droplets. The initial parameters were $\omega_1 = \omega_2 = .4$ and $\mathbf{V}_1 = .6[\cos(2\pi/3), \sin(2\pi/3)]^T, \mathbf{V}_2 = .6[-\cos(2\pi/3), \sin(2\pi/3)]^T, \Delta\Phi = 0$.

A typical experiment is illustrated in Figures 3.5-3.6. The two figures represent two presentations of the data. The first is sequential time data for m_z. It can be difficult to tell exactly what the motion is from one time step to the next. To clarify this, an annotated graph with all time slices superimposed is presented in Figure 3.6. In this experiment, the two droplets start with the same initial phase (i.e. $\Delta\Phi = 0$). When the droplets are close enough, they merge and then scatter along the axis of symmetry. Note that the two resultant droplets are not of equal mass, with a droplet of larger radius going up. This inequality can be tuned via the angle of interaction, with two identical droplets emerging from the intermediate merged state and scattering along the perpendicular when $V_{y,1} = V_{y,2} = 0$, i.e. a head-on collision. The opposite occurs for the interactions between droplets which start exactly out of phase, $\Delta\Phi = \pi$. A typical experiment illustrating these repulsive dynamics is illustrated in Figures 3.7-3.8. With such drastically different results determined exclusively by the relative initial phase,

it is natural to conjecture that there is a crossover point where the dynamics shift from generally attractive to generally repulsive.

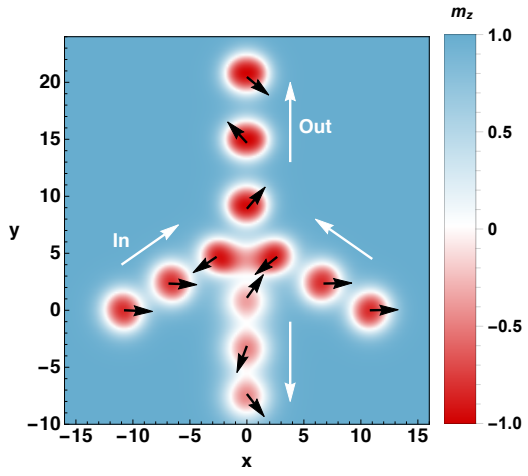

Figure 3.6 A time-lapsed image of an attractive droplet interaction. Color corresponds to m_z and the arrows represent the $[m_x, m_y]$ component at the center of the droplet. Initial parameters are the same as Fig. 3.5. The arrows indicate that droplets are in phase initially as well as just before and just after the strongly nonlinear interaction.

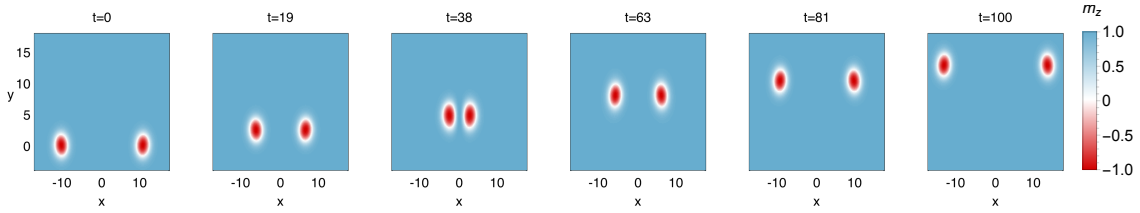

Figure 3.7 Time series of m_z during the repulsive interaction of two droplets. The initial parameters were $\omega_1 = \omega_2 = .4$ and $\mathbf{V}_1 = .6[\cos(2\pi/3), \sin(2\pi/3)]^T, \mathbf{V}_2 = .6[-\cos(2\pi/3), \sin(2\pi/3)]^T$, $\Delta\Phi = \pi$.

Indeed, there does exist a critical value of $\Delta\Phi = \Delta\Phi_{\text{cr}}$ which divides the attractive and repulsive regimes. This critical value depends on the frequencies and velocities of the initial droplets and is typically near $\Delta\Phi = \pi/2$, but not precisely this value. As $|\Delta\Phi|$ approaches $\Delta\Phi_{\text{cr}}$, the two droplets

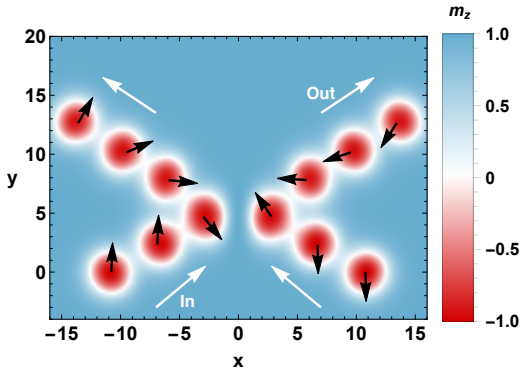

Figure 3.8 A time-lapsed image of an repulsive droplet interaction. Color corresponds to m_z and the arrows represent the $[m_x, m_y]$ component at the center of the droplet. The initial parameters were $\omega_1 = \omega_2 = .4$ and $\mathbf{V}_1 = .6[\cos(2\pi/3), \sin(2\pi/3)]^T$, $\mathbf{V}_2 = .6[-\cos(2\pi/3), \sin(2\pi/3)]^T$, $\Delta\Phi = \pi$. The arrows clearly show the droplets are out of phase initially as well as just before and just after the strongly nonlinear interaction.

collide with one preferentially absorbing the other, then transferring a significant portion of their energy into spin waves followed by the spontaneous formation of a breather state as shown in the head-on collision of Figure 3.9. The preferred direction in the interaction of Figure 3.9 is due to the choice $0 < \Delta\Phi < \pi$. A change in the sign of $\Delta\Phi$ reverses the asymmetry.

An examination of the m_z component over time reveals a significant decrease in the excitation amplitude, $1-m_z$, during the loss of energy to spin waves (magnons) and an amplitude coalescence associated with the formation of the breather. Because a single droplet can be interpreted as a bound state of magnon quasi-particles [Kos90], this sort of interaction can broadly be interpreted as a fission-type event. Annihilation is possible during the crossover from attractive to repulsive scattering where the incommensurate phases of the colliding droplets cannot be resolved at high kinetic energies, resulting in the explosive release of spin waves accompanied by an apparent breather bound state. Such observations of soilton annihilation are quite novel. Previous observations of soliton annihilation in optics were of a very different type [Kró98] where the simultaneous collision of three solitons could result in annihilation of only one of them.

The summary of phenomena presented here is not complete, but sufficient to introduce the

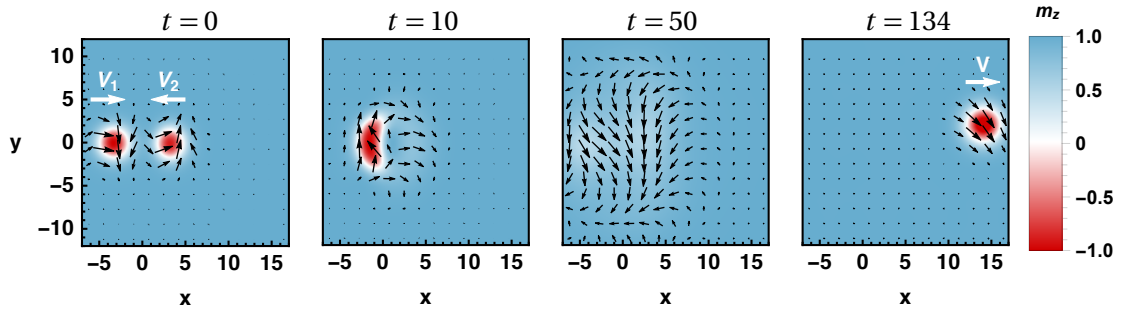

Figure 3.9 Time series of two droplets undergoing an annihilation type interaction. The initial parameters were $\omega_1 = \omega_2 = .4$ and $\mathbf{V}_1 = [.6, 0]^T = -\mathbf{V}_2$. The relative initial phase was chose at the critical value $\Delta\Phi = \Delta\Phi_{cr} \approx 1.61$

broad categories of interaction that the next section attempts to explain via the modulation equations. A more comprehensive discussion of this numerical investigation of droplet interaction can be found in [Mai14]. While the results presented here are for relatively high velocities, the same kinds of attractive and repulsive phenomena can be observed for weakly interacting stationary droplets. It is not possible, however, to achieve annihilation at low velocities. The attractive interaction of two stationary droplets appears to resolve in very long times to a stable-stationary breather in which the boundary of the droplet oscillates in time. This will be revisited in Chapter 5.

3.4.2 Modulation Theory for Interacting Droplets

The interactions studied studied so far are strongly nonlinear, hence a perturbation theory would be insufficient to study the full complement of observed phenomena. Nevertheless, it is possible to gain insight into the nature of the interaction (attractive/repulsive) by studying two well-separated droplets perturbatively, with the small parameter being the inverse of the droplet separation. This approach is well-known and has been applied successfully to several systems, including NLS-type models [ZY07; Abl09; Mal98].

In full generality, the perturbations arising from this analysis are complex. However, since the validity of these equations is strongly dependent on the separation of the two droplets, these equa-

tions are expected to be valid over short time scales. Hence, the aim of this section is only to describe the initial behavior of two stationary, weakly overlapping droplets. As the interaction immediately accelerates the two droplets, it would be necessary to incorporate $V_k \neq 0$ in the modulation equations for $t > 0$. Nevertheless, these assumptions make it possible to describe much of the behavior observed in full numerical simulations [Mai14]. The initial configuration places one droplet on the left (subscripted 1) and another droplet (subscripted 2) a distance d away along the $x-$axis. The relative phase difference will emerge as an important quantity in the modulation equations. Considering the modulation equations, two weakly interacting droplets with motion in the x direction *at the initial time only* yields

$$\dot{\Phi}_{0,k} = -\frac{\omega}{2\pi}\cos(\Delta\Phi)\int_{\mathbb{R}^2} \mathcal{K}_k(\mathbf{x})d\mathbf{x} \tag{3.13}$$

$$\dot{\xi}_k = \frac{\omega}{2\pi}(-1)^{k+1}\sin(\Delta\Phi)\int_{\mathbb{R}^2} \mathcal{K}_k(\mathbf{x})\mathrm{sech}\left(\rho-\frac{1}{\omega}\right)\cos\varphi\, d\mathbf{x} \tag{3.14}$$

$$\dot{\omega}_k = -\frac{\omega^3}{4\pi}(-1)^{k+1}\sin(\Delta\Phi)\int_{\mathbb{R}^2} \mathcal{K}_k(\mathbf{x})\mathrm{sech}\left(\rho-\frac{1}{\omega}\right)d\mathbf{x} \tag{3.15}$$

$$\dot{V}_k = \frac{\omega^3}{\pi}\cos(\Delta\Phi)\int_{\mathbb{R}^2} \mathcal{K}_k(\mathbf{x})\cos\varphi\, d\mathbf{x} \tag{3.16}$$

where

$$\mathcal{K}_k(\mathbf{x}) = \mathrm{sech}\left(\tilde{\rho}_k-\frac{1}{\omega}\right)\mathrm{sech}\left(\rho-\frac{1}{\omega}\right)\times\left[2\mathrm{sech}^2\left(\rho-\frac{1}{\omega}\right)-\omega\left(1-\tanh\left(\rho-\frac{1}{\omega}\right)\right)\right]. \tag{3.17}$$

$\mathcal{K}_k$ defines an interaction kernel which depends on the separation between the two droplets through $\tilde{\rho}_k = \sqrt{(x+(-1)^k d)^2+y^2}$. Throughout this section the notation $\dot{z}$ will be used for $\frac{dz}{dt}$ for notational simplicity. Utilizing this framework, it is now possible to offer some insight into the nature of two interacting droplets. The precise derivation of these equations is based on determining the perturbation of one droplet on the other via the overlapping exponential tails. Using the form of the approximate two-soliton solutions used in [Mai14], these perturbations are carefully worked out in

Appendix B.4.

3.4.3 Attraction and Repulsion

The attractive or repulsive nature of two droplets can be understood by considering Eq. 3.16. As $\Delta\Phi$ varies, the sign of $\cos(\Delta\Phi)$ is clear. Thus determining the accleration of motion of the droplet comes down to determining the sign of the integral term in (3.16). Figure 3.10, left shows the numerical

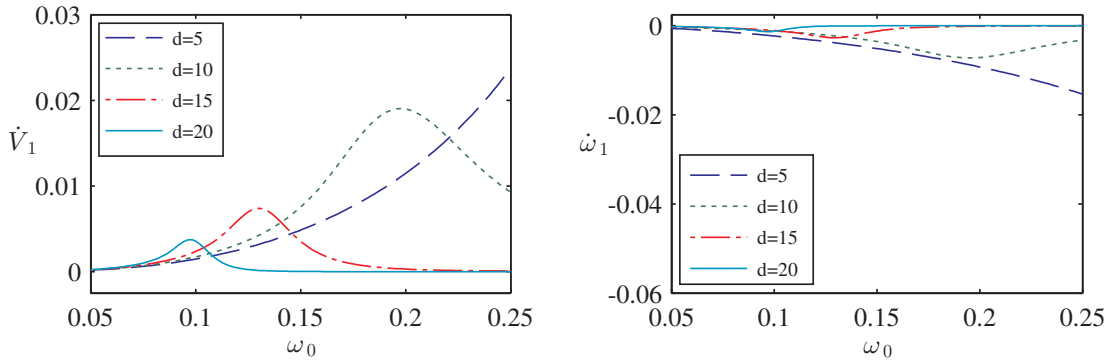

Figure 3.10 Left: Initial acceleration for varied initial ω and several values of separation. Right: Plot of $\frac{d\omega_1}{dt}$ as a function of initial ω for several values of separation. In both, the initial relative phase was $\Delta\Phi = 1$.

evaluation of the right hand side of $\dot{V}_1$ (droplet on left) when $\Delta\Phi = 1 < \pi/2$, leading to positive values only. Thus, the left droplet experiences a positive acceleration to the right, towards the other droplet when $|\Delta\Phi| < \pi/2$. Since the kernel exhibits symmetry with respect to droplet choice $\mathcal{K}_1(x,y) = \mathcal{K}_2(-x,y)$, the integral in (3.16) for the right droplet, $k = 2$, has the opposite sign. The right droplet experiences a negative acceleration to the left when $|\Delta\Phi| < \pi/2$. Therefore, two droplets are attractive when $|\Delta\Phi| < \pi/2$, i.e., when they are sufficiently in phase. Similarly, when $\pi/2 < |\Delta\Phi| < \pi$, the signs of $\dot{V}_k$ are reversed and the droplets move away from each other. Thus, two droplets are repulsive when they are sufficiently out of phase.

As was noted in [Mai14], by a nonlinear method of images, the attractive or repulsive nature

of two droplets with the special initial values $\Delta\Phi = 0$ or $\Delta\Phi = \pi$ describes the dynamics of a single droplet near a magnetic boundary with either a free spin (Neumann type) boundary condition or a fixed spin (Dirichlet type) boundary condition, respectively. The analysis presented here confirms this fact for any droplet that weakly interacts with a magnetic boundary. Such behavior was observed in micromagnetic simulations of a droplet in a NC-STO, nanowire geometry [Iac14].

3.4.4 Asymmetry

Despite a highly symmetric initial condition, an asymmetry was observed in so-called “head-on collisions" of two droplets in [Mai14]. Equation (3.15) provides an explanation of this in the limit of very small velocities. Figure 3.10, right contains the relevant information. The asymmetry is encoded in the sign of $\dot{\omega}_k$. The range of $\Delta\Phi$ considered in the numerical experiments of [Mai14] were between $\Delta\Phi = 0$ and $\Delta\Phi = \pi$. Since the sign of $\dot{\omega}_k$ is determined by the overall factor $(-1)^{k+1}\sin(\Delta\Phi)$, $\dot{\omega}_1 < 0$ and $\dot{\omega}_2 > 0$ for all the experiments considered here with $\Delta\Phi \geq 0$. Again using (3.15), and $\mathcal{K}_1(x,y) = \mathcal{K}_2(-x,y)$, it can be seen that the integrals involved in computing $\dot{\omega}_1$ and $\dot{\omega}_2$ are equal. Hence the sign of $\dot{\omega}_k$ is determined by $(-1)^{k+1}$, and the signs of $\dot{\omega}_1$ and $\dot{\omega}_2$ will always be opposite. For the parameters discussed here, this means that the frequency decreases for the droplet on the left and increases on the right. This change in droplet structure is asymmetric because a reduced (increased) frequency implies larger (smaller) droplet mass and corresponds precisely with the observations of [Mai14]. Such symmetry breaking has been explained in 1D systems [KM06] with a similar analysis to what is provided here for 2D droplets.

3.4.5 Acceleration

The discussion of attraction and repulsion in Section 3.4.3 suggests that the boundary between the two behaviors is $\Delta\Phi_{\text{cr}} = \pi/2$. But this does not agree with numerical experiments where the crossover $\Delta\Phi$ was found to vary with the initial droplet parameters [Mai14]. To offer an explanation for this, we must consider the total acceleration of the initial droplets, i.e., $\ddot{\xi}_k$. This incorporates higher order

information not included in $\dot{V}_k$. Since the full modulation equations for interacting droplets when $V \neq 0$ are complex, the framework laid out here does not access this information for all values of $\Delta\Phi$. However, at $\Delta\Phi = \frac{\pi}{2}$, $\dot{V}_k = 0$ (since $\cos(\Delta\Phi) = 0$) and those terms will not contribute. Similarly, $\dot{\Phi}_0 = 0$ at $\Delta\Phi = \frac{\pi}{2}$ for the same reason which simplifies the calculation. Figure 3.11 shows the initial, total droplet acceleration $\ddot{\xi}_1$, evaluated numerically, as the initial frequency and separation are varied. The variable sign of this quantity as parameters change demonstrates that subtle, higher

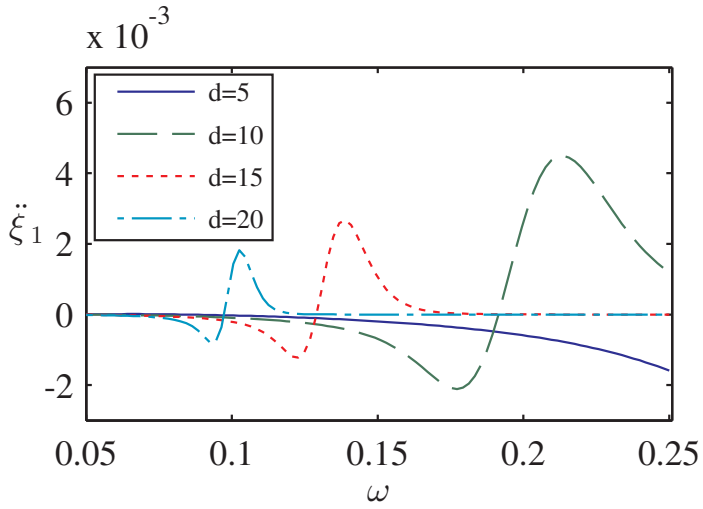

Figure 3.11 Numerical evaluation of $\ddot{\xi}_1$ initially for $\Delta\Phi = \pi/2$, variable droplet separation d and frequency ω. There is not one sign of acceleration, i.e., the left droplet can be repelled or attracted to the right droplet depending on the choice of parameters.

order effects cause the crossover value of $\Delta\Phi$ to deviate from its nominal value $\pi/2$.

The perturbations investigated in this chapter are far from exhaustive. Chapter 4, continues this investigation for perturbations which model spin transfer torque, a mechanism which can directly oppose the natural damping of a magnetic material. The above examples demonstrate a versatility of the modulation equations for modeling complex phenomena. The relatively simple results of a spatially varying applied field offer clean physical insight and intuition into the motion

of the droplet. In more complex perturbations, the higher-order parameters play an important role, leading to conclusions that could not be reached by relying upon dynamics of the frequency and velocity alone. The role of these phase parameters will continue to be important as the investigation is continued in Chapter 4.

CHAPTER

4

APPLICATIONS INVOLVING SPIN-TORQUE

As established in the previous chapter, damping has the tendency to cause the droplet to relax to the uniform state. Since damping is ubiquitous in magnetic materials, the droplet would remain a mathematical novelty if there did not exist a means to overcome this effect. The idea that dissipation can be compensated in solitonic systems is by no means unique to the droplet. Dissipative solitons have been extensively studied in the context of non-linear optics, with some early experimental observations made in [Pic91] and theoretical work for a dissipatively modified Korteweg de-Vries equation [CV95] and for the Swift-Hohenberg equation [AA05] (see [AA08] for a thorough discussion). In the context of magnetics, the idea that spin transfer torque could balance damping and stabilize the droplet was proposed and investigated in [Hoe10]. In this chapter, that idea is explored using the analytical framework of the previous chapters.

The primary focus of this chapter is on a device known as the nanocontact spin-torque oscillator (NC-STO), in which the spin accumulation due to polarized spin current exerts a torque on the

magnetization, the spin transfer torque [Ber96; Slo96]. This forcing can be confined to a localized region via a nanocontact [Slo99]. Perturbations of this sort can lead to dynamics within all the parameters of the droplet. In addition to spin torque, a droplet in a NC-STO also experiences damping and it is precisely the balance between the two that leads to the stable droplet observed in experiments. At the end of this chapter, other forms of spin-torque are investigated. As these do not appear to support the dissipative droplet, they are not investigated in detail.

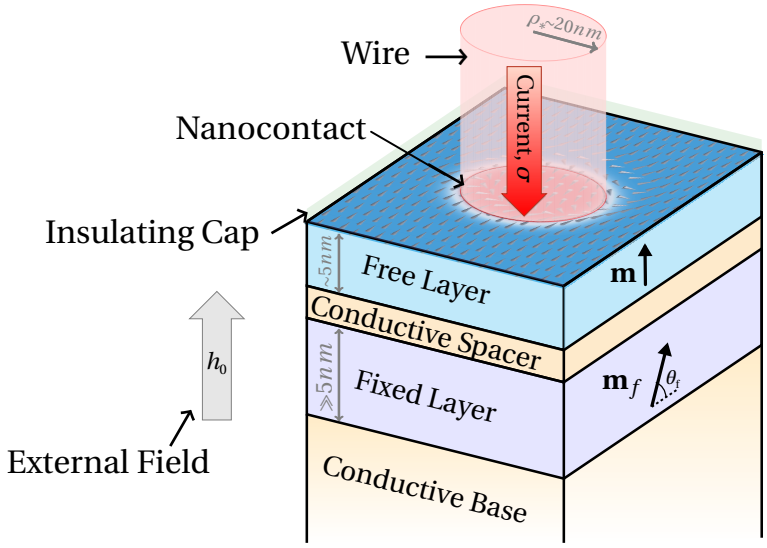

Figure 4.1 Schematic of nanocontact device. The magnetization dynamics in the free layer are modeled by the perturned Landau-Lifshitz equation, while the fixed layer acts a polarizer. The electrons in the current become spin polarized as they interact with the fixed layer and in turn the electrons exert a torque on the free layer.

4.1 Nanocontact Devices

4.1.1 Application to Stationary Droplets

This section considers the effects of damping and spin-transfer torque (STT) on a stationary droplet where $\mathbf{V} \equiv 0$. A NC-STO consists of two magnetic layers, one that acts as a spin polarizer of the

driving DC current and the other where the dynamics according to eq. (1.8) occur. This assumption corresponds to taking $\mathbf{m}_f = \mathbf{z}$ in Figure 4.1. For simplicity, the spin torque asymmetry, which introduces another parameter into the analysis but does not appear to have a significant effect on the dynamics [Hoe10] will be neglected. Under these assumptions, the perturbation $\mathbf{p}$ takes the form [Hoe10]

$$p_\Theta = -\alpha\omega\sin\Theta_0 + \sigma\mathscr{H}(\rho_* - \rho)\sin\Theta_0, \quad p_\Phi = 0, \tag{4.1}$$

where α is the damping coefficient, ρ_* is the nanocontact radius, and $\mathscr{H}$ is a localized function. For the following analysis, take $\mathscr{H}$ to be the Heaviside step function thus defining the region of spin polarized current flow as a disk with radius ρ_*. The STT coefficient $\sigma = I/I_0$ is proportional to the applied, dc current I with nondimensionalization $I_0 = 2M_s^2 e\mu_0\pi{\rho_*}^2\delta/(\hbar\epsilon)$ where ϵ is the spin-torque polarization, e is the electron charge, and $\hbar$ is the modified Planck's constant. For simplicity, take $\lambda_{\text{st}} = 1$, i.e., no asymmetry. Experiments [Moh13; Mac14] and analysis [Hoe10; BH13] have shown that the ratio of damping, α, to forcing strength, σ (proportional to current), are roughly order 1 for the existence of droplets to be satisfied. Since α is small in these systems ($\alpha \approx 0.0$ [Moh13]), α and σ can be taken as small parameters of the same order. Substituting this perturbation into (2.43)–(2.42) results in a system of three ordinary differential equations (ODEs). However, since rotational symmetry is not broken for a circular nanocontact, it is possible to rotate the plane so that motion occurs in the $x-$direction only and thereby eliminate one of the two equations for the center. The modulation system is

$$\begin{aligned}\frac{d\omega}{dt} =& \alpha\omega^2(\omega + h_0) \\ &- \frac{\sigma\omega^3}{4\pi}\int_{|\mathbf{x}|<\rho_*} \operatorname{sech}^2(|\mathbf{x}-\mathbf{x}_0| - 1/\omega)\,d\mathbf{x}\end{aligned} \tag{4.2}$$

$$\frac{dx_0}{dt} = -\frac{\sigma\omega^3}{2\pi}\int_{|\mathbf{x}|<\rho_*} \operatorname{sech}^2(|\mathbf{x}-\mathbf{x}_0| - 1/\omega)\frac{x - x_0}{|\mathbf{x}-\mathbf{x}_0|}\,d\mathbf{x}, \tag{4.3}$$

where the integrals are performed in a coordinate system centered on the nanocontact. Note that these equations do not depend upon the slowly varying phase Φ_0 so that the inclusion of nonlocal magnetostatic effects will lead to the same frequency shift given in eq. (3.12), decoupling from the ODEs (4.2) and (4.3). The fixed points of this system correspond to steady state conditions where there is a balance between uniform damping and localized spin torque, i.e., a dissipative droplet soliton. A fixed point at $(\omega, x_0) = (\omega_*, 0)$ leads to the relationship between current and precession frequency

$$\frac{\sigma}{\alpha} = \frac{2(\omega_* + h_0)}{1 + \omega_* \left(\log[\mathrm{sech}(\rho_* - \frac{1}{\omega_*})/2] + \rho_* \tanh\left(\rho_* - \frac{1}{\omega_*}\right)\right)}. \tag{4.4}$$

Note that there is an error in Eq. 17 of [BH13], where parentheses have been dropped. Linearizing about the fixed point, the eigenvalues of the system are found to be

$$\begin{aligned} \lambda_1 = \tfrac{1}{2}\omega_*[&\sigma \tanh(\rho_* - 1/\omega_*) \\ &+ \sigma - \rho_* \sigma \,\mathrm{sech}^2(\rho_* - 1/\omega_*) - 2\alpha h_0], \end{aligned} \tag{4.5}$$

$$\lambda_2 = -\tfrac{1}{2}\rho_* \sigma \omega_* \,\mathrm{sech}^2(\rho_* - 1/\omega_*). \tag{4.6}$$

For physical parameters, λ_2 is always negative, however λ_1 can change sign as ω_* is varied and hence the stability of the fixed point can change. This family of fixed points arises from a saddle-node bifurcation occurring as the current is increased through the minimum sustaining current (Fig. 4.2(a-d)). Figures 4.2(b)-(d) show the vector field of this system below onset and after the appearance of the stable and unstable equilibria. The stable branch of this saddle node bifurcation is the dissipative soliton. Furthermore, micromagnetic simulations verify the stable branch of Eq. (4.4) shown in Fig. 4.2(a). However, the dissipative soliton is not a global attractor. The saddle point's stable manifold (solid curve in Fig. 4.2(c-d)) denotes the upper boundary in phase space of the basin of attraction for the dissipative soliton. A droplet with frequency ω and position x_0 lying within the basin of attraction will generally increase in frequency and move toward the nanocontact center, then decrease in frequency to ω_*, converging to the dissipative soliton fixed point as illustrated in Figure 4.3. If initial

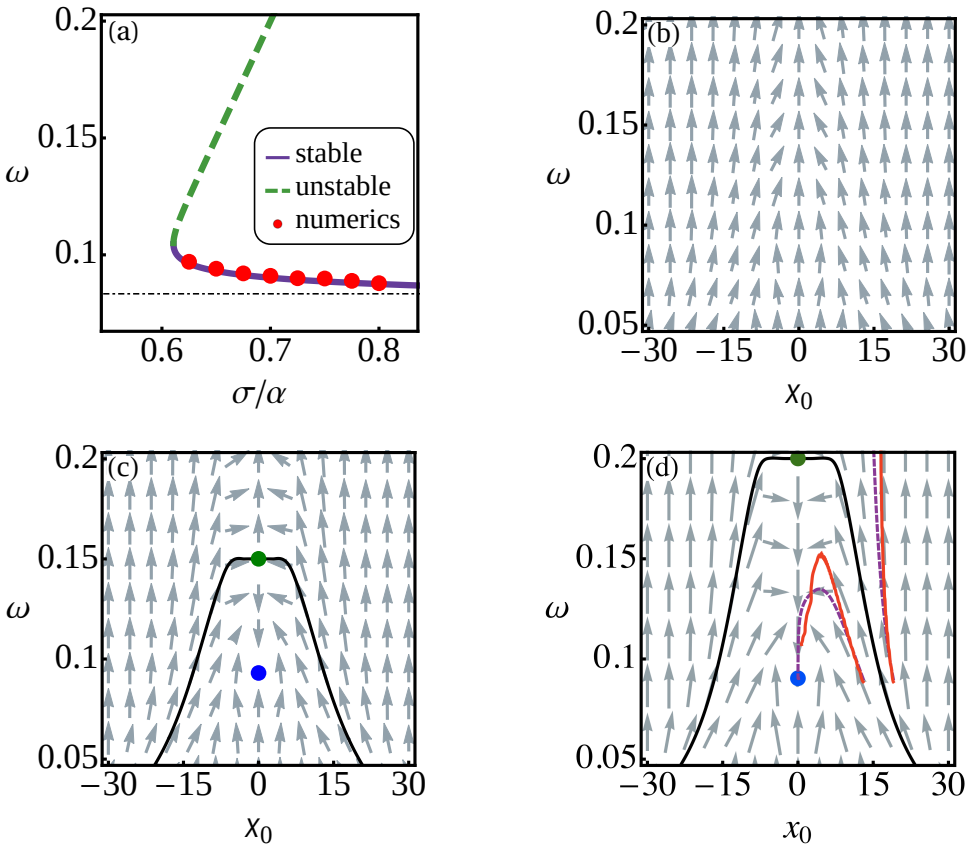

Figure 4.2 (a) Dissipative soliton relation (4.4). Horizontal line is $\omega = 1/\rho_\star$. (b-d) ODE vector fields corresponding to equations (4.4), (4.15) as σ varies (b) just before the saddle-node bifurcation (c), just after and (d) far past bifurcation. The upper/lower dot corresponds to the unstable/stable fixed point. The solid black curve encloses the basin of attraction. Parameters are $\rho_\star = 12$, $h_0 = 0.5$, and $\alpha = 0.01$. (d) includes trajectories from ODE theory (dashed) and micromagnetics (solid).

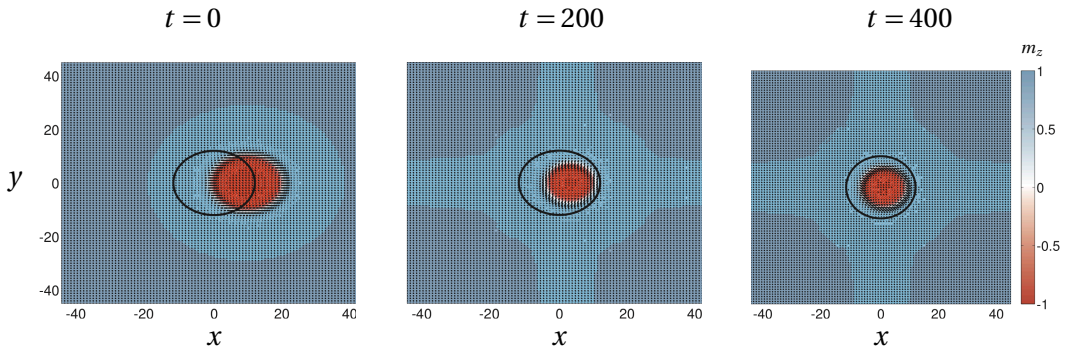

Figure 4.3 Time series plots of the magnetization illustrating the droplet centering on the nanocontact in long time. In the simulations presented here $\frac{\sigma}{\alpha} = .65$ and $\rho_* = 12$. The initial droplet frequency was selected as ω_*, but the initial droplet center is chosen just outside the nanocontact $x_0 = 13$.

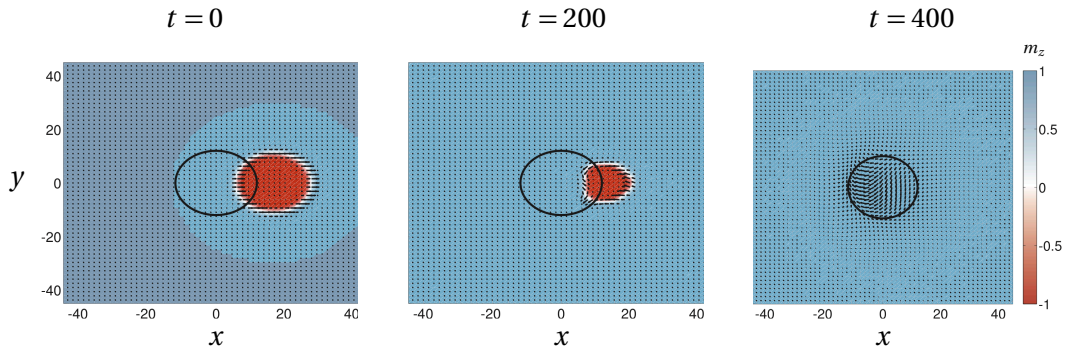

Figure 4.4 Time series plots of the magnetization illustrating the droplet outside the basin of attraction of the nanocontact decaying to the uniform state. In the simulations presented here $\frac{\sigma}{\alpha} = .65$ and $\rho_* = 12$. The initial droplet frequency was selected as ω_*, but the initial droplet center so that the droplet just overlaps the nanocontact $x_0 = 18$.

conditions lie outside the basin of attraction, the soliton will decay to spin waves (ω increases to 1) as in Figure 4.4.

That the dissipative soliton is not a global attractor was observed in micromagnetic simulations previously in the form of the drift instability [Hoe10]. As shown in Chapter 3, a magnetic field gradient can accelerate a stationary droplet, so it is reasonable to conjecture that STT provides a restoring force that could keep the droplet inside the nanocontact for a sufficiently small gradient. However, a sufficiently strong field gradient could lead to expulsion of the droplet, hence a drift instability. Further investigation of this requires the study of modulated propagating droplets in the presence of an NC-STO, because the perturbation due to an inhomogeneous field necessarily excites dynamics in V, see Eq. (3.4).

The other physical parameters in eq. (4.4) are h_0 and ρ_*. Figures 4.5 & 4.6 demonstrate that h_0 serves to shift the fixed point curves and that this shift is almost exactly h_0. Changes to h_0 have little to no visible impact on the corresponding frequency of the fixed point, ω_*, or phase portraits. The motivation for this observation is that in the limit of small ω and when the nanocontact and droplet radius are approximately equal, the denominator in the fixed point relation Eq. (4.4) is $\mathcal{O}(1)$.

Figure 4.7 depicts the basin of attraction radius ρ_b (the value of x_0 at the edge of the basin of attraction when $\omega = \omega_*$) scaled by ρ_*. As the current is increased, the basin radius rapidly exceeds

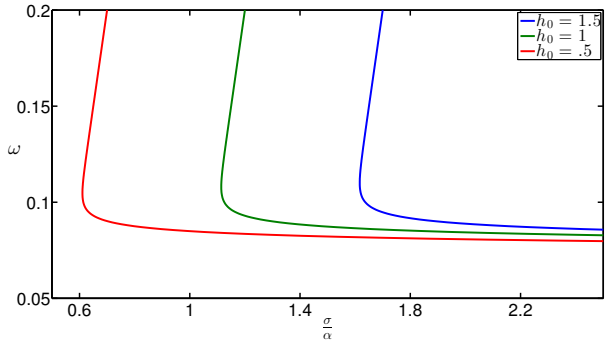

Figure 4.5 Fixed points, both stable and unstable for several values of h_0. The primary effect of h_0 is to shift these curves of fixed points along the $\frac{\sigma}{\alpha}$ axis. For the present purposes, it is not important to differentiate between the stable and unstable branches, since both are shifted in the same manner.

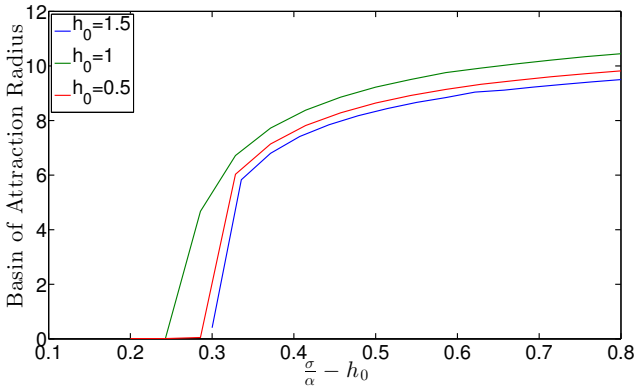

Figure 4.6 While the center of the basin of attraction depends on h_0, the width of the basin remains essentially unchanged as h_0 varies.

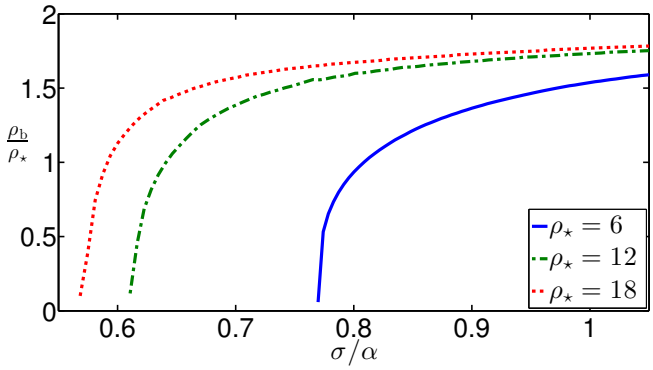

Figure 4.7 Basin of attraction radius, ρ_b at $\omega = \omega_*$ scaled by nanocontact radius, ρ_*.

$\frac{3}{2}\rho_*$ so that a droplet placed well outside the nanocontact may still experience a restoring force to the nanoncontact center.

The robustness of magnetic droplet solitons to symmetry breaking perturbations demonstrated here suggests that their initial observation in [Moh13] represents the beginning of a rich inquiry into novel nonlinear physics.

4.1.2 NC-STO and Spatially Inhomogeneous Applied Field

So far the focus has been on the stationary droplet. This was possible because the damping, Eq. 3.6 , and spin-torque, Eq. 4.1, perturbations satisfy the constraint that $\frac{d\mathbf{V}}{dt} = 0$ when $\mathbf{V} = 0$ which is shown by evaluating Eq. 2.40. In contrast, a spatially varying field cannot satisfy this constraint. In this section, the addition of weak spatial inhomogeneity of the applied magnetic field is considered, in addition to damping and spin-transfer torque. For simplicity, consideration will be restricted to a field that is linear in x.

This investigation has broader implications for the practical use and understanding of droplets in real devices. These three physical effects influence the system in competing ways, which can balance, allowing for the existence of stable droplets. Alternatively, a strong enough field gradient can push the droplet out of the NC-STO, giving rise to a previously unexplained drift instability [Hoe10].

As seen in Sec. 3.2, damping decreases the effective mass of the droplet. In Sec. 3.1, it was shown that a field inhomogeneity accelerates the droplet while leaving the mass of the droplet unaffected. The inclusion of forcing due to spin transfer torque in a nanocontact opposes both of these effects. As discussed in Section 4.1.1 the spin torque increases the droplet mass and generates an effective restoring force that centers the droplet in the nanocontact region. Hence, there could exist a delicate balance between all of these effects: the NC-STO restoring force balancing the potential force due to the field gradient and the mass gain due to spin-torque balancing the mass loss due to damping. Previous studies have been unable to identify when such a balance occurs and when it fails. Here, we analytically demonstrate stable droplets as fixed points of the modulation equations with all of these perturbations.

Because the perturbation components p_Θ and p_Φ appear linearly in the modulation equations (2.37)-(2.40), it is possible to simply add the field inhomogeneity eq. (3.3) and damping eq. (3.6) perturbations to those due to spin torque Eq. 4.1. The perturbation components are

$$p_\Theta = -\alpha(\omega + h_0 - \mathbf{V}\cdot\nabla\Phi)\sin\Theta + \sigma\mathscr{H}(\rho_* - r)\sin\Theta, \tag{4.7}$$

$$p_\Phi = \left(\nabla h_0 \cdot \hat{\boldsymbol{\rho}}\right)\rho - \alpha\mathbf{V}\cdot\nabla\Theta. \tag{4.8}$$

The coordinate r in the argument of the Heaviside function $\mathscr{H}$ is measured from the center of the nanocontact, which differs from the coordinates ρ and φ which are measured from the center of the droplet. The magnetic field is assumed to be spatially linear

$$h_0 = a + b\,x, \quad |b| \ll 1. \tag{4.9}$$

In this way, droplet motion is restricted to the x direction only. Insertion of the perturbations in Eq.

(4.7)- (4.8) into the modulation equations (2.37)-(2.40) results in the following system

$$\dot{\Phi}_0 = \frac{\alpha b V}{2\omega^2} - \frac{\sigma V}{4\pi}\int_\Xi \cos(\varphi)\operatorname{sech}^2\left(\rho - \frac{1}{\omega}\right)d\mathbf{x} \tag{4.10}$$

$$\dot{\xi} = V - \frac{\alpha b}{\omega} + \frac{\sigma\omega}{2\pi}\int_\Xi \cos(\varphi)\operatorname{sech}^2\left(\rho - \frac{1}{\omega}\right)d\mathbf{x} \tag{4.11}$$

$$\dot{\omega} = \alpha\omega^2(\omega + a) - \frac{\sigma\omega^3}{4\pi}\int_\Xi \operatorname{sech}^2\left(\rho - \frac{1}{\omega}\right)d\mathbf{x} \tag{4.12}$$

$$\dot{V} = -b\omega + \alpha V\omega(\omega + 2a) - \frac{\sigma V\omega}{4\pi}\int_\Xi \frac{(3\rho\omega + \cos(2\varphi) - 1)}{\rho}\operatorname{sech}^2\left(\rho - \frac{1}{\omega}\right)d\mathbf{x} \tag{4.13}$$

where $\xi = \xi_x$, $V = V_x$ and the integrals are performed over the nanocontact region, $\Xi = \left\{\mathbf{x} \in \mathbb{R}^2 \middle| |\mathbf{x}| < \rho_*\right\}$. None of the right hand sides in the equations above depend explicitly on the parameter Φ_0 so that the dynamics of the remaining parameters can be considered separately. For the remainder of the analysis the evolution of Φ_0 is ignored, noting that $\dot{\Phi}_0$ corresponds to a small frequency shift as in Eq. (3.1).

There is a complex interplay between the many small parameters in this problem. Since there is not an exact analytical solution, it is necessary that these perturbations dominate over the error terms in our approximate solution, while still remaining small. To keep an overall consistent error estimate it is required that $|V| \lesssim \omega^2$ for the approximate droplet. The variation in the applied field is a little more subtle. The actual requirement is that the applied field vary slowly compared to the length scale of the soliton. For the approximate droplet this length scale is roughly $1/\omega$, hence the requirement is that b/ω be small and $b \ll \omega$. In particular, this means b should be at least an order of magnitude smaller than the other parameters.

The stationary droplet without a field gradient is stable when centered on the nanocontact [Hoe10; BH13]. From the previous section, taking $\frac{dh_0}{dx} = b = 0$ and $V = 0$, the modulation equations (4.11)-(4.10) for propagating droplets exhibit the fixed point $(\xi, \omega, V) = (0, \omega_*, 0)$ when damping balances forcing. The precise relationship is the same as that given in Eq. 4.4 (taking $h_0 = a$). To be

explicit, in this context

$$\frac{\sigma}{\alpha}=\frac{2(a+\omega_*)}{1+\omega_*\left(\log\left(\frac{1}{2}\operatorname{sech}\left(\rho_*-\frac{1}{\omega_*}\right)\right)+\rho_*\tanh\left(\rho_*-\frac{1}{\omega_*}\right)\right)}. \tag{4.14}$$

For this section, a more careful analysis of the fixed point will be required. Recall, $\omega_* = \omega_*(\sigma)$ corresponds to the stable branch with a minimum sustaining value of the current corresponding to a saddle-node bifurcation. For σ sufficiently large, the stable branch quickly approaches

$$\omega_*=\rho_*^{-1}+\operatorname{arctanh}\left(\frac{2a\alpha}{\sigma}-1\right)\rho_*^{-2}+\mathcal{O}\left(\rho_*^{-3}\right),\quad \rho_*\gg 1,\quad 0<\omega_*-\rho_*^{-1}\ll 1. \tag{4.15}$$

Near the critical value $\sigma = 2a\alpha$, where the second term is zero, the asymptotic form is

$$\omega_*=\rho_*^{-1}+\left(\frac{2a\alpha}{\sigma}-1\right)\rho_*^{-2}+\left(\frac{2\alpha}{\sigma}+\ln 2\right)\rho_*^{-3}+\mathcal{O}\left(\rho_*^{-4}\right),\quad \left|\frac{2a\alpha}{\sigma}-1\right|=\mathcal{O}\left(\rho_*^{-1}\right). \tag{4.16}$$

Linearizing equations (4.11)- (4.13) about this fixed point, the Jacobian matrix is given by

$$J(0,\omega_*,0)=\begin{pmatrix}\lambda_1 & 0 & 1\\ 0 & \lambda_2 & 0\\ 0 & 0 & \lambda_3\end{pmatrix}, \tag{4.17}$$

$$\lambda_1=-\frac{1}{2}\sigma\rho_*\omega_*\operatorname{sech}^2\left(\rho_*-\frac{1}{\omega_*}\right), \tag{4.18}$$

$$\lambda_2=-\alpha a\omega_*+\lambda_1+\frac{1}{2}\sigma\omega_*\left(\tanh\left(\rho_*-\frac{1}{\omega_*}\right)+1\right), \tag{4.19}$$

$$\lambda_3=-2\alpha\omega_*^2+\lambda_2-\lambda_1. \tag{4.20}$$

Unlike the analysis on the stationary droplet, there is now a third eigenvalue (corresponding to the inclusion of velocity dynamics). This linearization therefore represents a generalization of that

considered in the previous section. Utilizing the approximation from Eq. (4.16),

$$\lambda_1 = -\frac{\sigma}{2} + \mathcal{O}\left(\rho_*^{-2}\right), \quad \lambda_2 \sim \lambda_1, \quad \lambda_3 = \left(-\alpha + \frac{\ln 2}{2}\sigma\right)\rho_*^{-2} + \mathcal{O}\left(\rho_*^{-4}\right), \quad \left|\frac{2a\alpha}{\sigma} - 1\right| = \mathcal{O}\left(\rho_*^{-1}\right). \quad (4.21)$$

Since $\rho_* > 1/\omega_*$, all three eigenvalues are negative when $\sigma > 2a\alpha$, so the fixed point will be stable. The critical forcing value $\sigma = 2a\alpha$, below which the droplet is predicted to be unstable could be considered as an estimate for the minimum sustaining current of a droplet [Hoe10]. Note, however, that this is a dubious estimate due to $\omega_* - \rho_*^{-1}$ not being a small quantity.

Next, consider the case of a small field gradient $0 < |b| \ll 1$. It will be shown that the droplet fixed point persists for very small $|b|$. These fixed points exist as a balance between the expulsive force provided by the field gradient and the attractive force provided by the nanocontact. This attraction manifests in nonzero ξ and V at the fixed point, so this balance can also be viewed as a balance between leading order effects (in V) and higher order effects (in $\dot{\xi}$). Unlike the $b = 0$ fixed point, exact analytical expressions for the fixed point cannot be found when $b \neq 0$ since the droplet is no longer centered on the nanocontact ($\xi \neq 0$). Nevertheless, it is possible to obtain an approximate form for these fixed points as follows. The structure of J in Eq. (4.17) yields very simple predictions in the regime of small field gradient. The key observation here is that the system of Eqs. (4.11)-(4.13) can be written as

$$\begin{pmatrix} \dot{\xi} \\ \dot{\omega} \\ \dot{V} \end{pmatrix} = F(\xi, \omega, V) - b \begin{pmatrix} \frac{\alpha}{\omega} \\ 0 \\ \omega \end{pmatrix}. \quad (4.22)$$

By virtue of the stationary fixed point, F satisfies $F(0, \omega_*, 0) = 0$. Next, seek a fixed point that slightly deviates from the stationary one according to $\xi = b\,\xi_1 + \cdots$, $\omega = \omega_* + b\,\omega_1 + \cdots$ and $V = b\,V_1 + \cdots$. Expanding and equating the right hand side of Eq. (4.22) to zero gives the correction

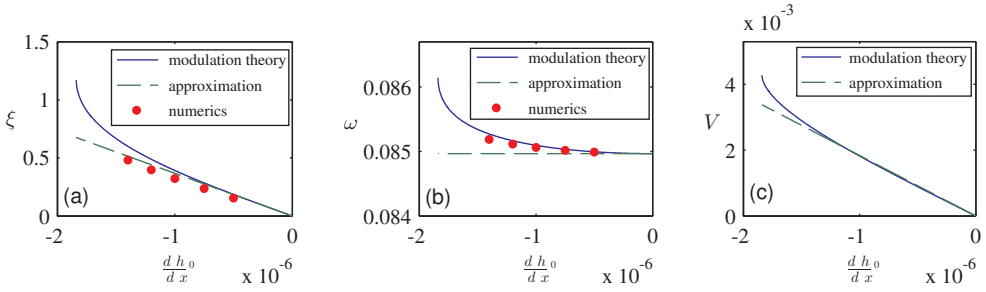

Figure 4.8 Fixed points from modulation theory, exact (solid) and approximate Eq. (4.23) (dashed), and direct numerical simulation of Eq. (1.8) (circles) when $\alpha = \sigma = 0.01$, $a = 0.5$, $\rho_* = 12$. In this case, the parameter V cannot be extracted from direct numerical simulations without additional assumptions (See Section 3.0.1). Accordingly, this data is not presented in (c).

$$\begin{pmatrix} \xi_1 \\ \omega_1 \\ V_1 \end{pmatrix} = J(0,\omega_*,0)^{-1} \begin{pmatrix} \frac{\alpha}{\omega_*} \\ 0 \\ w_* \end{pmatrix} = \begin{pmatrix} \frac{\alpha}{\lambda_1\omega_*} - \frac{\omega_*}{\lambda_1\lambda_3} \\ 0 \\ \frac{\omega_*}{\lambda_3} \end{pmatrix} \sim \begin{pmatrix} \frac{4\rho_*}{-2\alpha\sigma+\sigma^2\ln 2} \\ 0 \\ \frac{2\rho_*}{-2\alpha+\sigma\ln 2} \end{pmatrix}, \tag{4.23}$$

where the approximations (4.16) and (4.21) were used to obtain the large ρ_* estimate.

As summarized in Fig. 4.8, these simple expressions make predictions in good agreement with the fixed points found by numerical continuation in b and those observed in long time micromagnetic simulations of eq. (1.8) with perturbations (4.7) and (4.8) where the droplet relaxes to the fixed points shown in Fig. 4.8. The Jacobian matrix of Eqs. (4.11)-(4.13) can also be numerically evaluated, showing that all eigenvalues are negative, until continuation breaks down when one eigenvalue reaches zero. After this bifurcation, no fixed points were found. The condition of this eigenvalue reaching zero then corresponds exactly to the crossover where the attractive nanocontact is no longer strong enough to balance the expulsive force supplied by the field gradient. A strong enough field gradient, on the scale of $\alpha\sigma/2\rho_*$, can eject the droplet from the nanocontact, causing a drift instability previously observed in numerical simulations [Hoe10]. For the example studied here, $b \approx 10^{-6}$ compared to the NC-STO forcing magnitude $\sigma = 10^{-2}$ for a fixed point to no longer exist. This demonstrates that droplet attraction due to spin torque is quite weak. A strong enough field

gradient, sufficiently larger than $\frac{\alpha\sigma}{2\rho_*}$, can eject the droplet from the nanocontact, causing a drift instability previously observed in numerical simulations [Hoe10].

4.2 Other Forms of Spin Torque

Given the presence of damping, it is important to consider terms which could potentially oppose this in the medium and clearly the NC-STO offers just such a means to do so. However, in practice, it would be desirable to exploit a propagating droplet as a means of transferring information. While the field gradient offers a way to direct and control the droplet, the presence of damping will always cause the droplet to decay. The NC-STO is limited in that the droplet must be localized on or near the nanocontact. While it is theoretically possible to pattern a ferromagnetic wafer with nanocontact devices and push the droplet from one nanocontact to the next, this is unlikely to be practical in laboratory devices. It may be extremely difficult to find an appropriate balance of forcing and damping to observe this in experiment. As such it is desirable to consider other forms of spin-torque. Two other physical mechanisms are considered in this section: adiabatic spin-torque and the spin hall effect. Under the analysis provided by modulation theory, neither of these seem to be a suitable mechanism to stabilize the droplet. These forms of forcing are no longer localized and hypothetically could provide the appropriate balance to oppose damping globally in the medium, and hence a mechanism for a propagating dissipative droplet to be sustained. However, as the following analysis will show, this is not the case.

4.2.1 Adiabatic and Non-adiabatic Spin Torque

The form of spin torque considered here is exerted by a current as it flows in-plane interacting with the magnetization. The interaction of electrons with the magnetization can leave electron spins nearly parallel with the magnetization [Sti07], which is deemed an adiabatic response. Notably the adiabatic and non-adabatic spin-torques exert torques on the magnetization which are perpendicular to one another. This form of forcing has been of particular recent interest in manipulating the

dynamics of domain walls [LZ04; Sti07] and magnetic vortices [Shi06]. Therefore, it is reasonable to hypothesize that this form of forcing could stabilize the droplet. Following [Bea08], if the current flows uniformly in the **x** direction the model equation is

$$\frac{\partial \mathbf{m}}{\partial t} = -\mathbf{m} \times \mathbf{h}_{\text{eff}} - v \frac{\partial \mathbf{m}}{\partial x} + \beta \mathbf{m} \times \frac{\partial \mathbf{m}}{\partial x} \tag{4.24}$$

where $v \geq 0$ and $\beta \geq 0$ represent strength of the adiabatic and non-adiabatic spin-torques respectively. These constants are typically proportional to the current density in the medium. Executing a similar procedure as was used to derive the damping perturbations,

$$p_\Theta = -v \frac{\partial \Theta}{\partial x} - \beta \sin(\Theta) \frac{\partial \Phi}{\partial x} \tag{4.25}$$

and

$$p_\Phi = -v \sin(\Theta) \frac{\partial \Phi}{\partial x} + \beta \frac{\partial \Theta}{\partial x} \tag{4.26}$$

Substituting the approximate propagating droplet into Eqs 4.25 & 4.26 , adding the contribution from damping and using the result in Eqs 2.37-2.40 yields

$$\frac{d\xi_x}{dt} = V_x + v \tag{4.27}$$

$$\frac{d\xi_y}{dt} = V_y \tag{4.28}$$

$$\frac{d\omega}{dt} = \alpha\omega^2(h_0 + \omega) - \frac{1}{2}\beta\omega V_x \tag{4.29}$$

$$\frac{dV_x}{dt} = \beta\omega^2 + \alpha\omega(2h_0 + \omega) V_x \tag{4.30}$$

$$\frac{dV_y}{dt} = \alpha\omega(2h_0 + \omega) V_y - \beta V_x V_y \tag{4.31}$$

where terms have only been kept up to leading order in ω and V. By making the choice that the current flows in the $x-$direction only, the symmetry of the equations is broken and hence the

equations for V_x and V_y are not symmetric with respect to the exchange of x and y.

Stable fixed points are of particular interest here. Such fixed points would correspond to what might be observed in numerics or laboratory experiments. Accordingly, the first step in the analysis is to seek fixed points of the system in Eqs. 4.27-4.31. Eq. 4.27 is quite limiting. Seeking a solution in which the soliton center is not changing, i.e. $\dot{\xi}_x = 0$ requires that $V_x = -v$ This restriction implies there exists only one fixed point given by $\omega = 0$, $V_x = -v$ and $V_y = 0$, which corresponds to a reversed, uniform state. By instead working in a reference frame that moves to the right with velocity v, the restriction that $\dot{\xi}_x = 0$ is satisfied without requiring $V_x = -v$. Searching for fixed points in this frame yields the fixed points $V_y = 0$, $V_x = \frac{2\alpha\omega(\omega+h_0)}{\beta}$, and $\omega_\pm = -\frac{3h_0}{2} \pm \sqrt{h_0^2 - 2\frac{\beta^2}{\alpha^2}}$. However, for physically reasonable values of the parameters, $h_0^2 - 2\frac{\beta^2}{\alpha^2} < 0$ which leads to complex ω. Such solutions are not physically meaningful.

If the target is freely propagating droplets, however, it is natural to expect that $\dot{\xi}_x \neq 0$. Droplet the restriction of fixed point of the full system and looking instead for a fixed point of the subsystem Eqs. (4.29)-(4.30) does not lead to more desirable results. The restriction to two equations as opposed to three is made possible by taking $V_y = 0$ which trivially satisfies Eq. (4.31). This system admits three fixed points, none of which are physically relevant. The first $\omega = 0$, $V_x = 0$ again corresponds to a reversed, uniform state. The other two are complex conjugate pairs

$$\omega^\pm = -\frac{3h_0}{2} \pm \frac{\sqrt{-2\beta^2 + \alpha^2 h_0^2}}{2\alpha} \tag{4.32}$$

$$V_x^\pm = -\frac{\beta}{\alpha} + \frac{2h_0\left(\alpha h_0 \mp \sqrt{-2\beta^2 + \alpha^2 h_0^2}\right)}{\beta} \tag{4.33}$$

Again, to avoid the appearance of parameters, it is required that $h_0^2 - 2\frac{\beta^2}{\alpha^2} > 0$ which does not hold at physically reasonable values. Even if very large values of h_0 are chosen a straightforward stability analysis shows that for each of these fixed points at least one eigenvalue of the system is positive and such a fixed point would be unstable. While it remains possible that other terms could contribute to a complex balance which would stabilize the droplet in the presence of adiabatic and non-adiabatic

spin torques, it is the conclusion of this work that droplets are unlikely to be observed in this context.

4.2.2 Spin Hall Effect

Another mechanism for inducing spin torques is based on manipulation of the spin Hall effect [And08; Liu11; Liu12]. Like adiabatic spin torque, this form of spin-torque has its origin in a longitudinal charge current density. However, in the right experimental configuration, a transverse spin current density develops via spin-orbit scattering [Hir99]. Spin torque based on manipulation of the spin Hall effect offers a theoretical advantage in that the form of the forcing is relatively simple and therefore analytically tractable. In contrast, to the results of the preceeding section, this analysis does find the existence of a fixed point to the modulation equations in the presence of this kind of forcing that has physically admissible parameter values. However, this fixed point has two undesirable properties. First, the fixed point corresponds to a stationary droplet, whereas the hope was to sustain a propagating droplet. Worse, this fixed point is unstable and therefore unlikely to be observed in experiments.

Essentially, the spin Hall effect contributes the same term as the Slonczewski spin-torque contribution for the NC-STO, but the effect is global. The equation under study then is

$$\frac{\partial \mathbf{m}}{\partial t} = -\mathbf{m}\times\mathbf{h}_{\text{eff}} + \alpha\mathbf{m}\times(\mathbf{m}\times\mathbf{h}_{\text{eff}}) + \sigma\mathbf{m}\times(\mathbf{m}\times\hat{\mathbf{z}})$$

which is a modification of Eq. (1) from [Liu11]. The spin hall effect always induces an in plane stray field, which is neglected here. Assuming the droplet is propagating only in the $x-$direction, the modulation equations can be reduced to the 2×2 system below.

$$\begin{pmatrix} \frac{d\omega}{dt} \\ \\ \frac{dV}{dt} \end{pmatrix} = \begin{pmatrix} \frac{1}{2}\omega(2\omega(\alpha(h_0+\omega)-\sigma)) \\ \\ 2(h_0\alpha-\sigma)\omega V \end{pmatrix} \tag{4.34}$$

Eq. 4.34 admits 4 fixed points

$$\omega = 0 \qquad V = 0 \tag{4.35}$$

$$\omega = h_0 - \frac{\sigma}{\alpha} \qquad V = -2i\left(h_0 - \frac{\sigma}{\alpha}\right) \tag{4.36}$$

$$\omega = h_0 - \frac{\sigma}{\alpha} \qquad V = 2i\left(h_0 - \frac{\sigma}{\alpha}\right) \tag{4.37}$$

$$\omega = -h_0 + \frac{\sigma}{\alpha} \qquad V = 0 \tag{4.38}$$

Only the last of these fixed points is of physical interest. The fixed point in (4.35) corresponds to the uniform reversed state, $m_z = -1$. The fixed points in Eqs (4.36)&(4.37) have complex velocities, which are disregarded as physically meaningless. This leaves only the fixed point in Eq. (4.38) to consider, which requires the admissibility condition $\frac{\sigma}{\alpha} > h_0$. The linearization of this system about this fixed point is given by

$$\frac{d\mathbf{z}}{dt} = \begin{pmatrix} \frac{1}{2}\omega(2\alpha\omega + 2(\alpha(h_0+\omega)-\sigma)) + \frac{1}{2}\left(2\omega(\alpha(h_0+\omega)-\sigma)+\alpha V^2\right) & \alpha V\omega \\ 2V(\alpha h_0 - \sigma) + 2\alpha V\omega & \alpha\omega^2 + 2\omega(\alpha h_0 - \sigma) + \frac{9\alpha V^2}{4} \end{pmatrix}\mathbf{z} \tag{4.39}$$

Evaluating the Jacobian at the fixed point of interest yields

$$J = \begin{pmatrix} \frac{(\sigma-\alpha h_0)^2}{\alpha} & 0 \\ 0 & -\frac{(\sigma-\alpha h_0)^2}{\alpha} \end{pmatrix} \tag{4.40}$$

Since this matrix is diagonal, the eigenvalues are easily read off. Both are real and one strictly positive, the other strictly negative. The strictly positive eigenvalue corresponds to growth of ω and defines the unstable direction. Hence the fixed point will not be stable with the unstable manifold in the ω-direction. The conclusion of this analysis is that the droplet is unlikely to be observed in the presence of spin hall torque alone and the droplet is most likely to decay to the uniform state.

4.3 Summary

The analysis of this section offers a theoretical framework for understanding the observations of droplets made in [Moh13; Mac14]. In particular, spin-torque can balance the natural damping of a material and a droplet may be stabilized in a nanocontact. This process selects a single frequency dependent on the NC-STO's properties, suggesting a tuning mechanism for spin-torque oscillators. However, the geometric contribution of the nanocontact seems to play a critical role in the existence of the dissipative droplet. In the absence of a nanocontact, other mechanisms of spin-torque appear to not be able to stabilize the droplet on their own. Nevertheless, the droplet is quite robust in the context of the nanocontact and the theory here offers the first steps toward learning how to manipulate the droplet in experiments. Further work is still required to include more effects, such as the stochastic perturbation due to finite temperature, to move even closer to laboratory experiments.

CHAPTER

5

NUMERICAL COMPUTATION OF DROPLET SOLITONS

The previous chapters investigated extensions of the Landau-Lifshitz equation utilizing an approximate analytical framework. In one such example, Section 4.1.1, that analysis concluded the existence of a stable, time-periodic droplet-like structure in an extended model. These conclusions were backed up by direct numerical simulations and analysis on the resulting time series. Relying on time marching to compute time-periodic solitons in extended models is not only computationally expensive, but will only reveal stable solutions whose basin of attraction includes the initial data. The aim of this chapter is to take the initial steps toward developing an efficient numerical method suitable for the direct compution of solitons in this extended context. Such methods would enable direct computation of a bifurcation diagram (similar to Figure 4.2d) for truly time periodic solutions of the full nonlinear partial differential equation, offer a more accurate means of validating the conclusions of the previous chapters and enable the study of solitons when methods of the previous chapters are not applicable.

Much work has been devoted to the numerical computation of solitons and accordingly there are many strategies which have been employed. One common approach is the Petviashvili method, which was originally proposed to compute solitons for power-law nonlinearity [Pet76]. The Petviashvili method, crudely speaking, converts a partial differential equation of this type into a functional which can converge under fixed point iteration. This method remains popular today with recent application, for example, to solutions of the Dysthe equation (an NLS-type model for water waves with higher order corrections) [FD12]. However, the method does not guarantee a convergent iteration except in special cases [PS04] and extensions of the method to more general equations is an area of active research [LY07; ÁD14b; ÁD14a]. A similar scheme to the Petviashvili method called spectral renormalization was developed [AM05]. This method instead operates in Fourier space and obtains convergence by rescaling the Fourier coefficients by a constant self-consistently determined via an integral equation. The method has been successfully used in previous work to compute propagating droplet solitons [HS12]. In addition to these schemes, there exist other methods for computing solitons based on fixed point iteration such as the squared-operator iteration [YL07] and variational iteration methods [HW06; He07; Abb07] which also enjoy popularity. However, since all these methods are based on fixed point iteration, they all converge linearly and it may be desirable to use a scheme with faster nonlinear convergence properties.

In addition to these schemes, there exist Newton based approaches (e.g. [Yan09; Yan02]) which address exactly this concern. Similar to the methods already discussed, these methods convert the partial differential equation into a nonlinear functional where the roots of the functional correspond to the soliton. A variant on this idea called the adjoint continuation method has recently been employed in a number of systems [AW10b; AW10a; Wil11]. This method converts the problem of finding roots of the functional into a minimization problem and then leverages recent advances in numerical optimization to compute the soliton. The adjoint continuation method has the desirable property that it is no longer necessary for the number of unknowns (e.g. spatiotemporal Fourier components) to match the number of equations because the temporal dependency is enforced

via an adjoint calculation. Hence additional parameters can potentially be determined with the addition of specific constraints, provided a solution actually exists. This method is briefly explored in Section 5.2, but proves unsuitable for the computation of conservative droplet solitons.

As is done in Chapter 2, solitons are often viewed as fixed points of a nonlinear system. To do this, typically an ansatz is made such as is done for the droplet in Section 1.1.2. This converts the problem of soliton computation into a nonlinear eigenvalue problem and greatly reduces the complexity involved at the cost of generality. Often soliton solutions are time-periodic, as is the case for the Landau-Lifshitz equation. If the ansatz does not scale out the time-dependence, some generality can be regained, but at the cost of multiplying the size of the computational problem. Viewing the soliton either as a fixed point or a time-periodic orbit frames soliton computation in the classical terms of bifurcation analysis. Problems of this sort have been extensively studied in the context of ordinary differential equations. In principle, it would be possible to leverage well-established software packages in bifurcation analysis such as `AUTO` [Doe81] or `MATCONT` [Dho03]. Unfortunately, once discretized, partial differential equations often have too many unknowns for such packages to be practical and these investigations are typically limited to problems in (1+1)D with relatively coarse discretizations [CS07].

An additional motivation for pursuing a new method for the computation of droplets comes from interaction problems discussed earlier. In [Mai14], we observed that the interaction of two droplets could resolve into an apparently stable, time-periodic state which was not a droplet (called a breather). The simplest breather observed there arose from the interaction of two stationary droplets initially in phase. When situated far enough apart that the support of the droplets only weakly overlapped, these two droplets were attracted toward each other. An explanation of this phenomenon is given in Section 3.4.2. In long times the droplets merged, forming a droplet-like structure with a boundary that modulated shape with the precession frequency (See Figure 5.1) . Such a structure like this populates higher temporal Fourier harmonics than a stationary droplet residing in one Fourier component. Therefore, the computation cannot be approached as a nonlinear

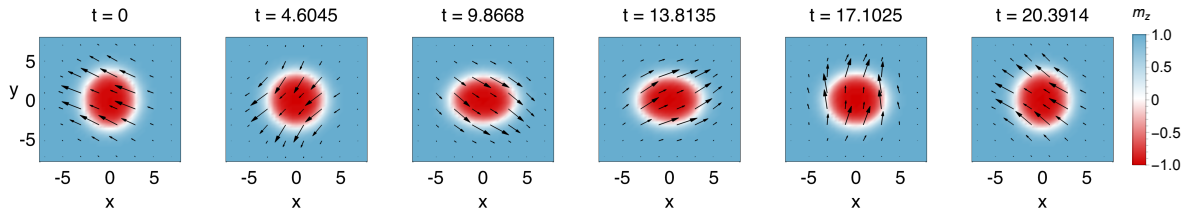

Figure 5.1 Time series of breather solution from [Mai14]. Notice that as time evolves, the boundary of this structure evolves as well. The structure is stationary and periodic with precession frequency $\omega \approx .3$

eigenvalue problem. Furthermore, while spectral renormalization is known to compute droplets as the solution to a nonlinear eigenvalue problem, this method is expected to converge to the ground state [PS04], the droplet for this problem. Even if the spectral renormalization method of [HS12] were generalized to include more than a single Fourier mode in time, it would not resolve this state and another method would be needed.

The next section makes precise the problem under consideration and subsequent sections outline different approaches taken, mostly based on Newton's method. The conclusion of this work is that the methods are unsuitable for a large scale numerical investigation of the droplet. Among other problems, these methods suffer from current limitations of computer memory. Even with Jacobian-free approaches such as Newton-GMRES, the cost of storing the Krylov basis becomes prohibitive in (2+1)D for discretizations necessary to fully resolve the droplet. While the method is demonstrated to work on the (2+1)D problem with large computational expense, the application of this method to the breather converges to the underlying droplet. This leaves the possibility that the initial data provided based on Figure 5.1 is not in the basin of attraction for Newton's method or that the observations in [Mai14] were of a metastable state that in longer time would have decayed to the droplet. If the latter, this would indicate that there may not exist exact breathers of this sort to the Landau-Lifshitz equation.

5.1 Problem Statement

The basic goal is to find localized, time-periodic solutions to the Landau-Lifshitz equation. The particular focus is to find (numerically) solutions which are valid in more realistic models of physical experiments or cannot be characterized by a single frequency mode. Since shooting methods and the adjoint continuation method have failed in the past, the approach tried here is to consider this as a boundary value problem in space and time. That is we seek solutions of

$$\begin{cases} \imath\left(\dfrac{\partial w}{\partial t} - \mathbf{V}\cdot\nabla w\right) - \nabla^2 w + \dfrac{2w^*\nabla w\cdot\nabla w + w\left(1-|w|^2\right)}{1+|w|^2} + \epsilon P[w] = 0 \\ \\ w(x,0) = w_0(x), \qquad w(x,T) = w_0(x), \qquad x\in\mathbb{R}^n, \qquad \lim\limits_{|x|\to\infty} w(x,t) \to \bar{w}\in\mathbb{C}, \quad t\in[0,T] \end{cases} \tag{5.1}$$

The unknowns in this problem are the period, T and the initial data $w_0(x)$. The term $\epsilon P[w]$ represents any number of arbitrary other terms which we wish to incorporate at a later date: damping, Slonczewski Spin-Torque etc. The $-\mathbf{V}\cdot\nabla w$ term comes from the fact that we may wish to consider propagating solutions. Such solutions will (in general) not be periodic in time in the "lab frame". As a result, we formulate the problem in the co-moving frame. The constant $\bar{w}$ satisfies the stationary problem,

$$\frac{\bar{w}(1-|\bar{w}|^2)}{1+|\bar{w}|^2} + \epsilon P[\bar{w}] = 0 \tag{5.2}$$

It is convenient to work with the stereographic form of because of (a) it's similarity to NLS where similar methods have been successful in the past and (b) there are obvious linear terms which suggest a preconditioner.

5.1.1 Simplest Problem

To start, this section considers the (1+1)D problem without additional terms ($\epsilon = 0$). In this case, a family of solutions is known and we will test the method by doing numerical continuation within the family of solutions. Since one of the parameters for this family of solutions is the frequency

ω, $T = \frac{2\pi}{\omega}$ will be fixed. Additionally, the spatial domain will be restricted to $[-L, L]$ instead of $\mathbb{R}$. Since the solution is required to decay to a constant $\bar{w}$, it is possible to utilize periodic boundary conditions in space as well. Hence, the target is a solution to

$$\begin{cases} \imath\left(\dfrac{\partial w}{\partial t} - V\dfrac{\partial w}{\partial x}\right) - \dfrac{\partial^2 w}{\partial x^2} + \dfrac{2w^*\left(\frac{\partial w}{\partial x}\right)^2 + w\left(1-|w|^2\right)}{1+|w|^2} = 0 \\ \\ w(x,0) = w(x,T) = w_0(x), \qquad w(-L,t) = w(L,t), \\ \\ \qquad x \in [-L,L], \qquad\qquad t \in [0,T] \end{cases} \tag{5.3}$$

Because of the periodic boundary conditions, a Fourier discretization may be used in space and time and the problem can be reformulated as a nonlinear function which vanishes for solutions of Eq. (5.3). That is, Eq. (5.3) is solved by zeroing

$$\begin{aligned} &F[w] = \imath\frac{\partial w}{\partial t} - \imath V\frac{\partial w}{\partial x} - \frac{\partial^2 w}{\partial x^2} + \frac{2w^*\left(\frac{\partial w}{\partial x}\right)^2 + w\left(1-|w|^2\right)}{1+|w|^2} = 0 \\ \\ &F : \mathcal{C}^2(\mathbb{R}\times[0,T],\mathbb{C}) \to \mathcal{C}(\mathbb{R}\times[0,T],\mathbb{C}) \end{aligned} \tag{5.4}$$

using Newton's method, where the periodic boundary conditions are encoded in the discretization.

5.2 Adjoint Continuation Method

This section explores the feasibility of the adjoint continuation method (ACM) for the Landau-Lifshitz equation. What follows describes the general setup of ACM as explained in Section 4 of [AW10b]. The basic problem attempts to minimize

$$G[w_0] = \int_{-\infty}^{\infty} \|w(x,T) - w_0(x)\|^2 \, dx \tag{5.5}$$

with respect to $w_0(x)$ where $w(x,t)$ satisfies Eq. (5.3). In principle, a minimization procedure could be used to compute the period T as well as the initial data, w_0, but for current purposes, the period is treated as given. The minimization is conducted by seeking a zero of the gradient. Hence it is necessary to find an efficient means to evaluate the gradient numerically. A brief explanation of how this is done is provided here. For notational simplicity $\mathcal{N}[w]$ will be defined to be such that the differential equation $\frac{\partial w}{\partial t} = \mathcal{N}[w]$ is equivalent to Eq. (5.3).

Computing the variational derivative of Eq. 5.5

$$\dot{G}[w_0,T] \equiv \frac{\partial}{\partial \epsilon} G(w_0+\epsilon v_0)\Big|_{\epsilon=0} = \int_{\mathbb{R}} [w(x,T)-w_0(x)][v(x,T)-v_0(x)]dx \equiv \int_{\mathbb{R}} \frac{\delta G}{\delta w_0} v_0 dx \equiv \left\langle \frac{\delta G}{\delta w_0}, v_0 \right\rangle \quad (5.6)$$

where v satisfies the PDE given by the linearization of $\mathcal{N}$, namely $\frac{\partial v}{\partial t} = D\mathcal{N}[w]v,\ v(x,0) = v_0(x)$ (an explicit expression will be given shortly). If this was where the computation was left, evaluation of the gradient, $\frac{\delta G}{\delta w_0}$, would require evolving the PDE for v N times where N is the number of grid-points in the discretization. However, significant gains can be made by evaluating the adjoint PDE $\frac{\partial u}{\partial s} = -D\mathcal{N}[w[T-s]]^\dagger u,\ u(x,0) = u_0(x) = w(x,T)-w_0(x)$. A brief digression explains why and exactly what properties the adjoint PDE satisfies. Defining u in the fashion described,

$$\left\langle \frac{\partial}{\partial s} u(\cdot,s), v(\cdot,T-s) \right\rangle = -\left\langle D\mathcal{N}^\dagger(w(\cdot,T-s))u, v(\cdot,T-s) \right\rangle \quad (5.7)$$

$$= -\langle u(\cdot,s), D\mathcal{N}(w(\cdot,T-s))v(\cdot,T-s)\rangle \quad \text{(by definition of the adjoint)} \quad (5.8)$$

$$= -\left\langle u(\cdot,s), \frac{\partial v(\cdot,T-s)}{\partial (T-s)} \right\rangle \quad (5.9)$$

The critical claim here is that $\frac{d}{ds}\langle u(\cdot,s), v(\cdot,T-s)\rangle = 0$.This is readily verified by the computation

$$\frac{\partial}{\partial s}\langle u(\cdot,s), v(\cdot,T-s)\rangle = -\left\langle \frac{\partial u(\cdot,s)}{\partial s}, v(\cdot,T-s) \right\rangle + \left\langle u(\cdot,s), \frac{\partial v(\cdot,T-s)}{\partial s} \right\rangle \quad (5.10)$$

$$= \left\langle u(\cdot,s), \frac{\partial v(\cdot,T-s)}{\partial (T-s)} \right\rangle - \left\langle u(\cdot,s), \frac{\partial v(\cdot,T-s)}{\partial (T-s)} \right\rangle \quad (5.11)$$

$$= 0 \quad (5.12)$$

This calculation implies that $\langle u(\cdot,s), v(\cdot,T-s)\rangle$ is constant and $\langle u(\cdot,0), v(\cdot,T)\rangle = \langle u(\cdot,T), v(\cdot,0)\rangle$. It is this relation which enables efficient evaluation of the gradient.

$$\begin{aligned}
\dot{G} &= \langle u_0(\cdot), v(\cdot,T) - v_0(\cdot)\rangle \\
&= \langle u_0(\cdot), v(\cdot,T)\rangle - \langle u_0(\cdot), v_0(\cdot)\rangle \\
&= \langle u(\cdot,T), v_0(\cdot)\rangle - \langle u_0(\cdot), v_0(\cdot)\rangle \\
&= \langle u(\cdot,T) - u_0(\cdot), v_0(\cdot)\rangle \\
&= \left\langle \frac{\delta G}{\delta w_0}, v_0(\cdot)\right\rangle.
\end{aligned}$$

With this property, evaluation of the gradient is reduced to a single evolution of the adjoint PDE to determine $u(x,t)$ and a series of inner products.

For Eq. (5.3), the linearization is given by

$$\begin{cases} i v_t = \quad v_{xx} - \frac{4w^* w_x v_x}{1+|w|^2} + \frac{\left(-1+2|w|^2+|w|^4+2w^{*2}w_x^2\right)}{(1+|w|^2)^2} v + \frac{\left(2w^2-2w_x^2\right)}{(1+|w|^2)^2} v^* \\ v(x,0) = v_0(x). \end{cases} \tag{5.13}$$

The algebraic details of this computation are in Appendix B.5.1. The adjoint of this linearization is given by

$$\begin{cases} -i u_t = \quad u_{xx} + \left(\frac{4w^* w_x u}{1+|w|^2}\right)_x + \frac{-1+2|w|^2+|w|^4+2w^2(w_x^{*2})}{(1+|w|^2)^2} u + \frac{2w_x^2-2w^2}{(1+|w|^2)^2} u^* \\ u(x,0) = u_0(x) = w(x,T) - w_0(x). \end{cases} \tag{5.14}$$

which is carefully derived in Appendix B.5.2. Numerical evaluation of the hessian remains computationally expensive. Accordingly a quasi-Newton method of the Broyden-Fletcher-Goldfarb-Shanno (BFGS) algorithm is the standard choice for optimization. In the studies attempted here, Tim Kelley's implementation `bfgswopt.m` [Kel11] was used to perform the optimization. The theory for Newton's method in the complex plane is more restrictive, requiring the function to be analytic to properly define the Newton iterates. To avoid this, optimization was performed over the real and imaginary

parts of w_0. BFGS requires an initial guess for the hessian, which was here taken to be the identity. Such a choice is not atypical [Kel11].

Time-marching for Eqs. (5.3) and (5.14) was performed with an 11-stage, 8th order explicit Runge-Kutta method [CV72]. The high order of the method significantly improved evaluation times compared to more traditional methods like the Runge-Kutta-Fehlberg algorithm without drastically altering the stability properties of the method. Similar high-order approaches have been used in previous implementations of ACM [WY12]. Figure 5.2 makes a comparison between the stability region of this method compared to the classical 4th order Runge-Kutta method. Spatial discretization

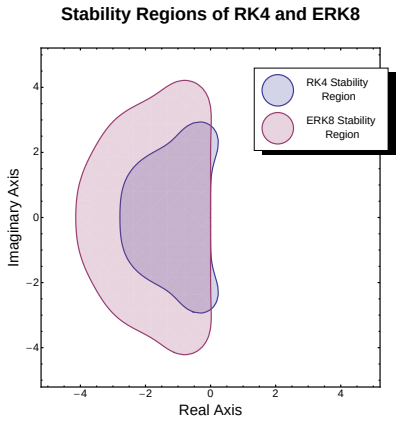

Figure 5.2 Plot comparing the stability regions of the explicit 8^{th} order Runge-Kutta method used here and the classical 4^{th} order Runge-Kutta method. The method chosen has a higher-order of accuracy, but does not suffer significantly decreased stability properties and is suitable for use on non-stiff problems.

of the PDEs was done via a Fourier spectral method. Since Eq. (5.3) admits an exact analytical solution [Kos90], the accuracy of the method can be directly queried. A careful investigation of the discretization was conducted to determine the impact of time-step size and spatial resolution on the accuracy of the solution. Taking the known solution, the difference between the initial and final states was used as a surrogate for the global error. The results of that investigation are summarized in Figure 5.3. Using these as a guide, the discretization parameters were chosen such that the

global error in the computed solution was less than 10^{-10}. Typical choices took the spatial domain where$L = 50$ with 512 grid points in space ($\delta x \approx .2$) and $\delta t \approx 0.03$ for the time step, yielding an estimated error in time on the order of 10^{-12}.

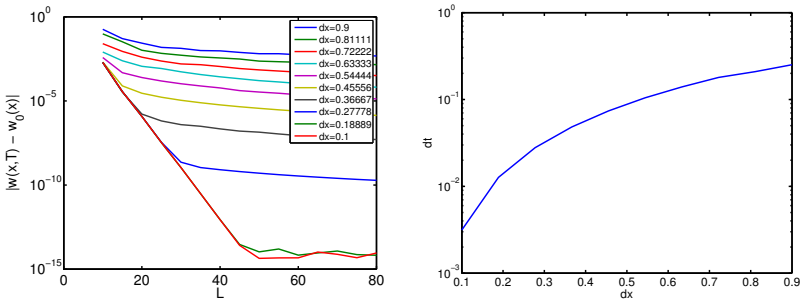

Figure 5.3 (left) The difference between the initial and final states using the known stationary soliton solution with $\omega = 0.5$, for a range of domain sizes L and mesh widths dx. The time step $dt = 10^{-4}$ was held fixed. (right) Holding $L = 50$ fixed, for a given dx the time step was increased until $\|w(x,T) - w_0(x)\|_\infty$ increased beyond 10^{-3}. The error increased dramatically as the edge of the stability region was reached. Together the right and left plots can be used as a guide for choosing optimal grid resolutions.

The evaluation of the gradient was also extensively validated. This was done in two ways. The first was based on comparison to a finite difference approximation of the gradient. For several randomly selected localized function w and v, the quantity $G(w+\epsilon v) - G(w) - \epsilon\langle G'[w], v\rangle = \mathcal{O}\left(\epsilon^2\right)$ was computed for a range of ϵ. The residual was then computed and fit to a function of the from $C\epsilon^p$, with the expectation that $p \approx 2$. For every test there was good agreement, supporting that the numerical implementation of the gradient was correct. An example is provided in Figure 5.4

An additional test was run by implementing the linearized PDE. Rather than evaluate the gradient using this method, the linearized PDE solution was used to verify numerically that the desired property of the adjoint PDE was satisfied, namely that $\langle u(s), v(T-s)\rangle$ is constant. This property held to a remarkable degree for a wide range of choices of w_0 and v_0 chosen to be exponentially localized solutions, but otherwise dissimilar to the analytical solution. An example of such a test is shown in Figure 5.5.

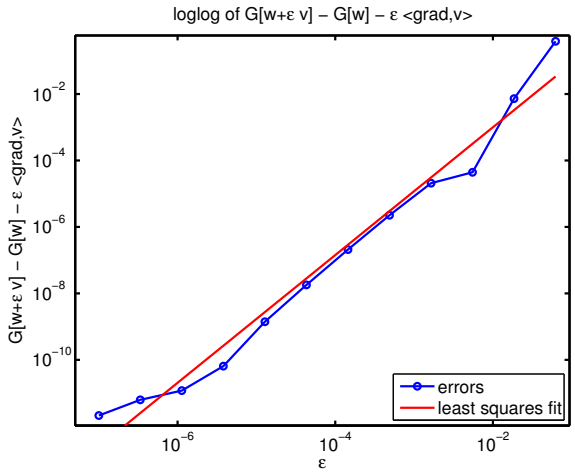

Figure 5.4 This plot is one example of the finite difference test done to validate the gradient. The functions w and v used in this test were Guassians of different length scales, chosen to be quite far from the known analytical solution. The least squares fit of the residuals is given by $6.95908 * \epsilon^{1.92215}$ which matches nicely with the theoretical expectation.

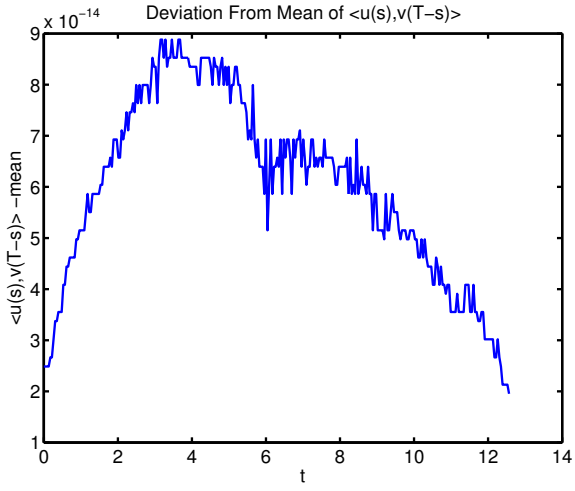

Figure 5.5 This graph shows the deviation from the mean of $\langle u(s), v(T-s)\rangle$.

Despite these efforts to validate the implementation, ACM never converged to the soliton solution. Private communications with the authors of [AW10b] revealed that the method worked best for problems for which the solution was a global attractor. This is not the case for the droplet. Further communication revealed that ACM used with BFGS is highly sensitive to the initial estimate of the hessian. Apparently it has been necessary in past work to allow many hundreds or thousands of iterations of a first line search for BFGS to sufficiently update the hessian estimate. Once the hessian estimate was sufficiently accurate, ACM did converge in those applications. Additionally it was recommended that the PDEs be solved in quadruple precision. Since the ultimate aim of this work was to compute droplet solitons in (2+1)D, it seemed unlikely that these requirements would allow ACM to be a viable option. At this point, ACM was abandoned in favor of a different Newton based method, which is discussed in the next section.

5.3 Newton-GMRES approach

The approach taken in this section simply attempts to solve Eq. (5.3) as a boundary value problem in space and time. Newton's method does typically converge for complex-valued functions of complex variables, as briefly discussed in the previous section. However, this issue is readily patched by converting a nonlinear function which maps real-valued functions to real-valued functions. To do this, let $w = u + \imath v$, where u and v represent the real and imaginary parts of w. Executing this procedure, an equivalent functional

$$G[u,v] = \begin{bmatrix} -\dfrac{\partial v}{\partial t} + V\dfrac{\partial v}{\partial x} - \dfrac{\partial^2 u}{\partial x^2} + \dfrac{2u\left(\left(\frac{\partial u}{\partial x}\right)^2 - \left(\frac{\partial v}{\partial x}\right)^2\right) + 4v\frac{\partial u}{\partial x}\frac{\partial v}{\partial x} + u(1-u^2-v^2)}{1+u^2+v^2} \\ \dfrac{\partial u}{\partial t} - V\dfrac{\partial u}{\partial x} - \dfrac{\partial^2 v}{\partial x^2} + \dfrac{-2v\left(\left(\frac{\partial u}{\partial x}\right)^2 - \left(\frac{\partial v}{\partial x}\right)^2\right) + 4u\frac{\partial u}{\partial x}\frac{\partial v}{\partial x} + v(1-u^2-v^2)}{1+u^2+v^2} \end{bmatrix} \tag{5.15}$$

$$G : \mathcal{C}^2(\mathbb{R}\times[0,T]) \times \mathcal{C}^2(\mathbb{R}\times[0,T]) \to \mathcal{C}(\mathbb{R}\times[0,T]) \times \mathcal{C}(\mathbb{R}\times[0,T])$$

is obtained. The function G is equivalent in the sense that $F[u+\imath v] = (G[u,v])_1 + \imath(G[u,v])_2$ (F as defined by Eq (5.4)). Most importantly, G vanishes exactly where F vanishes, thus solutions of G can be used to construct solutions to Eq. (5.3). In practice, it is not necessary to implement the function G numerically, rather G can be evaluated by composing F with maps which identify $\mathbb{R}^2$ with the complex plane and vice versa.

In order to apply Newton-GMRES it is not necessary to compute and store the Jacobian. However, an algorithm to compute the matrix vector product for the Jacobian is required. This is often done with finite differences, but in this case, an analytical form of the matrix vector product can be derived, which offers accuracy gains and little additional computational cost. This is done by computing the Frechét derivative of G which is done in Appendix B.5.3. The result is given by

$$DG[u,v]\begin{pmatrix} q \\ w \end{pmatrix} = \begin{pmatrix} \left\{ \begin{array}{r} -\frac{\partial w}{\partial t} + V\frac{\partial w}{\partial x} - \frac{\partial^2 q}{\partial x^2} + q\Big(-\frac{2u\left(u(1-u^2-v^2)+2u\left(\left(\frac{\partial u}{\partial x}\right)^2-\left(\frac{\partial v}{\partial x}\right)^2\right)+4v\left(\frac{\partial u}{\partial x}\right)\left(\frac{\partial v}{\partial x}\right)\right)}{(1+u^2+v^2)^2} + \frac{1-3u^2-v^2+2\left(\left(\frac{\partial u}{\partial x}\right)^2-\left(\frac{\partial v}{\partial x}\right)^2\right)}{1+u^2+v^2} \Big) \\ +\frac{4v\left(\left(\frac{\partial q}{\partial x}\right)\left(\frac{\partial v}{\partial x}\right)+\left(\frac{\partial u}{\partial x}\right)\left(\frac{\partial w}{\partial x}\right)\right)}{1+u^2+v^2} + \frac{4u\left(\left(\frac{\partial q}{\partial x}\right)\left(\frac{\partial u}{\partial x}\right)-\left(\frac{\partial v}{\partial x}\right)\left(\frac{\partial w}{\partial x}\right)\right)}{1+u^2+v^2} + w\left(\frac{4\left(\frac{\partial u}{\partial x}\right)\left(\frac{\partial v}{\partial x}\right)-2uv}{1+u^2+v^2} - \frac{2v\left(u(1-u^2-v^2)+2u\left(\left(\frac{\partial u}{\partial x}\right)^2-\left(\frac{\partial v}{\partial x}\right)^2\right)+4v\left(\frac{\partial u}{\partial x}\right)\left(\frac{\partial v}{\partial x}\right)\right)}{(1+u^2+v^2)^2} \right) \end{array} \right\} \\ \left\{ \begin{array}{r} \frac{\partial q}{\partial t} - V\frac{\partial q}{\partial x} - \frac{\partial^2 w}{\partial x^2} + q\Big(-\frac{2u\left(v(1-u^2-v^2)+4u\left(\frac{\partial u}{\partial x}\right)\left(\frac{\partial v}{\partial x}\right)-2v\left(\frac{\partial u}{\partial x}\right)^2-\left(\frac{\partial v}{\partial x}\right)^2\right)}{(1+u^2+v^2)^2} + \frac{4\left(\frac{\partial u}{\partial x}\right)\left(\frac{\partial v}{\partial x}\right)-2uv}{1+u^2+v^2} \Big) \\ +\frac{4u\left(\left(\frac{\partial q}{\partial x}\right)\left(\frac{\partial v}{\partial x}\right)+\left(\frac{\partial u}{\partial x}\right)\left(\frac{\partial w}{\partial x}\right)\right)}{1+u^2+v^2} - \frac{4v\left(\left(\frac{\partial q}{\partial x}\right)\left(\frac{\partial u}{\partial x}\right)-\left(\frac{\partial v}{\partial x}\right)\left(\frac{\partial w}{\partial x}\right)\right)}{1+u^2+v^2} + w\left(\frac{1-3v^2-u^2-2\left(\left(\frac{\partial u}{\partial x}\right)^2-\left(\frac{\partial v}{\partial x}\right)^2\right)}{1+u^2+v^2} - \frac{2v\left(v(1-u^2-v^2)+4u\left(\frac{\partial u}{\partial x}\right)\left(\frac{\partial v}{\partial x}\right)2v\left(\left(\frac{\partial u}{\partial x}\right)^2-\left(\frac{\partial v}{\partial x}\right)^2\right)\right)}{(1+u^2+v^2)^2} \right) \end{array} \right\} \end{pmatrix}. \quad (5.16)$$

As with the functional itself, there is an equivalent representation in terms of complex variables (See Appendix B.5.3) which offers computational efficiency gains.

In general, inverting the Jacobian of G would be a difficult task. In particular, the eigenvalues are quite spread out and a preconditioner is required to accelerate the convergence of GMRES. The linear part of the Jacobian, which is diagonalizable in Fourier space, is easy to invert. Furthermore, it is the continuous spectrum of the differential operator in Eq. (5.16) which causes the greatest difficulty for GMRES. A standard method of computing the continuous spectrum is to analyze the far field behavior of the linear operator [Yan10]. Therefore, linearizing around the far field of the soliton (decay to zero in this case) should give an operator with roughly an equivalent continuous

spectrum to the Jacobian in Eq. (5.16), which makes this a suitable candidate for a preconditioner.

$$G[u,v] \approx M \begin{bmatrix} u \\ v \end{bmatrix} = \begin{bmatrix} \left(1-\frac{\partial^2}{\partial x^2}\right) & \left(-\frac{\partial}{\partial t}+V\frac{\partial}{\partial x}\right) \\ \left(\frac{\partial}{\partial t}-V\frac{\partial}{\partial x}\right) & \left(1-\frac{\partial^2}{\partial x^2}\right) \end{bmatrix} \begin{bmatrix} u \\ v \end{bmatrix} \tag{5.17}$$

The differential operator M is a block 2×2 linear operator. Noting that in Fourier space, all the operators in sight are diagonal simplifies the computation. That is

$$\hat{M} = \begin{bmatrix} 1+k_x^2 & \imath(-k_t+Vk_x) \\ \imath(k_t-Vk_x) & 1+k_x^2 \end{bmatrix}, \tag{5.18}$$

where k_t is the discrete conjugate temporal frequency in Fourier space. Now, one can invert this 2×2 matrix and obtain

$$\hat{M}^{-1} = \frac{1}{\det(\hat{M})} \begin{bmatrix} 1+k_x^2 & \imath(k_t-Vk_x) \\ \imath(-k_t+Vk_x) & 1+k_x^2 \end{bmatrix} \tag{5.19}$$

This preconditioner works quite well for problems in (1+1)D, but in (2+1)D this preconditioner slowed convergence rather than accelerated it. This is due to catastrophic cancelation in $\frac{1}{\det(\hat{M})}$. Consequently, an ad-hoc constant was added to the preconditioner,

$$\hat{P}^{-1} = \frac{1}{\det(\hat{M})+C} \begin{bmatrix} 1+k_x^2 & \imath(k_t-Vk_x) \\ \imath(-k_t+Vk_x) & 1+k_x^2 \end{bmatrix} \tag{5.20}$$

which was found to exhibit satisfactory convergence properties.

Similar to what was done for the gradient in the adjoint continuation problem, a finite-difference based test was used to validate the Jacobian for the preconditioned problem. The results of one such experiment are shown in Fig. 5.6. The problem was discretized using the parameters $N_x = N_y = 1024$ and $N_t = 16$ where N_i is the number of grid points in the i^{th} direction. The domain of discretization

was $[-50,50]\times[-50,50]\times[0,4\pi]$. Using the approximate droplet formula, two localized structures with different parameters were generated. These were far out of the regime of validity of the droplet itself, but this is a convenient way to generate reasonable inputs. For the data shown, U was generated with the parameters $\omega = .6, V = .2, \Phi_0 = 0, x_0 = 0$. For W the parameters $\omega = .45, V = .3, \Phi_0 = \pi/3, x_0 = 4$ were taken. For several choices of ϵ. As before, a least squares fit of $F[U+\epsilon W]-F[U]-\epsilon DF[U]W$ was used to validate that the error term was $\mathcal{O}(\epsilon^2)$.

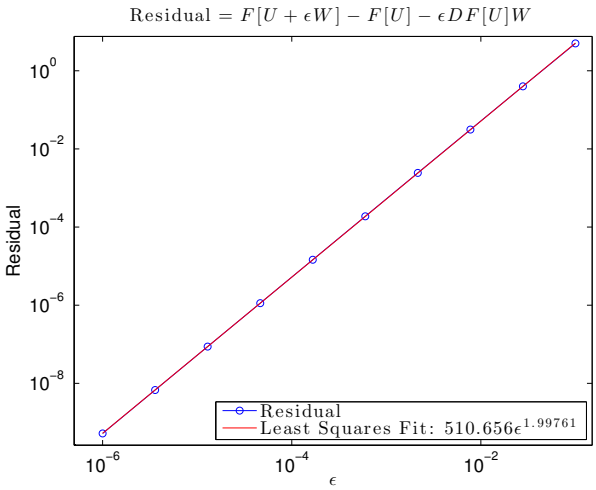

Figure 5.6 Loglog plot of $F[U+\epsilon W]-F[U]-\epsilon DF[U]W$ for several choices of ϵ. Also shown is a least squares fit to the data showing consistency with Taylor's theorem.

It is worth noting that the symmetries of the equation guarantee that the Jacobian is singular at the root. This can be seen readily by differentiating the functional evaluated at the known solution with respect to the parameters. This means that one of the theoretical gains of a Newton based approach (quadratic nonlinear convergence) is not guaranteed. In practice, for the (1+1)D method Newton's method avoided singular search directions and quadratic convergence was observed. Nevertheless, it is probable that significant improvements in this method could be realized if constraints were added to break these symmetries, although other exhaustive studies have not experienced difficulties due to a singular Jacobian [Yan09]. In the numerical computation of periodic orbits, this

is a well known problem and a standard phase constraint is typically imposed [CS07]. Unfortunately, such constraints significantly complicate the development of an effective preconditioner. It is likely that these constraints could be treated by application of the Sherman-Morrison-Woodbury formula. This is a goal for future work.

5.3.1 Results

In (1+1)D, the method above was used to compute a family of droplets parameterized by ω. Simple continuation was used taking the previous, final iterate of Newton's method as the initial iterate of the next continuation step. The discretization parameters used in this experiment were $N_x = 2^{13}$ and $N_t = 16$ on the domain $[-600, 600] \times [0, 2\pi/\omega]$. The large spatial domain was required to resolve droplets at lower frequencies which are characterized by longer length scales. Note that since the droplet corresponds to a nonlinear eigenfunction, only the first Fourier mode should be required to resolve the temporal structure of the droplet. $N_t = 16$ was chosen to verify that that the method would work with a nontrivial Fourier series in time. The results were then compared to the known solution to this problem. The $\|\cdot\|_\infty$ of the error is plotted in Figure 5.7. Also plotted is the residual–error owing only to the discretization and round off error–determined by evaluating the functional G on the known true solution. Visibly, the error of the computed solitons is on the order of the discretization error. Even with a large number of grid points, continuation managed to compute the ~ 100 solitons on the order of a few hours on a desktop with a 3.5 Ghz processor.

Armed with success in (1+1)D, a similar trial was run in (2+1)D. While individual solitons could be computed, there were serious limitations. The preconditioner proposed for the method required $10-200$ Krylov iterations per newton iteration. This held true across a wide range of choices of the acceleration parameter, C; however, the constant C had to be chosen such that $C > \max(k_t)$ to see reasonable performance. Spatial discretizations with more than ~ 1000 grid points in each separate spatial dimension were prohibitively expensive in terms of memory storage when the preconditioner was less efficient. This could be alleviated by utilizing GMRES with restarts, but this

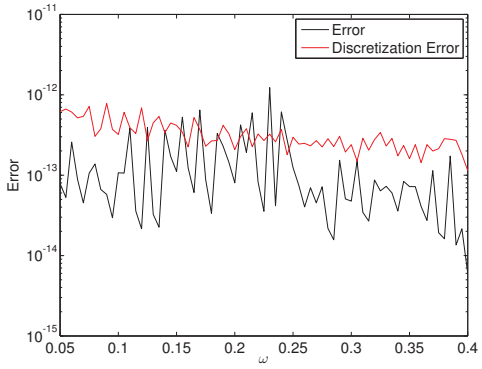

Figure 5.7 Plot of the inf-norm error of computed solitons based on (1+1) Newton-GMRES continuation

was not explored. At the cost of on the order of hours per newton iteration, individual continuation steps did successfully compute droplets. One such example computed is illustrated in Figures 5.8-5.9, which demonstrate sufficient spatial and temporal resolution by analysis of the Fourier coefficients. For all of the experiments presented in (2+1)D the numerical parameters were chosen to be $N_x = N_y = 256$, $N_t = 16$ and the computational domain was $[-40,40]\times[-40,40]\times[0,{}^{2\pi}/_{\omega}]$.

Given the high computational cost involved, it seems unlikely that this method is suitable for large scale exploration of solitons in perturbed Landau-Lifshitz equations. However, this method still offers the potential benefit of capturing solutions which are not the ground state. Consequently, the breather observed in [Mai14] was taken as an initial guess. Newton-GMRES converges to the underlying droplet (as illustrated in Figure 5.10-5.12). The slow convergence of Newton's method means the absolute and relative tolerances in this experiment were chosen to be quite coarse $\sim 10^{-6}$, but the trend is clear. It remains possible that with a more refined initial guess, a breather state could be computed via this method. It is the conclusion here that the breather is likely a meta-stable solution and does not precisely solve the boundary value problem. Such an interpretation is consistent with similar observations of [PZ98].

Neither of the methods explored in this chapter seem feasible for a large scale investigation. Given the apparent non-existence of a numerically exact breather state, it seems most likely that a proven method like spectral renormalization will be a more practical tool for investigating droplets

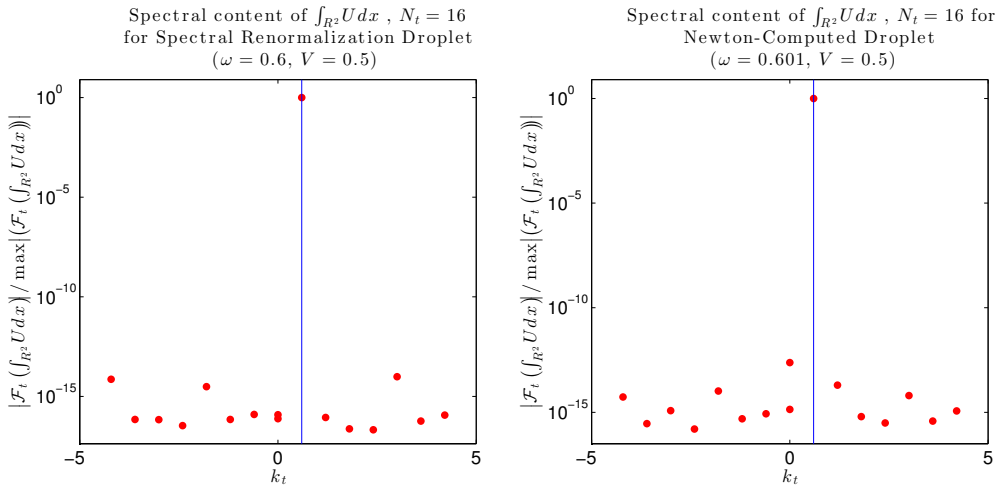

Figure 5.8 This plot shows the temporal resolution of the droplet. On the left is a droplet computed via spectral renormalization and lifted to (2+1)D. The quantity plotted is the integral over space of the droplet in stereographic form. The spectral content of the the resulting time series is concentrated in a single Fourier mode as is expected for a nonlinear eigenvalue problem. On the right, the same data is plotted for a droplet computed with Newton-GMRES, taking the droplet on the left as an initial iterate. In both plots, the vertical blue line corresponds to the target frequency of the droplet. This plot suggests that the solution computed is in fact a droplet and is resolved sufficiently in time.

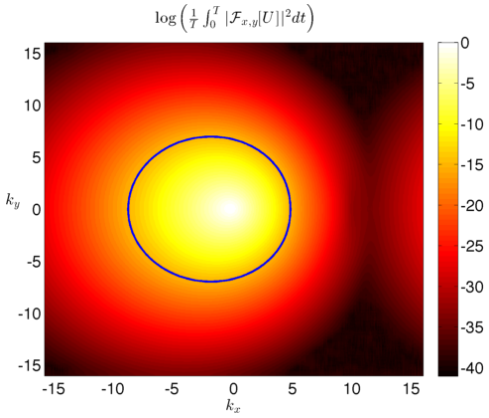

Figure 5.9 Spatial resolution of the droplet. The plotted quantity is the temporal average absolute spatial Fourier coefficients of the (2+1)D droplet computed via Newton-GMRES. The contour plotted reflects machine precision. There is clear decay in the spatial Fourier modes indicating that a sufficient number of spatial grid points were used.

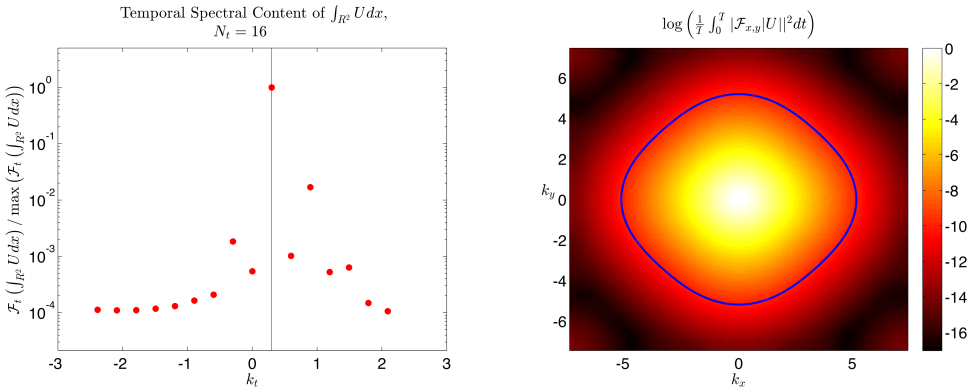

Figure 5.10 Spatial and temporal resolution of the breather in Fig 5.1. The contour plotted on the right is at 10^{-10}. The plot on the left shows the Fourier coefficients of the integral over space of the droplet. There is a peak at the expected frequency with slow decay in the Fourier coefficients. This is consistent with observations of time series where the period is slightly off the nominal value. The plot on the right indicates the spatial content of the breather is sufficiently resolved.

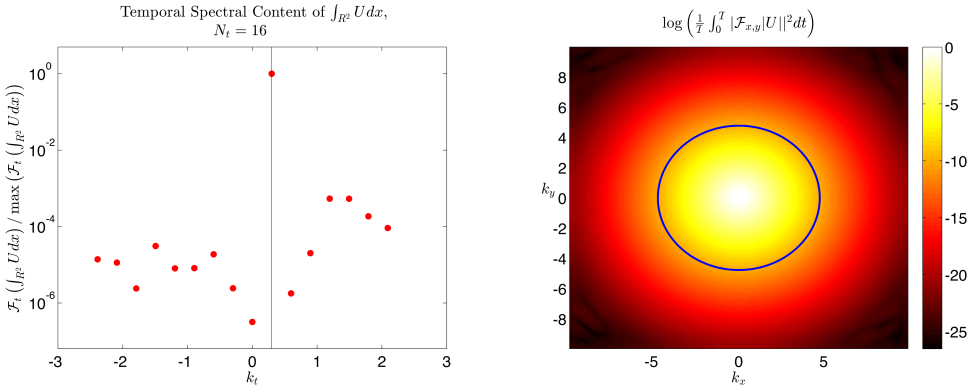

Figure 5.11 Spatial and temporal resolution of the breather in Fig 5.12. The contour plotted on the right is at 10^{-10}. The plot on the left shows the Fourier coefficients of the integral over space of the droplet. There is a peak at the expected frequency and Newton-GMRES seems to be driving the other Fourier modes in time to zero. The plot on the right shows that the structure is still quite well resolved in space after Newton's method has converged.

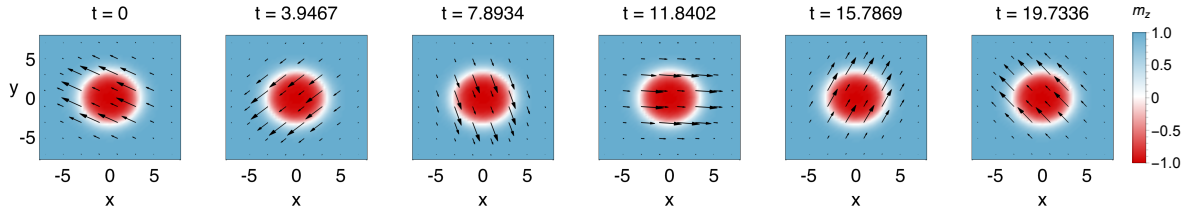

Figure 5.12 Time series of the structure after Newton's method. Compare this to the times series of the initial Newton iterate in Figure 5.1. Note the boundary of the structure remains nearly circular as time progresses and there is no modulation of the boundary.

in perturbed contexts. Fixed point iteration schemes would resolve the memory-constrained issues related to storing either the Jacobian or the Krylov-basis for Newton approaches. Even given these constraints, the approach outlined here does enjoy modest success and has the potential to investigate some regimes not accessible to spectral renormalization if further evidence of breathers in the Landau-Lifshitz equation should arise.

CHAPTER

6

CONCLUSION

The primary contribution of this thesis is two-fold: a mathematical result providing a simple formula for the evaluation of modulation equations in Hamiltonian systems and a physical result developing a general framework for investigating perturbations of droplet solitons. Each of these contributions provide a tool which can be used for further investigation. The straightforward evaluation of modulation equations for Hamiltonian systems makes evaluation simple, allowing new frameworks to be developed in solitonic systems when the appropriate structure can be recognized. The physical result presents a model which can be used to guide the recent experimental work where droplets have been observed [Moh13; Mac14]. These experiments are only beginning the exploration of properties of droplets in laboratory devices and theoretical input can help guide these experiments into physically practical devices.

In particular, the investigation of the NC-STO is of particular importance, providing insight into experimentally observed dissipative droplets. The combination of effects creates a complex balance in which a rich array of structures can be observed. One key theoretical prediction is that the higher order dynamics of soliton center can balance the small change in droplet velocity in

a nanocontact. This enables a stationary structure with nontrivial phase structure to be trapped by the an nanocontact. It opens up the possibility that wider array of solitons may be observed in experimental configurations than has previously been predicted [BH13]. Current work being done to directly image the magnetization [Bon15; Bac15] in nanocantact devices may reveal this complex structure, which the indirect measurements of past experiments would not reveal [Moh13].

The examples provided in this thesis are meant to demonstrate the many ways in which the modulation equations can be used to make predictions. For instance, in the example alluded to above, the droplet in a nanocontact appears robust in the presence of weak field gradients, but can be ejected from the nanocontact if the gradient becomes too large. This not only offers an explanation of the previously observed drift instability, but also highlights the importance of the higher order parameters (initial phase and position). In this example, the restoring force of the nanocontact, which arises from modulation of the soliton center, can balance the direct acceleration provided by the field gradient when the terms are of the same order. Observations of this sort are the first steps toward utilizing the droplet as a mechanism for information storage and transfer. The role of field gradients in propagation and control of droplets in the absence of a nanocontact has previously been understood in [Hoe12]. The key contribution here is to see that higher order effects, not considered in previous work, play an important role in modeling dissipative droplets.

In Chapter 4, perturbations relating to various experimental configurations were investigated. The conclusion that neither adiabatic spin torque or the spin hall effect can stabilize the droplet suggests the symmetry breaking provided by the nanocontact region plays a very important role in these experimental devices. The modulation equations make such analysis comparatively straightforward, offering a quick means to determine that experimental investigation of droplets should continue to focus the nanocontact and it is not simply that the nanocontact offers an expedient way of nucleating the droplet.

In the context of the nanocontact, a large number of physical perturbations can now be investigated providing many avenues for future work. There are countless additional perturbations that

could be investigated. In present work, the experiments are typically conducted at room temperature [Mac14] and thermal effects are likely to play a significant role. Temperature dependence has been neglected in this work. It is possible that initiation of the drift instability could be a thermally activated process and understanding the role of this stochastic perturbation could clarify the importance of temperature control in the lab. This is just one of a number of neglected effects which could prove important in laboratory experiments. Stray fields, canted applied fields and spin torque asymmetry are all likely to play some role in experimental devices and warrant further investigation as well.

Much more than being limited to the droplet, the Hamiltonian systems approach generalizes a long history of soliton perturbation theory. Work of this sort has a long history in physically relevant solitonic models. The early works of [Gor74] and [KM77b] posed these important questions in quite general settings. The work here provides an equation which is straightforward to use and offers significant generality in the systems to which it can be applied. The class of Hamiltonian systems considered here is quite general with the necessary properties a direct consequence of symmetry arguements [CS07]. Many new systems can now be readily investigated without extend asymptotic calculations, ad hoc balance laws or knowledge of the Lagrangian which have been required in past work [Wei85; KA81; KS95]. As a result modulation equations in new soliton bearing systems should be a more accessible tool for investigation.

Understanding the general framework for Hamiltonian systems accomplishes multiple goals. Not only is simpler to apply soliton perturbation theory to systems other than the Landau-Lifshitz equation, it is also straightforward to model other solitary wave solutions to to the torque equations such as magnetic vortices. In [BH15] it was proposed that the invariance of the Landau-Lifshitz equation under rotation of the domain suggests the possibility of structures which both rotate and precess. Such a solitary wave would be parameterized differently than the droplet, but if the relevant parameters could be understood and an approximate solution obtained, the framework could be extended to study perturbations of this structure readily.

For direct computation of solitons in these extended contexts, much work remains to be done. While the Newton based approaches seem impractical at this time, serious effort should be put into spectral renormalization. Computation of solitary waves in extended versions of the Landau-Lifshitz equation provides an avenue to probe questions of existence and stability directly in the context of the partial differential equation. Work of this sort provides another mechanism for probing experimental configurations which could support droplets. While potentially expensive to compute, these solitons could help to verify the validity of modulation theory, but can also draw conclusions well outside of the perturbative regime.

Numerically exact droplets can also be used to improve upon the existing modulation theory. While the approximate droplet utilized in this thesis represents the best current approximation, the limitation of studying only very slowly propagating droplets represents a significant limitation in the theory developed here. However, sufficient generality is preserved throughout much of this work that if a better approximation is presented, modulation equations not limited to slowly propagating droplets could readily be derived. A numerically exact droplet cannot provide an analytical tool for investigating droplet perturbations. However, with a sufficiently complete database, these exact droplets could be interpolated providing a better surrogate for the droplet in the modulation equations. These equations would then have to be integrated numerically. Such a tool could still offer significant insight and computational savings over micromagnetic simulations.

There is a wide gap that exists between the theory of the droplet and experimental work. At present, theoretical work can only make qualitative comparisons to physical experiments [Moh13]. The quantitative comparisons made in this thesis are to micromagnetic simulations, which also provide only qualitative insight into experimental work. This suggests that there additional effects present in experiment, but neglected by the fully nonlinear model that will need to be incorporated before quantitative comparison is realistic. While this thesis has detailed many perturbations, there is still much more which requires work. By continuing to investigate new effects in the torque equation and refining approximations, the theoretical models will be able to provide stronger

quantitative agreement with experimental work. It is through a combination of numerical and analytical techniques, like those provided in this thesis, that the critical connections will be made and that gap will be bridged.

BIBLIOGRAPHY

[Abb07] Abbasbandy, S. "Numerical solution of non-linear Klein–Gordon equations by variational iteration method". *International Journal for Numerical Methods in Engineering* **70**.7 (2007), pp. 876–881.

[AM05] Ablowitz, M. J. & Musslimani, Z. H. "Spectral renormalization method for computing self-localized solutions to nonlinear systems". *Optics letters* **30**.16 (2005), pp. 2140–2142.

[AS81] Ablowitz, M. J. & Segur, H. *Solitons and the inverse scattering transform*. Vol. 4. SIAM, 1981.

[Abl09] Ablowitz, M. J. et al. "Asymptotic Analysis of Pulse Dynamics in Mode-Locked Lasers". *Studies in Applied Mathematics* **122**.4 (2009), pp. 411–425.

[AA08] Akhmediev, N & Ankiewicz, A. "Three sources and three component parts of the concept of dissipative solitons". *Dissipative Solitons: From Optics to Biology and Medicine*. Springer, 2008, pp. 1–28.

[AA05] Akhmediev, N. & Ankiewicz, A. "Dissipative solitons in the complex Ginzburg-Landau and Swift-Hohenberg equations". *Dissipative solitons*. Springer, 2005, pp. 1–17.

[ÁD14a] Álvarez, J & Durán, A. "An extended Petviashvili method for the numerical generation of traveling and localized waves". *Communications in Nonlinear Science and Numerical Simulation* **19**.7 (2014), pp. 2272–2283.

[ÁD14b] Álvarez, J & Durán, A. "Petviashvili type methods for traveling wave computations: I. Analysis of convergence". *Journal of Computational and Applied Mathematics* **266** (2014), pp. 39–51.

[AW10a] Ambrose, D. M. & Wilkening, J. "Computation of symmetric, time-periodic solutions of the vortex sheet with surface tension". *Proceedings of the National Academy of Sciences* **107**.8 (2010), pp. 3361–3366.

[AW10b] Ambrose, D. M. & Wilkening, J. "Computation of time-periodic solutions of the Benjamin–Ono equation". *Journal of nonlinear science* **20**.3 (2010), pp. 277–308.

[And08] Ando, K et al. "Electric manipulation of spin relaxation using the spin Hall effect". *Physical review letters* **101**.3 (2008), p. 036601.

[Bac15] Backes, D et al. "Direct Observation of Large Amplitude Spin Excitations Localized in a Spin-Transfer Nanocontact". *arXiv preprint arXiv:1504.00488* (2015).

[Bar86] Baryakhtar, V. et al. "On relaxation of magnetic solitons". *Physics Letters A* **119**.4 (1986), pp. 191–196.

[Bea08] Beach, G. et al. "Current-induced domain wall motion". *Journal of magnetism and magnetic materials* **320**.7 (2008), pp. 1272–1281.

[Ber96] Berger, L. "Emission of spin waves by a magnetic multilayer traversed by a current". *Physical Review B* **54**.13 (1996), p. 9353.

[Bon15] Bonetti, S. et al. "Direct observation and imaging of a spin-wave soliton with $p-$ like symmetry". *arXiv preprint arXiv:1504.00144* (2015).

[BH13] Bookman, L. D. & Hoefer, M. "Analytical theory of modulated magnetic solitons". *Physical Review B* **88**.18 (2013), p. 184401.

[BH15] Bookman, L. & Hoefer, M. "Perturbation Theory for Propagating Magnetic Droplet Solitons". *arXiv preprint arXiv:1501.05276* (2015).

[Cal78] Calogero, F. *Nonlinear Evolution Equations Solvable by the Spectral Transform: F. Calogero (editor).* Vol. 26. Pitman Publishing, 1978.

[CS07] Champneys, A. R. & Sandstede, B. "Numerical computation of coherent structures". *Numerical Continuation Methods for Dynamical Systems*. Springer, 2007, pp. 331–358.

[CV95] Christov, C. & Velarde, M. "Dissipative solitons". *Physica D: Nonlinear Phenomena* **86**.1 (1995), pp. 323–347.

[CV72] Cooper, G. & Verner, J. "Some Explicit Runge-Kutta Methods of High Order". *SIAM Journal on Numerical Analysis* **9**.3 (1972), pp. 389–405.

[CS14] Cousins, W. & Sapsis, T. P. "Localized instabilities in unidirectional deep water wave envelope equations". *arXiv preprint arXiv:1411.4175* (2014).

[Cow07] Cowburn, R. P. "Spintronics: Change of direction". *Nature materials* **6**.4 (2007), pp. 255–256.

[CG11] Cullity, B. D. & Graham, C. D. *Introduction to magnetic materials*. John Wiley & Sons, 2011.

[DL80] De Leeuw, F. et al. "Dynamic properties of magnetic domain walls and magnetic bubbles". *Reports on Progress in Physics* **43**.6 (1980), p. 689.

[Dho03] Dhooge, A. et al. "MATCONT: a MATLAB package for numerical bifurcation analysis of ODEs". *ACM Transactions on Mathematical Software (TOMS)* **29**.2 (2003), pp. 141–164.

[Doe81] Doedel, E. J. "AUTO: A program for the automatic bifurcation analysis of autonomous systems". *Congr. Numer* **30** (1981), pp. 265–284.

[FD12] Fedele, F. & Dutykh, D. “Hamiltonian form and solitary waves of the spatial Dysthe equations”. *JETP letters* **94**.12 (2012), pp. 840–844.

[Fer13] Fert, A. et al. “Skyrmions on the track”. *Nature nanotechnology* **8**.3 (2013), pp. 152–156.

[Fin13] Finocchio, G et al. “Switching of a single ferromagnetic layer driven by spin Hall effect”. *Applied Physics Letters* **102**.21 (2013), p. 212410.

[GC04a] Garcia-Cervera, C. J. “One-Dimensional Magnetic Domain Walls”. *Eur. J. Appl. Math.* **15** (2004), p. 451.

[GCE01] Garcia-Cervera, C. J. & E, W. “Effective dynamics for ferromagnetic thin films”. *J. Appl. Phys.* **90** (2001), p. 370.

[GC04b] García-Cervera, C. J. “One-dimensional magnetic domain walls”. *European Journal of Applied Mathematics* **15**.04 (2004), pp. 451–486.

[Gor83] Gordon, J. “Interaction forces among solitons in optical fibers”. *optics letters* **8**.11 (1983), pp. 596–598.

[Gor74] Gorschkov, K. et al. “Some problems of asymptotic theory of nonlinear waves”. *Proceedings of the IEEE* **62**.11 (1974), pp. 1511–1517.

[Gri87] Grillakis, M. et al. “Stability theory of solitary waves in the presence of symmetry, I”. *Journal of Functional Analysis* **74**.1 (1987), pp. 160–197.

[Gri90] Grillakis, M. et al. “Stability theory of solitary waves in the presence of symmetry, II”. *Journal of Functional Analysis* **94**.2 (1990), pp. 308–348.

[He07] He, J.-H. “Variational iteration methodâĂŤsome recent results and new interpretations”. *Journal of computational and applied mathematics* **207**.1 (2007), pp. 3–17.

[HW06] He, J.-H. & Wu, X.-H. “Construction of solitary solution and compacton-like solution by variational iteration method”. *Chaos, Solitons & Fractals* **29**.1 (2006), pp. 108–113.

[Hir99] Hirsch, J. “Spin hall effect”. *Physical Review Letters* **83**.9 (1999), p. 1834.

[Hoe10] Hoefer, M. et al. “Theory for a dissipative droplet soliton excited by a spin torque nanocontact”. *Physical Review B* **82**.5 (2010), p. 054432.

[HS12] Hoefer, M. A. & Sommacal, M. “Propagating two-dimensional magnetic droplets”. *Physica D: Nonlinear Phenomena* **241**.9 (2012), pp. 890–901.

[Hoe12] Hoefer, M. A. et al. “Propagation and control of nanoscale magnetic-droplet solitons”. *Physical Review B* **85**.21 (2012), p. 214433.

[Iac14] Iacocca, E. et al. “Confined Dissipative Droplet Solitons in Spin-Valve Nanowires with Perpendicular Magnetic Anisotropy”. *Phys. Rev. Lett.* **112**.4 (2014), p. 047201.

[Iva01] Ivanov, B. A. et al. “Small-amplitude mobile solitons in the two-dimensional ferromagnet”. *Physical Review B* **63**.13 (2001), p. 134413.

[IS89] Ivanov, B. & Stephanovich, V. “Two-dimensional soliton dynamics in ferromagnets”. *Physics Letters A* **141**.1 (1989), pp. 89–94.

[KM77a] Karpman, V. & Maslov, E. “A perturbation theory for the Korteweg-de Vries equation”. *Physics Letters A* **60**.4 (1977), pp. 307–308.

[KS95] Kath, W. L. & Smyth, N. F. “Soliton evolution and radiation loss for the nonlinear Schrödinger equation”. *Physical Review E* **51**.2 (1995), p. 1484.

[KN78] Kaup, D. J. & Newell, A. C. “Solitons as particles, oscillators, and in slowly changing media: a singular perturbation theory”. *Proceedings of the Royal Society of London. A. Mathematical and Physical Sciences* **361**.1707 (1978), pp. 413–446.

[KM77b] Keener, J. P. & McLaughlin, D. W. “Solitons under perturbations”. *Physical Review A* **16** (1977), p. 777.

[Kel11] Kelley, C. T. *Implicit filtering*. Vol. 23. SIAM, 2011.

[KM06] Khaykovich, L. & Malomed, B. A. “Deviation from one dimensionality in stationary properties and collisional dynamics of matter-wave solitons”. *Physical Review A* **74**.2 (2006), p. 023607.

[KM89] Kivshar, Y. S. & Malomed, B. A. “Dynamics of solitons in nearly integrable systems”. *Reviews of Modern Physics* **61**.4 (1989), p. 763.

[KA81] Kodama, Y. & Ablowitz, M. J. “Perturbations of solitons and solitary waves”. *Studies in Applied Mathematics* **64** (1981), pp. 225–245.

[Kos86] Kosevich, A. M. et al. *Sov. Sci. Rev., Sect. A, Phys. Rev.* **6** (1986). Ed. by Chalatnikov, I. M., p. 171.

[Kos98] Kosevich, A. M. et al. “Magnetic soliton motion in a nonuniform magnetic field”. *J. Exp. Theor. Phys.* **87** (1998), pp. 401–407.

[Kos90] Kosevich, A. Ĭ. M. et al. “Magnetic solitons”. *Physics Reports* **194**.3 (1990), pp. 117–238.

[Kra12] Krasnov, V. M. “Radiative annihilation of a soliton and an antisoliton in the coupled sine-Gordon equation”. *Physical Review B* **85**.13 (2012), p. 134525.

[Kró98] Królikowski, W. et al. "Annihilation of photorefractive solitons". *Optics letters* **23**.2 (1998), pp. 97–99.

[LY07] Lakoba, T. I. & Yang, J. "A generalized Petviashvili iteration method for scalar and vector Hamiltonian equations with arbitrary form of nonlinearity". *Journal of Computational Physics* **226**.2 (2007), pp. 1668–1692.

[LL35] Landau, L. D. & Lifshitz, E. "On the theory of the dispersion of magnetic permeability in ferromagnetic bodies". *Phys. Z. Sowjetunion* **8**.153 (1935), pp. 101–114.

[LZ04] Li, Z & Zhang, S. "Domain-wall dynamics driven by adiabatic spin-transfer torques". *Physical Review B* **70**.2 (2004), p. 024417.

[Liu11] Liu, L. et al. "Spin-torque ferromagnetic resonance induced by the spin Hall effect". *Physical review letters* **106**.3 (2011), p. 036601.

[Liu12] Liu, L. et al. "Current-induced switching of perpendicularly magnetized magnetic layers using spin torque from the spin Hall effect". *Physical review letters* **109**.9 (2012), p. 096602.

[Mac14] Macià, F. et al. "Stable magnetic droplet solitons in spin-transfer nanocontacts". *Nat. Nanotechnol.* **9**.12 (2014), pp. 992–996.

[Mai14] Maiden, M. et al. "Attraction, merger, reflection, and annihilation in magnetic droplet soliton scattering". *Physical Review B* **89**.18 (2014), p. 180409.

[Mal98] Malomed, B. A. "Potential of interaction between two-and three-dimensional solitons". *Physical Review E* **58**.6 (1998), p. 7928.

[Moh13] Mohseni, S. M. et al. "Spin Torque–Generated Magnetic Droplet Solitons". *Science* **339**.6125 (2013), pp. 1295–1298.

[Olv84] Olver, P. J. "Hamiltonian and non-Hamiltonian models for water waves". *Trends and Applications of Pure Mathematics to Mechanics*. Springer, 1984, pp. 273–290.

[PT91] Papanicolaou, N & Tomaras, T. "Dynamics of magnetic vortices". *Nuclear Physics B* **360**.2 (1991), pp. 425–462.

[Par08] Parkin, S. S. et al. "Magnetic domain-wall racetrack memory". *Science* **320**.5873 (2008), pp. 190–194.

[PS04] Pelinovsky, D. E. & Stepanyants, Y. A. "Convergence of Petviashvili's iteration method for numerical approximation of stationary solutions of nonlinear wave equations". *SIAM Journal on Numerical Analysis* **42**.3 (2004), pp. 1110–1127.

[Pet76] Petviashvili, V. "Equation of an extraordinary soliton". *Fizika plazmy* **2** (1976), pp. 469–472.

[Pic91] Picholle, E. et al. "Observation of dissipative superluminous solitons in a Brillouin fiber ring laser". *Physical review letters* **66**.11 (1991), p. 1454.

[PZ98] Piette, B. & Zakrzewski, W. "Localized solutions in a two-dimensional Landau-Lifshitz model". *Physica D: Nonlinear Phenomena* **119**.3 (1998), pp. 314–326.

[RW88] Rose, H. A. & Weinstein, M. I. "On the bound states of the nonlinear Schrödinger equation with a linear potential". *Physica D: Nonlinear Phenomena* **30**.1 (1988), pp. 207–218.

[Shi06] Shibata, J. et al. "Current-induced magnetic vortex motion by spin-transfer torque". *Physical Review B* **73**.2 (2006), p. 020403.

[Siv08] Sivan, Y et al. "Qualitative and quantitative analysis of stability and instability dynamics of positive lattice solitons". *Physical Review E* **78**.4 (2008), p. 046602.

[Slo99] Slonczewski, J. "Excitation of spin waves by an electric current". *Journal of Magnetism and Magnetic Materials* **195**.2 (1999), pp. L261–L268.

[Slo96] Slonczewski, J. C. "Current-driven excitation of magnetic multilayers". *Journal of Magnetism and Magnetic Materials* **159**.1 (1996), pp. L1–L7.

[SS99] Stegeman, G. I. & Segev, M. "Optical spatial solitons and their interactions: universality and diversity". *Science* **286**.5444 (1999), pp. 1518–1523.

[Sti07] Stiles, M. et al. "Adiabatic domain wall motion and Landau-Lifshitz damping". *Physical Review B* **75**.21 (2007), p. 214423.

[VK73] Vakhitov, N. & Kolokolov, A. A. "Stationary solutions of the wave equation in a medium with nonlinearity saturation". *Radiophysics and Quantum Electronics* **16**.7 (1973), pp. 783–789.

[Wei85] Weinstein, M. I. "Modulational stability of ground states of nonlinear Schrödinger equations". *SIAM journal on mathematical analysis* **16**.3 (1985), pp. 472–491.

[WY12] Wilkening, J. & Yu, J. "Overdetermined shooting methods for computing standing water waves with spectral accuracy". *Computational Science & Discovery* **5**.1 (2012), p. 014017.

[Wil11] Williams, M. O. et al. "Continuation of periodic solutions in the waveguide array mode-locked laser". *Physica D: Nonlinear Phenomena* **240**.22 (2011), pp. 1791–1804.

[Yan10] Yang, J. *Nonlinear Waves in Integrable and Nonintegrable Systems*. Philadelphia: Society for Industrial and Applied Mathematics, 1, 2010.

[Yan02] Yang, J. "Internal oscillations and instability characteristics of (2+1)-dimensional solitons in a saturable nonlinear medium". *Physical Review E* **66**.2 (2002), p. 026601.

[Yan09] Yang, J. "Newton-conjugate-gradient methods for solitary wave computations". *Journal of Computational Physics* **228**.18 (2009), pp. 7007–7024.

[YL07] Yang, J. & Lakoba, T. I. "Universally-Convergent Squared-Operator Iteration Methods for Solitary Waves in General Nonlinear Wave Equations". *Studies in Applied Mathematics* **118**.2 (2007), pp. 153–197.

[ZK65] Zabusky, N. J. & Kruskal, M. D. "Interaction of solitons in a collisionless plasma and the recurrence of initial states". *Phys. Rev. Lett* **15**.6 (1965), pp. 240–243.

[ZY07] Zhu, Y. & Yang, J. "Universal fractal structures in the weak interaction of solitary waves in generalized nonlinear Schrödinger equations". *Phys. Rev. E* **75**.3 (2007), p. 036605.

APPENDICES

APPENDIX

A

NOTATIONAL CONVENTIONS

Unless otherwise stated, bold-face variables (e.g. **m**) will denote vector quantities. Generally, subscripts are reserved for labeling, not partial derivatives. However, in Appendix B, subscripts will be used to denote partial derivatives since many of the equations are quite long and this notation is more compact. The remainder of this appendix is dedicated to tables enumerating common notation throughout this thesis.

Symbol		Name	Typical Value
M_s	-	Saturation magnetization	$7.37\times10^5 A/m = .926T/\mu_0$
L_{ex}	-	Exchange Length	6 nm
δ	-	Free layer thickness	5 nm
r_*	-	nanocontact radius	75 nm
H_0	-	applied field	$5.57\times10^5 A/m = .7T/\mu_0$
H_k	-	anisotropy field	$9.36\times10^5 A/m = 1.18T/\mu_0$
I	-	applied current	$\sim$30mA
ϵ	-	spin torque efficiency	75 nm

Table A.1 Table of physical constants.

Symbol		Name	Relation to Physical Constants
Q	-	Quality factor	H_k/μ_0
I_0	-	Spin torque scaling	$\frac{4M_s^2 e\mu_0\pi r_*^2\delta(Q-1)}{\hbar\epsilon\Theta_p}$
τ	-	Time scale	$(\lvert\gamma\rvert\mu_0 M_s(Q-1))^{-1}$
L	-	Length scale	$L_{\text{ex}}/\sqrt{Q-1}$
h_0	-	Dimensionless perpendicular field	$H_0/M_s(Q-1)$
ρ_*	-	Dimensionless nanocontact radius	r_*/L
σ	-	Dimensionless current	I/I_0
α	-	Dimensionless damping	~ 0.01

Table A.2 Table of scaling parameters and dimensionless constants

$\mathbf{M}$	-	Magnetization vector, satisfying $\lvert\mathbf{M}\rvert = M_s$
M_i	-	i-component of the magnetization, i.e $\mathbf{M} = [M_x, M_y, M_z]$
$\mathbf{m}$	-	Nondimensional magnetization vector, satisfying $\lvert\mathbf{m}\rvert = 1$
m_i	-	i-component of the nondimensional magnetization, i.e $\mathbf{m} = [m_x, m_y, m_z]$
Θ	-	Azimuthal angle of magnetization, $\mathbf{m} = [\cos(\Phi)\sin(\Theta), \sin(\Phi)\sin(\Theta), \cos(\Theta)]$
Φ	-	Polar angle of magnetization, $\mathbf{m} = [\cos(\Phi)\sin(\Theta), \sin(\Phi)\sin(\Theta), \cos(\Theta)]$
w	-	Stereographic representation of the magnetization, $w = \frac{m_x + i m_y}{1+m_z} = \frac{e^{i\Phi}\sin\Theta}{1+\cos(\Theta)}$

Table A.3 Variables used for the magnetization

$\mathcal{E}$	-	Energy (See Eq. (1.15))
$\mathcal{N}$	-	Total spin (See Eq. (1.18))
$\mathcal{P}$	-	Momentum (See Eq. (1.21))
Φ_0	-	Overall droplet phase
$\mathbf{x}_0$	-	Initial soliton center
ω	-	Droplet frequency (above Zeeman)
$\mathbf{V}$	-	Droplet velocity
ξ	-	Droplet center ($\xi = \mathbf{x}_0 + \frac{1}{\epsilon}\int_0^{\epsilon t} \mathbf{V}(t')dt'$)

Table A.4 Droplet parameters and conserved quantites

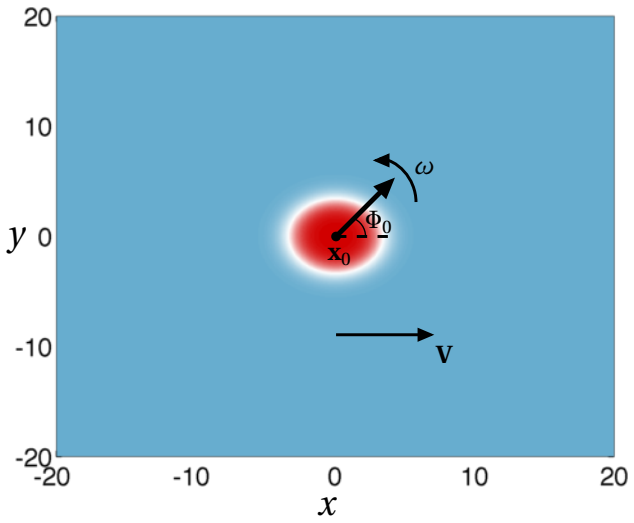

Figure A.1 Illustration of the droplet parameters. The vector in the middle represents the in-plane component of the magnetization at the center of the droplet.

APPENDIX

B

SUPPLEMENTARY CALCULATIONS

B.1 Hamiltonian of the Torque Equatioun

As is repeatedly referred to in the main body of Eq. (1.8) represents a Hamiltonian system. The canonical Hamiltonian variables are m_z and Φ where m_z is the vertical component of the magnetization and Φ is the phase. In these variables, the torque equation becomes

$$\frac{\partial m_z}{\partial t} = -\nabla \cdot \left((1-m_z^2)\nabla\Phi\right) \tag{B.1}$$

$$\frac{\partial \Phi}{\partial t} = \frac{\nabla^2 m_z}{1-m_z^2} + \frac{m_z |\nabla m_z|^2}{(1-m_z^2)^2} + m_z(1+|\nabla\Phi|^2). \tag{B.2}$$

The corresponding Hamiltonian for this system is

$$H(m_z,\Phi) = \frac{1}{2}\int_{\mathbb{R}^n} \left[\frac{|\nabla m_z|^2}{1-m_z^2} + (1-m_z^2)(1+|\nabla\Phi|^2)\right] d\mathbf{x} \tag{B.3}$$

It remains to verify that this is the Hamiltonian by computing the variational derivatives of the torque equation. However, this form is not suitable for modulation theory, so the verification will be suspended until the Hamiltonian is in the appropriate form. Shifting into the precessing, comoving frame: i.e

$$m_z(x,t) \to \tilde{m}_z(x - Vt, t) \tag{B.4}$$

$$\Phi(x,t) \to \omega t + \tilde{\Phi}(x - Vt, t) \tag{B.5}$$

the Landau-Lifshitz equation becomes

$$\frac{\partial m_z}{\partial t} = -\nabla \cdot \left((1-m_z^2)\nabla\Phi\right) + V \cdot \nabla m_z \tag{B.6}$$

$$\frac{\partial \Phi}{\partial t} = \frac{\nabla^2 m_z}{1-m_z^2} + \frac{m_z |\nabla m_z|^2}{(1-m_z^2)^2} + m_z(1+|\nabla\Phi|^2) + \mathbf{V}\cdot\nabla\Phi - \omega \tag{B.7}$$

where gradients are now with respect to $\xi = \mathbf{x} - \mathbf{V}t$ the comoving coordinate and $\tilde{}$'s will be dropped from variables for clarity. Since there are now new terms in the equation, the Hamiltonian must change correspondingly,

$$H(m_z,\Phi) = \frac{1}{2}\int_{\mathbb{R}^n} \left[\frac{|\nabla m_z|^2}{1-m_z^2} + (1-m_z^2)(1+|\nabla\Phi|^2) + \mathbf{V}\cdot(-m_z\nabla\Phi + \nabla m_z \Phi) + 2\omega m_z \right] d\mathbf{x} \tag{B.8}$$

This Hamiltonian now explicitly depends on the parameters ω and V. The next several computations verify that this is the Hamiltonian corresponding to the system in Eqs. (B.6)& (B.7).

$$\langle H_\Phi, \Psi; \omega, \mathbf{V}\rangle = \frac{d}{d\epsilon}\left[\frac{1}{2}\int_{\mathbb{R}^n}\left[\frac{|\nabla m_z|^2}{1-m_z^2}+(1-m_z^2)(1+|\nabla(\Phi+\epsilon\Psi)|^2)\right]d\mathbf{x}+\mathbf{V}\cdot(-m_z\nabla(\Phi+\epsilon\Psi)+\nabla m_z(\Phi+\epsilon\Psi)+2\omega m_z\right]\Big|_{\epsilon=0} \tag{B.9}$$

$$= \int_{\mathbb{R}^n}\left[(1-m_z^2)\nabla\Phi\nabla\Psi+\mathbf{V}\cdot(-m_z\nabla\Psi+\nabla m_z\Psi)\right]d\mathbf{x} \tag{B.10}$$

$$= \int_{\mathbb{R}^n}\left[-\nabla\cdot((1-m_z^2)\nabla\Phi)\Psi+\frac{1}{2}\mathbf{V}\cdot(-m_z\nabla\Psi+\nabla m_z\Psi)\right]d\mathbf{x} \tag{B.11}$$

by an application of Green's identities

$$= \int_{\mathbb{R}^n}\left[-\nabla\cdot((1-m_z^2)\nabla\Phi)\Psi+\frac{1}{2}\mathbf{V}\cdot(\nabla m_z\Psi+\nabla m_z\Psi)\right]d\mathbf{x} \tag{B.12}$$

by integration by parts on each component of the gradient

$$= \int_{\mathbb{R}^n}\left(-\nabla\cdot((1-m_z^2)\nabla\Phi)+\mathbf{V}\cdot\nabla m_z\right)\Psi d\mathbf{x} \tag{B.13}$$

$$\Rightarrow H_\Phi = -\nabla\cdot((1-m_z^2)\nabla\Phi)+\mathbf{V}\cdot\nabla m_z \tag{B.14}$$

$$\left\langle H_{m_z},\Psi\right\rangle = \frac{d}{d\epsilon}\left[\frac{1}{2}\int_{\mathbb{R}^n}\left[\frac{|\nabla(m_z+\epsilon\Psi)|^2}{1-(m_z+\epsilon\Psi)^2}\right.\right.$$
$$+(1-(m_z+\epsilon\Psi)^2)(1+|\nabla\Phi|^2)$$
$$\left.\left.+V(-(m_z+\epsilon\Psi)\nabla\Phi+\nabla(m_z+\epsilon\Psi)\Phi)+2\omega(m_z+\epsilon\Psi)\right]d\mathbf{x}\right]\Bigg|_{\epsilon=0} \tag{B.15}$$

$$=\int_{\mathbb{R}^n}\left[\frac{m_z|\nabla m_z|^2\Psi}{(1-m_z^2)^2}+\frac{\nabla m_z\cdot\nabla\Psi}{1-m_z^2}-m_z\Psi(1+|\nabla\Phi|^2)+\frac{1}{2}V\cdot(-\nabla\Phi\Psi+\Phi\nabla\Psi)+\omega\Psi\right]d\mathbf{x} \tag{B.16}$$

by elementary calculus

$$=\int_{\mathbb{R}^n}\left[\frac{m_z|\nabla m_z|^2}{(1-m_z^2)^2}\Psi-\nabla\cdot\left(\frac{\nabla m_z}{1-m_z^2}\right)\Psi-m_z(1+|\nabla\Phi|^2)\Psi+\frac{1}{2}V\cdot(-\nabla\Phi\Psi+\Phi\nabla\Psi)+\omega\Psi\right]d\mathbf{x} \tag{B.17}$$

by an application of Green's identities

$$=\int_{\mathbb{R}^n}\left[\frac{m_z|\nabla m_z|^2}{(1-m_z^2)^2}\Psi-\nabla\cdot\left(\frac{\nabla m_z}{1-m_z^2}\right)\Psi-m_z(1+|\nabla\Phi|^2)\Psi+\frac{1}{2}V\cdot(-\nabla\Phi\Psi-\nabla\Phi\Psi)+\omega\Psi\right]d\mathbf{x} \tag{B.18}$$

by integration by parts on each component of the gradient

$$=\int_{\mathbb{R}^n}\left[-\frac{\nabla^2 m_z}{1-m_z^2}-\frac{m_z|\nabla m_z|^2}{(1-m_z^2)^2}-m_z(1+|\nabla\Phi|^2)-V\cdot\nabla\Phi+\omega\right]\Psi d\mathbf{x} \tag{B.19}$$

by elementary calculus

$$\Rightarrow H_{m_z}=-\frac{\nabla^2 m_z}{1-m_z^2}-\frac{m_z|\nabla m_z|^2}{(1-m_z^2)^2}-m_z(1+|\nabla\Phi|^2)-V\cdot\nabla\Phi+\omega \tag{B.20}$$

Armed with this it is now clear that

$$\frac{\partial}{\partial t}\begin{pmatrix} m_z \\ \Phi\end{pmatrix}=\begin{pmatrix} 0 & 1 \\ -1 & 0\end{pmatrix}\nabla H(m_z,\Phi) \tag{B.21}$$

which verifies that indeed the Eq. 1.8 is Hamiltonian with the Hamiltonian given by Eq. B.3 and the skew-adjoint operator being $J=\begin{pmatrix} 0 & 1 \\ -1 & 0\end{pmatrix}$.

B.1.1 Second Variation of the Hamiltonian

It remains to compute the second variation of the functional in Eq. B.3 and verify that the resulting operator is self adjoint. This will require computing H_{m_z,m_z}, $H_{\Phi,\Phi}$, H_{Φ,m_z} and $H_{m_z,\Phi}$. Further, it remains to verify that $H_{m_z,m_z} = H^{\dagger}_{m_z,m_z}$,$H_{\Phi,\Phi} = H^{\dagger}_{\Phi,\Phi}$ and $H_{\Phi,m_z} = H^{\dagger}_{m_z,\Phi}$ which will verify that the second variation

$$\nabla^2 H = \begin{pmatrix} H_{m_z,m_z} & H_{m_z,\Phi} \\ H_{\Phi,m_z} & H_{\Phi,\Phi} \end{pmatrix} \tag{B.22}$$

is self adjoint.

These derivatives are readily computed,

$$H_{m_z,m_z}(m_z,\Phi)\Psi = \frac{d}{d\epsilon}\left[-\frac{\nabla^2 m_z}{1-m_z^2} - \frac{m_z|\nabla m_z|^2}{(1-m_z^2)^2} - m_z(1+|\nabla(\Phi+\epsilon\Psi)|^2) - V\cdot\nabla\Phi + \epsilon\Psi + \omega\right]\Big|_{\epsilon=0} \tag{B.23}$$

$$= -\frac{\nabla^2\Psi}{1-m_z^2} - \frac{2m_z\nabla m_z\nabla\Psi}{(1-m_z^2)^2} - \left(\frac{2\Delta m_z^2}{(1-m_z^2)^2} + \frac{(\nabla m_z)^2}{(1-m_z^2)^2} + \frac{4m_z^2(\nabla m_z)^2}{(1-m_z^2)^3} + (\nabla\Phi)^2 + 1\right)\Psi \tag{B.24}$$

$$H_{m_z,\Phi}(m_z,\Phi)\Psi = \frac{d}{d\epsilon}\left[-\frac{\nabla^2 m_z}{1-m_z^2} - \frac{m_z|\nabla m_z|^2}{(1-m_z^2)^2} - m_z(1+|\nabla(\Phi+\epsilon\Psi)|^2) - V\cdot\nabla(\Phi+\epsilon\Psi) + \omega\right]\Big|_{\epsilon=0} \tag{B.25}$$

$$= -2m_z\nabla\Phi\nabla\Psi - V\nabla\Psi \tag{B.26}$$

$$H_{\Phi,\Phi}(m_z,\Phi)\Psi = \frac{d}{d\epsilon}\left[-\nabla\cdot((1-m_z^2)\nabla(\Phi+\epsilon\Psi)) + \mathbf{V}\cdot\nabla m_z\right]\Big|_{\epsilon=0} = -\nabla\cdot((1-m_z^2)\nabla\Psi) \tag{B.27}$$

$$\Rightarrow H_{\Phi,\Phi}(m_z,\Phi) = -\nabla\cdot(1-m_z^2)\nabla \tag{B.28}$$

$$H_{\Phi,m_z}(m_z,\Phi)\Psi = \frac{d}{d\epsilon}\left[-\nabla\cdot((1-(m_z+\epsilon\Psi)^2)\nabla\Phi)+\mathbf{V}\cdot\nabla(m_z+\epsilon\Psi)\right]\Big|_{\epsilon=0} \tag{B.29}$$

$$= 2\nabla\cdot(m_z\Psi\nabla\Phi)+\mathbf{V}\cdot\nabla\Psi \tag{B.30}$$

The next step is to verify that $\nabla^2 H$ is self adjoint, which will be done by individually computing $\left\langle\Upsilon, H_{m_z,m_z}\Psi\right\rangle = \left\langle H_{m_z,m_z}\Upsilon,\Psi\right\rangle$, $\left\langle\Upsilon, H_{\Phi,\Phi}\Psi\right\rangle = \left\langle H_{\Phi,\Phi}\Upsilon,\Psi\right\rangle$ and $\left\langle\Upsilon, H_{m_z,\Phi}\Psi\right\rangle = \left\langle H_{\Phi,m_z}\Upsilon,\Psi\right\rangle$. First $H_{\Phi,\Phi}$ is famously self-adjoint which is shown by simply integrating by parts twice. Verifying that $H_{m_z,m_z} = H^\dagger_{m_z,m_z}$ is slightly more involved, $H_{\Phi,m_z} = H^\dagger_{m_z,\Phi}$ will be verified first.

$$\left\langle\Upsilon, H_{m_z,\Phi}\Psi\right\rangle = \int_{\mathbb{R}^n}\left[\Upsilon(-2m_z\nabla\Phi\nabla\Psi - V\nabla\Psi)\right]d\mathbf{x} \tag{B.31}$$

$$= -\int_{\mathbb{R}^n} 2\Upsilon m_z\nabla\Phi\nabla\Psi d\mathbf{x} - \int_{\mathbb{R}^n}\Upsilon V\nabla\Psi d\mathbf{x} \tag{B.32}$$

$$= \int_{\mathbb{R}^n}\nabla\cdot(2m_z\Upsilon\nabla\Phi)\Psi d\mathbf{x} - \int_{\mathbb{R}^n}\Upsilon V\nabla\Psi d\mathbf{x} \tag{B.33}$$

by Green's Identities

$$= \int_{\mathbb{R}^n} 2\nabla\cdot(m_z\Upsilon\nabla\Phi)\Psi d\mathbf{x} + \int_{\mathbb{R}^n} V\nabla\Upsilon\Psi d\mathbf{x} \tag{B.34}$$

by integration by parts

on each component of the gradient

$$= \int_{\mathbb{R}^n}\left[2\nabla\cdot(m_z\Upsilon\nabla\Phi)+V\nabla\Upsilon\right]\Psi d\mathbf{x} \tag{B.35}$$

$$= \left\langle H_{\Phi,m_z}\Upsilon,\Psi\right\rangle \tag{B.36}$$

Hence, $H_{\Phi,m_z} = H^\dagger_{m_z,\Phi}$ as desired. What remains to finish showing that $\nabla^2 H = \nabla^2 H^\dagger$ is that $H_{m_z,m_z} =$

$H^{\dagger}_{m_z,m_z}$.

$$\left\langle \Upsilon, H_{m_z,m_z}\Psi \right\rangle = \int_{\mathbb{R}^n} \left[\Upsilon \left(-\frac{\Delta\Psi}{1-m_z^2} - \frac{2m_z\nabla m_z\nabla\Psi}{\left(1-m_z^2\right)^2} - \left(\frac{2\Delta m_z^2}{\left(1-m_z^2\right)^2} + \frac{(\nabla m_z)^2}{\left(1-m_z^2\right)^2} + \frac{4m_z^2(\nabla m_z)^2}{\left(1-m_z^2\right)^3} + (\nabla\Phi)^2 + 1 \right)\Psi \right) \right] d\mathbf{x} \tag{B.37}$$

$$= \underbrace{-\int_{\mathbb{R}^n} \Upsilon \frac{\Delta\Psi}{1-m_z^2} d\mathbf{x}}_{①} \underbrace{-\int_{\mathbb{R}^n} \Upsilon \frac{2m_z\nabla m_z\nabla\Psi}{\left(1-m_z^2\right)^2} d\mathbf{x}}_{②} - \underbrace{\int_{\mathbb{R}^n} \left(\frac{2\Delta m_z^2}{\left(1-m_z^2\right)^2} + \frac{(\nabla m_z)^2}{\left(1-m_z^2\right)^2} + \frac{4m_z^2(\nabla m_z)^2}{\left(1-m_z^2\right)^3} + (\nabla\Phi)^2 + 1 \right)\Psi\Upsilon d\mathbf{x}}_{③} \tag{B.38}$$

Consider ① and ②. No further computation will be required on ③. So, ①:

$$\int_{\mathbb{R}^n} \Upsilon \frac{\Delta\Psi}{1-m_z^2} d\mathbf{x} = -\int_{\mathbb{R}^n} \nabla\left(\frac{\Upsilon}{1-m_z^2} \right) \cdot \nabla\Psi d\mathbf{x} \tag{B.39}$$

by Green's identities

$$= -\int_{\mathbb{R}^n} \left(\frac{\nabla\Upsilon}{1-m_z^2} + 2\frac{\Upsilon m_z\nabla m_z}{(1-m_z^2)^2} \right) \cdot \nabla\Psi d\mathbf{x} \tag{B.40}$$

by basic calculus

$$= \int_{\mathbb{R}^n} \nabla \cdot \left(\frac{\nabla\Upsilon}{1-m_z^2} + 2\frac{\Upsilon m_z\nabla m_z}{(1-m_z^2)^2} \right) \Psi d\mathbf{x} \tag{B.41}$$

by Green's identities

$$= \int_{\mathbb{R}^n} \left[\frac{\nabla^2\Upsilon}{1-m_z^2} + \frac{2m_z\nabla\Upsilon\cdot\nabla m_z}{1-m_z^2} + \nabla\cdot\left(\frac{2\Upsilon m_z\nabla m_z}{(1-m_z^2)^2} \right) \right] \Psi d\mathbf{x} \tag{B.42}$$

by basic calculus

Next, consider ②.

$$\int_{\mathbb{R}^n} \Upsilon \frac{2m_z \nabla m_z \nabla \Psi}{\left(1-m_z^2\right)^2} d\mathbf{x} = -\int_{\mathbb{R}^n} \nabla \cdot \left(\frac{2\Upsilon m_z \nabla m_z}{\left(1-m_z^2\right)^2} \right) \Psi d\mathbf{x} \tag{B.43}$$

by an application of Green's identities. All together this becomes

$$① + ② = \int_{\mathbb{R}^n} \left[\frac{\nabla^2 \Upsilon}{1-m_z^2} + \frac{2m_z \nabla \Upsilon \cdot \nabla m_z}{1-m_z^2} \right] \Psi d\mathbf{x} \tag{B.44}$$

which greatly simplifies the calculation. Finally,

$$\begin{aligned}
\left\langle \Upsilon, H_{m_z,m_z} \Psi \right\rangle = & \underbrace{-\int_{\mathbb{R}^n} \Upsilon \frac{\Delta \Psi}{1-m_z^2} d\mathbf{x}}_{①} \underbrace{-\int_{\mathbb{R}^n} \Upsilon \frac{2m_z \nabla m_z \nabla \Psi}{\left(1-m_z^2\right)^2} d\mathbf{x}}_{②} \\
& \underbrace{-\int_{\mathbb{R}^n} \left(\frac{2\Delta m_z^2}{\left(1-m_z^2\right)^2} + \frac{(\nabla m_z)^2}{\left(1-m_z^2\right)^2} + \frac{4m_z^2 (\nabla m_z)^2}{\left(1-m_z^2\right)^3} + (\nabla \Phi)^2 + 1 \right) \Psi \Upsilon d\mathbf{x}}_{③} \qquad \text{(B.45)} \\
= & -\int_{\mathbb{R}^n} \left[\frac{\nabla^2 \Upsilon}{1-m_z^2} + \frac{2m_z \nabla \Upsilon \cdot \nabla m_z}{1-m_z^2} \right] \Psi d\mathbf{x} \\
& -\int_{\mathbb{R}^n} \left(\frac{2\Delta m_z^2}{\left(1-m_z^2\right)^2} + \frac{(\nabla m_z)^2}{\left(1-m_z^2\right)^2} + \frac{4m_z^2 (\nabla m_z)^2}{\left(1-m_z^2\right)^3} + (\nabla \Phi)^2 + 1 \right) \Psi \Upsilon d\mathbf{x} \qquad \text{(B.46)} \\
= & \int_{\mathbb{R}^n} \left[-\frac{\nabla^2 \Upsilon}{1-m_z^2} - \frac{2m_z \nabla \Upsilon \cdot \nabla m_z}{1-m_z^2} \right. \\
& \left. -\left(\frac{2\Delta m_z^2}{\left(1-m_z^2\right)^2} + \frac{(\nabla m_z)^2}{\left(1-m_z^2\right)^2} + \frac{4m_z^2 (\nabla m_z)^2}{\left(1-m_z^2\right)^3} + (\nabla \Phi)^2 + 1 \right) \Upsilon \right] \Psi d\mathbf{x} \qquad \text{(B.47)} \\
= & \left\langle H_{m_z,m_z} \Upsilon, \Psi \right\rangle \qquad \text{(B.48)}
\end{aligned}$$

Therefore H_{m_z,m_z} is self-adjoint and it follow immediately that $\nabla^2 H$ is self-adjoint as desired.

B.1.2 Derivatives of the Hamiltonian

The final computation in this section regards the somewhat unusual assumption in Theorem 2.1.1. The assumption in question is assumption 4: $\forall\ 1 \leq k \leq m, \exists\ 1 \leq j \leq s$ such that $\frac{\partial}{\partial q_k}\nabla H(z,\mathbf{q})\Big|_{z=u} \in \text{span}\left\{J^{-1}\frac{\partial u}{\partial r_j}\right\}$. In the terminology of this section, it's necessary to compute $\partial_\omega \nabla H$ and $\partial_{V_i}\nabla H$,

$$\nabla H = \begin{pmatrix} -\dfrac{\nabla^2 m_z}{1-m_z^2} - \dfrac{m_z\,|\nabla m_z|^2}{(1-m_z^2)^2} - m_z(1+|\nabla\Phi|^2) - V\cdot\nabla\Phi + \omega \\ -\nabla\cdot((1-m_z^2)\nabla\Phi) + \mathbf{V}\cdot\nabla m_z \end{pmatrix} \tag{B.49}$$

The important observation is that when taking partial derivatives, the fact that m_z will later depend on ω and $\mathbf{V}$ does not impact the present calculation.

$$\partial_\omega \nabla H = \begin{pmatrix} 1 \\ 0 \end{pmatrix} \tag{B.50}$$

$$\partial_{V_i}\nabla H = \begin{pmatrix} -\Phi_{x_i} \\ m_{z,x_i} \end{pmatrix} \tag{B.51}$$

In order for the assumption of Theorem 2.1.1 to be satisfied either

$$\begin{pmatrix} 1 \\ 0 \end{pmatrix} = \begin{pmatrix} m_{z,s,\Phi_0} \\ \Phi_{s_{\Phi_0}} \end{pmatrix} \tag{B.52}$$

or

$$\begin{pmatrix} 1 \\ 0 \end{pmatrix} = \begin{pmatrix} m_{z,s,x_{0,i}} \\ \Phi_{s,x_{0,i}} \end{pmatrix}. \tag{B.53}$$

It will become clear which choice makes more sense. In order to verify the assumptions, it is necessary to understand the dependence on the parameters. This dependence, however, is entirely

encapsulated in the ansatz.

$$m_{z,s} = m_{z,s}(x + x_0 - V t; \omega) \tag{B.54}$$

$$\Phi_s = \Phi_0 + \omega t + \Psi(x + x_0 - V t; \omega). \tag{B.55}$$

Utilizing this ansatz,

$$\partial_{\Phi_0} \begin{pmatrix} m_{z,s} \\ \Phi_s \end{pmatrix} = \begin{pmatrix} 0 \\ 1 \end{pmatrix} \tag{B.56}$$

$$\partial_{x_{0,i}} \begin{pmatrix} m_{z,s} \\ \Phi_s \end{pmatrix} = \begin{pmatrix} m_{z,s,x_i} \\ \Phi_{s,x_i} \end{pmatrix} \tag{B.57}$$

it is immediate that

$$\partial_{\Phi_0} \begin{pmatrix} m_{z,s} \\ \Phi_s \end{pmatrix} = \begin{pmatrix} 0 \\ 1 \end{pmatrix} = -J\partial_\omega \nabla H \tag{B.58}$$

and

$$\partial_{x_{0,i}} \begin{pmatrix} m_{z,s} \\ \Phi_s \end{pmatrix} = \begin{pmatrix} m_{z,s,x_i} \\ \Phi_{s,x_i} \end{pmatrix} = -J\partial_{V_i} \nabla H \tag{B.59}$$

which verifies $\partial_{\Phi_0} \begin{pmatrix} m_{z,s} \\ \Phi_s \end{pmatrix} \in \text{span}\{-J\partial_\omega \nabla H\}$ and $\partial_{x_{0,i}} \begin{pmatrix} m_{z,s} \\ \Phi_s \end{pmatrix} \in \text{span}\left\{-J\partial_{V_i} \nabla H\right\}$ and the assumptions of Theorem 2.1.1 hold.

B.2 Direct Calculation of Landau-Lifshitz Modulation Equations

B.2.1 Setup for General Perturbations of the Landau Lifshitz Equation

As explained in the main body of this thesis (Section 2.1), determining the modulation equations in Hamiltonian variables is significantly easier than other coordinate systems. In the derivation that follows for the Landau-Lifshitz equation, the Hamiltonian variables will be used. These variables

have already been given names by other presentations of the Landau-Lifshitz equation, but for the sake of clarity, and minimization of subscripts, in this section take

$$u = m_z \tag{B.60}$$

$$\bar{\Phi} = \Phi. \tag{B.61}$$

Thus the Landau-Lifshitz equation becomes

$$u_t = -\nabla \cdot ((1-u^2)\nabla\bar{\Phi}) \tag{B.62}$$

$$\bar{\Phi}_t = \frac{\nabla^2 u}{1-u^2} + \frac{u|\nabla u|^2}{(1-u^2)^2} + u(1+\left|\nabla\bar{\Phi}\right|^2) + h_0 \tag{B.63}$$

Under the presence of perturbations Eq. B.62-Eq. B.63 become

$$u_t = -\nabla \cdot ((1-u^2)\nabla\bar{\Phi}) + \epsilon P_u \tag{B.64}$$

$$\bar{\Phi}_t = \frac{\nabla^2 u}{1-u^2} + \frac{u|\nabla u|^2}{(1-u^2)^2} + u(1+\left|\nabla\bar{\Phi}\right|^2) + h_0(\epsilon x, \epsilon t) + \epsilon P_{\bar{\Phi}} \tag{B.65}$$

Note that $P_u = -\sin(\Theta)P_\Theta$ and $P_{\bar{\Phi}} = \frac{P_\Phi}{\sin(\Theta)}$ relates these perturbations to the perturbations of the Landau-Lifshtiz equation in spherical variables as used in [BH13]. Also, as argued in the main body of this thesis (Section 2.1), the calculation becomes significantly easier in the co-moving frame. However, for the purposes of this computation, it is equivalent to build the necessary information into the form of the perturbation expansion.

Take the ansatz for $u, \bar{\Phi}$ given by

$$u(x,t) = U(x-\xi(t,T);\omega,V) + \epsilon\, u_1(x-\xi(t,T),t,T) + \dots \tag{B.66}$$

$$\bar{\Phi}(x,t) = \Phi_0(T) + \int_0^t \left(\omega(\epsilon t') + h_0(\epsilon t')\right) dt + \Psi(x-\xi(t,T);\omega,V) + \epsilon\Upsilon(x-\xi(t,T),t,T) + \dots \tag{B.67}$$

$$\xi(t,T) = x_0(T) + \int_0^t V(\epsilon t')dt' \tag{B.68}$$

where $T = \epsilon t$. Note this ansatz mandates the next order term is centered on the soliton. Further, this ansatz does not allow h_0 to vary slowly on space. Attempting to include such variation directly into h_0 leads to secularity which is not readily handled by this theory. Instead, as explained in (Section 3.1) it is possible to expand the field around a constant background and treat spatial variation as a perturbation so little generality is lost by this assumption .

Differentiating the anstaz in Eqs B.66-B.68 with respect to t,

$$u_t = -\nabla U(x-\xi)\cdot\xi_t + \epsilon\left(u_{1t} - \nabla u_1(x-\xi)\cdot\xi_t - \nabla U(x-\xi)\cdot\xi_T + U_\omega\omega'(T) + U_V V'(T)\right) + \mathcal{O}\left(\epsilon^2\right) \tag{B.69}$$

$$= -\nabla U\cdot V + \epsilon\left(u_{1t} - \nabla u_1\cdot V - \nabla U\cdot x_0'(T) + U_\omega\omega'(T) + U_V V'(T)\right) + \mathcal{O}\left(\epsilon^2\right) \tag{B.70}$$

$$\tag{B.71}$$

$$\bar{\Phi}_t = \omega + h_0 - V\cdot\nabla\Psi + \epsilon\left(\Upsilon_t - V\cdot\nabla\Upsilon + \Phi_0'(T) - \nabla\Psi\cdot x_0'(T) + \Psi_\omega\omega'(T) + \Psi_V V'(T)\right) + \mathcal{O}\left(\epsilon^2\right) \tag{B.72}$$

Next define,

$$H_{u,u}(u,\bar{\Phi}) = -\frac{\Delta}{1-u^2} - \frac{2u\nabla u\cdot\nabla}{(1-u^2)^2} - \left(\frac{2u\Delta u + |\nabla u|^2}{(1-u^2)^2} + \frac{4u^2|\nabla u|^2}{(1-u^2)^3} + (\nabla\bar{\Phi})^2 + 1\right) \tag{B.73}$$

$$H_{u,\bar{\Phi}}(u,\bar{\Phi}) = -2u\nabla\bar{\Phi}\nabla - V\cdot\nabla \tag{B.74}$$

$$H_{\bar{\Phi},u} = 2u\nabla\bar{\Phi}\cdot\nabla + \left(2u\nabla^2\bar{\Phi} + 2\nabla u\cdot\nabla\bar{\Phi}\right) + V\cdot\nabla \tag{B.75}$$

(i.e. $\Rightarrow H_{\bar{\Phi},u}(u,\bar{\Phi})(\star) = 2\nabla\cdot(u\nabla\bar{\Phi}\star)\,) + V\cdot\nabla\star\,)$

$$H_{\bar{\Phi},\bar{\Phi}}(u,\bar{\Phi}) = -\nabla\cdot(1-u^2)\nabla \tag{B.76}$$

$$L = \begin{pmatrix} H_{u,u} & H_{u,\bar{\Phi}} \\ H_{\bar{\Phi},u} & H_{\bar{\Phi},\bar{\Phi}} \end{pmatrix} \tag{B.77}$$

Note: $H^{\dagger}_{u,u} = H_{u,u}$, $H^{\dagger}_{\bar{\Phi},\bar{\Phi}} = H_{\bar{\Phi},\bar{\Phi}}$ and $H^{\dagger}_{u,\bar{\Phi}} = H_{\bar{\Phi},u}$ so that $L = L^{\dagger}$. L is exactly the Hessian of the Hamiltonian as it presents in the co-moving frame.

For computational simplicity, take $u = A + \epsilon B + \mathcal{O}\left(\epsilon^2\right)$ and $\bar{\Phi} = C + \epsilon D + \mathcal{O}\left(\epsilon^2\right)$ to evaluate the right hand sides. A, B, C and D will be substituted back in when the remainder of the calculation is complete.

$$-\nabla\cdot((1-u^2)\nabla\bar{\Phi}) = -\nabla\cdot((1-(A+\epsilon B)^2)\nabla(C)+\epsilon D)) + \mathcal{O}\left(\epsilon^2\right) \tag{B.78}$$

$$= -\nabla\cdot((1-A^2-\epsilon 2AB)(\nabla C + \epsilon(\nabla D))) + \mathcal{O}\left(\epsilon^2\right) \tag{B.79}$$

$$= -\left(\nabla\cdot((1-A^2-\epsilon 2AB)(\nabla C + \epsilon(\nabla D)))\right) + \mathcal{O}\left(\epsilon^2\right) \tag{B.80}$$

$$= -\left(\nabla\cdot((1-A^2)\nabla C + \epsilon\left((1-A^2)\nabla D - 2AB\nabla C\right)\right) + \mathcal{O}\left(\epsilon^2\right) \tag{B.81}$$

$$= -\nabla\cdot((1-A^2)\nabla C) + \epsilon\left(\nabla\cdot(2A\nabla C\, B) - \nabla\cdot(1-A^2)\nabla D\right) + \mathcal{O}\left(\epsilon^2\right) \tag{B.82}$$

$$= -\nabla\cdot((1-A^2)\nabla C) + \epsilon\left(H_{\bar{\Phi},u}(A,C)B - \mathbf{V}\cdot\nabla B + H_{\bar{\Phi},\bar{\Phi}}(A,C)D\right) + \mathcal{O}\left(\epsilon^2\right) \tag{B.83}$$

Now,

$$A = U \qquad B = u_1 \qquad C = \Phi_0 + \int_0^t \omega(\epsilon t')dt' + \Psi \qquad D = \Upsilon \tag{B.84}$$

and note that it's really only ∇C that enters these equations (anywhere) so it's enough to evaluate at

Ψ instead and

$$-\nabla\cdot((1-u^2)\nabla\bar{\Phi}) = -\nabla\cdot((1-U^2)\nabla\Psi) + \epsilon\left(H_{\bar{\Phi},u}u_1 + H_{\bar{\Phi},\bar{\Phi}}\Upsilon - \mathbf{V}\cdot\nabla u_1\right) + \mathcal{O}\left(\epsilon^2\right) \tag{B.85}$$

Similarly,

$$\frac{\nabla^2 u}{1-u^2} = \frac{\nabla^2(A+\epsilon B)}{1-(A+\epsilon B)^2} + \mathcal{O}\left(\epsilon^2\right) \tag{B.86}$$

$$= (\nabla^2 A + \epsilon\nabla^2 B)\left(\frac{1}{1-A^2} + \epsilon\left(\frac{2AB}{(1-A^2)^2}\right)\right) + \mathcal{O}\left(\epsilon^2\right) \tag{B.87}$$

$$= \frac{\nabla^2 A}{1-A^2} + \epsilon\left(\frac{\nabla^2 B}{1-A^2} + \frac{2A\nabla^2 AB}{(1-A^2)^2}\right) + \mathcal{O}\left(\epsilon^2\right) \tag{B.88}$$

$$\frac{u|\nabla u|^2}{(1-u^2)^2} = \frac{(A+\epsilon B)|\nabla(A+\epsilon B)|^2}{(1-(A+\epsilon B)^2)^2} + \mathcal{O}\left(\epsilon^2\right) \tag{B.89}$$

$$= \left((A+\epsilon B)(|\nabla A|^2 + \epsilon 2\nabla A\cdot\nabla B)\right)\left(\frac{1}{(1-A^2)^2} + \epsilon\left(\frac{4AB}{(1-A^2)^3}\right)\right) + \mathcal{O}\left(\epsilon^2\right) \tag{B.90}$$

$$= \left((A|\nabla A|^2 + \epsilon\left(B|\nabla A|^2 + 2A\nabla A\cdot\nabla B\right)\right)\left(\frac{1}{(1-A^2)^2} + \epsilon\left(\frac{4AB}{(1-A^2)^3}\right)\right) + \mathcal{O}\left(\epsilon^2\right) \tag{B.91}$$

$$= \left(\frac{A|\nabla A|^2}{(1-A^2)^2} + \epsilon\left(\frac{B|\nabla A|^2 + 2A\nabla A\cdot\nabla B}{(1-A^2)^2} + \frac{4A^2B|\nabla A|^2}{(1-A^2)^3}\right)\right) + \mathcal{O}\left(\epsilon^2\right) \tag{B.92}$$

$$u\left(1+\left|\nabla\bar{\Phi}\right|^2\right) = (A+\epsilon B)\left(1+|\nabla(C+\epsilon D)|^2\right) + \mathcal{O}\left(\epsilon^2\right) \tag{B.93}$$

$$= (A+\epsilon B)\left(1+|\nabla C + \epsilon(\nabla D)|^2\right) + \mathcal{O}\left(\epsilon^2\right) \tag{B.94}$$

$$= (A+\epsilon B)\left(1+|\nabla C|^2 + \epsilon 2\nabla C\cdot(\nabla D)\right) + \mathcal{O}\left(\epsilon^2\right) \tag{B.95}$$

$$= A\left(1+|\nabla C|^2\right) + \epsilon\left(2A\nabla C\cdot(\nabla D) + B\left(1+|\nabla C|^2\right)\right) + \mathcal{O}\left(\epsilon^2\right) \tag{B.96}$$

Note

$$\frac{\nabla^2 B}{1-A^2} + \frac{2A\nabla^2 AB}{(1-A^2)^2} + \frac{B|\nabla A|^2 + 2A\nabla A\cdot\nabla B}{(1-A^2)^2} + \frac{4A^2B|\nabla A|^2}{(1-A^2)^3} + B\left(1+|\nabla C|^2\right) = -H_{u,u}(A,C)B \tag{B.97}$$

and

$$2A\nabla C\cdot(\nabla D)=-H_{u,\bar{\Phi}}(A,C)D-V\cdot\nabla D \tag{B.98}$$

So putting this all together

$$\frac{\nabla^2 u}{1-u^2}+\frac{u|\nabla u|^2}{(1-u^2)^2}+u\left(1+\left|\nabla\bar{\Phi}\right|^2\right)=\frac{\nabla^2 A}{1-A^2}+\frac{A|\nabla A|^2}{(1-A^2)^2}+A\left(1+|\nabla C|^2\right) \tag{B.99}$$

$$+\epsilon\left(-H_{u,u}(A,C)B-H_{u,\bar{\Phi}}(A,C)D-V\cdot\nabla D\right)+\mathcal{O}\left(\epsilon^2\right) \tag{B.100}$$

$$=\frac{\nabla^2 U}{1-U^2}+\frac{U|\nabla U|^2}{(1-U^2)^2}+U\left(1+|\nabla\Psi|^2\right) \tag{B.101}$$

$$+\epsilon\left(-H_{u,u}u_1-H_{u,\bar{\Phi}}\Upsilon-\mathbf{V}\cdot\nabla\Upsilon\right)+\mathcal{O}\left(\epsilon^2\right) \tag{B.102}$$

Collecting terms of like order in the original PDE

$$\mathcal{O}(1):\quad\begin{cases}-\nabla U\cdot V &= -\nabla\cdot((1-U^2)\nabla\Psi)\\ \omega+\cancel{h_0}-\nabla\Psi\cdot V &= \frac{\nabla^2 U}{1-U^2}+\frac{U|\nabla U|^2}{(1-U^2)^2}+U\left(1+|\nabla\Psi|^2\right)+\cancel{h_0}\end{cases}$$

$$\mathcal{O}(\epsilon):\quad\begin{cases}u_{1\,t}-\cancel{V\cdot\nabla u_1}-\nabla U\cdot x_0'+U_\omega\omega'+U_V V' &= H_{\bar{\Phi},u}u_1+H_{\bar{\Phi},\bar{\Phi}}\Upsilon-\cancel{V\cdot\nabla u_1}+P_u\\ \Upsilon_t-\cancel{V\cdot\nabla\Upsilon}+\Phi_0'-\nabla\Psi\cdot x_0'+\Psi_\omega\omega'+\Psi_V V' &= -H_{u,u}u_1-H_{u,\bar{\Phi}}\Upsilon-\cancel{V\cdot\nabla\Upsilon}+P_{\bar{\Phi}}\end{cases}$$

Moving stuff over, the first order problem becomes

$$\mathcal{O}(\epsilon):\quad\begin{cases}u_{1\,t} &= H_{\bar{\Phi},u}u_1+H_{\bar{\Phi},\bar{\Phi}}\Upsilon+\nabla U\cdot x_0'-U_\omega\omega'-U_V V'+P_u\\ \Upsilon_t &= -H_{u,u}u_1-H_{u,\bar{\Phi}}\Upsilon-\Phi_0'+\nabla\Psi\cdot x_0'-\Psi_\omega\omega'-\Psi_V V'+P_{\bar{\Phi}}\end{cases}$$

Casting this in matrix form

$$\underbrace{\begin{pmatrix} u_1 \\ \Upsilon \end{pmatrix}_t}_{\Upsilon_t} = \underbrace{\begin{pmatrix} 0 & 1 \\ -1 & 0 \end{pmatrix}}_{J} \underbrace{\begin{pmatrix} H_{u,u} & H_{u,\bar{\Phi}} \\ H_{\bar{\Phi},u} & H_{\bar{\Phi},\bar{\Phi}} \end{pmatrix}}_{L} \underbrace{\begin{pmatrix} u_1 \\ \Upsilon \end{pmatrix}}_{\Upsilon} + \underbrace{\begin{pmatrix} \nabla U^T \\ \nabla \Psi^T \end{pmatrix} x_0' - \begin{pmatrix} 0 \\ \Phi_0' \end{pmatrix} - \begin{pmatrix} U \\ \Psi \end{pmatrix}_{\omega} \omega' - \begin{pmatrix} U \\ \Psi \end{pmatrix}_{V} V' + \begin{pmatrix} P_u \\ P_{\bar{\Phi}} \end{pmatrix}}_{f} \tag{B.103}$$

As explained in (Section 2.1.1), solvability on this ODE requires that f be orthogonal to the generalized null space of of $(JL)^\dagger = -LJ$ since L is self-adjoint and J is skew-adjoint. Define $E(LJ)$ to be this generalized null space. It is a fact, requiring justification, that

$$\operatorname{span}\left\{ \begin{pmatrix} -1 \\ 0 \end{pmatrix}, \begin{pmatrix} \Psi_{x_i} \\ -U_{x_i} \end{pmatrix}, \begin{pmatrix} -\Psi_{\omega} \\ U_{\omega} \end{pmatrix}, \begin{pmatrix} -\Psi_{V_i} \\ U_{V_i} \end{pmatrix} \right\} \subseteq E(LJ). \tag{B.104}$$

More specifically,

$$LJ \begin{pmatrix} -1 \\ 0 \end{pmatrix} = 0 \text{ and } LJ \begin{pmatrix} -\Psi_{x_{0,i}} \\ U_{x_{0,i}} \end{pmatrix} = 0 \tag{B.105}$$

and the remaining terms are generalized null vectors which can be seen by verifying

$$LJ \begin{pmatrix} -\Psi_{\omega} \\ U_{\omega} \end{pmatrix} = \begin{pmatrix} -1 \\ 0 \end{pmatrix} \text{ and } LJ \begin{pmatrix} -\Psi_{V_i} \\ U_{V_i} \end{pmatrix} = \begin{pmatrix} \Psi_{x_i} \\ -U_{x_i} \end{pmatrix}. \tag{B.106}$$

Next, verify these claims.

$$LJ \begin{pmatrix} -1 \\ 0 \end{pmatrix} = L \begin{pmatrix} 0 & 1 \\ -1 & 0 \end{pmatrix} \begin{pmatrix} -1 \\ 0 \end{pmatrix} = \begin{pmatrix} H_{u,u} & H_{u,\bar{\Phi}} \\ H_{\bar{\Phi},u} & H_{\bar{\Phi},\bar{\Phi}} \end{pmatrix} \begin{pmatrix} 0 \\ 1 \end{pmatrix} = \begin{pmatrix} H_{u,\bar{\Phi}} 1 \\ H_{\bar{\Phi},\bar{\Phi}} 1 \end{pmatrix} \tag{B.107}$$

But

$$H_{u,\bar{\Phi}} 1 = -2U \nabla \Psi \cancelto{0}{\nabla 1} = 0 \tag{B.108}$$

and

$$H_{\bar{\Phi},\bar{\Phi}}1 = -\nabla\cdot((1-U^2)\cancelto{0}{\nabla 1}) = 0 \tag{B.109}$$

and so evidently $(-1,0)^T \in \ker(LJ)$. The next claim was that

$$LJ\begin{pmatrix} -\bar{\Phi}_{x_i} \\ U_{x_i}\end{pmatrix} = L\begin{pmatrix} 0 & 1 \\ -1 & 0\end{pmatrix}\begin{pmatrix} -\Psi_{x_i} \\ U_{x_i}\end{pmatrix} = \begin{pmatrix} H_{u,u} & H_{u,\bar{\Phi}} \\ H_{\bar{\Phi},u} & H_{\bar{\Phi},\bar{\Phi}}\end{pmatrix}\begin{pmatrix} U_{x_i} \\ \Psi_{x_i}\end{pmatrix} = \begin{pmatrix} H_{u,u}U_{x_i} + H_{u,\bar{\Phi}}\Psi_{x_i} \\ H_{\bar{\Phi},u}U_{x_i} + H_{\bar{\Phi},\bar{\Phi}}\Psi_{x_i}\end{pmatrix} = 0. \tag{B.110}$$

Start by considering the first of the two $\mathcal{O}(1)$ equations:

$$-\nabla U\cdot V = -\nabla\cdot((1-U^2)\nabla\Psi). \tag{B.111}$$

Differentiating this equation with respect to $x_{0,i}$. Note that since the ansatz in Eqs B.66-B.66 has the form $U(x-x_0-Vt;\omega)$, $\partial_{x_{0,i}}U \to -\partial_{x_i}U$ and similarly for Ψ.

$$\partial_{x_{0,i}} - \nabla U\cdot V = \nabla U_{x_i}\cdot V = \partial_{x_{0,i}}\left(-\nabla\cdot((1-U^2)\nabla\Psi)\right) \tag{B.112}$$

$$= -\left(-\nabla\cdot\left(-2U_{x_i}\nabla\Psi + (1-U^2)\nabla\Psi_{x_i}\right)\right) \tag{B.113}$$

$$= -\nabla\cdot\left(2U_{x_i}\nabla\Psi\right) + \nabla\cdot\left((1-U^2)\nabla\Psi_{x_i}\right) \tag{B.114}$$

$$\cancel{\nabla U_{x_i}\cdot V} = -H_{\bar{\Phi},u}U_{x_i} + \cancel{\mathbf{V}\cdot\nabla U_{x_i}} - H_{\bar{\Phi},\bar{\Phi}}\Psi_{x_i} \tag{B.115}$$

$$0 = -(H_{\bar{\Phi},u}U_{x_i} + H_{\bar{\Phi},\bar{\Phi}}\Psi_{x_i}) \tag{B.116}$$

$$0 = (H_{\bar{\Phi},u}U_{x_i} + H_{\bar{\Phi},\bar{\Phi}}\Psi_{x_i}). \tag{B.117}$$

Next differentiate the other equation to verify the other component vanishes as desired.

$$\partial_{x_{0,i}}(\omega-\nabla\Psi\cdot V)=\nabla\Psi_{x_i}\cdot V=\partial_{x_{0,i}}\left(\frac{\nabla^2 U}{1-U^2}+\frac{U|\nabla U|^2}{(1-U^2)^2}+U\left(1+|\nabla\Psi|^2\right)\right) \tag{B.118}$$

$$=-\left[\left(\frac{\nabla^2 U_{x_i}}{1-U^2}+\frac{2U\nabla^2 U}{(1-U^2)^2}U_{x_i}\right)+\frac{4U^2|\nabla U|^2 U_{x_i}}{(1-U^2)^3}+\frac{2U\nabla U\cdot\nabla U_{x_i}}{(1-U^2)^2}\right. \tag{B.119}$$

$$\left.+\frac{U_{x_i}|\nabla U|^2}{(1-U^2)^2}+U_{x_i}\left(1+|\nabla\Psi|^2\right)+2U\nabla\Psi\cdot\nabla\Psi_{x_i}\right] \tag{B.120}$$

$$=-\left(\frac{\nabla^2}{1-U^2}+\frac{2U\nabla^2 U}{(1-U^2)^2}+\frac{4U^2|\nabla U|^2}{(1-U^2)^3}+\frac{2U\nabla U\cdot\nabla}{(1-U^2)^2}\right. \tag{B.121}$$

$$\left.+\frac{|\nabla U|^2}{(1-U^2)^2}+\left(1+|\nabla\Psi|^2\right)\right)U_{x_i} \tag{B.122}$$

$$-2U\nabla\Psi\cdot\nabla\Psi_{x_i}-V\cdot\nabla\Psi_{x_i}+\mathbf{V}\cdot\nabla\Psi_{x_i} \tag{B.123}$$

$$\cancel{\nabla\Psi_{x_i}\cdot V}=H_{u,u}U_{x_i}+H_{u,\bar{\Phi}}\Psi_{x_i}+\cancel{\mathbf{V}\cdot\nabla\Psi_{x_i}} \tag{B.124}$$

$$0=H_{u,u}U_{x_i}+H_{u,\bar{\Phi}}\Psi_{x_i} \tag{B.125}$$

which is precisely as desired and evidently $(\Psi_{x_i},-U_{x_i})^T\in\ker(LJ)$ for all i. There are two more computations to verify, namely the generalized kernel–or as much of it as can be known ahead of time. Next, verify the claim that

$$LJ\begin{pmatrix}-\Psi_\omega\\ U_\omega\end{pmatrix}=L\begin{pmatrix}0&1\\-1&0\end{pmatrix}\begin{pmatrix}-\Psi_\omega\\ U_\omega\end{pmatrix}=\begin{pmatrix}H_{u,u}&H_{u,\bar{\Phi}}\\ H_{\bar{\Phi},u}&H_{\bar{\Phi},\bar{\Phi}}\end{pmatrix}\begin{pmatrix}U_\omega\\ \Psi_\omega\end{pmatrix}=\begin{pmatrix}H_{u,u}U_\omega+H_{u,\bar{\Phi}}\Psi_\omega\\ H_{\bar{\Phi},u}U_\omega+H_{\bar{\Phi},\bar{\Phi}}\Psi_\omega\end{pmatrix}=\begin{pmatrix}-1\\ 0\end{pmatrix} \tag{B.126}$$

This calculation is essentially the same as the previous, so skipping a few steps:

$$\partial_\omega(\omega-\nabla\Psi\cdot V)=1-\nabla\Psi_\omega\cdot V \tag{B.127}$$

$$=\left(\frac{\nabla^2}{1-U^2}+\frac{2U\nabla^2U}{(1-U^2)^2}+\frac{4U^2|\nabla U|^2}{(1-U^2)^3}+\frac{2U\nabla U\cdot\nabla}{(1-U^2)^2}+\frac{|\nabla U|^2}{(1-U^2)^2}+\left(1+|\nabla\Psi|^2\right)\right)U_\omega \tag{B.128}$$

$$+2U\nabla\Psi\cdot\nabla\Psi_\omega+V\cdot\nabla\Psi_\omega-\mathbf{V}\cdot\nabla\Psi_\omega \tag{B.129}$$

$$1-\cancel{\nabla\Psi_\omega\cdot V}=-(H_{u,u}U_\omega+H_{u,\bar\Phi}\Psi_\omega)-\cancel{\mathbf{V}\cdot\nabla\Psi_\omega} \tag{B.130}$$

$$1=-\left(H_{u,u}U_\omega+H_{u,\bar\Phi}\Psi_\omega\right) \tag{B.131}$$

$$-1=\left(H_{u,u}U_\omega+H_{u,\bar\Phi}\Psi_\omega\right) \tag{B.132}$$

and

$$\partial_\omega(-\nabla U\cdot V)=-\nabla U_\omega\cdot V=\partial_\omega\left(-\nabla\cdot((1-U^2)\nabla\Psi)\right) \tag{B.133}$$

$$=-\nabla\cdot\left(-2U_\omega\nabla\Psi+(1-U^2)\nabla\Psi_\omega\right) \tag{B.134}$$

$$=\nabla\cdot(2U_\omega\nabla\Psi)-\nabla\cdot\left((1-U^2)\nabla\Psi_\omega\right) \tag{B.135}$$

$$\cancel{-\nabla U_\omega\cdot V}=H_{\bar\Phi,u}U_\omega-\cancel{\mathbf{V}\cdot\nabla U_\omega}+H_{\bar\Phi,\bar\Phi}\Psi_\omega \tag{B.136}$$

$$0=H_{\bar\Phi,u}U_\omega+H_{\bar\Phi,\bar\Phi}\Psi_\omega. \tag{B.137}$$

which again is precisely what had previously been asserted.

The final claim is

$$LJ\begin{pmatrix}-\Psi_{V_i}\\U_{V_i}\end{pmatrix}=L\begin{pmatrix}0&1\\-1&0\end{pmatrix}\begin{pmatrix}-\Psi_{V_i}\\U_{V_i}\end{pmatrix}=\begin{pmatrix}H_{u,u}&H_{u,\bar\Phi}\\H_{\bar\Phi,u}&H_{\bar\Phi,\bar\Phi}\end{pmatrix}\begin{pmatrix}U_{V_i}\\\Psi_{V_i}\end{pmatrix}=\begin{pmatrix}H_{u,u}U_{V_i}+H_{u,\bar\Phi}\Psi_{V_i}\\H_{\bar\Phi,u}U_{V_i}+H_{\bar\Phi,\bar\Phi}\Psi_{V_i}\end{pmatrix}=\begin{pmatrix}\Psi_{x_i}\\-U_{x_i}\end{pmatrix}. \tag{B.138}$$

Again, via the same exact calculation,

$$\partial_{V_i}(-\nabla\Psi\cdot V) = -\Psi_{x_i} - \nabla\Psi_{V_i}\cdot V \tag{B.139}$$

$$= \left(\frac{\nabla^2}{1-U^2} + \frac{2U\nabla^2 U}{(1-U^2)^2} + \frac{4U^2|\nabla U|^2}{(1-U^2)^3} + \frac{2U\nabla U\cdot\nabla}{(1-U^2)^2} + \frac{|\nabla U|^2}{(1-U^2)^2} + \left(1+|\nabla\Psi|^2\right)\right)U_{V_i} \tag{B.140}$$

$$+ 2U\nabla\Psi\cdot\nabla\Psi_{V_i} + V\cdot\nabla\Psi_{V_i} - \mathbf{V}\cdot\nabla\Psi_{V_i} \tag{B.141}$$

$$-\Psi_{x_i} - \cancel{\nabla\Psi_{V_i}\cdot V} = -(H_{u,u}U_{V_i} + H_{u,\bar{\Phi}}\Psi_{V_i}) - \cancel{\mathbf{V}\cdot\nabla\Psi_{V_i}} \tag{B.142}$$

$$-\Psi_{x_i} = -\left(H_{u,u}U_{V_i} + H_{u,\bar{\Phi}}\Psi_{V_i}\right) \tag{B.143}$$

$$\Psi_{x_i} = \left(H_{u,u}U_{V_i} + H_{u,\bar{\Phi}}\Psi_{V_i}\right) \tag{B.144}$$

and

$$\partial_{V_i}(-\nabla U\cdot V) = -U_{x_i} - \nabla U_{V_i}\cdot V = \partial_{V_i}\left(-\nabla\cdot((1-U^2)\nabla\Psi)\right) \tag{B.145}$$

$$= -\nabla\cdot\left(-2U_{V_i}\nabla\Psi + (1-U^2)\nabla\Psi_{V_i}\right) \tag{B.146}$$

$$= \nabla\cdot\left(2U_{V_i}\nabla\Psi\right) - \nabla\cdot\left((1-U^2)\nabla\Psi_{V_i}\right) \tag{B.147}$$

$$-U_{x_i} - \cancel{\nabla U_{V_i}\cdot V} = H_{\bar{\Phi},u}U_{V_i} - \cancel{\mathbf{V}\cdot\nabla U_{V_i}} + H_{\bar{\Phi},\bar{\Phi}}\Psi_{V_i} \tag{B.148}$$

$$-U_{x_i} = H_{\bar{\Phi},u}U_{V_i} + H_{\bar{\Phi},\bar{\Phi}}\Psi_{V_i}. \tag{B.149}$$

which is precisely as claimed.

Hence a subset of the generalized null space $E(LJ)$ has been properly characterized. It is important to note, that there may well be other elements of the generalized nullspace $E(LJ)$. These other elements would correspond to additional restrictions which may be placed on the admissible set of perturbations, but would not impact the validity of the equations derived with this subset of the generalized null space. It would be desirable to fully characterize $E(LJ)$; however, such undertakings often rely on the integrability of the underlying system [Yan10; KM77b]. Since the 2D Landau-Lifshitz

equation is not known to be integrable at this time, such a complete characterization would require novel techniques which are beyond the scope of this thesis. For this reason, the modulation equations are necessary, but not sufficient conditions, in order that the ansatz in Eqs B.66-B.68 remain well-ordered in ϵ for $t \ll \mathcal{O}\left(\epsilon^2\right)$.

B.2.2 Step down to 2D

Up to this point, no restrictions have been put on dimension in this problem. While possible to do, it will be cumbersome to write the general modulation equations for magnetics since it would require inverting a $2n+2\times 2n+2$ matrix (n =dimension). Nevertheless, since the $2D$ soliton is what is of interest in this work and the approximate droplet in 2D is what is known, there is now reason to continue on in full generality. From this point on, take $(x_1, x_2) = (x, y)$ and $V = (V_x, V_y)$ to hopefully keep subscripts to a minimum.

As discussed in the previous section, solvability requires that $f \perp E(LJ)$ where

$$E(LJ) = \text{span}\left\{\begin{pmatrix}-1\\0\end{pmatrix}, \begin{pmatrix}\Psi_x\\-U_x\end{pmatrix}, \begin{pmatrix}\Psi_y\\-U_y\end{pmatrix}, \begin{pmatrix}-\Psi_\omega\\U_\omega\end{pmatrix}, \begin{pmatrix}-\Psi_{V_x}\\U_{V_x}\end{pmatrix}, \begin{pmatrix}-\Psi_{V_y}\\U_{V_y}\end{pmatrix}\right\} = \text{span}\{k_1, k_2, k_3, k_4, k_5, k_6\} \tag{B.150}$$

where $k_1,\dots,k_6$ are defined by the above relation and

$$f=-\begin{pmatrix}0\\ \Phi_0'\end{pmatrix}+\begin{pmatrix}\nabla U^T\\ \nabla\Psi^T\end{pmatrix}x_0'-\begin{pmatrix}U\\ \Psi\end{pmatrix}_{\omega}\omega'-\begin{pmatrix}U\\ \Psi\end{pmatrix}_{V}V'+\begin{pmatrix}P_u\\ P_{\tilde{\Phi}}\end{pmatrix} \tag{B.151}$$

$$=-\begin{pmatrix}0\\ \Phi_0'\end{pmatrix}+\begin{pmatrix}U_x & U_y\\ \Psi_x & \Psi_y\end{pmatrix}\begin{pmatrix}x_0'\\ y_0'\end{pmatrix}-\begin{pmatrix}U_\omega\\ \Psi_\omega\end{pmatrix}\omega'-\begin{pmatrix}U_{V_x} & U_{V_y}\\ \Psi_{V_x} & \Psi_{V_y}\end{pmatrix}\begin{pmatrix}V_x{}'\\ V_y{}'\end{pmatrix}+\begin{pmatrix}P_u\\ P_{\tilde{\Phi}}\end{pmatrix} \tag{B.152}$$

$$=-\begin{pmatrix}0\\ \Phi_0'\end{pmatrix}+\begin{pmatrix}U_x & U_y\\ \Psi_x & \Psi_y\end{pmatrix}\begin{pmatrix}x_0'\\ y_0'\end{pmatrix}-\begin{pmatrix}U_\omega\\ \Psi_\omega\end{pmatrix}\omega'-\begin{pmatrix}U_{V_x} & U_{V_y}\\ \Psi_{V_x} & \Psi_{V_y}\end{pmatrix}\begin{pmatrix}V_x{}'\\ V_y{}'\end{pmatrix}+\begin{pmatrix}P_u\\ P_{\tilde{\Phi}}\end{pmatrix} \tag{B.153}$$

$$=\begin{pmatrix}U_x x_0'+U_y y_0'-U_\omega\omega'-U_{V_x}V_x{}'-U_{V_y}V_y{}'+P_u\\ -\Phi_0'+\Psi_x x_0'+\Psi_y y_0'-\Psi_\omega\omega'-\Psi_{V_x}V_x{}'-\Psi_{V_y}V_y{}'+P_{\tilde{\Phi}}\end{pmatrix}. \tag{B.154}$$

Orthogonality here is in the sense of the standard L^2 inner product, $\langle\mathbf{g},\mathbf{h}\rangle=\int_{\mathbb{R}^2}(\mathbf{g}^T\mathbf{h})d\mathbf{x}$. It remains to compute $\langle k_1,f\rangle,\langle k_2,f\rangle,\langle k_3,f\rangle,\langle k_4,f\rangle,\langle k_5,f\rangle$ and $\langle k_6,f\rangle$ to explicitly obtain the relations necessary for solvability (i.e. the modulation equations) .

$$0=\langle k_1,f\rangle=\int_{\mathbb{R}^2}\begin{pmatrix}-1 & 0\end{pmatrix}\begin{pmatrix}U_x x_0'+U_y y_0'-U_\omega\omega'-U_{V_x}V_x{}'-U_{V_y}V_y{}'+P_u\\ -\Phi_0'+\Psi_x x_0'+\Psi_y y_0'-\Psi_\omega\omega'-\Psi_{V_x}V_x{}'-\Psi_{V_y}V_y{}'+P_{\tilde{\Phi}}\end{pmatrix}d\mathbf{x} \tag{B.155}$$

$$=-\int_{\mathbb{R}^2}\left(U_x x_0'+U_y y_0'-U_\omega\omega'-U_{V_x}V_x{}'-U_{V_y}V_y{}'+P_u\right)d\mathbf{x} \tag{B.156}$$

$$=-\Bigg(\Big(\cancelto{0}{\int_{\mathbb{R}^2}U_x d\mathbf{x}}\Big)x_0'+\Big(\cancelto{0}{\int_{\mathbb{R}^2}U_y d\mathbf{x}}\Big)y_0'-\Big(\int_{\mathbb{R}^2}U_\omega d\mathbf{x}\Big)\omega' \tag{B.157}$$

$$-\Big(\int_{\mathbb{R}^2}U_{V_x}d\mathbf{x}\Big)V_x{}'-\Big(\int_{\mathbb{R}^2}U_{V_y}d\mathbf{x}\Big)V_y{}'+\int_{\mathbb{R}^2}P_u d\mathbf{x}\Bigg) \tag{B.158}$$

where the cancelation occurs since the boundary conditions on the soliton are decay at infinity.

Rearranging, this equation becomes

$$\begin{pmatrix} -\int_{\mathbb{R}^2} U_\omega d\mathbf{x} & -\int_{\mathbb{R}^2} U_{V_x} d\mathbf{x} & -\int_{\mathbb{R}^2} U_{V_y} d\mathbf{x} \end{pmatrix} \begin{pmatrix} \omega' \\ V_x' \\ V_y' \end{pmatrix} = -\int_{\mathbb{R}^2} P_u d\mathbf{x} \tag{B.159}$$

So now one of six equations has been obtained. Next,

$$0 = \langle k_2, f \rangle = \int_{\mathbb{R}^2} \begin{pmatrix} \Psi_x & -U_x \end{pmatrix} \begin{pmatrix} U_x x_0' + U_y y_0' - U_\omega \omega' - U_{V_x} V_x' - U_{V_y} V_y' + P_u \\ -\Phi_0' + \Psi_x x_0' + \Psi_y y_0' - \Psi_\omega \omega' - \Psi_{V_x} V_x' - \Psi_{V_y} V_y' + P_{\tilde{\Phi}} \end{pmatrix} d\mathbf{x} \tag{B.160}$$

$$= \int_{\mathbb{R}^2} \Psi_x \left(U_x x_0' + U_y y_0' - U_\omega \omega' - U_{V_x} V_x' - U_{V_y} V_y' + P_u \right) d\mathbf{x} \tag{B.161}$$

$$+ \int_{\mathbb{R}^2} -U_x \left(-\Phi_0' + \Psi_x x_0' + \Psi_y y_0' - \Psi_\omega \omega' - \Psi_{V_x} V_x' - \Psi_{V_y} V_y' + P_{\tilde{\Phi}} \right) d\mathbf{x} \tag{B.162}$$

$$-\int_{\mathbb{R}^2} (\Psi_x P_u - U_x P_{\tilde{\Phi}}) d\mathbf{x} = \cancelto{0}{\left(\int_{\mathbb{R}^2} U_x d\mathbf{x} \right)} \Phi_0' + \cancelto{0}{\left(\int_{\mathbb{R}^2} \Psi_x U_x - \Psi_x U_x d\mathbf{x} \right)} x_0' + \cancelto{0}{\left(\int_{\mathbb{R}^2} \Psi_x U_y - \Psi_y U_x d\mathbf{x} \right)} x_0' \tag{B.163}$$

$$- \left(\int_{\mathbb{R}^2} \Psi_x U_\omega - \Psi_\omega U_x d\mathbf{x} \right) \omega' - \left(\int_{\mathbb{R}^2} \Psi_x U_{V_x} - \Psi_{V_x} U_x d\mathbf{x} \right) V_x' \tag{B.164}$$

$$- \left(\int_{\mathbb{R}^2} \Psi_x U_{V_y} - \Psi_{V_y} U_x d\mathbf{x} \right) V_y' \tag{B.165}$$

Rearranging this becomes

$$\begin{pmatrix} \int_{\mathbb{R}^2} (\Psi_x U_\omega - \Psi_\omega U_x) d\mathbf{x} \\ \int_{\mathbb{R}^2} (\Psi_x U_{V_x} - \Psi_{V_x} U_x) d\mathbf{x} \\ \int_{\mathbb{R}^2} (\Psi_x U_{V_y} - \Psi_{V_y} U_x) d\mathbf{x} \end{pmatrix} \cdot \begin{pmatrix} \omega' \\ V_x' \\ V_y' \end{pmatrix} = \int_{\mathbb{R}^2} (\Psi_x P_u - U_x P_{\tilde{\Phi}}) d\mathbf{x} \tag{B.166}$$

The computation for $\langle k_3, f \rangle = 0$ is symmetric so it is possible to immediately write down the resulting expression

$$\begin{pmatrix} \int_{\mathbb{R}^2}(\Psi_y U_\omega - \Psi_\omega U_y)d\mathbf{x} \\ \int_{\mathbb{R}^2}(\Psi_y U_{V_x} - \Psi_{V_x} U_y)d\mathbf{x} \\ \int_{\mathbb{R}^2}(\Psi_y U_{V_y} - \Psi_{V_y} U_y)d\mathbf{x} \end{pmatrix} \cdot \begin{pmatrix} \omega' \\ V_x{}' \\ V_y{}' \end{pmatrix} = \int_{\mathbb{R}^2}(\Psi_x P_u - U_x P_{\bar{\Phi}})d\mathbf{x} \tag{B.167}$$

Now, half way to the general, 2D modulation equations. 3 more conditions, and then moving on to the small ω, small V limit where it is possible to obtain analytical expressions.

$$0 = \langle k_4, f \rangle = \int_{\mathbb{R}^2} \begin{pmatrix} -\Psi_\omega & U_\omega \end{pmatrix} \begin{pmatrix} U_x x_0' + U_y y_0' - U_\omega \omega' - U_{V_x} V_x{}' - U_{V_y} V_y{}' + P_u \\ -\Phi_0' + \Psi_x x_0' + \Psi_y y_0' - \Psi_\omega \omega' - \Psi_{V_x} V_x{}' - \Psi_{V_y} V_y{}' + P_{\bar{\Phi}} \end{pmatrix} d\mathbf{x} \tag{B.168}$$

$$= \int_{\mathbb{R}^2} -\Psi_\omega \left(U_x x_0' + U_y y_0' - U_\omega \omega' - U_{V_x} V_x{}' - U_{V_y} V_y{}' + P_u \right) d\mathbf{x} \tag{B.169}$$

$$+ \int_{\mathbb{R}^2} U_\omega \left(-\Phi_0' + \Psi_x x_0' + \Psi_y y_0' - \Psi_\omega \omega' - \Psi_{V_x} V_x{}' - \Psi_{V_y} V_y{}' + P_{\bar{\Phi}} \right) d\mathbf{x} \tag{B.170}$$

$$= -\int_{\mathbb{R}^2} \Psi_\omega P_u d\mathbf{x} + \int_{\mathbb{R}^2} U_\omega P_{\bar{\Phi}} d\mathbf{x} \tag{B.171}$$

$$+ \cancelto{0}{\left(\int_{\mathbb{R}^2} (\Psi_\omega U_\omega - U_\omega \Psi_\omega) d\mathbf{x} \right)} \omega' - \left(\int_{\mathbb{R}^2} (\Psi_\omega U_x - U_\omega \Psi_x) d\mathbf{x} \right) x_0' \tag{B.172}$$

$$- \left(\int_{\mathbb{R}^2} (\Psi_\omega U_y - U_\omega \Psi_y) d\mathbf{x} \right) y_0' + \left(\int_{\mathbb{R}^2} (\Psi_\omega U_{V_x} - U_\omega \Psi_{V_x}) d\mathbf{x} \right) V_x{}' \tag{B.173}$$

$$+ \left(\int_{\mathbb{R}^2} (\Psi_\omega U_{V_y} - U_\omega \Psi_{V_y}) d\mathbf{x} \right) V_y{}' - \left(\int_{\mathbb{R}^2} U_\omega d\mathbf{x} \right) \Phi_0' \tag{B.174}$$

Rearranging, this becomes

$$\begin{pmatrix} \int_{\mathbb{R}^2} U_\omega d\mathbf{x} \\ -\int_{\mathbb{R}^2}(\Psi_x U_\omega - \Psi_\omega U_x)d\mathbf{x} \\ -\int_{\mathbb{R}^2}(\Psi_y U_\omega - \Psi_\omega U_y)d\mathbf{x} \\ -\int_{\mathbb{R}^2}(\Psi_\omega U_{V_x} - U_\omega \Psi_{V_x})d\mathbf{x} \\ -\int_{\mathbb{R}^2}(\Psi_\omega U_{V_y} - U_\omega \Psi_{V_y})d\mathbf{x} \end{pmatrix} \cdot \begin{pmatrix} \Phi_0' \\ x_0' \\ y_0' \\ V_x{}' \\ V_y{}' \end{pmatrix} = -\int_{\mathbb{R}^2} \Psi_\omega P_u d\mathbf{x} + \int_{\mathbb{R}^2} U_\omega P_{\tilde{\Phi}} d\mathbf{x} \tag{B.175}$$

Now the last two (which again can be done simultaneously because of symmetry in the algebra)

$$0 = \langle k_5, f \rangle = \int_{\mathbb{R}^2} \begin{pmatrix} -\Psi_{V_x} & U_{V_x} \end{pmatrix} \begin{pmatrix} U_x x_0' + U_y y_0' - U_\omega \omega' - U_{V_x} V_x{}' - U_{V_y} V_y{}' + P_u \\ -\Phi_0' + \Psi_x x_0' + \Psi_y y_0' - \Psi_\omega \omega' - \Psi_{V_x} V_x{}' - \Psi_{V_y} V_y{}' + P_{\tilde{\Phi}} \end{pmatrix} d\mathbf{x} \tag{B.176}$$

$$= \int_{\mathbb{R}^2} -\Psi_{V_x} \left(U_x x_0' + U_y y_0' - U_\omega \omega' - U_{V_x} V_x{}' - U_{V_y} V_y{}' + P_u \right) d\mathbf{x} \tag{B.177}$$

$$+ \int_{\mathbb{R}^2} U_{V_x} \left(-\Phi_0' + \Psi_x x_0' + \Psi_y y_0' - \Psi_\omega \omega' - \Psi_{V_x} V_x{}' - \Psi_{V_y} V_y{}' + P_{\tilde{\Phi}} \right) d\mathbf{x} \tag{B.178}$$

$$+ \left(\int_{\mathbb{R}^2} (-\Psi_{V_x} U_x + \Psi_x U_{V_x}) d\mathbf{x} \right) x_0' \tag{B.179}$$

$$= \int_{\mathbb{R}^2} (-\Psi_{V_x} P_u + U_{V_x} P_{\tilde{\Phi}}) d\mathbf{x} - \left(\int_{\mathbb{R}^2} U_{V_x} d\mathbf{x} \right) \Phi_0' \tag{B.180}$$

$$+ \left(\int_{\mathbb{R}^2} (-\Psi_{V_x} U_y + \Psi_y U_{V_x}) d\mathbf{x} \right) y_0' + \left(\int_{\mathbb{R}^2} (\Psi_{V_x} U_\omega - \Psi_\omega U_{V_x}) d\mathbf{x} \right) \omega' \tag{B.181}$$

$$+ \left(\int_{\mathbb{R}^2} (\Psi_{V_x} U_{V_x} - \Psi_{V_x} U_{V_x}) d\mathbf{x} \right) V_x{}' + \left(\int_{\mathbb{R}^2} (\Psi_{V_x} U_{V_y} - \Psi_{V_y} U_{V_x}) d\mathbf{x} \right) V_y{}' \tag{B.182}$$

$\int_{\mathbb{R}^2} (\Psi_{V_x} U_{V_x} - \Psi_{V_x} U_{V_x}) d\mathbf{x} \to 0$

Rearranging this becomes

$$\begin{pmatrix} \int_{\mathbb{R}^2} U_{V_x} d\mathbf{x} \\ -\int_{\mathbb{R}^2} (\Psi_x U_{V_x} - \Psi_{V_x} U_x) d\mathbf{x} \\ -\int_{\mathbb{R}^2} (\Psi_y U_{V_x} - \Psi_{V_x} U_y) d\mathbf{x} \\ \int_{\mathbb{R}^2} (\Psi_\omega U_{V_x} - U_\omega \Psi_{V_x}) d\mathbf{x} \\ -\int_{\mathbb{R}^2} (\Psi_{V_x} U_{V_y} - U_{V_x} \Psi_{V_y}) d\mathbf{x} \end{pmatrix} \cdot \begin{pmatrix} \Phi_0' \\ x_0' \\ y_0' \\ \omega' \\ V_y{}' \end{pmatrix} = -\int_{\mathbb{R}^2} \Psi_{V_x} P_u d\mathbf{x} + \int_{\mathbb{R}^2} U_{V_x} P_{\tilde{\Phi}} d\mathbf{x} \tag{B.183}$$

and the symmetric condition induced by $\langle k_6, f \rangle = 0$ is simply

$$\begin{pmatrix} \int_{\mathbb{R}^2} U_{V_y} d\mathbf{x} \\ -\int_{\mathbb{R}^2} (\Psi_x U_{V_y} - \Psi_{V_y} U_x) d\mathbf{x} \\ -\int_{\mathbb{R}^2} (\Psi_y U_{V_y} - \Psi_{V_y} U_y) d\mathbf{x} \\ \int_{\mathbb{R}^2} (\Psi_\omega U_{V_y} - U_\omega \Psi_{V_y}) d\mathbf{x} \\ \int_{\mathbb{R}^2} (\Psi_{V_x} U_{V_y} - U_{V_x} \Psi_{V_y}) d\mathbf{x} \end{pmatrix} \cdot \begin{pmatrix} \Phi_0' \\ x_0' \\ y_0' \\ \omega' \\ V_x{}' \end{pmatrix} = -\int_{\mathbb{R}^2} \Psi_{V_y} P_u d\mathbf{x} + \int_{\mathbb{R}^2} U_{V_y} P_{\tilde{\Phi}} d\mathbf{x} \tag{B.184}$$

Eqs. B.159-B.184, can be recast in matrix form

$$\begin{pmatrix} 0 & 0 & 0 & -\int_{\mathbb{R}^2} U_\omega d\mathbf{x} & -\int_{\mathbb{R}^2} U_{V_x} d\mathbf{x} & -\int_{\mathbb{R}^2} U_{V_y} d\mathbf{x} \\ 0 & 0 & 0 & \int_{\mathbb{R}^2} (\Psi_x U_\omega - \Psi_\omega U_x) d\mathbf{x} & \int_{\mathbb{R}^2} (\Psi_x U_{V_x} - \Psi_{V_x} U_x) d\mathbf{x} & \int_{\mathbb{R}^2} (\Psi_x U_{V_y} - \Psi_{V_y} U_x) d\mathbf{x} \\ 0 & 0 & 0 & \int_{\mathbb{R}^2} (\Psi_y U_\omega - \Psi_\omega U_y) d\mathbf{x} & \int_{\mathbb{R}^2} (\Psi_y U_{V_x} - \Psi_{V_x} U_y) d\mathbf{x} & \int_{\mathbb{R}^2} (\Psi_y U_{V_y} - \Psi_{V_y} U_y) d\mathbf{x} \\ \int_{\mathbb{R}^2} U_\omega d\mathbf{x} & -\int_{\mathbb{R}^2} (\Psi_x U_\omega - \Psi_\omega U_x) d\mathbf{x} & -\int_{\mathbb{R}^2} (\Psi_y U_\omega - \Psi_\omega U_y) d\mathbf{x} & 0 & -\int_{\mathbb{R}^2} (\Psi_\omega U_{V_x} - U_\omega \Psi_{V_x}) d\mathbf{x} & -\int_{\mathbb{R}^2} (\Psi_\omega U_{V_y} - U_\omega \Psi_{V_y}) d\mathbf{x} \\ \int_{\mathbb{R}^2} U_{V_x} d\mathbf{x} & -\int_{\mathbb{R}^2} (\Psi_x U_{V_x} - \Psi_{V_x} U_x) d\mathbf{x} & -\int_{\mathbb{R}^2} (\Psi_y U_{V_x} - \Psi_{V_x} U_y) d\mathbf{x} & \int_{\mathbb{R}^2} (\Psi_\omega U_{V_x} - U_\omega \Psi_{V_x}) d\mathbf{x} & 0 & -\int_{\mathbb{R}^2} (\Psi_{V_x} U_{V_y} - U_{V_x} \Psi_{V_y}) d\mathbf{x} \\ \int_{\mathbb{R}^2} U_{V_y} d\mathbf{x} & -\int_{\mathbb{R}^2} (\Psi_x U_{V_y} - \Psi_{V_y} U_x) d\mathbf{x} & -\int_{\mathbb{R}^2} (\Psi_y U_{V_y} - \Psi_{V_y} U_y) d\mathbf{x} & \int_{\mathbb{R}^2} (\Psi_\omega U_{V_y} - U_\omega \Psi_{V_y}) d\mathbf{x} & \int_{\mathbb{R}^2} (\Psi_{V_x} U_{V_y} - U_{V_x} \Psi_{V_y}) d\mathbf{x} & 0 \end{pmatrix} \begin{pmatrix} \Phi_0 \\ x_0 \\ y_0 \\ \omega \\ V_x \\ V_y \end{pmatrix}' = \begin{pmatrix} -\int_{\mathbb{R}^2} P_u d\mathbf{x} \\ \int_{\mathbb{R}^2} (\Psi_x P_u - U_x P_{\tilde{\Phi}}) d\mathbf{x} \\ \int_{\mathbb{R}^2} (\Psi_x P_u - U_x P_{\tilde{\Phi}}) d\mathbf{x} \\ -\int_{\mathbb{R}^2} \Psi_\omega P_u d\mathbf{x} + \int_{\mathbb{R}^2} U_\omega P_{\tilde{\Phi}} d\mathbf{x} \\ -\int_{\mathbb{R}^2} \Psi_{V_x} P_u d\mathbf{x} + \int_{\mathbb{R}^2} U_{V_x} P_{\tilde{\Phi}} d\mathbf{x} \\ -\int_{\mathbb{R}^2} \Psi_{V_y} P_u d\mathbf{x} + \int_{\mathbb{R}^2} U_{V_y} P_{\tilde{\Phi}} d\mathbf{x} \end{pmatrix} \tag{B.185}$$

This matrix is antisymmetric as the theory suggests it would be (Section 2.1). In fact, this matrix is written out almost exactly (Section 2.4) (as is the right hand side). From here on out in this appendix, the notation M will be used to refer to the matrix in Eq. B.185.

There's a little more processing that can be done. Recall $\mathcal{N} = \int_{\mathbb{R}^2}(1-u)d\mathbf{X}$. For the soliton solution it is evident that $-\mathcal{N}_\omega = \int_{\mathbb{R}^2} U_\omega\, d\mathbf{x}$, $-\mathcal{N}_{V_x} = \int_{\mathbb{R}^2} U_{V_x}\, d\mathbf{x}$, and $-\mathcal{N}_{V_y} = \int_{\mathbb{R}^2} U_{V_y}\, d\mathbf{x}$. Further note, if $\nabla\Psi$ goes to a constant at infinity,

$$\int_{\mathbb{R}^2}(\Psi_x U_y - \Psi_y U_x)d\mathbf{x} = \int_{\mathbb{R}^2}\Psi_x U_y\, d\mathbf{x} - \int_{\mathbb{R}^2}\Psi_y U_x\, d\mathbf{x} \tag{B.186}$$

$$= -\int_{\mathbb{R}^2}\Psi_x(1-U)_y\, d\mathbf{x} + \int_{\mathbb{R}^2}\Psi_y(1-U)_x\, d\mathbf{x} \tag{B.187}$$

integrating by parts this becomes (B.188)

$$= \Psi_x(1-U)\Big|_{y\to\pm\infty}^{\to 0} + \int_{\mathbb{R}^2}\Psi_{xy}(1-U)d\mathbf{x} + \int_{\mathbb{R}^2}\Psi_y(1-U)_x\, d\mathbf{x} \tag{B.189}$$

integrating by parts again (B.190)

$$= \Psi_x(1-U)\Big|_{x\to\pm\infty}^{\to 0} - \int_{\mathbb{R}^2}\Psi_{xy}(1-U)d\mathbf{x} + \int_{\mathbb{R}^2}\Psi_y(1-U)_x\, d\mathbf{x} \tag{B.191}$$

$$= -\int_{\mathbb{R}^2}\Psi_{xy}(1-U)d\mathbf{x} + \int_{\mathbb{R}^2}\Psi_y(1-U)_x\, d\mathbf{x} = 0. \tag{B.192}$$

So that integral vanishes identically as well. A few more comments, recall $\mathcal{P} = -\int_{\mathbb{R}^2}\nabla\Psi(1-U)d\mathbf{x}$. Consider the first component of this vector-valued conserved quantity. $\mathcal{P}_1 = -\int_{\mathbb{R}^2}\Psi_x(1-U)d\mathbf{x}$.

Differentiate this with respect to ω.

$$\partial_\omega(-\int_{\mathbb{R}^2}\Psi_x(1-U)d\mathbf{x}) = -\int_{\mathbb{R}^2}\Psi_{x\omega}(1-U)d\mathbf{x} - \int_{\mathbb{R}^2}\Psi_x(1-U)_\omega d\mathbf{x} \tag{B.193}$$

$$= -\int_{\mathbb{R}^2}\Psi_{x\omega}(1-U)d\mathbf{x} + \int_{\mathbb{R}^2}\Psi_x U_\omega d\mathbf{x} \tag{B.194}$$

integrating by parts, (B.195)

$$= \Psi_\omega(1-U)\Big|_{x\to\pm\infty}^{0} + \int_{\mathbb{R}^2}\Psi_\omega(1-U)_x d\mathbf{x} + \int_{\mathbb{R}^2}\Psi_x U_\omega d\mathbf{x} \tag{B.196}$$

$$= -\int_{\mathbb{R}^2}\Psi_\omega U_x d\mathbf{x} + \int_{\mathbb{R}^2}\Psi_x U_\omega d\mathbf{x} \tag{B.197}$$

$$= \int_{\mathbb{R}^2}\Psi_x U_\omega - \Psi_\omega U_x d\mathbf{x} \tag{B.198}$$

which is a recognizable term in the matrix above. Similar calculations hold for differentiation with respect to V_x, V_y and will not be presented here. The computations are identical for the second component of the momentum. With these observations it is possible to write the matrix in blockwise form as follows.

$$M = \begin{pmatrix} 0 & \mathbf{0} & -\mathcal{N}_\omega & -(\nabla_V\mathcal{N})^T \\ \mathbf{0} & \mathbf{0} & \mathcal{P}_\omega & (\nabla_V\mathcal{P})^T \\ \mathcal{N}_\omega & -\mathcal{P}_\omega & 0 & (\nabla_V\mathcal{K})^T \\ \nabla_V\mathcal{N} & -\nabla_V\mathcal{P} & -\nabla_V\mathcal{K} & \nabla_V\mathcal{W} \end{pmatrix} \tag{B.199}$$

where generally ∇_V is the gradient operation with respect to the components (V_x, V_y). However, defining

$$\nabla_V\mathcal{K} = \begin{pmatrix} -\int_{\mathbb{R}^2}(\Psi_\omega U_{V_x} - \Psi_{V_x}U_\omega)d\mathbf{x} \\ -\int_{\mathbb{R}^2}(\Psi_\omega U_{V_y} - \Psi_{V_y}U_\omega)d\mathbf{x} \end{pmatrix} \tag{B.200}$$

and

$$\nabla_V\mathcal{W} = \begin{pmatrix} 0 & -\int_{\mathbb{R}^2}(\Psi_{V_x}U_{V_y} - \Psi_{V_y}U_{V_x})d\mathbf{x} \\ \int_{\mathbb{R}^2}(\Psi_{V_x}U_{V_y} - \Psi_{V_y}U_{V_x})d\mathbf{x} & 0 \end{pmatrix}. \tag{B.201}$$

This notation has been chosen to emphasize the hypothesis that $\mathcal{K}$ and $\mathcal{W}$ represent two other conserved quantities that have not yet been recognized. If this is so (and it may not be) then the chain rule (differentiating with respect to time and therefore the parameters) would require that

$$\mathcal{N}_\omega = \mathcal{K}_{\Phi_0}, -\mathcal{P}_\omega = -\nabla_{\mathbf{x}_0}\mathcal{K}, \mathcal{K}_\omega = 0, \nabla_V \mathcal{N} = \mathcal{W}_{\Phi_0}, -\nabla_V \mathcal{P} = \nabla_{\mathbf{x}_0}\mathcal{W} \text{ and } \nabla_V \mathcal{W} = -\nabla_V \mathcal{W}^T. \quad \text{(B.202)}$$

B.2.3 Small ω, small $|\mathbf{V}|$

The conserved quantities form of the matrix will now be used and computations will be executed as explicitly as possible. Another step down in generality must be taken at this point. The step down to $2D$ was moderately optional, but now it is necessary to evaluate a bunch of integrals and nothing further can be done without an explicit solution. The approximate soliton solution is

$$u = \tanh\left(\rho - \frac{1}{\omega}\right) + \mathcal{O}\left(\omega^2, V^2\right) \quad \text{(B.203)}$$

$$\bar{\Phi} = \omega t + \Phi_0 - \underbrace{\frac{\mathbf{V}\cdot\hat{\rho}}{\omega^2}}_{\Psi} + \mathcal{O}\left(\frac{V}{\omega}\right) \quad \text{(B.204)}$$

where ρ is the coordinate measured from the droplet center. This approximation is carefully derived in detail in Section 1.1.2.

The derivatives with respect to all the parameters can now be computed

$$U_\omega \approx \partial_\omega \tanh\left(\rho - \frac{1}{\omega}\right) = \frac{1}{\omega^2}\operatorname{sech}^2\left(\rho - \frac{1}{\omega}\right) \tag{B.205}$$

$$U_x \approx \partial_x \tanh\left(\rho - \frac{1}{\omega}\right) = \operatorname{sech}^2\left(\rho - \frac{1}{\omega}\right)\rho_x = \operatorname{sech}^2\left(\rho - \frac{1}{\omega}\right)\cos(\varphi) \tag{B.206}$$

$$U_y \approx \partial_y \tanh\left(\rho - \frac{1}{\omega}\right) = \operatorname{sech}^2\left(\rho - \frac{1}{\omega}\right)\rho_y = \operatorname{sech}^2\left(\rho - \frac{1}{\omega}\right)\sin(\varphi) \tag{B.207}$$

$$U_{V_x} \approx \partial_{V_x} \tanh\left(\rho - \frac{1}{\omega}\right) = 0 \tag{B.208}$$

$$U_{V_y} \approx \partial_{V_y} \tanh\left(\rho - \frac{1}{\omega}\right) = 0 \tag{B.209}$$

and

$$\Psi_\omega \approx \partial_\omega\left(\frac{-\mathbf{V}\cdot\hat{\rho}}{\omega^2}\right) = \frac{2(\mathbf{V}\cdot\hat{\rho})}{\omega^3} = \frac{2\left(V_x\cos(\varphi) + V_y\sin(\varphi)\right)}{\omega^3} \tag{B.210}$$

$$\Psi_x \approx \partial_x\left(-\frac{\mathbf{V}\cdot\hat{\rho}}{\omega^2}\right) \tag{B.211}$$

$$= -\partial_x\left(\frac{\left(V_x\cos(\varphi) + V_y\sin(\varphi)\right)}{\omega^2}\right) \tag{B.212}$$

$$= -\frac{1}{\omega^2}\left(-V_x\sin(\varphi) + V_y\cos(\varphi)\right)\varphi_x \tag{B.213}$$

$$= \frac{\sin(\varphi)}{\rho\,\omega^2}\left(-V_x\sin(\varphi) + V_y\cos(\varphi)\right) \tag{B.214}$$

$$\Psi_y \approx \partial_y\left(-\frac{\mathbf{V}\cdot\hat{\rho}}{\omega^2}\right) \tag{B.215}$$
$$=-\partial_y\left(\frac{\left(V_x\cos(\varphi)+V_y\sin(\varphi)\right)}{\omega^2}\right) \tag{B.216}$$
$$=\frac{-1}{\omega^2}\left(-V_x\sin(\varphi)+V_y\cos(\varphi)\right)\varphi_y \tag{B.217}$$
$$=\frac{-\cos(\varphi)}{\rho\,\omega^2}\left(-V_x\sin(\varphi)+V_y\cos(\varphi)\right) \tag{B.218}$$

$$\Psi_{V_x} \approx \partial_{V_x}\left(-\frac{\mathbf{V}\cdot\hat{\rho}}{\omega^2}\right)=-\partial_{V_x}\left(\frac{\left(V_x\cos(\varphi)+V_y\sin(\varphi)\right)}{\omega^2}\right)=\frac{-\cos(\varphi)}{\omega^2} \tag{B.219}$$
$$\Psi_{V_y} \approx \partial_{V_y}\left(-\frac{\mathbf{V}\cdot\hat{\rho}}{\omega^2}\right)=-\partial_{V_y}\left(\frac{\left(V_x\cos(\varphi)+V_y\sin(\varphi)\right)}{\omega^2}\right)=\frac{-\sin(\varphi)}{\omega^2}. \tag{B.220}$$

The first step is to start evaluating integrals.

$$\int_{\mathbb{R}^2} U_\omega d\mathbf{x}=\int_0^\infty\int_0^{2\pi}\frac{1}{\omega^2}\operatorname{sech}^2\left(\rho-\frac{1}{\omega}\right)\rho\,d\varphi\,d\rho \tag{B.221}$$
$$=\frac{2\pi}{\omega^2}\int_0^\infty\operatorname{sech}^2\left(\rho-\frac{1}{\omega}\right)\rho\,d\rho \tag{B.222}$$
$$=\frac{2\pi}{\omega^2}\log\left(1+e^{2/\omega}\right) \tag{B.223}$$
$$\approx\frac{2\pi}{\omega^2}\log\left(e^{2/\omega}\right) \tag{B.224}$$
$$\int_{\mathbb{R}^2} U_\omega d\mathbf{x}=\frac{4\pi}{\omega^3} \tag{B.225}$$

$$\int_{\mathbb{R}^2} U_{V_x} d\mathbf{x}=\int_0^\infty\int_0^{2\pi}(0)\rho\,d\varphi\,d\rho=0 \tag{B.226}$$

$$\int_{\mathbb{R}^2} U_{V_y} d\mathbf{x}=\int_0^\infty\int_0^{2\pi}(0)\rho\,d\varphi\,d\rho=0 \tag{B.227}$$

Breaking up $\int_{\mathbb{R}^2}(\Psi_x U_y - \Psi_y U_x)d\mathbf{x}$ into $\int_{\mathbb{R}^2}(\Psi_x U_y)d\mathbf{x}$ and $\int_{\mathbb{R}^2}(\Psi_y U_x)d\mathbf{x}$

$$\int_{\mathbb{R}^2}(\Psi_x U_y)d\mathbf{x} = \int_0^\infty \int_0^{2\pi} \left(\frac{\sin(\varphi)}{\rho\omega^2}\left(-V_x\sin(\varphi)+V_y\cos(\varphi)\right)\right)\left(\operatorname{sech}^2\left(\rho-\frac{1}{\omega}\right)\sin(\varphi)\right)\rho\, d\varphi\, d\rho \tag{B.228}$$

$$= \frac{-1}{\omega^2}\left[V_x\int_0^\infty\left(\operatorname{sech}^2\left(\rho-\frac{1}{\omega}\right)\cancelto{0}{\int_0^{2\pi}\sin^3(\varphi)d\varphi}\right)d\rho\right. \tag{B.229}$$

$$\left. + V_y\int_0^\infty\left(\operatorname{sech}^2\left(\rho-\frac{1}{\omega}\right)\cancelto{0}{\int_0^{2\pi}\left(-\cos(\varphi)\sin^2(\varphi)\right)d\varphi}\right)d\rho\right] \tag{B.230}$$

$$\int_{\mathbb{R}^2}(\Psi_x U_y)d\mathbf{x} = 0 \tag{B.231}$$

$$\int_{\mathbb{R}^2}(\Psi_y U_x)d\mathbf{x} = \int_0^\infty \int_0^{2\pi} \left(\frac{-\cos(\varphi)}{\rho\omega^2}\left(-V_x\sin(\varphi)+V_y\cos(\varphi)\right)\right)\left(\operatorname{sech}^2\left(\rho-\frac{1}{\omega}\right)\cos(\varphi)\right)\rho\, d\varphi\, d\rho$$

(B.232)

$$= \frac{-1}{\omega^2}\left[V_x\int_0^\infty\left(\operatorname{sech}^2\left(\rho-\frac{1}{\omega}\right)\cancelto{0}{\int_0^{2\pi}\left(-\sin(\varphi)\cos^2(\varphi)\right)d\varphi}\right)d\rho\right. \tag{B.233}$$

$$\left. + V_y\int_0^\infty\left(\operatorname{sech}^2\left(\rho-\frac{1}{\omega}\right)\cancelto{0}{\int_0^{2\pi}\left(\cos^3(\varphi)\right)d\varphi}\right)d\rho\right] \tag{B.234}$$

$$= 0 \tag{B.235}$$

Hence $\int_{\mathbb{R}^2}(\Psi_x U_y - \Psi_y U_x)d\mathbf{x} = 0$. Next, breaking up $\left(\int_{\mathbb{R}^2}(\Psi_x U_\omega - \Psi_\omega U_x)d\mathbf{x}\right)$ into $\int_{\mathbb{R}^2}(\Psi_x U_\omega)d\mathbf{x}$ and $\int_{\mathbb{R}^2}(\Psi_\omega U_x)d\mathbf{x}$

$$\int_{\mathbb{R}^2}(\Psi_x U_\omega)d\mathbf{x} = \int_0^\infty\int_0^{2\pi}\left(\frac{\sin(\varphi)}{\rho\omega^2}\left(-V_x\sin(\varphi)+V_y\cos(\varphi)\right)\right)\left(\frac{1}{\omega^2}\mathrm{sech}^2\left(\rho-\frac{1}{\omega}\right)\right)\rho\, d\varphi\, d\rho \tag{B.236}$$

$$= \frac{-1}{\omega^4}\left[V_x\int_0^\infty\left(\mathrm{sech}^2\left(\rho-\frac{1}{\omega}\right)\int_0^{2\pi}(\sin^2(\varphi))d\varphi\right)d\rho\right. \tag{B.237}$$

$$\left. + V_y\int_0^\infty\left(\mathrm{sech}^2\left(\rho-\frac{1}{\omega}\right)\underbrace{\int_0^{2\pi}\left(-\cos(\varphi)\sin(\varphi)\right)d\varphi}_{0}\right)d\rho\right] \tag{B.238}$$

$$= \frac{-\pi}{\omega^4}V_x\int_0^\infty\left(\mathrm{sech}^2\left(\rho-\frac{1}{\omega}\right)\right)d\rho \tag{B.239}$$

$$= \frac{-\pi}{\omega^4}V_x\left(1+\tanh\left(\frac{1}{\omega}\right)\right) \tag{B.240}$$

$$\approx \frac{-\pi}{\omega^4}V_x(1+1) = \frac{-2\pi}{\omega^4}V_x \tag{B.241}$$

$$\int_{\mathbb{R}^2}(\Psi_\omega U_x)d\mathbf{x} = \int_0^\infty\int_0^{2\pi}\left(\frac{2\left(V_x\cos(\varphi)+V_y\sin(\varphi)\right)}{\omega^3}\right)\left(\mathrm{sech}^2\left(\rho-\frac{1}{\omega}\right)\cos(\varphi)\right)\rho\, d\varphi\, d\rho \tag{B.242}$$

$$= \frac{2}{\omega^3}\int_0^\infty\mathrm{sech}^2\left(\rho-\frac{1}{\omega}\right)\rho\left[V_x\int_0^{2\pi}\cos^2(\varphi)d\varphi + V_y\underbrace{\int_0^{2\pi}\sin(\varphi)\cos(\varphi)d\varphi}_{0}\right]d\rho \tag{B.243}$$

$$= \frac{2\pi}{\omega^3}V_x\int_0^\infty\mathrm{sech}^2\left(\rho-\frac{1}{\omega}\right)\rho\, d\rho \tag{B.244}$$

$$= \frac{2\pi}{\omega^3}V_x\log\left(1+e^{\frac{2}{\omega}}\right) \tag{B.245}$$

$$\approx \frac{2\pi}{\omega^3}V_x\log\left(e^{\frac{2}{\omega}}\right) \tag{B.246}$$

$$\approx \frac{4\pi}{\omega^4}V_x \tag{B.247}$$

Putting this together,

$$\left(\int_{\mathbb{R}^2}(\Psi_x U_\omega - \Psi_\omega U_x)d\mathbf{x}\right) = \frac{-2\pi}{\omega^4}V_x - \frac{4\pi}{\omega^4}V_x = -\frac{6\pi}{\omega^4}V_x \tag{B.248}$$

Next consider $\left(\int_{\mathbb{R}^2}(\Psi_x U_{V_x}-\Psi_{V_x}U_x)d\mathbf{x}\right)$ again by separating out into $\int_{\mathbb{R}^2}(\Psi_x U_{V_x})d\mathbf{x}$ and $\int_{\mathbb{R}^2}(\Psi_{V_x}U_x)d\mathbf{x}$. The first of these is immediately zero since $U_{V_x}=0$.

$$\int_{\mathbb{R}^2}(\Psi_{V_x}U_x)d\mathbf{x}=\int_0^\infty\int_0^{2\pi}\left(\frac{-\cos(\varphi)}{\omega^2}\right)\left(\operatorname{sech}^2\left(\rho-\frac{1}{\omega}\right)\cos(\varphi)\right)\rho\,d\varphi\,d\rho \tag{B.249}$$

$$=\frac{-1}{\omega^2}\int_0^\infty\operatorname{sech}^2\left(\rho-\frac{1}{\omega}\right)\rho\left[\int_0^{2\pi}\left(\cos^2(\varphi)\right)d\varphi\right]d\rho \tag{B.250}$$

$$=\frac{-\pi}{\omega^2}=\frac{-\pi}{\omega^2}\log\left(1+e^{\frac{2}{\omega}}\right)\approx\frac{-\pi}{\omega^2}\log\left(e^{\frac{2}{\omega}}\right) \tag{B.251}$$

$$\approx\frac{-2\pi}{\omega^3} \tag{B.252}$$

So

$$\int_{\mathbb{R}^2}(\Psi_x U_{V_x}-\Psi_{V_x}U_x)d\mathbf{x}=\frac{2\pi}{\omega^3} \tag{B.253}$$

Next consider $\left(\int_{\mathbb{R}^2}(\Psi_x U_{V_y}-\Psi_{V_y}U_x)d\mathbf{x}\right)$ again by separating out into $\int_{\mathbb{R}^2}(\Psi_x U_{V_y})d\mathbf{x}$ and $\int_{\mathbb{R}^2}(\Psi_{V_y}U_x)d\mathbf{x}$. The first of these is immediately zero since $U_{V_y}=0$.

$$\int_{\mathbb{R}^2}(\Psi_{V_y}U_x)d\mathbf{x}=\int_0^\infty\int_0^{2\pi}\left(\frac{-\sin(\varphi)}{\omega^2}\right)\left(\operatorname{sech}^2\left(\rho-\frac{1}{\omega}\right)\cos(\varphi)\right)\rho\,d\varphi\,d\rho \tag{B.254}$$

$$=\frac{-1}{\omega^2}\int_0^\infty\operatorname{sech}^2\left(\rho-\frac{1}{\omega}\right)\rho\left[\int_0^{2\pi}\left(\cos(\varphi)\sin(\varphi)\right)d\varphi\right]^{0}_{0}d\rho \tag{B.255}$$

$$=0 \tag{B.256}$$

So

$$\int_{\mathbb{R}^2}(\Psi_x U_{V_y}-\Psi_{V_y}U_x)d\mathbf{x}=0 \tag{B.257}$$

Next consider $\left(\int_{\mathbb{R}^2}(\Psi_y U_\omega - \Psi_\omega U_y)d\mathbf{x}\right)$. As always, separate out into $\int_{\mathbb{R}^2}\Psi_y U_\omega d\mathbf{x}$ and $\int_{\mathbb{R}^2}\Psi_\omega U_y d\mathbf{x}$

$$\int_{\mathbb{R}^2}(\Psi_y U_\omega)d\mathbf{x} = \int_0^\infty\int_0^{2\pi}\left(\frac{-\cos(\varphi)}{\rho\omega^2}\left(-V_x\sin(\varphi)+V_y\cos(\varphi)\right)\right)\left(\frac{1}{\omega^2}\operatorname{sech}^2\left(\rho-\frac{1}{\omega}\right)\right)\rho\, d\varphi\, d\rho \tag{B.258}$$

$$= \frac{1}{\omega^4}\left[V_x\int_0^\infty\left(\operatorname{sech}^2\left(\rho-\frac{1}{\omega}\right)\cancelto{0}{\int_0^{2\pi}\left(\cos(\varphi)\sin(\varphi)\right)d\varphi}\right)d\rho\right)d\rho \tag{B.259}$$

$$+ V_y\int_0^\infty\left(\operatorname{sech}^2\left(\rho-\frac{1}{\omega}\right)\int_0^{2\pi}(-\sin^2(\varphi))d\varphi\right] \tag{B.260}$$

$$= \frac{-\pi}{\omega^4}V_y\int_0^\infty\left(\operatorname{sech}^2\left(\rho-\frac{1}{\omega}\right)\right)d\rho \tag{B.261}$$

$$= \frac{-\pi}{\omega^4}V_y\left(1+\tanh\left(\frac{1}{\omega}\right)\right) \tag{B.262}$$

$$\approx \frac{-\pi}{\omega^4}V_y(1+1) = \frac{-2\pi}{\omega^4}V_y \tag{B.263}$$

$$\int_{\mathbb{R}^2}(\Psi_\omega U_y)d\mathbf{x} = \int_0^\infty\int_0^{2\pi}\left(\frac{2\left(V_x\cos(\varphi)+V_y\sin(\varphi)\right)}{\omega^3}\right)\left(\operatorname{sech}^2\left(\rho-\frac{1}{\omega}\right)\sin(\varphi)\right)\rho\, d\varphi\, d\rho \tag{B.264}$$

$$= \frac{2}{\omega^3}\int_0^\infty\operatorname{sech}^2\left(\rho-\frac{1}{\omega}\right)\rho\left[V_x\cancelto{0}{\int_0^{2\pi}\cos(\varphi)\sin(\varphi)d\varphi} + V_y\int_0^{2\pi}\sin^2(\varphi)d\varphi\right]d\rho \tag{B.265}$$

$$= \frac{2\pi}{\omega^3}V_y\int_0^\infty\operatorname{sech}^2\left(\rho-\frac{1}{\omega}\right)\rho\, d\rho \tag{B.266}$$

$$= \frac{2\pi}{\omega^3}V_y\log\left(1+e^{\frac{2}{\omega}}\right) \tag{B.267}$$

$$\approx \frac{2\pi}{\omega^3}V_y\log\left(e^{\frac{2}{\omega}}\right) \tag{B.268}$$

$$\approx \frac{4\pi}{\omega^4}V_y \tag{B.269}$$

and

$$\left(\int_{\mathbb{R}^2}(\Psi_y U_\omega - \Psi_\omega U_y)d\mathbf{x}\right) = \frac{-2\pi}{\omega^4}V_y - \frac{4\pi}{\omega^4}V_y = -\frac{6\pi}{\omega^4}V_y \tag{B.270}$$

Next consider $\left(\int_{\mathbb{R}^2}(\Psi_y U_{V_x}-\Psi_{V_x}U_y)d\mathbf{x}\right)$. As always, separate out into $\int_{\mathbb{R}^2}\Psi_y U_{V_x}d\mathbf{x}$ and $\int_{\mathbb{R}^2}\Psi_{V_x}U_y d\mathbf{x}$. Note the first of these integrals immediately vanishes since $U_{V_x}=0$.

$$\int_{\mathbb{R}^2}(\Psi_{V_x}U_y)d\mathbf{x}=\int_0^\infty\int_0^{2\pi}\left(\frac{-\cos(\varphi)}{\omega^2}\right)\left(\operatorname{sech}^2\left(\rho-\frac{1}{\omega}\right)\sin(\varphi)\right)\rho\,d\varphi\,d\rho \tag{B.271}$$

$$=\frac{-1}{\omega^2}\int_0^\infty\operatorname{sech}^2\left(\rho-\frac{1}{\omega}\right)\rho\left[\int_0^{2\pi}\left(\cos(\varphi)\sin(\varphi)\right)d\varphi\right]d\rho \tag{B.272}$$

$$=0 \tag{B.273}$$

Hence

$$\int_{\mathbb{R}^2}(\Psi_y U_{V_x}-\Psi_{V_x}U_y)d\mathbf{x}=0 \tag{B.274}$$

Next consider $\left(\int_{\mathbb{R}^2}(\Psi_y U_{V_y}-\Psi_{V_y}U_y)d\mathbf{x}\right)$ again by separating out into $\int_{\mathbb{R}^2}(\Psi_y U_{V_y})d\mathbf{x}$ and $\int_{\mathbb{R}^2}(\Psi_{V_y}U_y)d\mathbf{x}$. The first of these is immediately zero since $U_{V_y}=0$.

$$\int_{\mathbb{R}^2}(\Psi_{V_y}U_y)d\mathbf{x}=\int_0^\infty\int_0^{2\pi}\left(\frac{-\sin(\varphi)}{\omega^2}\right)\left(\operatorname{sech}^2\left(\rho-\frac{1}{\omega}\right)\sin(\varphi)\right)\rho\,d\varphi\,d\rho \tag{B.275}$$

$$=\frac{-1}{\omega^2}\int_0^\infty\operatorname{sech}^2\left(\rho-\frac{1}{\omega}\right)\rho\left[\int_0^{2\pi}\left(\sin^2(\varphi)\right)d\varphi\right]d\rho \tag{B.276}$$

$$=\frac{-\pi}{\omega^2}=\frac{-\pi}{\omega^2}\log\left(1+e^{\frac{2}{\omega}}\right)\approx\frac{-\pi}{\omega^2}\log\left(e^{\frac{2}{\omega}}\right) \tag{B.277}$$

$$\approx\frac{-2\pi}{\omega^3} \tag{B.278}$$

So

$$\int_{\mathbb{R}^2}(\Psi_y U_{V_y}-\Psi_{V_y}U_y)d\mathbf{x}=\frac{2\pi}{\omega^3} \tag{B.279}$$

The last three are easier. It is immediately evident that they will all be zero, but to be explicit they will be computed. Consider $\int_{\mathbb{R}^2}(\Psi_\omega U_{V_x}-\Psi_{V_x}U_\omega)d\mathbf{x}$. $\int_{\mathbb{R}^2}(\Psi_\omega U_{V_x}-\Psi_{V_x}U_\omega)d\mathbf{x}=-\int_{\mathbb{R}^2}\Psi_{V_x}U_\omega\,d\mathbf{x}$ since

$U_{V_x} = 0$. Next

$$\int_{\mathbb{R}^2} \Psi_{V_x} U_\omega \, d\mathbf{x} = \int_0^\infty \int_0^{2\pi} \left(\frac{-\cos(\varphi)}{\omega^2}\right)\left(\frac{1}{\omega^2}\operatorname{sech}^2\left(\rho - \frac{1}{\omega}\right)\right)\rho \, d\varphi \, d\rho \tag{B.280}$$

$$= \frac{-1}{\omega^4}\int_0^\infty \left(\operatorname{sech}^2\left(\rho - \frac{1}{\omega}\right)\right)\rho \left[\int_0^{2\pi} \cos(\varphi) d\varphi \right] d\rho \tag{B.281}$$

$$= 0 \tag{B.282}$$

and therefore $\int_{\mathbb{R}^2}(\Psi_\omega U_{V_x} - \Psi_{V_x} U_\omega) d\mathbf{x} = 0$. Similarly $\int_{\mathbb{R}^2}(\Psi_\omega U_{V_y} - \Psi_{V_y} U_\omega) d\mathbf{x} == -\int_{\mathbb{R}^2} \Psi_{V_y} U_\omega \, d\mathbf{x}$ since $U_{V_x} = 0$.

$$\int_{\mathbb{R}^2} \Psi_{V_y} U_\omega \, d\mathbf{x} = \int_0^\infty \int_0^{2\pi} \left(\frac{-\sin(\varphi)}{\omega^2}\right)\left(\frac{1}{\omega^2}\operatorname{sech}^2\left(\rho - \frac{1}{\omega}\right)\right)\rho \, d\varphi \, d\rho \tag{B.283}$$

$$= \frac{-1}{\omega^4}\int_0^\infty \left(\operatorname{sech}^2\left(\rho - \frac{1}{\omega}\right)\right)\rho \left[\int_0^{2\pi} \sin(\varphi) d\varphi \right] d\rho \tag{B.284}$$

$$= 0 \tag{B.285}$$

and therefore $\int_{\mathbb{R}^2}(\Psi_\omega U_{V_y} - \Psi_{V_y} U_\omega)d\mathbf{x} = 0$. Finally, $\int_{\mathbb{R}^2}(\Psi_{V_x} U_{V_y} - \Psi_{V_y} U_{V_x})d\mathbf{x} = 0$ since $U_{V_x} = U_{V_y} = 0$. Finally all the integrals are done and

$$M = \begin{pmatrix} 0 & 0 & 0 & -\frac{4\pi}{\omega^3} & 0 & 0 \\ 0 & 0 & 0 & -\frac{6\pi V_x}{\omega^4} & \frac{2\pi}{\omega^3} & 0 \\ 0 & 0 & 0 & -\frac{6\pi V_y}{\omega^4} & 0 & \frac{2\pi}{\omega^3} \\ \frac{4\pi}{\omega^3} & \frac{6\pi V_x}{\omega^4} & \frac{6\pi V_y}{\omega^4} & 0 & 0 & 0 \\ 0 & -\frac{2\pi}{\omega^3} & 0 & 0 & 0 & 0 \\ 0 & 0 & -\frac{2\pi}{\omega^3} & 0 & 0 & 0 \end{pmatrix} \tag{B.286}$$

This matrix is easily inverted to find

$$M^{-1} = \begin{pmatrix} 0 & 0 & 0 & \frac{\omega^3}{4\pi} & \frac{3V_x\omega^2}{4\pi} & \frac{3V_y\omega^2}{4\pi} \\ 0 & 0 & 0 & 0 & -\frac{\omega^3}{2\pi} & 0 \\ 0 & 0 & 0 & 0 & 0 & -\frac{\omega^3}{2\pi} \\ -\frac{\omega^3}{4\pi} & 0 & 0 & 0 & 0 & 0 \\ -\frac{3V_x\omega^2}{4\pi} & \frac{\omega^3}{2\pi} & 0 & 0 & 0 & 0 \\ -\frac{3V_y\omega^2}{4\pi} & 0 & \frac{\omega^3}{2\pi} & 0 & 0 & 0 \end{pmatrix} \tag{B.287}$$

That's about as nice as the story gets. The next step is to try to simplify f, but since it includes arbitrary perturbations very little can be done.

$$\begin{pmatrix} \Phi_0 \\ x_0 \\ y_0 \\ \omega \\ V_x \\ V_y \end{pmatrix}' = \begin{pmatrix} \frac{3f_5V_x\omega^2}{4\pi} + \frac{3f_6V_y\omega^2}{4\pi} + \frac{f_4\omega^3}{4\pi} \\ -\frac{f_5\omega^3}{2\pi} \\ -\frac{f_6\omega^3}{2\pi} \\ -\frac{f_1\omega^3}{4\pi} \\ -\frac{3f_1V_x\omega^2}{4\pi} + \frac{f_2\omega^3}{2\pi} \\ -\frac{3f_1V_y\omega^2}{4\pi} + \frac{f_3\omega^3}{2\pi} \end{pmatrix} \tag{B.288}$$

where $(f_1, f_2, f_3, f_4, f_5, f_6)$ are the components of f and are defined by what follows. Note that it is possible to write this in vector form by grouping f_2, f_3 together and f_5, f_6 together since the coefficients on these terms are the same.

$$f_1 = -\int_{\mathbb{R}^2} P_u \, d\mathbf{x} \tag{B.289}$$

Next consider f_2 and f_3 together.

$$f_2 = \int_{\mathbb{R}^2} \Psi_x P_u \, d\mathbf{x} - \int_{\mathbb{R}^2} U_x P_{\bar{\Phi}} \, d\mathbf{x} \tag{B.290}$$

$$f_3 = \int_{\mathbb{R}^2} \Psi_y P_u \, d\mathbf{x} - \int_{\mathbb{R}^2} U_y P_{\bar{\Phi}} \, d\mathbf{x} \tag{B.291}$$

$$\begin{pmatrix} f_2 \\ f_3 \end{pmatrix} = \int_{\mathbb{R}^2} \nabla\Psi P_u \, d\mathbf{x} - \int_{\mathbb{R}^2} \nabla U P_{\bar{\Phi}} \, d\mathbf{x} \tag{B.292}$$

The following identities will prove useful.

$$\begin{pmatrix} f_2 \\ f_3 \end{pmatrix} = -\int_{\mathbb{R}^2} \frac{1}{\rho\omega^2}\left(\mathbf{V}\cdot\hat{\varphi}\right)\hat{\varphi}P_u d\mathbf{x} - \int_{\mathbb{R}^2} \operatorname{sech}^2\left(\rho - \frac{1}{\omega}\right)\hat{\rho}P_{\bar{\Phi}} d\mathbf{x} \tag{B.293}$$

Next, f_4

$$f_4 = -\int_{\mathbb{R}^2} \Psi_\omega P_u d\mathbf{x} + \int_{\mathbb{R}^2} U_\omega P_{\bar{\Phi}} d\mathbf{x} \tag{B.294}$$

$$= -\int_{\mathbb{R}^2} \frac{2\mathbf{V}\cdot\hat{\rho}}{\omega^3} P_u d\mathbf{x} + \int_{\mathbb{R}^2} \frac{1}{\omega^2}\operatorname{sech}^2\left(\rho - \frac{1}{\omega}\right) P_{\bar{\Phi}} d\mathbf{x} \tag{B.295}$$

Finally, consider f_5, f_6 together.

$$f_5 = -\int_{\mathbb{R}^2} \Psi_{V_x} P_u d\mathbf{x} + \int_{\mathbb{R}^2} U_{V_x} P_{\bar{\Phi}} d\mathbf{x} \tag{B.296}$$

$$f_6 = -\int_{\mathbb{R}^2} \Psi_{V_y} P_u d\mathbf{x} + \int_{\mathbb{R}^2} U_{V_y} P_{\bar{\Phi}} d\mathbf{x} \tag{B.297}$$

$$\begin{pmatrix} f_5 \\ f_6 \end{pmatrix} = -\int_{\mathbb{R}^2} \nabla_{\mathbf{V}}\Psi P_u d\mathbf{x} + \int_{\mathbb{R}^2} \nabla_{\mathbf{V}} U P_{\bar{\Phi}} d\mathbf{x} \tag{B.298}$$

where $\nabla_{\mathbf{V}} = \begin{pmatrix} \partial_{V_x} \\ \partial_{V_y} \end{pmatrix}$. $\nabla_{\mathbf{V}} U = 0$ and $\nabla_{\mathbf{V}}\Psi = -\frac{1}{\omega^2}\hat{\rho}$ hence

$$\begin{pmatrix} f_5 \\ f_6 \end{pmatrix} = \frac{1}{\omega^2}\int_{\mathbb{R}^2} (P_u\hat{\rho}) d\mathbf{x} \tag{B.299}$$

So the equations for (x_0', y_0') only depend on f_5, f_6 in the following way

$$\mathbf{x_0}'(T) = -\frac{\omega^3}{2\pi}\begin{pmatrix} f_5 \\ f_6 \end{pmatrix} \tag{B.300}$$

$$= -\frac{\omega^3}{2\pi}\left(\frac{1}{\omega^2}\int_{\mathbb{R}^2}(P_u\hat{\rho})d\mathbf{x}\right) \tag{B.301}$$

$$= -\frac{\omega}{2\pi}\int_{\mathbb{R}^2}(P_u\hat{\rho})d\mathbf{x} \tag{B.302}$$

The next simplest equation to unpack is for $\omega'(T)$ since it just depends on f_1

$$\omega'(T) = -\frac{f_1\omega^3}{4\pi} \tag{B.303}$$

$$= \frac{\omega^3}{4\pi}\left(\int_{\mathbb{R}^2} P_u d\mathbf{x}\right) \tag{B.304}$$

Next consider $\mathbf{V}'(T)$

$$\mathbf{V}'(T) = -\frac{3\mathbf{V}\omega^2}{4\pi}f_1 + \frac{\omega^3}{2\pi}\begin{pmatrix} f_2 \\ f_3 \end{pmatrix} \tag{B.305}$$

$$= \frac{3\mathbf{V}\omega^2}{4\pi}\left(\int_{\mathbb{R}^2} P_u d\mathbf{x}\right) + \frac{\omega^3}{2\pi}\left(-\int_{\mathbb{R}^2}\frac{1}{\rho\,\omega^2}\left(\mathbf{V}\cdot\hat{\varphi}\right)\hat{\varphi}P_u d\mathbf{x} - \int_{\mathbb{R}^2}\operatorname{sech}^2\left(\rho-\frac{1}{\omega}\right)\hat{\rho}P_{\tilde{\Phi}}d\mathbf{x}\right) \tag{B.306}$$

$$= \frac{3\mathbf{V}\omega^2}{4\pi}\left(\int_{\mathbb{R}^2} P_u d\mathbf{x}\right) - \frac{\omega}{2\pi}\int_{\mathbb{R}^2}\frac{1}{\rho}\left(\mathbf{V}\cdot\hat{\varphi}\right)\hat{\varphi}P_u d\mathbf{x} - \frac{\omega^3}{2\pi}\int_{\mathbb{R}^2}\operatorname{sech}^2\left(\rho-\frac{1}{\omega}\right)\hat{\rho}P_{\tilde{\Phi}}d\mathbf{x} \tag{B.307}$$

Note that the contributions to Φ_0' from f_5, f_6 can be written in terms of $\mathbf{V}\cdot\begin{pmatrix} f_5 \\ f_6 \end{pmatrix}$

$$\Phi_0' = \frac{3\omega^2}{4\pi}\mathbf{V}\cdot\begin{pmatrix} f_5 \\ f_6 \end{pmatrix} + \frac{f_4\omega^3}{4\pi} \tag{B.308}$$

$$= \frac{3\omega^2}{4\pi}\mathbf{V}\cdot\left(\frac{1}{\omega^2}\int_{\mathbb{R}^2}(P_u\hat{\rho})d\mathbf{x}\right) + \frac{f_4\omega^3}{4\pi} \tag{B.309}$$

$$= \frac{3\omega^2}{4\pi}\mathbf{V}\cdot\left(\frac{1}{\omega^2}\int_{\mathbb{R}^2}(P_u\hat{\rho})d\mathbf{x}\right) + \frac{\omega^3}{4\pi}\left(-\int_{\mathbb{R}^2}\frac{2\mathbf{V}\cdot\hat{\rho}}{\omega^3}P_u d\mathbf{x} + \int_{\mathbb{R}^2}\frac{1}{\omega^2}\operatorname{sech}^2\left(\rho-\frac{1}{\omega}\right)P_{\bar{\Phi}}d\mathbf{x}\right) \tag{B.310}$$

$$= \frac{3\mathbf{V}}{4\pi}\cdot\left(\int_{\mathbb{R}^2}(P_u\hat{\rho})d\mathbf{x}\right) - \frac{\mathbf{V}}{2\pi}\cdot\int_{\mathbb{R}^2}\hat{\rho}\,P_u d\mathbf{x} + \frac{\omega}{4\pi}\int_{\mathbb{R}^2}\operatorname{sech}^2\left(\rho-\frac{1}{\omega}\right)P_{\bar{\Phi}}d\mathbf{x} \tag{B.311}$$

$$= \frac{\mathbf{V}}{4\pi}\cdot\left(\int_{\mathbb{R}^2}(P_u\hat{\rho})d\mathbf{x}\right) + \frac{\omega}{4\pi}\int_{\mathbb{R}^2}\operatorname{sech}^2\left(\rho-\frac{1}{\omega}\right)P_{\bar{\Phi}}d\mathbf{x} \tag{B.312}$$

So the modulation equations are a mess, but here's my best attempt at presenting them:

$$\begin{pmatrix} \Phi_0 \\ \mathbf{x}_0 \\ \omega \\ \mathbf{V} \end{pmatrix}' = \begin{pmatrix} \frac{\mathbf{V}}{4\pi}\cdot\left(\int_{\mathbb{R}^2}(P_u\hat{\rho})d\mathbf{x}\right) + \frac{\omega}{4\pi}\int_{\mathbb{R}^2}\operatorname{sech}^2\left(\rho-\frac{1}{\omega}\right)P_{\bar{\Phi}}d\mathbf{x} \\ -\frac{\omega}{2\pi}\int_{\mathbb{R}^2}(P_u\hat{\rho})d\mathbf{x} \\ \frac{\omega^3}{4\pi}\int_{\mathbb{R}^2}P_u d\mathbf{x} \\ \frac{3\mathbf{V}\omega^2}{4\pi}\left(\int_{\mathbb{R}^2}P_u d\mathbf{x}\right) - \frac{\omega}{2\pi}\int_{\mathbb{R}^2}\frac{1}{\rho}\left(\mathbf{V}\cdot\hat{\varphi}\right)\hat{\varphi}P_u d\mathbf{x} - \frac{\omega^3}{2\pi}\int_{\mathbb{R}^2}\operatorname{sech}^2\left(\rho-\frac{1}{\omega}\right)\hat{\rho}P_{\bar{\Phi}}d\mathbf{x} \end{pmatrix} \tag{B.313}$$

Taking $V = 0$.

$$\begin{pmatrix} \Phi_0 \\ \mathbf{x}_0 \\ \omega \\ \mathbf{0} \end{pmatrix}' = \begin{pmatrix} \frac{\omega}{4\pi}\int_{\mathbb{R}^2}\operatorname{sech}^2\left(\rho-\frac{1}{\omega}\right)P_{\bar{\Phi}}d\mathbf{x} \\ -\frac{\omega}{2\pi}\int_{\mathbb{R}^2}(P_u\hat{\rho})d\mathbf{x} \\ \frac{\omega^3}{4\pi}\int_{\mathbb{R}^2}P_u d\mathbf{x} \\ -\frac{\omega^3}{2\pi}\int_{\mathbb{R}^2}\operatorname{sech}^2\left(\rho-\frac{1}{\omega}\right)\hat{\rho}P_{\bar{\Phi}}d\mathbf{x} \end{pmatrix} \tag{B.314}$$

or in more natural variables,

$$\begin{pmatrix} \Phi_0 \\ \mathbf{x}_0 \\ \omega \\ \mathbf{0} \end{pmatrix}' = \begin{pmatrix} \frac{\omega}{4\pi}\int_{\mathbb{R}^2} \operatorname{sech}\left(\rho - \frac{1}{\omega}\right) P_\Phi \, d\mathbf{x} \\ \frac{\omega}{2\pi}\int_{\mathbb{R}^2} \operatorname{sech}\left(\rho - \frac{1}{\omega}\right) \hat{\rho} P_u \, d\mathbf{x} \\ -\frac{\omega^3}{4\pi}\int_{\mathbb{R}^2} \operatorname{sech}\left(\rho - \frac{1}{\omega}\right) P_u \, d\mathbf{x} \\ -\frac{\omega^3}{2\pi}\int_{\mathbb{R}^2} \operatorname{sech}\left(\rho - \frac{1}{\omega}\right) \hat{\rho} P_\Phi \, d\mathbf{x} \end{pmatrix} \tag{B.315}$$

which is precisely what had previously been found.

B.3 Calculation of the Magnetostatic Field Perturbation

Before beginning a discussion of how the magnetostatic field perturbation presented in Chapter 3 is derived it is important to understand the asymptotic reduction of the nonlocal magnetostatic field to the local contribution overall equation. The derivation here closely follows work in [GC04b; HS12] where more complete descriptions are given. Recall, that the contribution to the effective field in the torque equation is given by $\mathbf{h}_m = \nabla U$ where U solves

$$\begin{aligned} \nabla^2 U &= \begin{cases} \nabla \cdot \mathbf{m} & |z| < \frac{\delta}{2}, \\ 0 & |z| > \frac{\delta}{2} \end{cases} \\ \left.\frac{\partial U}{\partial z}\right|_{z=\pm\delta/2} &= \mp m_z\left(x, y, \pm\tfrac{\delta}{2}\right). \end{aligned} \tag{B.316}$$

Eq. B.316 admits an exact solution

$$U(x,y,z) = \int_{-\frac{\delta}{2}}^{\frac{\delta}{2}} \left[N(\cdot,\cdot,z-z') * \nabla\cdot\mathbf{m}(\cdot,\cdot,z')\right](x,y)\,dz' - [N(\cdot,\cdot,z-\delta/2) * (\mathbf{m}(\cdot,\cdot,\delta/2) - 1)] + [N(\cdot,\cdot,z+\delta/2) * (\mathbf{m}(\cdot,\cdot,-\delta/2) - 1)] - z \tag{B.317}$$

where $*$ denotes convolution with respect to x, y and N represents the Newtonian potential

$$N(x,y,z) = -\frac{1}{4\pi\sqrt{x^2+y^2+z^2}}. \tag{B.318}$$

Progress can be made in simplifying the given expression for U by working in Fourier space and by assuming that the magnetization is independent of z. Under this assumption the Fourier transform of U, denoted by $\mathcal{F}[U]$, is given by

$$\mathcal{F}[U(\cdot,\cdot,z)+z](k_x,k_y) = (ik_x\mathcal{F}[m_x]+ik_y\mathcal{F}[m_x])\int_{-\frac{\delta}{2}}^{\frac{\delta}{2}}\mathcal{F}[N(\cdot,\cdot,z-z')]dz' + \mathcal{F}[m_z-1](-N(\cdot,\cdot,\delta/2)]+N(\cdot,\cdot,-\delta/2)]) \tag{B.319}$$

Utilizing the fact $\mathcal{F}[N(\cdot,\cdot,z)] = -\frac{e^{-k|z|}}{2k}$ where $k=\sqrt{k_x^2+k_y^2}$, it is readily computed that $\int_{-\frac{\delta}{2}}^{\frac{\delta}{2}}\mathcal{F}[N(\cdot,\cdot,z-z')]dz' = \frac{e^{k\delta/2}\cosh(kz)-1}{k^2}$ and $(-N(\cdot,\cdot,\delta/2)]+N(\cdot,\cdot,-\delta/2)]) = \frac{e^{k\delta/2}}{k}\sinh(kz)$. Hence,

$$\mathcal{F}[U(\cdot,\cdot,z)+z](k_x,k_y) = (ik_x\mathcal{F}[m_x]+ik_y\mathcal{F}[m_x])\left(\frac{e^{k\delta/2}\cosh(kz)-1}{k^2}\right)+\mathcal{F}[m_z-1]\frac{e^{k\delta/2}}{k}\sinh(kz) \tag{B.320}$$

The above expression can then be used to determine an approximate expression for $\mathbf{h}_m$.

$$\mathcal{F}[\mathbf{h}_m+\mathbf{e}_z] = \mathcal{F}[\nabla U+\mathbf{e}_z] = \mathcal{F}[\nabla(U+z)] \tag{B.321}$$

$$\begin{aligned} &= \begin{pmatrix}k_x\\k_y\end{pmatrix}(k_x\mathcal{F}[m_x]+k_y\mathcal{F}[m_x])\left(\frac{e^{k\delta/2}\cosh(kz)-1}{k^2}\right)+i\begin{pmatrix}k_x\\k_y\end{pmatrix}\mathcal{F}[m_z-1]\frac{e^{k\delta/2}}{k}\sinh(kz)\\ &\quad -i\begin{pmatrix}k_x\\k_y\end{pmatrix}(k_x\mathcal{F}[m_x]+k_y\mathcal{F}[m_x])\left(\frac{e^{k\delta/2}\sinh(kz)}{k}\right)\mathbf{e}_z-\begin{pmatrix}k_x\\k_y\end{pmatrix}\mathcal{F}[m_z-1]e^{k\delta/2}\cosh(kz)\mathbf{e}_z \end{aligned} \tag{B.322}$$

where the final two terms come from taking the $z-$derivative of Eq B.320. In the thin film limit it is natural to assume that $\mathbf{h}_m$ does not vary much from the mean value in z. That is, the assumption

$\mathbf{h}_m \approx \frac{1}{\delta}\int_{-\frac{\delta}{2}}^{\frac{\delta}{2}} \mathbf{h}_m dz$ will not be imposed. As a result,

$$\mathcal{F}[\mathbf{h}_m + \mathbf{e}_z] = \approx \frac{1}{\delta}\int_{-\frac{\delta}{2}}^{\frac{\delta}{2}} \mathcal{F}[\mathbf{h}_m + \mathbf{e}_z] dz \tag{B.323}$$

$$= -\frac{k_x \mathcal{F}[m_x] + k_y \mathcal{F}[m_x]}{k^2}\begin{pmatrix} k_x \\ k_y \end{pmatrix}(1-\hat{\Gamma}(k\delta)) - (\mathcal{F}[m_z - 1])\hat{\Gamma}(k\delta)\mathbf{e}_z \tag{B.324}$$

where $\hat{\Gamma}(\kappa) = \frac{1-e^{-\kappa}}{\kappa}$. From this, the magnetostatic field expansion can be determined utilizing an inverse Fourier transform to obtain

$$(\mathbf{h}_m)_z = -m_z + \frac{\delta}{2}\mathcal{F}^{-1}[k\mathcal{F}[m_z - 1]] \tag{B.325}$$

$$(\mathbf{h}_m)_\perp = -\frac{\delta}{2}\mathcal{F}^{-1}\left[\mathbf{k}\frac{\mathbf{k}}{k}\mathcal{F}[\mathbf{m}_\perp]\right] \tag{B.326}$$

where $\mathbf{k} = \begin{pmatrix} k_x \\ k_y \end{pmatrix}$ and $\perp$ denotes the (x, y) directions.

The relevant contributions to the torque equation for the magnetostatic field are then given by $\mathbf{e}_\Phi \cdot \mathbf{h}_m$ to $\frac{\partial \Theta}{\partial t}$ and $-\mathbf{e}_\Theta \cdot \mathbf{h}_m$ to $\frac{\partial \Phi}{\partial t}$ where

$$\mathbf{e}_\Phi = \begin{pmatrix} -\sin\Phi \\ \cos\Phi \\ 0 \end{pmatrix} \tag{B.327}$$

and

$$\mathbf{e}_\Theta = \begin{pmatrix} \cos\Phi\cos\Theta \\ \sin\Phi\cos\Theta \\ -\sin\Theta \end{pmatrix} \tag{B.328}$$

First consider $\mathbf{e}_\Phi \cdot \mathbf{h}_m$

$$\mathbf{e}_\Phi \cdot \mathbf{h}_m = -\frac{\delta}{2}\mathbf{e}_\Phi \cdot \mathcal{F}^{-1}\left[\mathbf{k}\frac{\mathbf{k}}{k}\mathcal{F}[\mathbf{m}_\perp]\right] \tag{B.329}$$

$$= \frac{\delta}{2}\mathbf{e}_\Phi \cdot \nabla\left(\mathcal{F}^{-1}\left[\frac{i\mathbf{k}}{k}\mathcal{F}[\mathbf{m}_\perp]\right]\right) \tag{B.330}$$

$$= -\frac{\delta}{2}\left\{\sin(\varphi-\Phi)\frac{\partial}{\partial\rho}\left(\mathcal{F}^{-1}\left[\frac{i\mathbf{k}}{k}\mathcal{F}[\mathbf{m}_\perp]\right]\right) + \frac{\cos(\varphi-\Phi)}{\rho}\frac{\partial}{\partial\varphi}\left(\mathcal{F}^{-1}\left[\frac{i\mathbf{k}}{k}\mathcal{F}[\mathbf{m}_\perp]\right]\right)\right\}. \tag{B.331}$$

From this point on only stationary droplets will be consider which greatly simplifies the calculation. The stationary droplet is independent of φ and consequently $\frac{\partial}{\partial\varphi}\left(\mathcal{F}^{-1}\left[\frac{i\mathbf{k}}{k}\mathcal{F}[\mathbf{m}_\perp]\right]\right) = 0$.

Next consider $\mathbf{e}_\Theta \cdot \mathbf{h}_m$

$$\mathbf{e}_\Theta \cdot \mathbf{h}_m = \tfrac{1}{2}\sin(2\Theta) - \frac{\delta}{2}\left\{\sin(\Theta)\mathcal{F}^{-1}[k\mathcal{F}[m_z-1]] + \cos(\Theta)\cos(\varphi-\Phi)\frac{\partial}{\partial\rho}\left(\mathcal{F}^{-1}\left[\frac{i\mathbf{k}}{k}\mathcal{F}[\mathbf{m}_\perp]\right]\right) - \frac{\cos(\Theta)\sin(\varphi-\Phi)}{\rho}\frac{\partial}{\partial\varphi}\left(\mathcal{F}^{-1}\left[\frac{i\mathbf{k}}{k}\mathcal{F}[\mathbf{m}_\perp]\right]\right)\right\}^{0} \tag{B.332}$$

Recall that $m_z = \cos(\Theta)$ and

$$\mathbf{e}_\Theta \cdot \mathbf{h}_m = \frac{1}{2}\sin(2\Theta) - \frac{\delta}{2}\left\{\sin(\Theta)\mathcal{F}^{-1}[k\mathcal{F}[\cos(\Theta)-1]] + \cos(\Theta)\cos(\varphi-\Phi)\frac{\partial}{\partial\rho}\left(\mathcal{F}^{-1}\left[\frac{i\mathbf{k}}{k}\mathcal{F}[\mathbf{m}_\perp]\right]\right)\right\} \tag{B.333}$$

The final step is to recognize what terms of the contribution of the magnetostatic field contribute to the perturbations P_Θ and P_Φ. Note that the term $\frac{1}{2}\sin(2\Theta)$ in Eq. B.333 represents the leading order behavior for the magnetostatic field which has already be incorporated into the torque equations (Eqs. 1.11-1.12). The contributions to P_Φ from this equation, then are only from $\mathcal{O}(\delta)$ terms. Additionally, the terms involving $\frac{\partial}{\partial\rho}\left(\mathcal{F}^{-1}\left[\frac{i\mathbf{k}}{k}\mathcal{F}[\mathbf{m}_\perp]\right]\right)$ in both contributions constitute a regular perturbation to the equation. That is, considered on their own an exact solution to those perturbations can be found without appealing to secularity. Accordingly, these terms do not play a role in the modulation equations (or the evolution of soliton parameters) and will be neglected from the forms of P_Θ and P_Φ. This neglects the only term in $\mathbf{e}_\Phi \cdot \mathbf{h}_m$ that would contribute to P_Θ. The final result is that

$$P_\Theta = 0 \tag{B.334}$$

and

$$P_\Phi = -\frac{\delta}{2}\left\{\sin(\Theta)\mathcal{F}^{-1}\left[k\mathcal{F}[\cos(\Theta)-1]\right]\right\} \tag{B.335}$$

exactly what is claimed in Eq. 3.11.

B.4 Calcualignlation of the Interacting Droplet Perturbation

The approximate two-soliton droplet solutions studied in [Mai14] were constructed as follows

$$\begin{pmatrix}\tilde{m}_x\\ \tilde{m}_y\\ \tilde{m}_z\end{pmatrix} = \begin{pmatrix} m_{x,1}+m_{x,2}\\ m_{y,1}+m_{y,2}\\ m_{z,1}+\left(m_{z,2}-1\right)\end{pmatrix} \tag{B.336}$$

where the numbered subscript denotes “droplet 1" or “droplet 2" . Since it is required that **m** is normalized to unit length, after a superposition of the form above this condition was subsequently enforced. Note that near the center of droplet 1, the quantities $\gamma = m_{2,x}, \delta = m_{2,y}$ and $\epsilon = m_{2,z}-1$ are all small in absolute value since $\lim_{|\mathbf{x}|} m_2 \to e_z$, so this can be used to simplify the normalization process. Note that it is required that $m_{x,1}^2 + m_{y,1}^2 + m_{z,1}^2 = 1$ and $\gamma^2+\delta^2+(1+\epsilon)^2 = 1$, since they represent magnetization of droplets independently. The second of these can be rearranged to conclude that $\gamma^2+\delta^2+\epsilon^2 = -2\epsilon$ which implies a) $\epsilon < 0$ and b) $\gamma^2+\delta^2+\epsilon^2$ is of order ϵ not higher order. To get the appropriate form of the perturbation we need to normalize $\tilde{\mathbf{m}}$. Compute $\|\tilde{\mathbf{m}}\|$.

$$\|\tilde{\mathbf{m}}\| = (m_{x,1}+\gamma)^2 + (m_{y,1}+\delta)^2 + (m_{z,1}+\epsilon)^2 \tag{B.337}$$

$$= m_{x,1}^2 + 2\gamma m_{x,1} + \gamma^2 + m_{y,1}^2 + 2\delta m_{y,1} + \delta^2 + m_{z,1}^2 + 2\epsilon m_{z,1} + \epsilon^2 \qquad \text{regrouping} \tag{B.338}$$

$$= \underbrace{m_{x,1}^2 + m_{y,1}^2 + m_{z,1}^2}_{=1} + 2(\gamma m_{x,1} + \delta m_{y,1} + \epsilon m_{z,1}) + \underbrace{\gamma^2+\delta^2+\epsilon^2}_{=-2\epsilon} \tag{B.339}$$

$$= 1 + 2(\gamma m_{x,1} + \delta m_{y,1} + \epsilon(m_{z,1}-1)) = \zeta \tag{B.340}$$

The perturbed magnetization will then be

$$\mathbf{m} = \frac{\tilde{\mathbf{m}}}{\|\tilde{\mathbf{m}}\|} = \frac{1}{1+2(\gamma m_{x,1} + \delta m_{y,1} + \epsilon(m_{z,1}-1))} \begin{pmatrix} m_{x,1}+\gamma \\ m_{y,1}+\delta \\ m_{z,1}+\epsilon \end{pmatrix} = \begin{pmatrix} m_x, m_y, m_z \end{pmatrix} \tag{B.341}$$

However, it will ultimately be necessary to work in spherical coordinates. Consider how this might be expressed in Θ and Φ variables. By definition

$$\Theta = \arccos(m_z) \text{ and } \Phi = \arctan({}^{m_y}/_{m_x}) \tag{B.342}$$

Expanding

$$\begin{aligned} \Theta &= \arccos(m_z) && \text{(B.343)} \\ &= \arccos\left(\frac{m_{z,1}+\epsilon}{\zeta}\right) && \text{(B.344)} \\ &= \arccos\left(\frac{m_{z,1}+\epsilon}{1+(\zeta-1)}\right) && \text{(B.345)} \\ &= \arccos(m_{z,1} - \frac{\epsilon-(\zeta-1)m_{z,1}}{\sqrt{1-m_{z,1}^2}}) + \mathcal{O}\left(\epsilon^2\right) && \text{(B.346)} \end{aligned}$$

Viewing, $\mathbf{m}_1$ in polar coordinates, $\Theta_1 = \arccos(m_{z,1})$ and it follows that

$$\Theta = \Theta_1 - \frac{\epsilon-(\zeta-1)\cos(\Theta_1)}{\sin(\Theta_1)} + \mathcal{O}\left(\epsilon^2, (\zeta-1)^2\right) \tag{B.347}$$

It is also the case that $\cos(\Theta_2) = m_{z,2}$. Hence, $m_z - 1 = \epsilon \Rightarrow \epsilon = -1 + \cos(\Theta_2)$. More generally,

$$(m_{x,1}, m_{y,1}, m_{z,1}) = (\sin(\Theta_1)\cos(\Phi_1), \sin(\Theta_1)\sin(\Phi_1), \cos(\Theta_1)) \tag{B.348}$$

and

$$(m_{x,2}, m_{y,2}, m_{z,2}) = (\sin(\Theta_2)\cos(\Phi_2), \sin(\Theta_2)\sin(\Phi_2), \cos(\Theta_2)) = (\gamma, \delta, 1+\epsilon) \tag{B.349}$$

by definition. Substituting these in, I find

$$\frac{\zeta-1}{2} = \gamma m_{x,1} + \delta m_{y,1} + \epsilon(m_{z,1}-1) \tag{B.350}$$

$$= \sin(\Theta_2)\cos(\Phi_2)(\sin(\Theta_1)\cos(\Phi_1) + \sin(\Theta_2)\sin(\Phi_2)\sin(\Theta_1)\sin(\Phi_1) + \epsilon(\cos(\Theta_1)-1) \tag{B.351}$$

$$= \sin(\Theta_2)\sin(\Theta_1)(\cos(\Phi_2)\cos(\Phi_1) + \sin(\Phi_2)\sin(\Phi_1)) + \epsilon(\cos(\Theta_1)-1) \tag{B.352}$$

$$= \sin(\Theta_2)\sin(\Theta_1)\cos(\Phi_1-\Phi_2) + \epsilon(\cos(\Theta_1)-1) \tag{B.353}$$

$$\text{letting } \Delta\Phi = \Phi_2 - \Phi_1 \tag{B.354}$$

$$= \sin(\Theta_2)\sin(\Theta_1)\cos(\Delta\Phi) + \epsilon(\cos(\Theta_1)-1) \tag{B.355}$$

Consequently

$$\Rightarrow \epsilon - 2(\gamma m_{x,1} + \delta m_{y,1} + \epsilon(m_{z,1}-1) = \epsilon - 2(\sin(\Theta_2)\sin(\Theta_1)\cos(\Delta\Phi) + \epsilon(\cos(\Theta_1)-1)) \tag{B.356}$$

$$= \epsilon(3-2\cos(\Theta_1)) - 2\sin(\Theta_2)\sin(\Theta_1)\cos(\Delta\Phi) \tag{B.357}$$

$$\Rightarrow \frac{\epsilon - 2(\gamma m_{x,1} + \delta m_{y,1} + \epsilon(m_{z,1}-1)}{\sqrt{1-m_{z,1}^2}} = \frac{(1-\cos(\Theta_2))(3-2\cos(\Theta_1)) - 2\sin(\Theta_2)\cancel{\sin(\Theta_1)}\cos(\Delta\Phi)}{\cancel{\sin(\Theta_1)}} \tag{B.358}$$

$$= \frac{(1-\cos(\Theta_2))(3-2\cos(\Theta_1))}{\sin(\Theta_1)} - 2\sin(\Theta_2)\cos(\Delta\Phi) \tag{B.359}$$

So,

$$\Theta = \Theta_1 + \underbrace{2\sin(\Theta_2)\cos(\Delta\Phi)}_{\alpha} \tag{B.360}$$

where α is small. The next case is for Φ

$$\Phi = \arctan(m_y/m_x) \tag{B.361}$$
$$= \arctan\left(\frac{\frac{m_{y,1}+\delta}{\not{\gamma}}}{\frac{m_{x,1}+\gamma}{\not{\gamma}}}\right) \tag{B.362}$$
$$= \arctan\left(\frac{m_{y,1}+\delta}{m_{x,1}+\gamma}\right) \tag{B.363}$$
$$= \arctan\left(\frac{m_{y,1}}{m_{x,1}}\right) + \frac{m_{x,1}\delta - m_{y,1}\gamma}{m_{x,1}^2+m_{y,1}^2} + \mathcal{O}\left(\delta^2,\gamma^2\right) \qquad \text{Note: } m_{x,1}^2+m_{y,1}^2+m_{z,1}^2=1 \tag{B.364}$$
$$= \arctan\left(\frac{m_{y,1}}{m_{x,1}}\right) + \frac{m_{x,1}\delta - m_{y,1}\gamma}{1-m_{z,1}^2} + \mathcal{O}\left(\delta^2,\gamma^2\right) \qquad \text{Note: } \arctan\left(\frac{m_{y,1}}{m_{x,1}}\right)=\Phi_1 \tag{B.365}$$

Using that

$$(m_{x,1}, m_{y,1}, m_{z,1}) = (\sin(\Theta_1)\cos(\Phi_1), \sin(\Theta_1)\sin(\Phi_1), \cos(\Theta_1)) \tag{B.366}$$

and

$$(m_{x,2}, m_{y,2}, m_{z,2}) = (\sin(\Theta_2)\cos(\Phi_2), \sin(\Theta_2)\sin(\Phi_2), \cos(\Theta_2)) = (\gamma, \delta, 1+\epsilon) \tag{B.367}$$

by definition,

$$\Phi = \Phi_1 + \frac{1}{\sin(\Theta_1)\not{\gamma}}\left(\delta\cancel{\sin(\Theta_1)}\cos(\Phi_1) - \gamma\cancel{\sin(\Theta_1)}\sin(\Phi_1)\right) + \mathcal{O}\left(\delta^2,\gamma^2\right) \tag{B.368}$$
$$= \Phi_1 + \frac{1}{\sin(\Theta_1)}(\sin(\Theta_2)\sin(\Phi_2)\cos(\Phi_1) - \sin(\Theta_2)\cos(\Phi_2)\sin(\Phi_1)) + \mathcal{O}\left(\delta^2,\gamma^2\right) \tag{B.369}$$
$$= \Phi_1 + \frac{\sin(\Theta_2)}{\sin(\Theta_1)}(\sin(\Phi_2)\cos(\Phi_1) - \cos(\Phi_2)\sin(\Phi_1)) + \mathcal{O}\left(\delta^2,\gamma^2\right) \tag{B.370}$$
$$= \Phi_1 + \frac{\sin(\Theta_2)}{\sin(\Theta_1)}\sin(\Phi_2-\Phi_1) + \mathcal{O}\left(\delta^2,\gamma^2\right) \tag{B.371}$$

Defining $\Delta\Phi = \Phi_2 - \Phi_1$, we note $\Phi = \Phi_1 + \underbrace{\frac{\sin(\Theta_2)}{\sin(\Theta_1)}\sin(\Delta\Phi)}_{\beta} + \mathcal{O}\left(\delta^2,\gamma^2\right)$ where β is small (just like α.

Because of the exponential decay of the soliton tails it is evident that $\Theta_2 \ll 1$. Accordingly it can be

deduced that α, β ought to be small contributions to Θ and Φ. Summarizing this section

$$\alpha = 2\sin(\Theta_2)\cos(\Delta\Phi) \text{ and } \beta = \frac{\sin(\Theta_2)}{\sin(\Theta_1)}\sin(\Delta\Phi) \tag{B.372}$$

B.4.1 Linearization

The target has now shifted. Since the small contribution of one droplet on the other has now been expressed in terms of α and β, it suffices to consider general perturbations based on small deviations away from the droplet itself. The interaction initial condition gives $\Theta \approx \Theta_1 + \alpha$ and $\Phi \approx \Phi_1 + \beta$ where α and β are small. For simplicity subscripts will be dropped until they are required again. First consider the torque equation in spherical coordinates,

$$\frac{\partial \Theta}{\partial t} = \frac{\nabla \cdot \left(\sin^2(\Theta)\nabla\Phi\right)}{\sin(\Theta)} \tag{B.373}$$

$$\sin(\Theta)\frac{\partial \Phi}{\partial t} = \frac{1}{2}\sin(2\Theta)\left(|\nabla\Phi|^2 + 1\right) - \nabla^2\Theta \tag{B.374}$$

Here are some necessary expansions:

$$\sin(\Theta+\alpha) = \sin(\Theta) + \cos(\Theta)\alpha + \mathcal{O}\left(\alpha^2\right) \tag{B.375}$$

$$\sin^2(\Theta+\alpha) = \sin^2(\Theta) + 2\sin(\Theta)\cos(\Theta)\alpha + \mathcal{O}\left(\alpha^2\right) \tag{B.376}$$

$$\sin^2(\Theta+\alpha)\nabla\left(\Phi+\beta\right) = \left(\sin^2(\Theta) + 2\sin(\Theta)\cos(\Theta)\alpha\right)\left(\nabla\Phi + \nabla\beta\right) + \mathcal{O}\left(\alpha^2\right) = \sin^2(\Theta)\nabla\Phi + 2\sin(\Theta)\cos(\Theta)\alpha\nabla\Phi + \sin^2(\Theta)\nabla(\beta) + \mathcal{O}\left(\alpha^2, ||\nabla(\beta)||\right) \tag{B.377}$$

$$\frac{1}{\sin(\Theta+\alpha)} = \frac{1}{\sin(\Theta)} - \frac{\cos(\Theta)}{\sin^2(\Theta)}\alpha + \mathcal{O}\left(\alpha^2\right) \tag{B.378}$$

Putting all of these things together,

$$\frac{\partial \Theta}{\partial t} + \frac{\partial \alpha}{\partial t} = \frac{\nabla \cdot \left(\sin^2(\Theta+\alpha)\nabla(\Phi+\beta)\right)}{\sin(\Theta+\alpha)} \tag{B.379}$$

$$= \left(\frac{1}{\sin(\Theta)} - \frac{\cos(\Theta)}{\sin^2(\Theta)}\alpha\right)\nabla \cdot \left(\left(\sin^2(\Theta) + (2\sin\Theta\cos\Theta)\alpha\right)\left(\nabla\Phi + \nabla\beta\right)\right) + \mathcal{O}\left(\alpha^2, \left\|\nabla\beta\right\|^2\right) \tag{B.380}$$

$$= \left(\frac{1}{\sin(\Theta)} - \frac{\cos(\Theta)}{\sin^2(\Theta)}\alpha\right)\nabla \cdot \left(\sin^2(\Theta)\nabla\Phi + (2\sin\Theta\cos\Theta)\alpha\nabla\Phi + \sin^2(\Theta)\nabla\beta\right) + \mathcal{O}\left(\alpha^2, \left\|\nabla\beta\right\|^2\right) \tag{B.381}$$

$$= \frac{\nabla \cdot \left(\sin^2(\Theta)\nabla\Phi\right)}{\sin(\Theta)} + \left[-\frac{\cos(\Theta)\alpha\nabla \cdot \left(\sin^2\Theta\nabla\Phi\right)}{\sin^2\Theta} + \frac{\nabla \cdot \left((2\sin\Theta\cos\Theta)\alpha\nabla\Phi\right)}{\sin\Theta}\right] + \frac{\nabla \cdot \left(\sin^2(\Theta)\nabla\beta\right)}{\sin(\Theta)} + \mathcal{O}\left(\alpha^2, \left\|\nabla\beta\right\|^2\right) \tag{B.382}$$

So

$$\frac{\partial \Theta}{\partial t} = \frac{\nabla \cdot \left(\sin^2(\Theta)\nabla\Phi\right)}{\sin(\Theta)} + \underbrace{\left[-\frac{\cos(\Theta)\alpha\nabla \cdot \left(\sin^2\Theta\nabla\Phi\right)}{\sin^2\Theta} + \frac{\nabla \cdot \left((2\sin\Theta\cos\Theta)\alpha\nabla\Phi\right)}{\sin\Theta}\right] + \frac{\nabla \cdot \left(\sin^2(\Theta)\nabla\beta\right)}{\sin(\Theta)} - \frac{\partial \alpha}{\partial t}}_{P_\Theta} + \mathcal{O}\left(\alpha^2, \left\|\nabla\beta\right\|^2\right) \tag{B.383}$$

An additional expansion is still required:

$$\frac{1}{2}\sin(2(\Theta+\alpha)) = \frac{1}{2}\sin(2\Theta) + \cos(2\Theta)\alpha + \mathcal{O}\left(\alpha^2\right). \tag{B.384}$$

Doing a similar calculation on the Φ equation yields,

$$\frac{\partial \Phi}{\partial t}+\frac{\partial \beta}{\partial t}=\frac{1}{\sin(\Theta+\alpha)}\left(\frac{1}{2}\sin(2(\Theta+\alpha))\left(\left\|\nabla\Phi+\nabla\beta\right\|^2+1\right)-\nabla^2(\Theta+\alpha)\right) \tag{B.385}$$

$$=\left(\tfrac{1}{\sin(\Theta)}-\tfrac{\cos(\Theta)}{\sin^2(\Theta)}\alpha\right)\left(\left(\tfrac{1}{2}\sin(2\Theta)+\cos(2\Theta)\alpha\right)\left(\|\nabla\Phi\|^2+2\nabla\Phi\nabla\beta+1\right)-\nabla^2\Theta-\nabla^2\alpha\right)+\mathcal{O}\left(\alpha^2,\left\|\nabla\beta\right\|^2\right) \tag{B.386}$$

$$=\left(\tfrac{1}{\sin(\Theta)}-\tfrac{\cos(\Theta)}{\sin^2(\Theta)}\alpha\right)\left(\left[\tfrac{1}{2}\sin(2\Theta)\left(\|\nabla\Phi\|^2+1\right)-\nabla^2\Theta\right]+\left[\cos(2\Theta)\alpha\left(\|\nabla\Phi\|^2+1\right)-\nabla^2\alpha\right]+\sin(2\Theta)\nabla\Phi\nabla\beta\right)+\mathcal{O}\left(\alpha^2,\left\|\nabla\beta\right\|^2\right) \tag{B.387}$$

$$\begin{aligned}=&\frac{1}{\sin(\Theta)}\left[\frac{1}{2}\sin(2\Theta)\left(\|\nabla\Phi\|^2+1\right)-\nabla^2\Theta\right]\\&+\left[\frac{1}{\sin(\Theta)}\left(\cos(2\Theta)\alpha\left(\|\nabla\Phi\|^2+1\right)-\nabla^2\alpha\right)-\frac{\cos(\Theta)}{\sin^2(\Theta)}\alpha\left(\frac{1}{2}\sin(2\Theta)\left(\|\nabla\Phi\|^2+1\right)-\nabla^2\Theta\right)\right]\\&+\frac{\sin(2\Theta)}{\sin(\Theta)}\nabla\Phi\nabla\beta+\mathcal{O}\left(\alpha^2,\left\|\nabla\beta\right\|^2\right)\end{aligned} \tag{B.388}$$

$$\begin{aligned}\sin(\Theta)\frac{\partial\Phi}{\partial t}=&\left[\frac{1}{2}\sin(2\Theta)\left(\|\nabla\Phi\|^2+1\right)-\nabla^2\Theta\right]\\&\underbrace{+\left[\left(\cos(2\Theta)\alpha\left(\|\nabla\Phi\|^2+1\right)-\nabla^2\alpha\right)-\frac{\cos(\Theta)}{\sin(\Theta)}\alpha\left(\frac{1}{2}\sin(2\Theta)\left(\|\nabla\Phi\|^2+1\right)-\nabla^2\Theta\right)\right]+\sin(2\Theta)\nabla\Phi\nabla\beta-\sin(\Theta)\frac{\partial\beta}{\partial t}}_{P_\Phi}\\&+\mathcal{O}\left(\alpha^2,\left\|\nabla\beta\right\|^2\right)\end{aligned} \tag{B.389}$$

To summarize this section:

$$P_\Theta(\Theta,\Phi,\alpha,\beta)=\left[-\frac{\cos(\Theta)\alpha\nabla\cdot\left(\sin^2\Theta\nabla\Phi\right)}{\sin^2\Theta}+\frac{\nabla\cdot((2\sin\Theta\cos\Theta)\alpha\nabla\Phi)}{\sin\Theta}\right]+\frac{\nabla\cdot\left(\sin^2(\Theta)\nabla\beta\right)}{\sin(\Theta)}-\frac{\partial\alpha}{\partial t} \tag{B.390}$$

and

$$P_\Phi(\Theta,\Phi,\alpha,\beta)=\left[\left(\cos(2\Theta)\alpha\left(\|\nabla\Phi\|^2+1\right)-\nabla^2\alpha\right)-\frac{\cos(\Theta)}{\sin(\Theta)}\alpha\left(\frac{1}{2}\sin(2\Theta)\left(\|\nabla\Phi\|^2+1\right)-\nabla^2\Theta\right)\right]+\sin(2\Theta)\nabla\Phi\nabla\beta-\sin(\Theta)\frac{\partial\beta}{\partial t} \tag{B.391}$$

B.4.2 Evaluating only the right hand side at $t=0$

At this point the calculation becomes vastly easier under the assumption that both droplets are initially stationary. The most important simplification is that these stationary droplets will have trivial phase gradient. This assumption implies other conditions that will break down immediately.

Under these conditions it is possible to choose $\omega_1 = \omega_2 = \omega$ and $V_1 = V_2 = 0$

That is,

$$\frac{\partial \Theta_1}{\partial t} = 0 = \frac{\nabla \cdot \left(\sin^2(\Theta_1)\nabla\Phi_1\right)}{\sin(\Theta_1)} \tag{B.392}$$

$$\sin(\Theta_1)\frac{\partial \Phi_1}{\partial t} = \omega \sin(\Theta_1) = \frac{1}{2}\sin(2\Theta_1)\left(|\nabla\Phi_1|^2 + 1\right) - \nabla^2\Theta_1 \tag{B.393}$$

and

$$\frac{\partial \Theta_2}{\partial t} = 0 = \frac{\nabla \cdot \left(\sin^2(\Theta_2)\nabla\Phi_2\right)}{\sin(\Theta_2)} \tag{B.394}$$

$$\sin(\Theta_2)\frac{\partial \Phi_2}{\partial t} = \omega \sin(\Theta_2) = \frac{1}{2}\sin(2\Theta_2)\left(|\nabla\Phi_2|^2 + 1\right) - \nabla^2\Theta_2 \tag{B.395}$$

In this case the approximate solutions are given by

$$\Theta_1 = \arccos(\tanh(\rho - \frac{1}{\omega}) \tag{B.396}$$

$$\Phi_1 = \omega t + \Phi_{0,1} \tag{B.397}$$

$$\Theta_2 = \arccos(\tanh(\tilde{\rho} - \frac{1}{\omega}) \tag{B.398}$$

$$\Phi_2 = \omega t + \Phi_{0,2} \tag{B.399}$$

where (B.400)

$$\rho = \sqrt{x^2 + y^2} \text{ and } \tilde{\rho} = \sqrt{(x-\delta)^2 + y^2} \tag{B.401}$$

where δ is the separation between the droplets (and assumed large).

B.4.3 Evaluation of P_Θ

$$P_\Theta(\Theta, \Phi, \alpha, \beta) = \left[-\frac{\cos(\Theta)\alpha\nabla\cdot\left(\sin^2\Theta\nabla\Phi\right)}{\sin^2\Theta} + \frac{\nabla\cdot((2\sin\Theta\cos\Theta)\alpha\nabla\Phi)}{\sin\Theta}\right] + \frac{\nabla\cdot\left(\sin^2(\Theta)\nabla\beta\right)}{\sin(\Theta)} - \frac{\partial\alpha}{\partial t} \tag{B.402}$$

First consider $\frac{\partial \alpha}{\partial t}$.

$$\frac{\partial \alpha}{\partial t} = \frac{\partial}{\partial t}\left(2\sin(\Theta_2)\cos(\Phi_2-\Phi_1)\right) \tag{B.403}$$

$$= 2\left[\cos(\Theta_2)\cancelto{0}{\frac{\partial \Theta_2}{\partial t}}\cos(\Delta\Phi) - \sin(\Theta_2)\sin(\Delta\Phi)\cancelto{0}{\left(\frac{\partial \Phi_2}{\partial t} - \frac{\partial \Phi_2}{\partial t}\right)}\right] = 0 \tag{B.404}$$

Note $\nabla\Phi_1 = 0$ so the first term in P_Θ vanishes. All that remains is the middle term.

$$\frac{\nabla\cdot\left(\sin^2(\Theta)\nabla\beta\right)}{\sin(\Theta)} = \frac{\nabla\cdot\left(\sin^2(\Theta_1)\nabla\left(\frac{\sin(\Theta_2)}{\sin(\Theta_1)}\sin(\Delta\Phi)\right)\right)}{\sin(\Theta_1)} \tag{B.405}$$

note that $\Delta\Phi$ is independent of space

$$= \sin(\Delta\Phi)\frac{\nabla\cdot\left(\sin^2(\Theta_1)\nabla\left(\frac{\sin(\Theta_2)}{\sin(\Theta_1)}\right)\right)}{\sin(\Theta_1)} \tag{B.406}$$

$$= \sin(\Delta\Phi)\frac{\nabla\cdot(\cos\Theta_2\sin\Theta_1\nabla\Theta_2 - \cos\Theta_1\sin\Theta_2\nabla\Theta_1)}{\sin\Theta_1} \tag{B.407}$$

$$= \sin(\Delta\Phi)\Big[\Big(\cos(\Theta_2)\nabla^2\Theta_2\sin\Theta_1 - \sin(\Theta_2)|\nabla\Theta_2|^2\sin(\Theta_1) + \cancel{\cos(\Theta_1)\cos(\Theta_2)\nabla\Theta_1\cdot\nabla\Theta_2}\Big)$$
$$-\Big(\cos(\Theta_1)\nabla^2\Theta_1\sin\Theta_2 - \sin(\Theta_1)|\nabla\Theta_1|^2\sin(\Theta_2) + \cancel{\cos(\Theta_1)\cos(\Theta_2)\nabla\Theta_1\cdot\nabla\Theta_2}\Big)\Big] \tag{B.408}$$

Note that for the droplet

$$\omega\sin(\Theta) = \frac{1}{2}\sin(2\Theta)\left(|\nabla\Phi|^2+1\right) - \nabla^2\Theta \tag{B.409}$$

$$\Rightarrow \nabla^2\Theta = \sin\Theta\cos\Theta\left(|\nabla\Phi|^2\right) - \omega\sin(\Theta) = \underbrace{\sin\Theta\cos\Theta - \omega\sin\Theta}_{\text{for stationary droplet}} = \sin(\Theta)(\cos(\Theta)-\omega) \tag{B.410}$$

Hence,

$$\frac{\nabla\cdot\left(\sin^2(\Theta)\nabla\beta\right)}{\sin(\Theta)} = \sin(\Delta\Phi)\left[\sin\left(\Theta_1\left(\cos(\Theta_2)(\sin(\Theta_2)(\cos(\Theta_2)-\omega)) - \sin(\Theta_2)|\nabla\Theta_2|^2\right) - \sin\Theta_2\left(\cos(\Theta_1)(\sin(\Theta_1)(\cos(\Theta_1)-\omega)) - \sin(\Theta_1)|\nabla\Theta_1|^2\right)\right] \tag{B.411}$$

$$= \sin(\Delta\Phi)\sin(\Theta_1)\sin(\Theta_2)\left(\cos^2(\Theta_2) - \cos^2(\Theta_1) - \omega(\cos\Theta_2 - \cos\Theta_1) - |\nabla\Theta_2|^2 + |\nabla\Theta_1|^2\right) \tag{B.412}$$

Noting that Θ_2 is small it is possible make the additional simplification that $\cos(\Theta_2) \approx 1$ obtaining that

$$P_\Theta = \sin(\Delta\Phi)\sin(\Theta_1)\sin(\Theta_2)\left(\sin^2(\Theta_1) - \omega(1-\cos\Theta_1) + |\nabla\Theta_1|^2\right) \tag{B.413}$$

B.4.4 Evaluation of P_Φ

$$P_\Phi(\Theta,\Phi,\alpha,\beta) = \left[\left(\cos(2\Theta)\alpha\left(\|\nabla\Phi\|^2+1\right) - \nabla^2\alpha\right) - \frac{\cos(\Theta)}{\sin(\Theta)}\alpha\left(\frac{1}{2}\sin(2\Theta)\left(\|\nabla\Phi\|^2+1\right) - \nabla^2\Theta\right)\right] + \sin(2\Theta)\nabla\Phi\nabla\beta - \sin(\Theta)\frac{\partial\beta}{\partial t} \tag{B.414}$$

Observing that the middle term is the defining relationship for the droplet and noting that $\nabla\Phi = 0$, this relation can be drastically simplified.

$$P_\Phi(\Theta,\Phi,\alpha,\beta) = (\cos(2\Theta_1) - \omega\cos\Theta_1)\alpha - \nabla^2\alpha - \sin(\Theta)\frac{\partial\beta}{\partial t} \tag{B.415}$$

First compute $\frac{\partial\beta}{\partial t}$

$$\frac{\partial\beta}{\partial t} = \frac{\partial}{\partial t}\left(\frac{\sin(\Theta_2)}{\sin(\Theta_1)}\sin(\Delta\Phi)\right) = \frac{\sin(\Theta_2)}{\sin(\Theta_1)}\frac{\partial}{\partial t}(\sin(\Delta\Phi)) \tag{B.416}$$

$$= \frac{\sin(\Theta_2)}{\sin(\Theta_1)}\cos(\Delta\Phi)\cancelto{0}{\left(\frac{\partial\Phi_2}{\partial t} - \frac{\partial\Phi_1}{\partial t}\right)} = 0 \tag{B.417}$$

Next compute $\nabla^2\alpha$

$$\nabla^2\alpha = \nabla\cdot\nabla(2\sin(\Theta_2)\cos(\Delta\Phi)) \tag{B.418}$$

$$= 2\cos(\Delta\Phi)\nabla\cdot\nabla(\sin(\Theta_2)) = 2\cos(\Delta\Phi)\nabla\cdot(\cos(\Theta_2)\nabla\Theta_2) \tag{B.419}$$

$$= 2\cos(\Delta\Phi)\left(\cos(\Theta_2)\nabla^2\Theta_2 - \sin(\Theta_2)|\nabla\Theta_2|^2\right) \tag{B.420}$$

$$= 2\cos(\Delta\Phi)\left(\cos(\Theta_2)(\sin(\Theta_2)(\cos(\Theta_2)-\omega)) - \sin(\Theta_2)|\nabla\Theta_2|^2\right) \quad \text{using droplet equation} \tag{B.421}$$

Using that Θ_2 is small (and nearly flat) (i.e. $\cos(\Theta_2) \approx 1$ and $\nabla\Theta_2 = 0$)

$$\nabla^2\alpha = 2\cos(\Delta\Phi)\sin(\Theta_2)(1-\omega). \tag{B.422}$$

So all together,

$$P_\Phi = (\cos(2\Theta_1) - \omega\cos\Theta_1)(2\sin(\Theta_2)\cos(\Delta\Phi)) - (2\cos(\Delta\Phi)\sin(\Theta_2)(1-\omega)) \tag{B.423}$$

$$= 2\cos(\Delta\Phi)\sin(\Theta_2)[\cos(2\Theta_1) - \omega\cos\Theta_1 - 1 + \omega] \tag{B.424}$$

$$= 2\cos(\Delta\Phi)\sin(\Theta_2)\left[\cos^2(\Theta_1) - \sin^2(\Theta_1) - \omega\cos\Theta_1 - 1 + \omega\right] \tag{B.425}$$

$$= 2\cos(\Delta\Phi)\sin(\Theta_2)\left[\left(\cos^2(\Theta_1) - 1\right) - \sin^2(\Theta_1) + \omega(1-\cos\Theta_1)\right] \tag{B.426}$$

$$P_\Phi = 2\cos(\Delta\Phi)\sin(\Theta_2)\left[-2\sin^2(\Theta_1) + \omega(1-\cos\Theta_1)\right] \tag{B.427}$$

B.4.5 Evaluating the Right Hand Side of the Modulation Equations

First evaluate P_Θ, P_Φ for the approximate Θ_1.

$$P_\Theta = \sin(\Delta\Phi)\sin(\Theta_2)\text{sech}\left(\rho - \frac{1}{\omega}\right)\left(2\text{sech}^2\left(\rho - \frac{1}{\omega}\right) - \omega\left(1 - \tanh\left(\rho - \frac{1}{\omega}\right)\right)\right) \tag{B.428}$$

and

$$P_\Phi = 2\cos(\Delta\Phi)\sin(\Theta_2)\left[-2\text{sech}^2\left(\rho - \frac{1}{\omega}\right) + \omega\left(1 - \tanh\left(\rho - \frac{1}{\omega}\right)\right)\right] \tag{B.429}$$

In general, the modulation equations are

$$\begin{pmatrix} \Phi_0 \\ \mathbf{x}_0 \\ \omega \\ \mathbf{V} \end{pmatrix}' = \begin{pmatrix} \frac{\mathbf{V}}{4\pi}\cdot\left(\int_{\mathbb{R}^2}(P_u\hat{\rho})d\mathbf{x}\right) + \frac{\omega}{4\pi}\int_{\mathbb{R}^2}\text{sech}^2\left(\rho - \frac{1}{\omega}\right)P_{\tilde{\Phi}}d\mathbf{x} \\ -\frac{\omega}{2\pi}\int_{\mathbb{R}^2}(P_u\hat{\rho})d\mathbf{x} \\ \frac{\omega^3}{4\pi}\int_{\mathbb{R}^2}P_u d\mathbf{x} \\ \frac{3\mathbf{V}\omega^2}{4\pi}\left(\int_{\mathbb{R}^2}P_u d\mathbf{x}\right) - \frac{\omega}{2\pi}\int_{\mathbb{R}^2}\frac{1}{\rho}\left(\mathbf{V}\cdot\hat{\varphi}\right)\hat{\varphi}P_u d\mathbf{x} - \frac{\omega^3}{2\pi}\int_{\mathbb{R}^2}\text{sech}^2\left(\rho - \frac{1}{\omega}\right)\hat{\rho}P_{\tilde{\Phi}}d\mathbf{x} \end{pmatrix} \tag{B.430}$$

These simplify somewhat under the assumption that $V=0$ initially.

$$\begin{pmatrix} \Phi_0 \\ \mathbf{x}_0 \\ \omega \\ \mathbf{V} \end{pmatrix}' \Bigg|_{t=0} = \begin{pmatrix} \frac{\omega}{4\pi}\int_{\mathbb{R}^2} \operatorname{sech}^2\left(\rho-\frac{1}{\omega}\right) P_{\bar{\Phi}}\, d\mathbf{x} \\ -\frac{\omega}{2\pi}\int_{\mathbb{R}^2} (P_u\hat{\rho})\, d\mathbf{x} \\ \frac{\omega^3}{4\pi}\int_{\mathbb{R}^2} P_u\, d\mathbf{x} \\ -\frac{\omega^3}{2\pi}\int_{\mathbb{R}^2} \operatorname{sech}^2\left(\rho-\frac{1}{\omega}\right)\hat{\rho}\, P_{\bar{\Phi}}\, d\mathbf{x} \end{pmatrix} \tag{B.431}$$

Using that $P_u = -\sin(\Theta)P_\Theta = -\operatorname{sech}\left(\rho-\frac{1}{\omega}\right)P_\Theta$ and $P_{\bar{\Phi}} = \frac{P_\Phi}{\sin(\Theta)} = \frac{P_\Phi}{\operatorname{sech}\left(\rho-\frac{1}{\omega}\right)}$ and substituting the precise form of the perturbation

$$\begin{pmatrix} \Phi_{0,1} \\ \mathbf{x}_{0,1} \\ \omega_1 \\ \mathbf{V}_1 \end{pmatrix}' \Bigg|_{t=0} = \begin{pmatrix} \frac{\omega}{2\pi}\cos(\Delta\Phi)\int_{\mathbb{R}^2}\left[\operatorname{sech}\left(\rho-\frac{1}{\omega}\right)\left(\sin(\Theta_2)\left[-2\operatorname{sech}^2\left(\rho-\frac{1}{\omega}\right)+\omega\left(1-\tanh\left(\rho-\frac{1}{\omega}\right)\right)\right]\right)\right] d\mathbf{x} \\ \frac{\omega}{2\pi}\sin(\Delta\Phi)\int_{\mathbb{R}^2}\left[\operatorname{sech}\left(\rho-\frac{1}{\omega}\right)\hat{\rho}\left(\sin(\Theta_2)\operatorname{sech}\left(\rho-\frac{1}{\omega}\right)\left(2\operatorname{sech}^2\left(\rho-\frac{1}{\omega}\right)-\omega\left(1-\tanh\left(\rho-\frac{1}{\omega}\right)\right)\right)\right)\right] d\mathbf{x} \\ -\frac{\omega^3}{4\pi}\sin(\Delta\Phi)\int_{\mathbb{R}^2}\left[\operatorname{sech}\left(\rho-\frac{1}{\omega}\right)\left(\sin(\Theta_2)\operatorname{sech}\left(\rho-\frac{1}{\omega}\right)\left(2\operatorname{sech}^2\left(\rho-\frac{1}{\omega}\right)-\omega\left(1-\tanh\left(\rho-\frac{1}{\omega}\right)\right)\right)\right)\right] d\mathbf{x} \\ -\frac{\omega^3}{\pi}\cos(\Delta\Phi)\int_{\mathbb{R}^2}\left[\operatorname{sech}\left(\rho-\frac{1}{\omega}\right)\hat{\rho}\left(\sin(\Theta_2)\left[-2\operatorname{sech}^2\left(\rho-\frac{1}{\omega}\right)+\omega\left(1-\tanh\left(\rho-\frac{1}{\omega}\right)\right)\right]\right)\right] d\mathbf{x} \end{pmatrix} \tag{B.432}$$

Obviously there is a duplicate set of equations for the action droplet 1 on droplet 2–but these can be deduced by symmetry arguments (some signs will flip). These expressions can be further simplified by defining the quantity

$$I(\rho,\omega,\delta) = \sin(\Theta_2)\operatorname{sech}\left(\rho-\frac{1}{\omega}\right)\left[2\operatorname{sech}^2\left(\rho-\frac{1}{\omega}\right)-\omega\left(1-\tanh\left(\rho-\frac{1}{\omega}\right)\right)\right] \tag{B.433}$$

$$\begin{pmatrix} \Phi_0 \\ \mathbf{x}_0 \\ \omega \\ \mathbf{V} \end{pmatrix}' \Bigg|_{t=0} = \begin{pmatrix} -\frac{\omega}{2\pi}\cos(\Delta\Phi)\int_{\mathbb{R}^2} I(\rho,\omega,\delta)d\mathbf{x} \\ \frac{\omega}{2\pi}\sin(\Delta\Phi)\int_{\mathbb{R}^2} I(\rho,\omega,\delta)\mathrm{sech}\left(\rho-\frac{1}{\omega}\right)\hat{\rho}\,d\mathbf{x} \\ -\frac{\omega^3}{4\pi}\sin(\Delta\Phi)\int_{\mathbb{R}^2} I(\rho,\omega,\delta)d\mathbf{x} \\ \frac{\omega^3}{\pi}\cos(\Delta\Phi)\int_{\mathbb{R}^2} I(\rho,\omega,\delta)\mathrm{sech}\left(\rho-\frac{1}{\omega}\right)\hat{\rho}\,d\mathbf{x} \end{pmatrix} \tag{B.434}$$

These equations are equivalent to those presented in Section 3.4.

B.5 Supplementary Calculations for Numerical Methods

B.5.1 Gradient Evaluation for Adjoint Continuation

The first step is to compute the linearization for

$$\begin{cases} \imath\, w_t = \Delta w - \frac{2w^*\nabla w\cdot\nabla w + w(1-|w|^2)}{1+|w|^2} \\ w(\pm\infty) = 0, \quad w(x,0) = w_0 \end{cases} \tag{B.435}$$

Let w denote the solution to Eq. B.435. Let $\hat{w} = w + \epsilon v + \mathcal{O}\left(\epsilon^2\right)$ denote the solution to the Eq. B.435 with initial data $w_0 + \epsilon v_0$.

$$\imath\,\hat{w}_t = \imath\, w_t + \epsilon(i\, v_t) + \mathcal{O}\left(\epsilon^2\right) \tag{B.436}$$

$$\Delta\hat{w} = \Delta w + \epsilon\Delta v. \tag{B.437}$$

$$2\hat{w}^*\nabla\hat{w}\cdot\nabla\hat{w} = 2(w+\epsilon v)^*\nabla(w+\epsilon v)\cdot\nabla(w+\epsilon v)+\mathcal{O}\left(\epsilon^2\right) \tag{B.438}$$

$$= 2(w^*+\epsilon v^*)(\nabla w+\epsilon\nabla v)\cdot(\nabla w+\epsilon\nabla v)+\mathcal{O}\left(\epsilon^2\right) \tag{B.439}$$

$$= 2(w^*+\epsilon v^*)(\nabla w\cdot\nabla w+\epsilon(2\nabla w\cdot\nabla v)+\mathcal{O}\left(\epsilon^2\right) \tag{B.440}$$

$$= 2w^*\nabla w\cdot\nabla w+\epsilon(4w^*\nabla w\cdot\nabla v+2v^*\nabla w\cdot\nabla w)+\mathcal{O}\left(\epsilon^2\right) \tag{B.441}$$

$$|\hat{w}|^2 = |w+\epsilon v|^2+\mathcal{O}\left(\epsilon^2\right) \tag{B.442}$$

$$= (w+\epsilon v)^*(w+\epsilon v)+\mathcal{O}\left(\epsilon^2\right) \tag{B.443}$$

$$= w^*w+\epsilon(w^*v+v^*w)+\mathcal{O}\left(\epsilon^2\right)+\mathcal{O}\left(\epsilon^2\right) \tag{B.444}$$

$$= |w|^2+\epsilon(w^*v+v^*w)+\mathcal{O}\left(\epsilon^2\right) \tag{B.445}$$

$$\hat{w}(1-|\hat{w}|^2) = (w+\epsilon v)(1-(w^*w+\epsilon(w^*v+v^*w)))+\mathcal{O}\left(\epsilon^2\right) \tag{B.446}$$

$$= w(1-|w|^2)+\epsilon\left(v(1-|w|^2)-w(w^*v+v^*w)\right)+\mathcal{O}\left(\epsilon^2\right) \tag{B.447}$$

$$= w(1-|w|^2)+\epsilon\left(v(1-|w|^2)-v|w|^2-v^*w^2)\right)+\mathcal{O}\left(\epsilon^2\right) \tag{B.448}$$

$$= w(1-|w|^2)+\epsilon\left(v(1-2|w|^2)-v^*w^2)\right)+\mathcal{O}\left(\epsilon^2\right) \tag{B.449}$$

The following approximation will be useful.

$$\frac{1}{a+\epsilon b} = \frac{1}{a}-\frac{\epsilon b}{a^2}+\mathcal{O}\left(\epsilon^2\right) = \frac{1}{a}\left(1-\epsilon\frac{b}{a}\right)+\mathcal{O}\left(\epsilon^2\right) \tag{B.450}$$

to expand the denominator.

$$\frac{1}{1+|\hat{w}^2|} = \frac{1}{\underbrace{1+|w|^2}_{a}+\epsilon\underbrace{(w^*v+v^*w)}_{b}+\mathcal{O}(\epsilon^2)} \tag{B.451}$$

$$= \frac{1}{1+|w|^2}\left(1-\epsilon\frac{w^*v+v^*w}{1+|w|^2}\right)+\mathcal{O}\left(\epsilon^2\right) \tag{B.452}$$

Substituting this into the PDE for $\hat{w}$, namely

$$\begin{cases} \imath\,\hat{w}_t = \Delta\hat{w} - \frac{2\hat{w}^*\nabla\hat{w}\cdot\nabla\hat{w}+\hat{w}(1-|\hat{w}|^2)}{1+|\hat{w}|^2} \\ \hat{w}(\pm\infty)=0, \quad \hat{w}(x,0)=w_0+\epsilon v_0 \end{cases} \tag{B.453}$$

yields

$$\imath\,\hat{w}_t = \Delta\hat{w} - \frac{2\hat{w}^*\nabla\hat{w}\cdot\nabla\hat{w}+\hat{w}(1-|\hat{w}|^2)}{1+|\hat{w}|^2} \tag{B.454}$$

$$\begin{aligned} &= (\Delta w+\epsilon\Delta v) \\ &\quad -\left(\tfrac{1}{1+|w|^2}\left(1-\epsilon\tfrac{w^*v+v^*w}{1+|w|^2}\right)\right)(2w^*\nabla w\cdot\nabla w+\epsilon(4w^*\nabla w\cdot\nabla v+2v^*\nabla w\cdot\nabla w) \\ &\qquad +w(1-|w|^2)+\epsilon\left(v(1-2|w|^2)-v^*w^2\right))+\mathcal{O}\left(\epsilon^2\right) \end{aligned} \tag{B.455}$$

$$\begin{aligned} \cancel{\imath w_t}+\epsilon(\imath v_t) = (\cancel{\Delta w}+\epsilon\Delta v) &- \left(\frac{2w^*\nabla w\cdot\nabla w+\cancel{w(1-|w|^2)}}{1+|w|^2}\right. \\ &\left.+\epsilon\left(\frac{4w^*\nabla w\cdot\nabla v+2v^*\nabla w\cdot\nabla w+v(1-2|w|^2)-v^*w^2}{1+|w|^2}\right)\right) \\ &-\epsilon\left(\frac{-(w^*v+v^*w)\left(2w^*\nabla w\cdot\nabla w+w(1-|w|^2)\right)}{(1+|w|^2)^2}\right)+\mathcal{O}\left(\epsilon^2\right) \end{aligned} \tag{B.456}$$

$$\begin{aligned} \imath\,v_t = \Delta v &- \left(\frac{4w^*\nabla w\cdot\nabla v+2v^*\nabla w\cdot\nabla w+v(1-2|w|^2)-v^*w^2}{1+|w|^2}\right. \\ &\left.+\frac{-(w^*v+v^*w)\left(2w^*\nabla w\cdot\nabla w+w(1-|w|^2)\right)}{\left(1+|w|^2\right)^2}\right)+\mathcal{O}(\epsilon) \end{aligned} \tag{B.457}$$

With a little more processing this becomes

$$\imath v_t = \Delta v - \left(\frac{4w^*\nabla w\cdot\nabla v}{1+|w|^2} + \left(\frac{1-2|w|^2}{1+|w|^2} - \frac{2w^{*2}\nabla w\cdot\nabla w + |w|^2(1-|w|^2}{\left(1+|w|^2\right)^2} \right) v + \left(\frac{2\nabla w\cdot\nabla w - w^2}{1+|w|^2} - \frac{2|w|^2\nabla w\cdot\nabla w + w^2(1-|w|^2}{\left(1+|w|^2\right)^2} \right) v^* \right) \tag{B.458}$$

B.5.2 Adjoint Calculation

Taking the complex conjugate of Eq. (B.458),

$$-\imath v_t^* = \Delta v^* - \frac{4w\nabla w^*\cdot\nabla v^*}{1+|w|^2} - \left(\frac{1-2|w|^2}{1+|w|^2} - \frac{2w^2\nabla w^*\cdot\nabla w^* + |w|^2(1-|w|^2)}{\left(1+|w|^2\right)^2} \right) v^* - \left(\frac{2\nabla w^*\cdot\nabla w^* - w^{*2}}{1+|w|^2} - \frac{2|w|^2\nabla w^*\cdot\nabla w^* + w^{*2}(1-|w|^2)}{\left(1+|w|^2\right)^2} \right) v \tag{B.459}$$

Recall that,

$$G(w_0,T) = \frac{1}{2}\int_{\mathbb{R}^2} |w(x,T) - w_0(x)|^2\, dx \tag{B.460}$$

$$= \frac{1}{2}\int_{\mathbb{R}^2} (w(x,T) - w_0(x))^*(w(x,T) - w_0(x))dx \tag{B.461}$$

With this formulation, the functional G is guaranteed to map to real numbers. Further this functional corresponds to a L^2 norm over the set of complex functions. As a result, this functional exhibits the same convexity structure of traditional least squares minimization problems. If minimization of G will include variation of the period, T, it is necessary to compute

$$\frac{\partial}{\partial t}G(w_0,T) = \frac{1}{2}\int_{\mathbb{R}^2} |w(x,T) - w_0(x)|^2\, dx \tag{B.462}$$

$$= \frac{\partial}{\partial t}\frac{1}{2}\int_{\mathbb{R}^2} (w(x,T) - w_0(x))^*(w(x,T) - w_0(x))dx \tag{B.463}$$

$$= \frac{1}{2}\int_{\mathbb{R}^2} ((w_t(x,T))^*(w(x,T) - w_0(x)) + (w(x,T) - w_0(x))^*(w_t(x,T)))\, dx \tag{B.464}$$

$$= \mathcal{R}e\left(\int_{\mathbb{R}^2} (w(x,T) - w_0(x))^*(w_t(x,T))dx \right) \tag{B.465}$$

The more important quantity is the variational derivative with respect to the initial condition. Let $\hat{w}(x,T,\epsilon)$ denote the solution to the equation with perturbed initial data, then

$$G(w_0+\epsilon v_0)=\frac{1}{2}\int_{\mathbb{R}^2}(\hat{w}(x,T,\epsilon)-w_0(x)-\epsilon v_0(x))^*(\hat{w}(x,T,\epsilon)-w_0(x)-\epsilon v_0(x))\,dx \tag{B.466}$$

Differentiating with respect to ϵ

$$\frac{\partial}{\partial\epsilon}G(w_0+\epsilon v_0)=\frac{\partial}{\partial\epsilon}\frac{1}{2}\int_{\mathbb{R}^2}(\hat{w}(x,T,\epsilon)-w_0(x)-\epsilon v_0(x))^*(\hat{w}(x,T,\epsilon)-w_0(x)-\epsilon v_0(x))\,dx \tag{B.467}$$

$$=\frac{1}{2}\int_{\mathbb{R}^2}(\hat{w}_\epsilon(x,T,\epsilon)-v_0(x))^*(\hat{w}(x,T,\epsilon)-w_0(x)-\epsilon v_0(x))$$

$$+(\hat{w}(x,T,\epsilon)-w_0(x)-\epsilon v_0(x))^*(\hat{w}(x,T,\epsilon)-v_0(x))\,dx \tag{B.468}$$

$$=\mathcal{R}e\left(\int_{\mathbb{R}^2}(\hat{w}_\epsilon(x,T,\epsilon)-v_0(x))^*(\hat{w}(x,T,\epsilon)-w_0(x)-\epsilon v_0(x))\,dx\right) \tag{B.469}$$

Finally the variation derivative becomes

$$\dot{G}=\frac{\partial}{\partial\epsilon}G(w_0+\epsilon v_0)\bigg|_{\epsilon=0}=\mathcal{R}e\left(\int_{\mathbb{R}^2}(\hat{w}_\epsilon(x,T,0)-v_0(x))^*(\hat{w}(x,T,0)-w_0(x))\,dx\right) \tag{B.470}$$

Note that $\hat{w}(x,T,0)=w(x,T)$ and that $\hat{w}_\epsilon(x,T,0)$ is the solution to the linearized problem with initial data v_0, therefore call $\hat{w}_\epsilon(x,T,0)=v(x,T)$. Finally, define $u(x,0)=u_0=w(x,T)-w_0(x)$ and obtain

$$\dot{G}=\mathcal{R}e\left(\int_{\mathbb{R}^2}(v(x,T)-v_0(x))^*(w(x,T)-w_0(x))\,dx\right)=\mathcal{R}e\left(\int_{\mathbb{R}^2}(v(x,T)-v_0(x))^*\,u_0(x)dx\right) \tag{B.471}$$

This is fundamentally similar to the anlaysis in [AW10b], only the inner product has changed. Expanding a little further $\dot{G}=\mathcal{R}e\left(\int_{\mathbb{R}^2}(v(x,T)^*u_0(x)-v_0(x)^*u_0(x))\,dx\right)$.

Letting $\langle p(x), q(x)\rangle = \mathcal{R}e\left(\int_{\mathbb{R}^2} p(x)^* q(x) dx\right)$, it is clear that u needs to be such that

$$\langle v(x,T), u_0\rangle = \langle v_0(x), u(x,T)\rangle \equiv \langle u(x,T), v_0(x)\rangle \tag{B.472}$$

To understand why this is the adjoint requires a short digression. Let $s = T - s$ and define $u(x,s)$ be the adjoint.

Remark

Note $\mathcal{R}e\left(\int_{\mathbb{R}^2} p(x)^* q(x) dx\right) = \frac{1}{2}\int_{\mathbb{R}^2}\left(p(x)^* q(x) + p(x) q(x)^*\right) dx$ The distinction between simply proceeding as though the operators were acting on a scalar or as though they were acting on the vector $[w, w^*]^T$ amounts to a factor of 2 difference in how we view the inner product. This will not be significant.

The adjoint is meant to satisfy the relation,

$$\langle v_t, u\rangle = \langle v, u_s\rangle \tag{B.473}$$

$$\int_{\mathbb{R}^2}\left(v_t^* u + v_t u^*\right) dx = \int_{\mathbb{R}^2}\left(v^* u_s + v u_s^*\right) dx \tag{B.474}$$

This computation will be done in several pieces. Consider $v_t u^*$.

$$v_t u^* = -\imath\left(\Delta v - \frac{4w^*\nabla w\cdot\nabla v}{1+|w|^2} - \left(\frac{1-2|w|^2}{1+|w|^2} - \frac{2w^{*2}\nabla w\cdot\nabla w + |w|^2(1-|w|^2)}{\left(1+|w|^2\right)^2}\right) v\right. \tag{B.475}$$

$$\left. -\left(\frac{2\nabla w\cdot\nabla w - w^2}{1+|w|^2} - \frac{2|w|^2\nabla w\cdot\nabla w + w^2(1-|w|^2)}{\left(1+|w|^2\right)^2}\right) v^*\right) u^* \tag{B.476}$$

$$= -\imath\left(\underbrace{\Delta v\, u^*}_{(1)} - \underbrace{\frac{4w^*\nabla w\cdot\nabla v}{1+|w|^2} u^*}_{(2)} - \left(\frac{1-2|w|^2}{1+|w|^2} - \frac{2w^{*2}\nabla w\cdot\nabla w + |w|^2(1-|w|^2)}{\left(1+|w|^2\right)^2}\right) v u^*\right. \tag{B.477}$$

$$\left. -\left(\frac{2\nabla w\cdot\nabla w - w^2}{1+|w|^2} - \frac{2|w|^2\nabla w\cdot\nabla w + w^2(1-|w|^2)}{\left(1+|w|^2\right)^2}\right) v^* u^*\right) \tag{B.478}$$

Only terms (1) and (2) will require further processing. The next step is to apply the integral and integrate by parts to turn this into an operator acting on u^* instead of v. Not that by the boundary conditions, $\lim_{|x|\to\infty} w(x) = 0$. Assuming that perturbations do not destroy this property requires that $\lim_{|x|\to\infty} v(x) = 0$. Note that if $\lim_{|x|\to\infty} v(x) = 0$ goes to zero smoothly, requires that $\lim_{|x|\to\infty} \frac{\partial v}{\partial x} = 0$ as well. Assuming that $\frac{\partial v}{\partial x} \to 0$ as $x \to \pm\infty$, it is immediate that term (1) yields

$$\int_{\mathbb{R}^2} \Delta v\, u^* d\,x = \int_{\mathbb{R}^2} v \Delta u^* d\,x. \tag{B.479}$$

Consider term (2). Let $\alpha = x$, y or z, then

$$\int_{\mathbb{R}^2} \frac{4w^* w_\alpha \cdot v_\alpha}{1+|w|^2} u^* d\,\alpha = \cancelto{0}{\frac{4w^* w_\alpha \cdot v}{1+|w|^2} u^*}\Big|_{\alpha=\pm\infty} - \int_{\mathbb{R}^2} \left(\frac{4w^* w_\alpha}{1+|w|^2} u^*\right)_\alpha v\, d\,\alpha. \tag{B.480}$$

More compactly, ,

$$\int_{\mathbb{R}^2} \frac{4w^* \nabla w \cdot \nabla v}{1+|w|^2} u^* d\,x = -\int_{\mathbb{R}^2} \nabla \cdot \left(\frac{4w^* \nabla w\, u^*}{1+|w|^2}\right) v\, d\,x. \tag{B.481}$$

Putting these pieces of information together,

$$\int_{\mathbb{R}^2} v_t\, u^* d\,x = \int_{\mathbb{R}^2} -\imath \left(\Delta v - \frac{4w^*\nabla w\cdot\nabla v}{1+|w|^2} - \left(\frac{1-2|w|^2}{1+|w|^2} - \frac{2w^{*2}\nabla w\cdot\nabla w + |w|^2(1-|w|^2)}{\left(1+|w|^2\right)^2} \right) v \right.$$
$$\left. - \left(\frac{2\nabla w\cdot\nabla w - w^2}{1+|w|^2} - \frac{2|w|^2\nabla w\cdot\nabla w + w^2(1-|w|^2)}{\left(1+|w|^2\right)^2} \right) v^* \right) u^* d\,x \quad \text{(B.482)}$$

$$= \int_{\mathbb{R}^2} -\imath \left(\left(\Delta u^* + \nabla\cdot\left(\frac{4w^*\nabla w\, u^*}{1+|w|^2} \right) - \left(\frac{1-2|w|^2}{1+|w|^2} - \frac{2w^{*2}\nabla w\cdot\nabla w + |w|^2(1-|w|^2)}{\left(1+|w|^2\right)^2} \right) u^* \right) v \right.$$
$$\left. - \left(\frac{2\nabla w\cdot\nabla w - w^2}{1+|w|^2} - \frac{2|w|^2\nabla w\cdot\nabla w + w^2(1-|w|^2)}{\left(1+|w|^2\right)^2} \right) u^* \right) v^* d\,x \quad \text{(B.483)}$$

$$= \int_{\mathbb{R}^2} \imath \left(\left(-\Delta u^* - \nabla\cdot\left(\frac{4w^*\nabla w\, u^*}{1+|w|^2} \right) + \left(\frac{1-2|w|^2}{1+|w|^2} - \frac{2w^{*2}\nabla w\cdot\nabla w + |w|^2(1-|w|^2)}{\left(1+|w|^2\right)^2} \right) u^* \right) v \right.$$
$$\left. + \left(\frac{2\nabla w\cdot\nabla w - w^2}{1+|w|^2} - \frac{2|w|^2\nabla w\cdot\nabla w + w^2(1-|w|^2)}{\left(1+|w|^2\right)^2} \right) u^* v^* \right) d\,x \quad \text{(B.484)}$$

Next consider the very similar term $v_t^* u$.

$$v_t^* u = \imath \left(\underbrace{\Delta v^* - \frac{4w\nabla w^*\cdot\nabla v^*}{1+|w|^2}}_{(3)} - \left(\frac{1-2|w|^2}{1+|w|^2} - \frac{2w^2\nabla w^*\cdot\nabla w^* + |w|^2(1-|w|^2)}{\left(1+|w|^2\right)^2} \right) v^* \right. \quad \text{(B.485)}$$
$$\left. - \left(\frac{2\nabla w^*\cdot\nabla w^* - w^{*2}}{1+|w|^2} - \frac{2|w|^2\nabla w^*\cdot\nabla w^* + w^{*2}(1-|w|^2)}{\left(1+|w|^2\right)^2} \right) v \right) u \quad \text{(B.486)}$$

Again here only term (3) will require any attention from integration by parts and it will very closely mimic the work above. So putting these pieces of information together,

$$\int_{\mathbb{R}^2} v_t^* u\, d\,x = \int_{\mathbb{R}^2} \imath \left(\left(\Delta u + \nabla\cdot\left(\frac{4w\nabla w^* u}{1+|w|^2} \right) - \left(\frac{1-2|w|^2}{1+|w|^2} - \frac{2w^2\nabla w^*\cdot\nabla w^* + |w|^2(1-|w|^2)}{\left(1+|w|^2\right)^2} \right) u \right) v^* \right.$$
$$\left. - \left(\frac{2\nabla w^*\cdot\nabla w^* - w^{*2}}{1+|w|^2} - \frac{2|w|^2\nabla w^*\cdot\nabla w^* + w^{*2}(1-|w|^2)}{\left(1+|w|^2\right)^2} \right) u\, v \right) d\,x \quad \text{(B.487)}$$

Grouping terms by v and v^* in $\int_{\mathbb{R}^2}(v_t u^* + v_t^* u)dx$.

$$\begin{aligned}\int_{\mathbb{R}^2}(v_t u^* + v_t^* u)dx = \int_{\mathbb{R}^2} \imath\Bigg(\Bigg(\Delta u + \nabla\cdot\left(\frac{4w\nabla w^* u}{1+|w|^2}\right) - \left(\frac{1-2|w|^2}{1+|w|^2} - \frac{2w^2\nabla w^*\cdot\nabla w^* + |w|^2(1-|w|^2)}{\left(1+|w|^2\right)^2}\right)u \\ + \left(\frac{2\nabla w\cdot\nabla w - w^2}{1+|w|^2} - \frac{2|w|^2\nabla w\cdot\nabla w + w^2(1-|w|^2)}{\left(1+|w|^2\right)^2}\right)u^*\Bigg)v^* \\ - \Bigg(\Delta u^* + \nabla\cdot\left(\frac{4w^*\nabla w\, u^*}{1+|w|^2}\right) \\ - \left(\frac{1-2|w|^2}{1+|w|^2} - \frac{2w^{*2}\nabla w\cdot\nabla w + |w|^2(1-|w|^2)}{\left(1+|w|^2\right)^2}\right)u^* \\ + \Bigg(\frac{2\nabla w^*\cdot\nabla w^* - w^{*2}}{1+|w|^2} - \\ \frac{2|w|^2\nabla w^*\cdot\nabla w^* + w^{*2}(1-|w|^2)}{\left(1+|w|^2\right)^2}\Bigg)u\Bigg)v\Bigg)dx \end{aligned} \tag{B.488}$$

By inspection, this expression is of the form

$$\int_{\mathbb{R}^2} (v^* L^\dagger(u) + v(L^\dagger(u))^*) d\,x \tag{B.489}$$

where

$$L^\dagger(u) = \imath \left(\Delta u + \nabla \cdot \left(\frac{4w\nabla w^* u}{1+|w|^2} \right) - \left(\frac{1-2|w|^2}{1+|w|^2} - \frac{2w^2 \nabla w^* \cdot \nabla w^* + |w|^2(1-|w|^2)}{\left(1+|w|^2\right)^2} \right) u \right.$$
$$\left. + \left(\frac{2\nabla w \cdot \nabla w - w^2}{1+|w|^2} - \frac{2|w|^2 \nabla w \cdot \nabla w + w^2(1-|w|^2)}{\left(1+|w|^2\right)^2} \right) u^* \right) \tag{B.490}$$

If $u_s = L^\dagger u$, then the adjoint condition is met. This implies the adjoint equation to solve is

$$-\imath\, u_s = \Delta u + \nabla \cdot \left(\frac{4w\nabla w^* u}{1+|w|^2} \right) - \left(\frac{1-2|w|^2}{1+|w|^2} - \frac{2w^2 \nabla w^* \cdot \nabla w^* + |w|^2(1-|w|^2)}{\left(1+|w|^2\right)^2} \right) u$$
$$+ \left(\frac{2\nabla w \cdot \nabla w - w^2}{1+|w|^2} - \frac{2|w|^2 \nabla w \cdot \nabla w + w^2(1-|w|^2)}{\left(1+|w|^2\right)^2} \right) u^* \tag{B.491}$$

with $u_0 = w(x,T) - w_0(x)$.

B.5.3 Computation of the Jacobian

The challenge is to evaluate the matrix-vector product of the Jacobian so that Newton's method may be applied to the Landau-Lifshitz equation as formulated as a boundary value problem. The boundary conditions will be ignored for the time being, since these can be encapsulated in the discretization instead. The solution to the Landau-Lifshitz equation can be found as a root of the equation

$$F[U] = i\left(\frac{\partial U}{\partial t} - V_x \frac{\partial U}{\partial x} - V_y \frac{\partial U}{\partial y} \right) - \frac{\partial^2 U}{\partial x^2} - \frac{\partial^2 U}{\partial y^2} + \frac{2U^* \left(\left(\frac{\partial U}{\partial x}\right)^2 + \left(\frac{\partial U}{\partial y}\right)^2 \right) + U(1-|U|^2)}{1+|U|^2} \tag{B.492}$$

Equivalently F can be expressed as a function of the real and imaginary parts of $U = u + i\,v$,

$$G[u,v] = \begin{pmatrix} -\frac{\partial v}{\partial t} - \frac{\partial^2 u}{\partial x^2} - \frac{\partial^2 u}{\partial y^2} + V_x \frac{\partial v}{\partial x} + V_y \frac{\partial v}{\partial y} + \frac{u\left(1-u^2-v^2\right)+2u\left(\left(\frac{\partial u}{\partial x}\right)^2+\left(\frac{\partial u}{\partial y}\right)^2-\left(\frac{\partial v}{\partial x}\right)^2-\left(\frac{\partial v}{\partial y}\right)^2\right)+4v\left(\left(\frac{\partial u}{\partial x}\right)\left(\frac{\partial v}{\partial x}\right)+\left(\frac{\partial u}{\partial y}\right)\left(\frac{\partial v}{\partial y}\right)\right)}{1+u^2+v^2} \\ \frac{\partial u}{\partial t} - \frac{\partial^2 v}{\partial x^2} - \frac{\partial^2 v}{\partial y^2} - V_x \frac{\partial u}{\partial x} - V_y \frac{\partial u}{\partial y} + \frac{v\left(1-u^2-v^2\right)-2v\left(\left(\frac{\partial u}{\partial x}\right)^2+\left(\frac{\partial u}{\partial y}\right)^2-\left(\frac{\partial v}{\partial x}\right)^2-\left(\frac{\partial v}{\partial y}\right)^2\right)+4u\left(\left(\frac{\partial u}{\partial x}\right)\left(\frac{\partial v}{\partial x}\right)+\left(\frac{\partial u}{\partial y}\right)\left(\frac{\partial v}{\partial y}\right)\right)}{1+u^2+v^2} \end{pmatrix} \tag{B.493}$$

and the reader may verify that F is equivalent to G (as described above).

B.5.4 Computing the action of the Jacobian

What follows is the most explicit expression of the derivation of the jacobian, but it is not the most efficient derivation.

$$\frac{d}{d\epsilon} G[u+\epsilon q, v+\epsilon w]\Big|_{\epsilon=0} = DG[u,v]\begin{pmatrix} q \\ w \end{pmatrix} \tag{B.494}$$

The linear portion of this is a trivial calculation and will be skipped. The remaining parts will be computed in several steps. Of the rest, there are only four really distinct calculations, so rather than do it all out, only examples of the distinct parts will be presented. First, compute the variational derivative for the term $\frac{2u\left(\left(\frac{\partial u}{\partial x}\right)^2+\left(\frac{\partial u}{\partial y}\right)^2\right)}{1+u^2+v^2}$:

$$\begin{aligned} \frac{2(u+\epsilon q)\left(\left(\frac{\partial u}{\partial x}+\epsilon\frac{\partial q}{\partial x}\right)^2+\left(\left(\frac{\partial u}{\partial y}+\epsilon\frac{\partial q}{\partial y}\right)\right)^2\right)}{1+(u+\epsilon q)^2+(v+\epsilon w)^2} &= \frac{2\left(u\left(\frac{\partial u}{\partial x}\right)^2+u\left(\frac{\partial u}{\partial y}\right)^2\right)}{\epsilon(2qu+2vw)+1+u^2+v^2} \\ &\quad + \frac{2\epsilon\left(q\left(\frac{\partial u}{\partial x}\right)^2+q\left(\frac{\partial u}{\partial y}\right)^2+2\left(\frac{\partial q}{\partial x}\right)u\left(\frac{\partial u}{\partial x}\right)+2\left(\frac{\partial q}{\partial y}\right)u\left(\frac{\partial u}{\partial y}\right)\right)}{\epsilon(2qu+2vw)+1+u^2+v^2}+\mathcal{O}(\epsilon^2) \end{aligned} \tag{B.495}$$

Differentiating the above expression with respect to ϵ yields

$$\begin{aligned} \frac{d}{d\epsilon}\left(\frac{2(u+\epsilon q)\left(\left(\frac{\partial u}{\partial x}+\epsilon\frac{\partial q}{\partial x}\right)^2+\left(\left(\frac{\partial u}{\partial y}+\epsilon\frac{\partial q}{\partial y}\right)\right)^2\right)}{1+(u+\epsilon q)^2+(v+\epsilon w)^2}\right) &= \frac{2\left(q\left(\frac{\partial u}{\partial x}\right)^2+q\left(\frac{\partial u}{\partial y}\right)^2+2\left(\frac{\partial q}{\partial x}\right)u\left(\frac{\partial u}{\partial x}\right)+2\left(\frac{\partial q}{\partial y}\right)u\left(\frac{\partial u}{\partial y}\right)\right)}{\epsilon(2qu+2vw)+1+u^2+v^2} \\ &\quad - \frac{2\left(u\left(\frac{\partial u}{\partial x}\right)^2+u\left(\frac{\partial u}{\partial y}\right)^2\right)(2qu+2vw)}{\left(\epsilon(2qu+2vw)+1+u^2+v^2\right)^2}+\mathcal{O}(\epsilon) \end{aligned} \tag{B.496}$$

Evaluating at $\epsilon = 0$ this becomes

$$\frac{d}{d\epsilon}\left(\frac{2(u+\epsilon q)\left(\left(\frac{\partial u}{\partial x}+\epsilon\frac{\partial q}{\partial x}\right)^2+\left(\left(\frac{\partial u}{\partial y}+\epsilon\frac{\partial q}{\partial y}\right)\right)^2\right)}{1+(u+\epsilon q)^2+(v+\epsilon w)^2}\right)\Bigg|_{\epsilon=0} = \frac{2\left(q\left(\frac{\partial u}{\partial x}\right)^2+q\left(\frac{\partial u}{\partial y}\right)^2+2\left(\frac{\partial q}{\partial x}\right)u\left(\frac{\partial u}{\partial x}\right)+2\left(\frac{\partial q}{\partial y}\right)u\left(\frac{\partial u}{\partial y}\right)\right)}{1+u^2+v^2} - \frac{2\left(u\left(\frac{\partial u}{\partial x}\right)^2+u\left(\frac{\partial u}{\partial y}\right)^2\right)(2qu+2vw)}{(1+u^2+v^2)^2} \tag{B.497}$$

Next compute the variational derivative of $\frac{2u\left(-\left(\frac{\partial v}{\partial x}\right)^2-\left(\frac{\partial v}{\partial y}\right)^2\right)}{1+u^2+v^2}$:

$$\frac{2(u+\epsilon q)\left(-\left(\left(\frac{\partial v}{\partial x}\right)+\epsilon\left(\frac{\partial w}{\partial x}\right)\right)^2-\left(\left(\frac{\partial v}{\partial y}\right)+\epsilon\left(\frac{\partial w}{\partial y}\right)\right)^2\right)}{1+(u+\epsilon q)^2+(v+\epsilon w)^2} = \frac{2\epsilon\left(-q\left(\frac{\partial v}{\partial x}\right)^2-q\left(\frac{\partial v}{\partial y}\right)^2-2u\left(\frac{\partial v}{\partial x}\right)\left(\frac{\partial w}{\partial x}\right)-2u\left(\frac{\partial v}{\partial y}\right)\left(\frac{\partial w}{\partial y}\right)\right)}{\epsilon(2qu+2vw)+1+u^2+v^2} + \frac{2\left(-u\left(\frac{\partial v}{\partial x}\right)^2-u\left(\frac{\partial v}{\partial y}\right)^2\right)}{\epsilon(2qu+2vw)+1+u^2+v^2}+\mathcal{O}(\epsilon^2) \tag{B.498}$$

Differentiating the above expression with respect to ϵ yields

$$\frac{d}{d\epsilon}\left(\frac{2(u+\epsilon q)\left(-\left(\left(\frac{\partial v}{\partial x}\right)+\epsilon\left(\frac{\partial w}{\partial x}\right)\right)^2-\left(\left(\frac{\partial v}{\partial y}\right)+\epsilon\left(\frac{\partial w}{\partial y}\right)\right)^2\right)}{1+(u+\epsilon q)^2+(v+\epsilon w)^2}\right) = \frac{2\left(-q\left(\frac{\partial v}{\partial x}\right)^2-q\left(\frac{\partial v}{\partial y}\right)^2-2u\left(\frac{\partial v}{\partial x}\right)\left(\frac{\partial w}{\partial x}\right)-2u\left(\frac{\partial v}{\partial y}\right)\left(\frac{\partial w}{\partial y}\right)\right)}{\epsilon(2qu+2vw)+1+u^2+v^2} - \frac{2\left(-u\left(\frac{\partial v}{\partial x}\right)^2-u\left(\frac{\partial v}{\partial y}\right)^2\right)(2qu+2vw)}{\left(\epsilon(2qu+2vw)+1+u^2+v^2\right)^2}+\mathcal{O}(\epsilon) \tag{B.499}$$

Evaluating at $\epsilon = 0$ this becomes

$$\frac{d}{d\epsilon}\left(\frac{2(u+\epsilon q)\left(-\left(\left(\frac{\partial v}{\partial x}\right)+\epsilon\left(\frac{\partial w}{\partial x}\right)\right)^2-\left(\left(\frac{\partial v}{\partial y}\right)+\epsilon\left(\frac{\partial w}{\partial y}\right)\right)^2\right)}{1+(u+\epsilon q)^2+(v+\epsilon w)^2}\right)\Bigg|_{\epsilon=0} = \frac{-2\left(q\left(\frac{\partial v}{\partial x}\right)^2+q\left(\frac{\partial v}{\partial y}\right)^2+2u\left(\frac{\partial v}{\partial x}\right)\left(\frac{\partial w}{\partial x}\right)+2u\left(\frac{\partial v}{\partial y}\right)\left(\frac{\partial w}{\partial y}\right)\right)}{1+u^2+v^2} + \frac{2\left(u\left(\frac{\partial v}{\partial x}\right)^2+u\left(\frac{\partial v}{\partial y}\right)^2\right)(2qu+2vw)}{(1+u^2+v^2)^2} \tag{B.500}$$

Next compute the variational derivative of $\frac{4v\left(\left(\frac{\partial u}{\partial x}\right)\left(\frac{\partial v}{\partial x}\right)+\left(\frac{\partial u}{\partial y}\right)\left(\frac{\partial v}{\partial y}\right)\right)}{1+u^2+v^2}$:

$$\frac{4(v+\epsilon w)\left(\left(\frac{\partial u}{\partial x}+\epsilon\frac{\partial q}{\partial x}\right)\left(\frac{\partial v}{\partial x}+\epsilon\frac{\partial w}{\partial x}\right)+\left(\frac{\partial u}{\partial y}+\epsilon\frac{\partial q}{\partial y}\right)\left(\frac{\partial v}{\partial y}+\epsilon\frac{\partial w}{\partial y}\right)\right)}{1+(u+\epsilon q)^2+(v+\epsilon w)^2} = \frac{4\epsilon\left(\left(\frac{\partial q}{\partial x}\right)v\left(\frac{\partial v}{\partial x}\right)+\left(\frac{\partial q}{\partial y}\right)v\left(\frac{\partial v}{\partial y}\right)+\left(\frac{\partial u}{\partial x}\right)v\left(\frac{\partial w}{\partial x}\right)+\left(\frac{\partial u}{\partial x}\right)\left(\frac{\partial v}{\partial x}\right)w+\left(\frac{\partial u}{\partial y}\right)v\left(\frac{\partial w}{\partial y}\right)+\left(\frac{\partial u}{\partial y}\right)\left(\frac{\partial v}{\partial y}\right)w\right)}{\epsilon(2qu+2vw)+1+u^2+v^2} + \frac{4\left(\left(\frac{\partial u}{\partial x}\right)v\left(\frac{\partial v}{\partial x}\right)+\left(\frac{\partial u}{\partial y}\right)v\left(\frac{\partial v}{\partial y}\right)\right)}{\epsilon(2qu+2vw)+1+u^2+v^2}+\mathcal{O}\left(\epsilon^2\right) \tag{B.501}$$

Differentiating the above expression with respect to ϵ yields

$$\begin{aligned}\frac{d}{d\epsilon}\left(\frac{4(v+\epsilon w)\left(\left(\frac{\partial u}{\partial x}+\epsilon\frac{\partial q}{\partial x}\right)\left(\frac{\partial v}{\partial x}+\epsilon\frac{\partial w}{\partial x}\right)+\left(\frac{\partial u}{\partial y}+\epsilon\frac{\partial q}{\partial y}\right)\left(\frac{\partial v}{\partial y}+\epsilon\frac{\partial w}{\partial y}\right)\right)}{1+(u+\epsilon q)^2+(v+\epsilon w)^2}\right)=\\ \frac{4\left(\left(\frac{\partial q}{\partial x}\right)v\left(\frac{\partial v}{\partial x}\right)+\left(\frac{\partial q}{\partial y}\right)v\left(\frac{\partial v}{\partial y}\right)+\left(\frac{\partial u}{\partial x}\right)v\left(\frac{\partial w}{\partial x}\right)+\left(\frac{\partial u}{\partial x}\right)\left(\frac{\partial v}{\partial x}\right)w+\left(\frac{\partial u}{\partial y}\right)v\left(\frac{\partial w}{\partial y}\right)+\left(\frac{\partial u}{\partial y}\right)\left(\frac{\partial v}{\partial y}\right)w\right)}{\epsilon(2qu+2vw)+1+u^2+v^2}\\ -\frac{4(2qu+2vw)\left(\left(\frac{\partial u}{\partial x}\right)v\left(\frac{\partial v}{\partial x}\right)+\left(\frac{\partial u}{\partial y}\right)v\left(\frac{\partial v}{\partial y}\right)\right)}{\left(\epsilon(2qu+2vw)+1+u^2+v^2\right)^2}+\mathcal{O}(\epsilon)\end{aligned} \tag{B.502}$$

Evaluating at $\epsilon=0$ this becomes

$$\begin{aligned}\left.\frac{d}{d\epsilon}\left(\frac{4(v+\epsilon w)\left(\left(\frac{\partial u}{\partial x}+\epsilon\frac{\partial q}{\partial x}\right)\left(\frac{\partial v}{\partial x}+\epsilon\frac{\partial w}{\partial x}\right)+\left(\frac{\partial u}{\partial y}+\epsilon\frac{\partial q}{\partial y}\right)\left(\frac{\partial v}{\partial y}+\epsilon\frac{\partial w}{\partial y}\right)\right)}{1+(u+\epsilon q)^2+(v+\epsilon w)^2}\right)\right|_{\epsilon=0}=\\ \frac{4\left(\left(\frac{\partial q}{\partial x}\frac{\partial v}{\partial x}+\frac{\partial q}{\partial y}\frac{\partial v}{\partial y}+\frac{\partial u}{\partial x}\frac{\partial w}{\partial x}+\frac{\partial u}{\partial y}\frac{\partial w}{\partial y}\right)v+\left(\frac{\partial u}{\partial x}\frac{\partial v}{\partial x}+\frac{\partial u}{\partial y}\frac{\partial v}{\partial y}\right)w\right)}{1+u^2+v^2}-\frac{4v(2qu+2vw)\left(\frac{\partial u}{\partial x}\frac{\partial v}{\partial x}+\frac{\partial u}{\partial y}\frac{\partial v}{\partial y}\right)}{(1+u^2+v^2)^2}\end{aligned} \tag{B.503}$$

Finally, compute the variational derivative of $\frac{u\left(-u^2-v^2+1\right)}{1+u^2+v^2}$:

$$\frac{(u+\epsilon q)\left(-(u+\epsilon q)^2-(v+\epsilon w)^2+1\right)}{(u+\epsilon q)^2+(v+\epsilon w)^2+1}=\frac{\epsilon\left(-3qu^2-qv^2+q-2uvw\right)}{\epsilon(2qu+2vw)+1+u^2+v^2}+\frac{-u^3-uv^2+u}{\epsilon(2qu+2vw)+1+u^2+v^2}+\mathcal{O}\left(\epsilon^2\right) \tag{B.504}$$

Differentiating the above expression with respect to ϵ yields

$$\frac{d}{d\epsilon}\left(\frac{(u+\epsilon q)\left(-(u+\epsilon q)^2-(v+\epsilon w)^2+1\right)}{(u+\epsilon q)^2+(v+\epsilon w)^2+1}\right)=\frac{-3qu^2-qv^2+q-2uvw}{\epsilon(2qu+2vw)+1+u^2+v^2}-\frac{\left(-u^3-uv^2+u\right)(2qu+2vw)}{\left(\epsilon(2qu+2vw)+1+u^2+v^2\right)^2}+\mathcal{O}(\epsilon) \tag{B.505}$$

Evaluating at $\epsilon=0$ this becomes

$$\left.\frac{d}{d\epsilon}\left(\frac{(u+\epsilon q)\left(-(u+\epsilon q)^2-(v+\epsilon w)^2+1\right)}{(u+\epsilon q)^2+(v+\epsilon w)^2+1}\right)\right|_{\epsilon=0}=\frac{-3qu^2-qv^2+q-2uvw}{1+u^2+v^2}-\frac{\left(-u^3-uv^2+u\right)(2qu+2vw)}{(1+u^2+v^2)^2} \tag{B.506}$$

All together this yields,

$$DG[u,v]\begin{pmatrix} q \\ w \end{pmatrix} = \begin{pmatrix} \left\{ \begin{array}{r} -\frac{\partial w}{\partial t} + V_x \frac{\partial w}{\partial x} + V_y \frac{\partial w}{\partial y} - \frac{\partial^2 q}{\partial x^2} - \frac{\partial^2 q}{\partial y^2} + q\left(-\frac{2u\left(u\left(1-u^2-v^2\right)+2u\left(\left(\frac{\partial u}{\partial x}\right)^2+\left(\frac{\partial u}{\partial y}\right)^2-\left(\frac{\partial v}{\partial x}\right)^2-\left(\frac{\partial v}{\partial y}\right)^2\right)+4v\left(\left(\frac{\partial u}{\partial x}\right)\left(\frac{\partial v}{\partial x}\right)+\left(\frac{\partial u}{\partial y}\right)\left(\frac{\partial v}{\partial y}\right)\right)\right)}{\left(1+u^2+v^2\right)^2} \right. \\ \left. + \frac{1-3u^2-v^2+2\left(\left(\frac{\partial u}{\partial x}\right)^2+\left(\frac{\partial u}{\partial y}\right)^2-\left(\frac{\partial v}{\partial x}\right)^2-\left(\frac{\partial v}{\partial y}\right)^2\right)}{1+u^2+v^2} \right) \\ + \frac{4v\left(\left(\frac{\partial q}{\partial x}\right)\left(\frac{\partial v}{\partial x}\right)+\left(\frac{\partial q}{\partial y}\right)\left(\frac{\partial v}{\partial y}\right)+\left(\frac{\partial u}{\partial x}\right)\left(\frac{\partial w}{\partial x}\right)+\left(\frac{\partial u}{\partial y}\right)\left(\frac{\partial w}{\partial y}\right)\right)}{1+u^2+v^2} + \frac{2u\left(2\left(\frac{\partial q}{\partial x}\right)\left(\frac{\partial u}{\partial x}\right)+2\left(\frac{\partial q}{\partial y}\right)\left(\frac{\partial u}{\partial y}\right)-2\left(\frac{\partial v}{\partial x}\right)\left(\frac{\partial w}{\partial x}\right)-2\left(\frac{\partial v}{\partial y}\right)\left(\frac{\partial w}{\partial y}\right)\right)}{1+u^2+v^2} \\ + w\left(\frac{4\left(\left(\frac{\partial u}{\partial x}\right)\left(\frac{\partial v}{\partial x}\right)+\left(\frac{\partial u}{\partial y}\right)\left(\frac{\partial v}{\partial y}\right)\right)-2uv}{1+u^2+v^2} - \frac{2v\left(u\left(1-u^2-v^2\right)+2u\left(\left(\frac{\partial u}{\partial x}\right)^2+\left(\frac{\partial u}{\partial y}\right)^2-\left(\frac{\partial v}{\partial x}\right)^2-\left(\frac{\partial v}{\partial y}\right)^2\right)+4v\left(\left(\frac{\partial u}{\partial x}\right)\left(\frac{\partial v}{\partial x}\right)+\left(\frac{\partial u}{\partial y}\right)\left(\frac{\partial v}{\partial y}\right)\right)\right)}{\left(1+u^2+v^2\right)^2} \right) \end{array} \right\} \\ \left\{ \begin{array}{r} \frac{\partial q}{\partial t} - V_x \frac{\partial q}{\partial x} - V_y \frac{\partial q}{\partial y} - \frac{\partial^2 w}{\partial x^2} - \frac{\partial^2 w}{\partial y^2} + q\left(-\frac{2u\left(v\left(1-u^2-v^2\right)+4u\left(\left(\frac{\partial u}{\partial x}\right)\left(\frac{\partial v}{\partial x}\right)+\left(\frac{\partial u}{\partial y}\right)\left(\frac{\partial v}{\partial y}\right)\right)-2v\left(\left(\frac{\partial u}{\partial x}\right)^2+\left(\frac{\partial u}{\partial y}\right)^2-\left(\frac{\partial v}{\partial x}\right)^2-\left(\frac{\partial v}{\partial y}\right)^2\right)\right)}{\left(1+u^2+v^2\right)^2} \right. \\ \left. + \frac{4\left(\left(\frac{\partial u}{\partial x}\right)\left(\frac{\partial v}{\partial x}\right)+\left(\frac{\partial u}{\partial y}\right)\left(\frac{\partial v}{\partial y}\right)\right)-2uv}{1+u^2+v^2} \right) \\ + \frac{4u\left(\left(\frac{\partial q}{\partial x}\right)\left(\frac{\partial v}{\partial x}\right)+\left(\frac{\partial q}{\partial y}\right)\left(\frac{\partial v}{\partial y}\right)+\left(\frac{\partial u}{\partial x}\right)\left(\frac{\partial w}{\partial x}\right)+\left(\frac{\partial u}{\partial y}\right)\left(\frac{\partial w}{\partial y}\right)\right)}{1+u^2+v^2} - \frac{2v\left(2\left(\frac{\partial q}{\partial x}\right)\left(\frac{\partial u}{\partial x}\right)+2\left(\frac{\partial q}{\partial y}\right)\left(\frac{\partial u}{\partial y}\right)-2\left(\frac{\partial v}{\partial x}\right)\left(\frac{\partial w}{\partial x}\right)-2\left(\frac{\partial v}{\partial y}\right)\left(\frac{\partial w}{\partial y}\right)\right)}{1+u^2+v^2} \\ + w\left(\frac{1-3v^2-u^2-2\left(\left(\frac{\partial u}{\partial x}\right)^2+\left(\frac{\partial u}{\partial y}\right)^2-\left(\frac{\partial v}{\partial x}\right)^2-\left(\frac{\partial v}{\partial y}\right)^2\right)}{1+u^2+v^2} - \frac{2v\left(v\left(1-u^2-v^2\right)+4u\left(\left(\frac{\partial u}{\partial x}\right)\left(\frac{\partial v}{\partial x}\right)+\left(\frac{\partial u}{\partial y}\right)\left(\frac{\partial v}{\partial y}\right)\right)-2v\left(\left(\frac{\partial u}{\partial x}\right)^2+\left(\frac{\partial u}{\partial y}\right)^2-\left(\frac{\partial v}{\partial x}\right)^2-\left(\frac{\partial v}{\partial y}\right)^2\right)\right)}{\left(1+u^2+v^2\right)^2} \right) \end{array} \right\} \end{pmatrix} \tag{B.507}$$

B.5.4.1 An alternate approach

Both analytically and computationally the formulation of the Jacobian in Eq. (B.507) is extremely inefficient. It takes a lot more algebra than necessary to arrive at that equation by decoupling into real an imaginary parts from the start. Evaluating this computationally is inefficient since it requires more FFTs than necessary, unless you take derivatives of u, v and q, w together (which essentially brings you to the main point of this section). Define $\mathscr{C} : \mathbb{R}^{2n} \to \mathbb{C}^n$ to be the canonical map from the real numbers to the complex numbers. taking the variational derivative of F yields

$$\begin{aligned} \left.\frac{d}{d\epsilon} F[U+\epsilon W]\right|_{\epsilon=0} &= DF[U]W \\ &= i\left(\frac{\partial W}{\partial t} - \mathbf{V}\cdot\nabla W\right) - \Delta W \\ &\quad - \frac{2W^*\nabla U\cdot\nabla U + 4U^*\nabla U\cdot\nabla W - U\left(U^*W + UW^*\right) + \left(1-UU^*\right)W}{1+UU^*} \\ &\quad + \frac{\left(2U^*\nabla U\cdot\nabla U + U\left(1-UU^*\right)\right)\left(U^*W+UW^*\right)}{\left(1+UU^*\right)^2} \end{aligned} \tag{B.508}$$

The computation has been skipped since it essentially repeats the calculations of the previous sections. It is both intuitively obvious and a fact readily verified that

$$DG[u,v]\begin{pmatrix} q \\ w \end{pmatrix} = \mathscr{C}^{-1}\left(DF\left[\mathscr{C}\left(\begin{bmatrix} u \\ v \end{bmatrix} \right) \right] \mathscr{C}\left(\begin{bmatrix} q \\ w \end{bmatrix} \right) \right) \tag{B.509}$$

It is via this equation that the Jacobian has actually been evaluated numerically. In reality, this is just a consequence of the chain rule since $G = \mathscr{C}^{-1} \circ F \circ \mathscr{C}$.

APPENDIX

C

PERTURBED CONSERVATION OF ENERGY

While this thesis utilizes singular perturbation theory to derive the modulation equation, another quite popular method exists based on the conserved quantities of the underlying equation. As can be seen in this section, the calculation under this method is quite straightforward. The method is limited, however, by knowledge of the conserved quantities. In order to determine the evolution of the higher order parameters, the conserved quantities must be supplemented by balance law conditions. Such balance laws are either ad hoc or must be derived by asymptotic expansions of the conserved quantities and balancing higher order corrections. In such cases, the computational advantages of this method are often negated. For those who wish to pursue this approach, a simple example, based on determining the evolution of the energy in the presence of a perturbation is provided here.

C.1 Derivation in Spherical Variables

C.1.1 Problem Formulation

The challenge is to determine the time evolution of the energy for a perturbed version of the Landau-Lifshitz equation. This calculation will be done in two ways. First, based on the spherical variables. Since these are closely related to the Hamiltonian structure of the Landau-Lifshitz equation, the derivation is considerably simplified.

$$\frac{\partial \Theta}{\partial t} = F[\Theta,\Phi] + P_\Theta \tag{C.1}$$

$$\sin(\Theta)\frac{\partial \Phi}{\partial t} = G[\Theta,\Phi] + P_\Phi \tag{C.2}$$

where P_Θ and P_Φ represent arbitrary additional terms to the Landau-Lifshitz equation (damping, Oersted field etc.) and F and G are defined by

$$F[\Theta,\Phi] = \frac{\nabla\cdot\left(\sin^2(\Theta)\nabla\Phi\right)}{\sin(\Theta)} \tag{C.3}$$

$$G[\Theta,\Phi] = \frac{1}{2}\sin(2\Theta)\left(|\nabla\Phi|^2+1\right) - \nabla^2\Theta \tag{C.4}$$

respectively. The definitions F and G will make the subsequent calculation much easier. The energy equation is given by

$$\mathscr{E}[\Theta,\Phi] = \frac{1}{2}\int_{\mathbb{R}^2}\left[|\nabla\Theta|^2 + \sin^2(\Theta)\left(1+|\nabla\Phi|^2\right)\right]d\mathbf{x} \tag{C.5}$$

C.1.2 Calculation

Let's differentiate the energy with respect to time

$$\frac{d}{dt}\mathscr{E}[\Theta,\Phi] = \frac{d}{dt}\frac{1}{2}\int_{\mathbb{R}^2}\left[|\nabla\Theta|^2 + \sin^2(\Theta)\left(1+|\nabla\Phi|^2\right)\right]d\mathbf{x} \tag{C.6}$$

move time derivative inside derivative

$$= \frac{1}{\cancel{2}}\int_{\mathbb{R}^2}\left[\cancel{2}\nabla\Theta\cdot\nabla\left(\frac{\partial\Theta}{\partial t}\right) + \cancel{2}\sin(\Theta)\cos(\Theta)\left(1+|\nabla\Phi|^2\right)\frac{\partial\Theta}{\partial t} + \sin^2(\Theta)\cancel{2}\nabla\Phi\cdot\nabla\left(\frac{\partial\Phi}{\partial t}\right)\right]d\mathbf{x} \tag{C.7}$$

integrate by parts so that it is not necessary to differentiate Eqs. (1.9)& (1.10) (C.8)

(Green's first identity, boundary terms vanish)

$$= \int_{\mathbb{R}^2}\left[-\nabla^2\Theta\left(\frac{\partial\Theta}{\partial t}\right) + \sin(\Theta)\cos(\Theta)\left(1+|\nabla\Phi|^2\right)\frac{\partial\Theta}{\partial t} - \nabla\cdot\left(\sin^2(\Theta)\nabla\Phi\right)\left(\frac{\partial\Phi}{\partial t}\right)\right]d\mathbf{x} \tag{C.9}$$

At this point things should start to look familiar

$$\frac{d}{dt}\mathscr{E}[\Theta,\Phi] = \int_{\mathbb{R}^2}\left[\underbrace{\left(-\nabla^2\Theta + \sin(\Theta)\cos(\Theta)\left(1+|\nabla\Phi|^2\right)\right)}_{G[\Theta,\Phi]}\frac{\partial\Theta}{\partial t} - \nabla\cdot\left(\sin^2(\Theta)\nabla\Phi\right)\left(\frac{\partial\Phi}{\partial t}\right)\right]d\mathbf{x} \tag{C.10}$$

$$= \int_{\mathbb{R}^2}\left[G[\Theta,\Phi]\frac{\partial\Theta}{\partial t} - \underbrace{\frac{\nabla\cdot\left(\sin^2(\Theta)\nabla\Phi\right)}{\sin\Theta}}_{F[\Theta,\Phi]}\left(\sin\Theta\frac{\partial\Phi}{\partial t}\right)\right]d\mathbf{x} \tag{C.11}$$

Substituting based on Eqs. (C.1)- (C.2)

$$\frac{d}{dt}\mathscr{E}[\Theta,\Phi] = \int_{\mathbb{R}^2}\left(G[\Theta,\Phi](F[\Theta,\Phi]+P_\Theta) - F[\Theta,\Phi](G[\Theta,\Phi]+P_\Phi)\right)d\mathbf{x} \tag{C.12}$$

$$= \int_{\mathbb{R}^2}\left(\cancel{G[\Theta,\Phi]F[\Theta,\Phi]} + G[\Theta,\Phi]P_\Theta - \cancel{F[\Theta,\Phi]G[\Theta,\Phi]} - F[\Theta,\Phi]P_\Phi\right)d\mathbf{x} \tag{C.13}$$

Hence, the time evolution for the energy is governed by

$$\boxed{\frac{d\mathscr{E}}{dt} = \int_{\mathbb{R}^2} (G[\Theta,\Phi]P_\Theta - F[\Theta,\Phi]P_\Phi)\, d\mathbf{x}} \tag{C.14}$$

C.2 Derivation in Stereographic Variables

While the preceding section is certainly sufficient for determining the modulation equations, often a problem is presented in variables that are not so closely linked with the Hamiltonian structure. In such cases, the calculation may be some what less straightforward. The procedure remains essentially the same no matter how the equation is presented. This section provides the derivation in stereographic variables to provide an example. Additionally, knowing the evolution of the energy based on the stereographic formulation may be of some use in future work, and the transformation of Eq (C.14) to stereographic variables is a nontrivial exercise.

C.2.1 Problem Formulation

The Landau-Lifshitz equation in stereographic variables

$$\imath \frac{\partial w}{\partial t} = N[w] + P_w \tag{C.15}$$

where

$$N[w] = \nabla^2 w - \frac{2w^*\nabla w\cdot\nabla w + w(1-w^*w)}{1+w^*w} \tag{C.16}$$

and P_w is some arbitrary additional term to the Landau-Lifshitz equation in stereographic form. The energy is given by

$$\mathscr{E}[w] = 2\int \frac{\nabla w^*\cdot\nabla w + w^*w}{1+w^*w}\, d\mathbf{x} \tag{C.17}$$

C.2.2 Calculation

$$\frac{d\mathscr{E}}{dt} = 2\int \left\{ \frac{\frac{d}{dt}(\nabla w^* \cdot \nabla w + w^* w)(1+w^* w)^2 - (\nabla w^* \cdot \nabla w + w^* w)\,\frac{d}{dt}(1+w^* w)^2}{(1+w^* w)^4} \right\} d\mathbf{x} \tag{C.18}$$

$$= 2\int \left\{ \frac{\left(\nabla\left(\frac{\partial w^*}{\partial t}\right)\cdot\nabla w + \nabla w^*\cdot\nabla\left(\frac{\partial w}{\partial t}\right) + w^*\frac{\partial w}{\partial t} + \frac{\partial w^*}{\partial t}w\right)\cancel{(1+w^* w)^2} - 2(\nabla w^*\cdot\nabla w + w^* w)\cancel{(1+w^* w)}\left(w^*\frac{\partial w}{\partial t} + \frac{\partial w^*}{\partial t}w\right)}{(1+w^* w)^{\cancel{4}}} \right\} d\mathbf{x} \tag{C.19}$$

$$= 2\int \left\{ \frac{\nabla w}{(1+w^* w)^2}\cdot\nabla\left(\frac{\partial w^*}{\partial t}\right) + \frac{\nabla w^*}{(1+w^* w)^2}\cdot\nabla\left(\frac{\partial w}{\partial t}\right) + \frac{w^*\frac{\partial w}{\partial t} + \frac{\partial w^*}{\partial t}w}{(1+w^* w)^2} + \frac{-2(\nabla w^*\cdot\nabla w + w^* w)\left(w^*\frac{\partial w}{\partial t} + \frac{\partial w^*}{\partial t}w\right)}{(1+w^* w)^3} \right\} d\mathbf{x} \tag{C.20}$$

integrate the first two terms by parts, boundary terms will vanish...

$$= 2\int \left\{ -\nabla\cdot\left(\frac{\nabla w}{(1+w^* w)^2}\right)\left(\frac{\partial w^*}{\partial t}\right) - \nabla\cdot\left(\frac{\nabla w^*}{(1+w^* w)^2}\right)\left(\frac{\partial w}{\partial t}\right) + \frac{w^*\frac{\partial w}{\partial t} + \frac{\partial w^*}{\partial t}w}{(1+w^* w)^2} + \frac{-2(\nabla w^*\cdot\nabla w + w^* w)\left(w^*\frac{\partial w}{\partial t} + \frac{\partial w^*}{\partial t}w\right)}{(1+w^* w)^3} \right\} d\mathbf{x} \tag{C.21}$$

The first of these derivative terms expands to become

$$-\nabla\cdot\left(\frac{\nabla w}{(1+w^* w)^2}\right)\left(\frac{\partial w^*}{\partial t}\right) = \frac{\partial w^*}{\partial t}\left(-\frac{\nabla^2 w}{(1+w^* w)^2} + \frac{2\nabla w\cdot(w^*\nabla w + \nabla w^* w)}{(1+w^* w)^3}\right). \tag{C.22}$$

The other term expands in a similar fashion. Substituting based on these results and collecting like terms in $\frac{\partial w^*}{\partial t}$ and $\frac{\partial w}{\partial t}$,

$$\frac{d\mathscr{E}}{dt} = 2\int \frac{1}{(1+w^*w)^2}\left\{\left(\frac{\partial w^*}{\partial t}\right)\left(-\nabla^2 w + w + \frac{2w^*\nabla w\cdot\nabla w + 2w\nabla w\cdot\nabla w^*}{(1+w^*w)} + \frac{-2(\nabla w^*\cdot\nabla w + w^*w)(w)}{(1+w^*w)}\right)\right.$$
$$\left. + \left(\frac{\partial w}{\partial t}\right)\left(-\nabla^2 w^* + w^* + \frac{2w\nabla w^*\cdot\nabla w^* + 2w^*\nabla w^*\cdot\nabla w}{(1+w^*w)} + \frac{-2(\nabla w^*\cdot\nabla w + w^*w)(w^*)}{(1+w^*w)}\right)\right\} d\mathbf{x} \quad \text{(C.23)}$$

$$= 2\int \frac{1}{(1+w^*w)^2}\left\{\left(\frac{\partial w^*}{\partial t}\right)\left(-\nabla^2 w + \frac{w(1+w^*w)}{(1+w^*w)} + \frac{2w^*\nabla w\cdot\nabla w}{(1+w^*w)} + \cancel{\frac{2w\nabla w^*\cdot\nabla w}{(1+w^*w)}} - \cancel{\frac{2w\nabla w^*\cdot\nabla w}{(1+w^*w)}} - \frac{2w^*w^2}{(1+w^*w)}\right)\right.$$
$$\left. + \left(\frac{\partial w}{\partial t}\right)\left(-\nabla^2 w^* + \frac{w^*(1+w^*w)}{(1+w^*w)} + \frac{2w\nabla w^*\cdot\nabla w^*}{(1+w^*w)} + \cancel{\frac{2w^*\nabla w^*\cdot\nabla w}{(1+w^*w)}} - \cancel{\frac{2w^*\nabla w^*\cdot\nabla w}{(1+w^*w)}} - \frac{2(w^*)^2 w}{(1+w^*w)}\right)\right\} d\mathbf{x} \quad \text{(C.24)}$$

$$= 2\int \frac{1}{(1+w^*w)^2}\left\{\left(\frac{\partial w^*}{\partial t}\right)\left(-\nabla^2 w + \frac{w}{(1+w^*w)} + \cancel{\frac{w^*w^2}{(1+w^*w)}} + \frac{2w^*\nabla w\cdot\nabla w}{(1+w^*w)} - \frac{2w^*w^2}{(1+w^*w)}\right)\right.$$
$$\left. + \left(\frac{\partial w}{\partial t}\right)\left(-\nabla^2 w^* + \frac{w^*}{(1+w^*w)} + \cancel{\frac{(w^*)^2 w}{(1+w^*w)}} + \frac{2w\nabla w^*\cdot\nabla w^*}{(1+w^*w)} - \frac{2(w^*)^2 w}{(1+w^*w)}\right)\right\} d\mathbf{x} \quad \text{(C.25)}$$

$$= 2\int \frac{1}{(1+w^*w)^2}\left\{\left(\frac{\partial w^*}{\partial t}\right)\left(-\nabla^2 w + \frac{2w^*\nabla w\cdot\nabla w + w - w^*w^2}{(1+w^*w)}\right)\right.$$
$$\left. + \left(\frac{\partial w}{\partial t}\right)\left(-\nabla^2 w^* + \frac{2w\nabla w^*\cdot\nabla w^* + w^* - (w^*)^2 w}{(1+w^*w)}\right)\right\} d\mathbf{x} \quad \text{(C.26)}$$

$$= 2\int \frac{1}{(1+w^*w)^2}\left\{\left(\frac{\partial w^*}{\partial t}\right)\left(-\nabla^2 w + \frac{2w^*\nabla w\cdot\nabla w + w(1-w^*w)}{(1+w^*w)}\right)\right.$$
$$\left. + \left(\frac{\partial w}{\partial t}\right)\left(-\nabla^2 w^* + \frac{2w\nabla w^*\cdot\nabla w^* + w^*(1-w^*w)}{(1+w^*w)}\right)\right\} d\mathbf{x} \quad \text{(C.27)}$$

$$= 2\int \frac{1}{(1+w^*w)^2}\left\{\left(\frac{\partial w^*}{\partial t}\right)(-N[w]) + \left(\frac{\partial w}{\partial t}\right)(-N[w^*])\right\} d\mathbf{x} \quad \text{(C.28)}$$

From Eq. (C.15), $\frac{\partial w}{\partial t} = -\imath\,(N[w]+P_w) \Rightarrow \frac{\partial w^*}{\partial t} = \imath\left((N[w])^* + P_w^*\right) = \imath\left(N[w^*]+P_w^*\right)$. Substituting into the previous relation,

$$\frac{d\mathscr{E}}{dt} = 2\int \frac{1}{(1+w^*w)^2}\left\{\imath\left(N[w^*]+P_w^*\right)(-N[w]) - \imath\,(N[w]+P_w)(-N[w^*])\right\} d\mathbf{x} \tag{C.29}$$

$$= 2\imath\int \frac{1}{(1+w^*w)^2}\left\{-\cancel{N[w]N[w^*]} - N[w]P_w^* + \cancel{N[w]N[w^*]} + N[w^*]P_w\right\} d\mathbf{x} \tag{C.30}$$

$$= 2\imath\int \frac{1}{(1+w^*w)^2}\left\{N[w^*]P_w - N[w]P_w^*\right\} d\mathbf{x} \tag{C.31}$$

$$= -4\,\mathscr{I}m\left(\int \frac{N[w^*]P_w}{(1+w^*w)^2} d\mathbf{x}\right) \tag{C.32}$$

where $\mathscr{I}m(z)$ denotes the imaginary part of z. So that's my final answer

$$\boxed{\frac{d\mathscr{E}}{dt} = -4\,\mathscr{I}m\left(\int \frac{N[w^*]P_w}{(1+w^*w)^2} d\mathbf{x}\right)} \tag{C.33}$$

This calculation has some bearing on the numerical computation of droplets. The methods outlined in Chapter 5 attempt to calculate the droplet in stereographic form. If a constraint based on the energy is to be employed, it is reasonable to additionally assume that the energy is periodic with period T

$$\int_0^T \frac{d\mathscr{E}}{dt} dt = \mathscr{E}(T) - \mathscr{E}(0) = 0 = -4\int_0^T \mathscr{I}m\left(\int \frac{N[w^*]P_w}{(1+w^*w)^2} d\mathbf{x}\right) dt\,. \tag{C.34}$$

Hence, $0 = \int_0^T \mathscr{I}m\left(\int \frac{N[w^*]P_w}{(1+w^*w)^2} d\mathbf{x}\right) dt$ could be the additional constraint for the droplet system. Such a constraint would make it possible to solve for the necessary forcing while keeping the overall energy of the computed family of droplets constant.